

**Quantum dot - molecularly imprinted polymer
nanomaterials for the fluorescence sensing of
selected pharmaceutical and personal care products**

by

Hanieh Montaseri

Submitted in partial fulfilment of the requirements for the
degree

Doctor of Philosophy (Chemistry)

In the Faculty of Natural & Agricultural Sciences

University of Pretoria

Pretoria

December 2018

Declaration

I, Hanieh Montaseri declare that the thesis, which I hereby submit for the degree Doctor of Philosophy at the University of Pretoria, is my own work and has not previously been submitted by me for a degree at this or any other tertiary institution.

Signature:

Date:

Acknowledgments

Writing this thesis has certainly been a long and arduous journey, but it would not have been at all possible were it not for the help and support of a rather special group of people.

First and foremost I would like to thank my supervisor, Professor Patricia B.C. Forbes, for repeatedly going above and beyond throughout my postgraduate career. You continually motivate me to strive to become a better chemist. I have learned so much and would not be where I am today without your support.

My thanks also extend to Dr. Oluwasesan Adegoke for his scientific contribution in Paper 4 and above all, moral support.

I would also like to thank the amazing friends that I have made here in Pretoria; Sifiso, Chiedza, Genna, Kedibone, Amanda and Basil. You have been my family away from home and I will always treasure the memories we made here. I truly believe I have made true and lasting friendships.

I would also like to show gratitude towards the Water Research Commission (WRC) and the Photonics Initiative of South Africa (PISA) for funding and encouraging quantum dot research at the University of Pretoria.

I specially want to thank my mother and father for their tremendous support over my entire 26 years of education. Finally, I would like to dedicate this thesis to my family and my best company, Saeid, for believing in me and supporting me in many different ways to help me achieve my goals. Even when I did not believe in myself, you have always believed in me and what I could achieve. Without your endless love, support and encouragement, the completion of this thesis would not have been possible.

Abstract

This research was aimed at fabricating and applying cadmium based core/shell quantum dots (QDs) as fluorescence probes for the detection in aquatic compartments of triclosan (TCS) and acetaminophen (AC) which fall within the pharmaceutical and personal care products (PPCPs) subclass of emerging chemical pollutants (ECPs). Semiconductor quantum dots possess significant advantages such as high fluorescence intensity, long-term photostability, narrow emission and broad absorption as well as high photoluminescence quantum yields, and they have thus attracted considerable research attention for environmental monitoring and sensing applications.

Core/shell CdSe/ZnS QDs were synthesized through the one-pot organometallic approach in order to explore the fluorescence sensing of the QDs towards triclosan. A ligand exchange reaction was also performed with glutathione (GSH) as a surface capping agent to convert hydrophobic QDs to water soluble QDs, where the mercapto moiety of GSH binds onto the surface of the QDs and their carboxyl groups provide water solubility. The resultant quantum dots were characterized using various state of the art instruments including fluorescence and UV/Vis spectroscopy, powder X-ray diffraction (XRD), Fourier transform infrared spectroscopy (FTIR), high resolution transmission electron microscopy (HRTEM), and energy dispersive X-ray spectroscopy (EDS). Characterization techniques confirmed the successful synthesis of QDs and the formation of a GSH coating thereon. The synthesized GSH-CdSe/ZnS QDs had a high photoluminescence quantum yield of 89% and an average particle size of 3.3 ± 1.3 nm, as determined by HRTEM analysis, which agreed well with the size determined from the first excitonic absorption peak (3.7 nm). In addition, the QDs exhibited strong and narrow fluorescence intensity with an estimated full width at half maximum of 32.7 nm.

The presence of triclosan in the proximity of the QDs enhanced the fluorescence intensity of the QDs. The experimental results showed that under optimum conditions (i.e. 1.5 mg GSH-CdSe/ZnS QDs in 3.0 mL of Millipore water with an incubation time of 5 min and excitation and emission wavelengths of 300 nm and 598 nm, respectively), the calibration plot of $F-F_0/F_0$ of the GSH-CdSe/ZnS QDs was proportional to triclosan concentration in the range of 10-300 nmol L⁻¹ (F and F₀ are the fluorescence intensity of the QDs in the presence and absence of triclosan respectively). The mechanism was likely based on Förster resonance energy transfer (FRET) from the analyte to the QDs which provided a fluorescence “turn-on” nanosensor for the sensing of triclosan. The Förster distance in the system of GSH-CdSe/ZnS QDs-TCS was found to be approximately 4.0 nm which meets the distance required (<10 nm) for FRET to occur. The developed QDs were found to be a sensitive probe for the determination of triclosan with a very low detection limit of 3.7 nmol L⁻¹ in the presence of other

structurally related compounds. The applicability of the probe was evaluated for the determination of triclosan in South African tap and river water matrices which indicated good recoveries of 94%-117.5%.

In the next study, the performance of three QD-ligand systems were tested to find the optimum system with high sensitivity to acetaminophen. In this regard, three water-soluble QDs were synthesized through the use of hot, coordinating solvents of octadec-1-ene and oleic acid. In addition, ligand exchange reactions using L-cysteine (L-cys), N-acetyl-L-cysteine (NAC) and glutathione (reported earlier for triclosan detection) as thiol capping agents were performed. L-cys-CdSe/ZnS QDs produced enough sensitivity and were utilized as the optimized system for the determination of acetaminophen. Therefore, characterizations and analytical performance of the sensor for acetaminophen detection were investigated by using aqueous L-cys-CdSe/ZnS QDs.

L-cys bound efficiently to the surface of the QDs which was confirmed by different characterisation techniques such as Fourier-transform infrared spectroscopy, high resolution transmission electron microscopy, and energy dispersive X-ray spectroscopy. The photoluminescence properties of the synthesized L-cys-CdSe/ZnS QDs included a quantum yield of 77% with a low full width at half maxima value of 38.5 nm for L-cys-CdSe/ZnS QDs, which indicated the formation of a uniform and homogenous particle size distribution. The average particle size of the L-cys-CdSe and L-cys-CdSe/ZnS QDs determined from HRTEM were 2.1 ± 0.5 and 5.1 ± 0.8 nm, respectively which correlated well with the size from the first excitonic absorption peaks (2.8 nm and 4.0 nm respectively).

The utilization of the L-cys-CdSe/ZnS QDs as fluorescent probes for the determination of acetaminophen in water samples was optimised for various parameters including concentration of L-cys-CdSe/ZnS QDs and incubation time. The optimum amount of L-cys-CdSe/ZnS QDs was found to be 1.0 mg in 3.0 mL Millipore water with an incubation time of 5 min. The reaction mechanism proved that the fluorescence “turn-on” effect of the L-cys-CdSe/ZnS QDs in the presence of acetaminophen was due to Förster resonance energy transfer from acetaminophen (donor) to the QDs (acceptor) with a Förster distance of 6.1 nm. Experimental investigation showed that the FRET-sensitized QD emission intensity at 595 nm was enhanced with the introduction of acetaminophen over the linear range of 3.0-100 nmol L⁻¹. The applicability of the QDs to determine AC concentrations in the presence of some related pharmaceuticals including epinephrine hydrochloride, L-ascorbic acid, uric acid, dopamine hydrochloride and 4-aminophenol were tested and no significant interferences were found. In addition, the probe could be applied for the detection of acetaminophen in water matrices at concentrations as low as 1.6 nmol L⁻¹ with recoveries of 90-108% which is environmentally relevant.

Further work on the performance of a molecularly imprinted polymer (MIP) on the surface of the QDs was examined to improve the selectivity of the L-cys-CdSe/ZnS QDs-AC system which was applied in the previous study. In this research, MIP-capped QDs (MIP@QDs) were prepared using 3-aminopropyltriethoxysilane (APTES) as the functional monomer, tetraethyl orthosilicate (TEOS) as the cross-linker, aqueous ammonia solution as the catalyst and acetaminophen as the template via an adapted Stöber method (sol-gel approach) and surface imprinting technique. L-cys-CdSe/ZnS QDs were thus used as scaffolds in the preparation of molecularly imprinted composites for the determination of acetaminophen. Non-imprinted polymer (NIP) was synthesized under the same reaction conditions without the addition of the template. Different characterization techniques were carried out to confirm the polymer coating such as Fourier-transform infrared spectroscopy, high resolution transmission electron microscopy, energy dispersive X-ray spectroscopy as well as thermogravimetric analysis (TGA).

The template was imprinted near the proximity of the surface so there were no deeper lying cavities which may result in slow releasing of the template and subsequently template bleeding from the MIP material. Carboxyl groups covering the surface of L-cys-CdSe/ZnS QDs were conjugated to the amine groups of the functional monomer (APTES) through electrostatic interactions which resulted in the tight binding of the QDs in the sol-gel. Moreover, acetaminophen had hydroxyl and carboxyl groups which formed hydrogen bonds with APTES. As a result, the fluorescence intensity of the MIP@QDs did not decline significantly after 5 days. The synthesized MIP had a large surface area to volume ratio which facilitated mass transfer and rebinding of the template due to the accessibility of the recognition sites. The information that was garnered from characterization techniques confirmed the polymer coating and the resultant MIP demonstrated high thermal and photo stabilities. The binding capacity, sensitivity, response time, inter and intra-day stability and selectivity of the sensor were investigated systematically.

The nano-molar detection ($LOD = 0.34 \text{ nmol L}^{-1}$) of acetaminophen was accomplished via charge transfer from MIP@QDs to acetaminophen which caused fluorescence quenching. The relative fluorescence intensity of the MIP@QDs exhibited good linearity in the range of $1.0\text{-}300 \text{ nmol L}^{-1}$ of acetaminophen. Moreover, the evaluation of the imprinting factor indicated the higher selectivity of MIP@QDs relative to non-imprinted polymer capped QDs (NIP@QDs), which was found to be 6.0 based on the Stern-Volmer slopes of MIP@QDs to NIP@QDs. Selectivity studies on a group of structural analogues to acetaminophen revealed that the adsorption capacities for these compounds were much lower than those for the AC which confirmed that the recognition mechanism of acetaminophen was based on shape, size and functional groups. Good reproducibility was also attained with a relative standard deviation

(RSD) of 3.7% for three parallel detections. Further work on the monitoring of acetaminophen in real water samples, including tap and river water, validated the high selectivity of the developed probe in practical applications with satisfactory recoveries of 95% to 114%.

Publications and Manuscripts

This thesis is based on the following papers:

1. Montaseri, H., & Forbes, P.B.C. (2016). A review of monitoring methods for triclosan and its occurrence in aquatic environments. *TrAC Trends in Analytical Chemistry*, 85, 221-231. Impact Factor 7.034. <https://doi.org/10.1016/j.trac.2016.09.010>
2. Montaseri, H., & Forbes, P.B.C. (2018). Analytical techniques for the determination of acetaminophen: A review, *TrAC Trends in Analytical Chemistry*, 108, 122-134. Impact Factor 7.034. <https://doi.org/10.1016/j.trac.2018.08.023>
3. Montaseri, H., & Forbes, P.B.C. (2018). A triclosan turn-ON fluorescence sensor based on thiol-capped core/shell quantum dots. *Spectrochimica Acta Part A: Molecular and Biomolecular Spectroscopy*, 204, 370-379. Impact Factor 2.536. <https://doi.org/10.1016/j.saa.2018.06.043>
4. Montaseri, H., Adegoke, O., & Forbes, P.B.C. Development of a thiol-capped core/shell quantum dot sensor for acetaminophen. *South African Journal of Chemistry*. Under review.
5. Montaseri, H., & Forbes, P.B.C. (2018). Molecularly imprinted polymer coated quantum dots for fluorescence sensing of acetaminophen. *Materials Today Communications*, 17, 480-492. <https://doi.org/10.1016/j.mtcomm.2018.10.007>

Two additional journal papers were produced as a co-author responsible for the characterisation of the synthesised quantum dots:

1. Adegoke, O., Montaseri, H., Nsiband, S.A., & Forbes, P.B.C. (2017). Alloyed quaternary/binary core/shell quantum dot-graphene oxide nanocomposite: Preparation, characterization and application as a fluorescence “switch ON” probe for environmental pollutants. *Journal of Alloys and Compounds*, 720, 70-78.

2. Adegoke, O., Montaseri, H., Nsibande, S.A., & Forbes, P.B.C. (2019). Passivating effect of ternary alloyed AgZnSe shell layer on the structural and luminescent properties of CdS quantum dots. *Materials Science in Semiconductor Processing*. 90, 162-170.

Conference Presentations

1. Montaseri, H., & Forbes, P.B.C., "Synthesis and characterization of L-cysteine capped CdSe/ZnS quantum dots coated with a molecularly imprinted polymer", The South African Chemical Institute Inorganic Conference **2017**, 25-29 June 2017, Arabella Hotel & Spa, Hermanus, South Africa.
2. Montaseri, H., & Forbes, P.B.C. "Synthesis and characterization of L-cysteine capped CdSe/ZnS quantum dots coated with a molecularly imprinted polymer", South African Nanotechnology Initiative, 7th Annual Gauteng Nanosciences Young Researchers' Symposium, 20 October **2017**, Tshwane University of Pretoria, Pretoria, South Africa.
3. Montaseri, H., & Forbes, P.B.C. "Fluorescence sensor probe for the detection of acetaminophen using L-cysteine CdSe/ZnS quantum dots and molecular imprinted polymer@quantum dots", IEEE Sensors **2017**, 29 October – 1 November 2017, Glasgow, Scotland. DOI: [10.1109/ICSENS.2017.8234129](https://doi.org/10.1109/ICSENS.2017.8234129)
4. Montaseri, H., & Forbes, P.B.C. "A novel fluorescence sensor for acetaminophen", Analitika **2018**, 22-25 July 2018, Legend Gold and Safari Resort, Mookgophong, Limpopo, South Africa.

Table of Contents

Declaration.....	i
Acknowledgments.....	ii
Abstract.....	iii
Publications and Manuscripts.....	vii
Conference Presentations.....	ix
Table of Contents.....	x
List of Figures	xiii
List of Tables	xix
List of Schemes	xxi
List of Symbols.....	xxii
List of Abbreviations.....	xxiii
Chapter 1 Background and Motivation	1
1.1 Problem statement and motivation.....	2
1.2 Aims and objectives of the thesis	3
1.2.1 General aim of the thesis.....	3
1.2.2 Objectives	3
1.3 Context of the thesis	3
1.4 References	5
Chapter 2 Introduction	6
2.1 Background.....	7
2.2 Quantum dots (QDs).....	9
2.3 Core/shell nanoparticles.....	12
2.4 Toxicity considerations.....	14
2.5 Synthesis of QDs	14
2.5.1 Organometallic synthesis of QDs	15
2.5.1.1 Water-solubilisation of QDs.....	16

2.5.2	Wet chemistry	16
2.6.	Comparison of aqueous and organometallic synthetic approaches.....	16
2.7	Characterization techniques.....	17
2.7.1	Ultraviolet-visible absorption spectroscopy (UV/Vis).....	17
2.7.2	Fluorescence spectroscopy.....	18
2.7.3	Powder X-ray diffraction (XRD)	19
2.7.4	Fourier-transform infrared spectroscopy analysis (FT-IR).....	20
2.7.5	High resolution transmission electron microscopy analysis (HRTEM).....	20
2.7.6	High resolution scanning electron microscopy analysis (HRSEM)	20
2.7.7	Raman analysis.....	21
2.7.8	Energy-dispersive X-ray spectroscopy analysis (EDS)	21
2.7.9	Thermogravimetric analysis (TGA)	22
2.8	QDs utilized in this work.....	22
2.9	Application of CdSe/ZnS QDs in fluorescence sensing.....	26
2.10	Fluorescence quantum yield	29
2.11	Principle of optical sensing using QDs	29
2.12	Molecularly imprinted polymers (MIPs)	30
2.13	Mechanisms involved in MIP preparation.....	32
2.14	Polymers utilized in this work	33
2.14.1	Functional monomers.....	35
2.14.2	Cross linkers	35
2.14.3	Template	36
2.14.4	Solvents	36
2.15	Principle of optical sensing using MIP-capped QDs (MIP@QDs).....	37
2.16	Toxicity of triclosan	37
2.16.1	Toxicity threshold of triclosan	39
2.16.2	Legal limit of triclosan	45
2.17	Toxicity of acetaminophen	46
2.17.1	Toxicity threshold of acetaminophen	47

2.17.2 Legal limits of acetaminophen	50
2.18 References	50
Chapter 3 Literature Review	69
3.1 Paper 1	70
3.2 Paper 2	82
Chapter 4 Experimental Methods, Results and Discussion	97
4.1 Paper 3	98
4.1.1 Paper 3 - Supplementary information	110
4.2 Paper 4	114
4.2.1 Paper 4 - Supplementary information	138
4.3 Paper 5	146
4.3.1 Paper 5 - Supplementary information	161
Chapter 5 Overall Conclusions and Future Work	168
5.1 Overall conclusions	169
5.2 Future work	171
5.3 References	172
Appendices	173
Appendix A	173
Appendix B	175
Appendix C	177
C.1 Paper 1	178
C.2 Paper 2	188

List of Figures

Chapter 2

Figure 1. Electronic energy states of a semiconductor in the transition from discrete molecules to nanosized crystals and bulk crystals.	10
Figure 2. (a) Sixteen emission colors from small (blue) to large (red) QDs excited by a near-ultraviolet lamp; size of QDs can be from ~1 nm to ~10 nm. (b) Creation of an exciton upon photon absorption followed by fluorescence emission or relaxation through trap states.	11
Figure 3. The structure of a quantum dot showing its three main features: core, shell and ligands	13
Figure 4. (a) Zinc blende and (b) wurtzite crystal structures of ZnS.	20
Figure 5. QDs utilized in this work: (A) L-cys-CdSe QDs, (B) NAC-CdSe QDs, (C) GSH-CdSe QDs, (D) L-cys-CdSe/ZnS QDs, (E) NAC-CdSe/ZnS QDs, (F) GSH-CdSe/ZnS QDs.....	25
Figure 6. Synthesized QDs under UV irradiation with an excitation wavelength 365 nm, (A) L-cys-CdSe QDs (left), L-cys-CdSe/ZnS QDs (right); (B) NAC-CdSe QDs (left), NAC-CdSe/ZnS QDs (right); (C) GSH-CdSe QDs (left), GSH-CdSe/ZnS QDs (right).	25
Figure 7. Polymers utilized in this work: (A) MIP@QDs without template removed, (B) MIP@QDs with template removed and (C) NIP@QDs polymer.	34
Figure 8. Synthesized polymers with template removed under UV irradiation with an excitation wavelength 365 nm; MIP@QDs (left), NIP@QDs (right).	34
Figure 9. Structure of 3-aminopropyltriethoxysilane.....	35
Figure 10. Structure of tetraethyl orthosilicate.	36
Figure 11. Chemical structure of triclosan.	38
Figure 12. Comparison of environmental occurrence data of triclosan and toxicity threshold values for different organisms.	39
Figure 13. Structure of acetaminophen.....	46
Figure 14. Environmental occurrence data for acetaminophen in comparison to available toxicity threshold values for various indicator organisms.	47

Chapter 3

Paper 1

Figure 1. Chemical structure of triclosan.	72
Figure 2. Scheme for the synthesis of carbon nanotubes@triclosan – molecularly imprinted polymer (CNTs@TCS-MIPs): (a) formation of template triclosan (TCS)-aminosilica monomer 3-aminopropyltriethoxysilane (APTES) complex; (b) transformation of the surface of purified CNTs to silica shell by a sol–gel process using tetraethoxysilane (TEOS) and APTES in the	

presence of cetyltrimethylammonium bromide (CTAB) to obtain core@shell carbon nanotubes coated with silica (CNTs@SiO₂); (c) reaction of CNTs@ SiO₂ with template silica monomer complex to produce silica surface functionalized with TCS-imprinted polymer; (d) removal of the TCS from polymer shells to obtain the CNTs@TCS-MIPs.77

Paper 2

Figure 1. The typical procedure followed for the analysis of pharmaceuticals in aqueous matrices by chromatography-mass spectrometry.88

Figure 2. Publications relating to acetaminophen electrochemical sensors applied to a range of matrices within the period of 2010-2017 inclusive, (A) number of publications per year and (B) cumulative counts (n=334).91

Figure 3. Fluorescence quenching emission spectra of L-cysteine capped CdTe NPs in the absence and presence of acetaminophen in the concentration range 1.5×10^3 to 2.4×10^4 ng L⁻¹.93

Chapter 4

Paper 3

Figure 1. Chemical structure of triclosan.101

Figure 2. Absorption spectra of the water-soluble GSH-capped CdSe/ZnS QDs in Millipore water (A) and PL emission spectra of the water-soluble GSH-capped CdSe QDs (B) and GSH-capped CdSe/ZnS QDs measured in Millipore water (C) at 470 nm. The inset shows GSH-CdSe QDs (left) and GSH-CdSe/ZnS QDs under UV irradiation with an excitation wavelength of 365 nm.102

Figure 3. Powder XRD pattern of the GSH-CdSe and GSH-CdSe/ZnS QDs.103

Figure 4. The FT-IR spectra of GSH-CdSe QDs, GSH-CdSe/ZnS QDs, and GSH.103

Figure 5. TEM images of GSH-CdSe QDs (A) and GSH-CdSe/ZnS QDs (B) and particle size distribution of GSH-CdSe QDs (A1) and GSH-CdSe/ZnS QDs (B1).104

Figure 6. EDS spectra of GSH-CdSe QDs (A) and GSH-CdSe/ZnS QDs (B).105

Figure 7. Effect of the concentration of aqueous GSH-CdSe/ZnS QDs in the presence of 70 nmol L⁻¹ TCS, fluorescence intensity without TCS (F₀), fluorescence intensity with TCS (F). The experimental conditions were excitation wavelength, 300 nm; slit widths of excitation and emission, 5 nm.105

Figure 8. Effect of reaction time on the fluorescence intensity of GSH capped CdSe/ZnS QDs in the presence of 70 nmol L⁻¹ TCS. The experimental conditions were GSH-CdSe/ZnS QDs 1.5 mg in 3.0 mL Millipore water; excitation wavelength, 300 nm; slit widths of excitation and emission, 5 nm.106

Figure 9. The fluorescence spectra of GSH-CdSe/ZnS QDs in the presence of different concentrations of triclosan. The experimental conditions were GSH-CdSe/ZnS QDs 1.5 mg in 3.0 mL Millipore water; excitation wavelength, 300 nm; slit widths of excitation and emission, 5 nm.	106
Figure 10. Linear graph of $F-F_0/F_0$ versus TCS concentration. The experimental conditions were GSH-CdSe/ZnS QDs 1.5 mg in 3.0 mL Millipore water; excitation wavelength, 300 nm; slit widths of excitation and emission, 5 nm.	106
Figure 11. Effect of other analytes on the fluorescence emission intensity of the GSH-CdSe/ZnS QDs probe at an emission wavelength of 598 nm. The concentration of TCS and each of the other analytes was 180 nmol L^{-1} and GSH-CdSe/ZnS QDs was 1.5 mg in 3.0 mL Millipore water. $F-F_0/F_0$ relates to the fluorescence intensity of the QDs in the presence and absence of the analytes. Excitation wavelength was 300 nm. Analytes were 2,4,6-trichlorophenol (2,4,6-TCP), 2,3,4-trichlorophenol (2,3,4-TCP), 2,4-dichlorophenol (2,4-DCP), 4-chlorophenol (4-CP), 4-hydroxybenzoic acid (Paraben), Bisphenol A (BPA), and Triclocarban (TCC).	107
Figure 12. Florescence spectrum of TCS ($1.4 \times 10^{-5} \text{ mol L}^{-1}$) at excitation wavelength 310 nm (A) and UV–Vis absorption spectrum of GSH-CdSe/ZnS QDs (B).	108
Figure S1. Florescence spectrum of TCS ($1.4 \times 10^{-5} \text{ mol L}^{-1}$) at excitation wavelength 310 nm.	111
Figure S2. PL stability of the hydrophilic CdSe/ZnS QDs measured before and after 5 days of exposure to ambient light. The experimental conditions were GSH-CdSe/ZnS QDs 1.5 mg in 3.0 mL Millipore water; excitation wavelength, 300 nm; slit widths of excitation and emission, 5 nm.	111
Paper 4	
Figure 1. Structure of acetaminophen.	117
Figure 2. Comparison of the sensitivity of three QD-ligand systems (L-cys-CdSe/ZnS, NAC-CdSe/ZnS and GSH-CdSe/ZnS QDs) towards 5.0 nmol L^{-1} of AC.	121
Figure 3. The FT-IR spectra of (A) L-cys, (B) L-cys-CdSe QDs and (C) L-cys-CdSe/ZnS QDs.	123
Figure 4. TEM images of (A) L-cys-CdSe QDs and (B) L-cys-CdSe/ZnS QDs, scale bar 100 nm; and (A1) particle size distribution of L-cys-CdSe QDs and (B1) L-cys-CdSe/ZnS QDs	125
Figure 5. Effect of the concentration of aqueous L-cys-CdSe/ZnS QDs on fluorescence in the absence and presence of 5.0 nmol L^{-1} AC at excitation wavelength 300 nm (values are the average of three measurements).	127

Figure 6. (A) PL “turn-on” emission spectra for the determination of AC using L-cys-CdSe/ZnS QDs for different concentrations of AC at an excitation wavelength of 300 nm and (B) linear graph of $F-F_0$, versus AC concentration (values are the average of three measurements).	128
Figure 7. UV-Vis absorption spectrum of (A) L-cys-CdSe/ZnS QDs and (B) fluorescence spectrum of acetaminophen (1.0×10^{-5} mol L ⁻¹) at excitation wavelength 300 nm.	130
Figure 8. Fluorescence intensity change of 1.0 mg/3.0 mL of L-cys-CdSe/ZnS QDs in the presence of AC and various analytes (100 nmol L ⁻¹) at an excitation and emission wavelengths of 300 nm and 595 nm respectively. Epinephrine hydrochloride (EP), L-ascorbic acid (AA), uric acid (UA), dopamine hydrochloride (DA), 4-aminophenol (4-AP), (values are the average of three measurements).	132
Figure S1. Absorption spectra of the water-soluble (A) L-cys-capped CdSe/ZnS QDs; (B) L-cys-CdSe QDs in Millipore water; (C) PL emission spectra of the water-soluble L-cys-capped CdSe QDs at excitation wavelength 470 nm; (D) L-cys-capped CdSe/ZnS QDs at excitation wavelength 410 nm measured in Millipore water.....	139
Figure S2. EDS spectra of (A) L-cys-CdSe QDs and (B) L-cys-CdSe/ZnS QDs.	139
Figure S3. Powder XRD pattern of the (A) L-cys-CdSe and (B) L-cys-CdSe/ZnS QDs.	140
Figure S4. Raman spectra of (A) L-cys-CdSe and (B) L-cys-CdSe/ZnS QDs.	141
Figure S5. Florescence spectrum of acetaminophen in water (1.0×10^{-5} mol L ⁻¹) at an excitation wavelength of 300 nm.	142
Figure S6. PL stability of the hydrophilic QDs measured before and after 5 days of exposure to ambient light (300 nm excitation).	142
Figure S7. Effect of interaction time on the fluorescence intensity of the L-cys capped CdSe/ZnS QD-AC system at an excitation wavelength of 300 nm (values are the average of three measurements).	143
Paper 5	
Figure 1. FT-IR spectra of AC, L-cys, L-cys-CdSe QDs, L-cys-CdSe/ZnS QDs, MIP@QDs (with template removed) and NIP@QDs.	151
Figure 2. HRTEM images of (A) L-cys-CdSe QDs (B) L-cys-CdSe/ZnS QDs (C) MIP@QDs and (D) NIP@QDs.	152
Figure 3. Size distribution histogram of (A) L-cys-CdSe QDs (B) L-cys-CdSe/ZnS QDs, (C) MIP@QDs and (D) NIP@QDs.	153
Figure 4. Thermogravimetric analysis of the synthesized MIP@QDs and NIP@QDs.	154

Figure 5. Effect of the MIP@QD concentration on PL quenching efficiency (n=3). The concentration of AC was fixed at 300.0 nmol L⁻¹. The experimental conditions were excitation wavelength 350 nm; slit widths of excitation and emission, 5.0 nm.155

Figure 6. Effect of incubation time on relative fluorescence of MIP@QDs with AC (n=3). The experimental conditions were MIP@QDs: 0.8 mg in 3.0 mL⁻¹; AC: 300.0 nmol L⁻¹; excitation wavelength, 350 nm; slit widths of excitation and emission, 5 nm.155

Figure 7. Photostability of MIP@QDs over 40 min (values are the average of three measurements). The experimental conditions were MIP@QDs, 0.8 mg in 3.0 mL; excitation wavelength, 350 nm; slit widths of excitation and emission, 5.0 nm.155

Figure 8. Fluorescence emission spectra of MIP@QDs (A) and NIP@QDs (B) in the presence of varying concentrations of AC. The experimental conditions were MIP@QDs or NIP@QDs at 0.8 mg in 3.0 mL; excitation wavelength, 350 nm; slit widths of excitation and emission, 5 nm. The inset graphs display the corresponding Stern–Volmer plots of MIP@QDs and NIP@QDs with the addition of AC (all results are the average of three replicates).156

Figure 9. Fluorescence quenching of MIP@QDs and NIP@QDs by different analytes at 300.0 nmol L⁻¹. The experimental conditions were MIP@QDs, or NIP@QDs 0.8 mg in 3.0 mL; excitation wavelength 350 nm; 5 nm excitation and emission slit widths. L-tryptophan (TRY), ascorbic acid (AA), epinephrine hydrochloride (EP), uric acid (UA), dopamine hydrochloride (DA), ketoprofen (KTP), sulfamethoxazole (SM), diclofenac sodium salt (Dic), estradiol (ES), L-3,4-dihydroxyphenylalanine (L-Dopa) and 4-aminophenol (4-AP) (results are the average of three replicates).157

Figure 10. UV/Vis absorption spectrum of AC (A) and MIP@QDs (B) and fluorescence emission spectrum of MIP coated QDs (C).157

Figure S1. (A) Photoluminescence spectra of the L-cys-CdSe/ZnS QDs, MIP@QDs and NIP@QDs in Millipore water, excitation wavelength 350 nm; slit widths of excitation and emission, 5 nm. (Inset: (b) photoluminescence spectra of the L-cys-CdSe QDs with an intensity of 6.4×10⁴ at an emission wavelength of 568 nm which could not be included in graph (A) due to the low intensity, (c) L-cys-CdSe/ZnS QDs (left) MIP@QDs (middle) and NIP@QDs (right) under UV irradiation with an excitation wavelength of 365 nm).162

Figure S2. HRSEM image of NIP@QDs.162

Figure S3. EDS spectra of MIP@QDs (A) and NIP@QDs (B).163

Figure S4. Average photostability of MIP@QDs and NIP@QDs over 5 days (n=3). The experimental conditions were MIP@QDs or NIP@QDs, 0.8 mg in 3.0 mL⁻¹; excitation wavelength, 350 nm; slit widths of excitation and emission, 5.0 nm.163

Appendices

Appendix C

Paper 1

- Figure 1.** PL emission (A) and UV/vis absorption spectra (B) of unconjugated L-cysteine-capped CdSeTeS/ZnS QDs and the QD-GO nanocomposite.181
- Figure 2.** TEM images of (A) L-cysteine CdSeTeS/ZnS QDs and (B) GO. (C) SEM image of GO and (D) HRSEM image of GO. (E) TEM image of the QD-GO nanocomposite.182
- Figure 3.** PXRD spectra of GO, unconjugated QDs and the QD-GO nanocomposite.183
- Figure 4.** EDS spectra of (A) CdSeTeS core and (B) CdSeTeS/ZnS QDs.183
- Figure 5.** Raman spectra of GO, unconjugated QDs and the QD-GO nanocomposite.184
- Figure 6.** FT-IR spectra of GO, unconjugated QDs and the QD-GO nanocomposite.184
- Figure 7.** Effects of PAHs on the PL emission of QD-GO nanocomposite. [PAH]= 5×10^{-7} M. Effect of incubation time (0-40 min) (B) and concentration (C) on the PL emission of the QD-GO nanocomposite in the presence of 5×10^{-7} M Phe target. Error bars represent standard deviation of 3 successive measurements.185
- Figure 8.** (A) PL “switch ON” emission spectra for the detection of Phe using the QD-GO nanocomposite for a range of phenanthrene concentrations and (B) corresponding fluorescence signal calibration curve.186

Paper 2

- Figure 1.** TEM images (A, B and C) and average particle size distribution (A1, B1 and C1) of CdS core QDs.190
- Figure 2.** TEM images (A, B, C and D) and average particle size distribution (A1, B1, C1 and D1) of CdS/AgZnSe core/alloyed shell QDs synthesized via method 1.191
- Figure 3.** TEM images (A, B and C) and average particle size distribution (A1, B1 and C1) of CdS/AgZnSe core/alloyed shell QDs synthesized via method 2.193
- Figure 4.** PXRD plots of CdS, CdS/AgZnSe₅₈₈, CdS/AgZnSe₅₉₃, CdS/AgZnSe₅₉₉ and CdS/AgZnS₆₀₁ QDs.194
- Figure 5.** Raman spectra of CdS, CdS/AgZnSe₅₈₈, CdS/AgZnSe₅₉₃, CdS/AgZnSe₅₉₉ and CdS/AgZnS₆₀₁ QDs.194
- Figure 6.** PL and UV/vis absorption spectra of the different sized CdS (A and B) and CdS/AgZnSe core/alloyed shell QDs (C and D) synthesized via method 1.195
- Figure 7.** PL (A) and UV/vis absorption (B) spectra of the different sized and CdS/AgZnSe core/alloyed shell QDs synthesized via method 2.196

List of Tables

Chapter 2

Table 1. Examples of emerging compound classes.	8
Table 2. List of the precursors, stabilizing agents and particle sizes for the synthesis of CdSe/ZnS QDs reported in the literature and target analytes which have been detected, where appropriate.....	28
Table 3. Effects of TCS on freshwater (FW) and marine (SW) organisms.....	41
Table 4. Acute toxicity data of triclosan.....	43
Table 5. Chronic toxicity data of triclosan.....	43
Table 6. Effects of acetaminophen on different organisms.....	49

Chapter 3

Paper 1

Table 1. Examples of green techniques compared to conventional analytical methods and their relative advantages and disadvantages.	73
Table 2. Proposed QC acceptance criteria for triclosan.	74
Table 3. Comparison of selected chromatography-based methods for triclosan determinations in water samples.	75
Table 4. Comparison of linear ranges and limits of detection (LODs) for triclosan obtained using a range of electrode based systems.	77
Table 5. Comparison of typical analytical parameters pertaining to liquid chromatography and capillary electrophoresis.	78

Paper 2

Table 1. Selected chromatography based methods for the determination of acetaminophen in water and wastewater applications.	89
Table 2. Comparison of the performance of selected electrochemical sensors and biosensors for acetaminophen sensing in date order for the two year period from 2016 to the end of 2017.	92

Chapter 4

Paper 3

Table 1. Comparison of some analytical methods for the determination of TCS in water samples.	107
Table 2. Analytical results for the determination of TCS in tap and river water samples using GSHcapped CdSe/ZnS QDs.	107

Table S1 Chemical structures of potentially interfering analytes.	112
---	-----

Paper 4

Table 1. Optical characterization values of the water-soluble L-cys-CdSe and L-cys-CdSe/ZnS QDs.	122
--	-----

Table 2. Comparison of the particle size of L-cys-CdSe and L-cys-CdSe/ZnS QDs.	125
--	-----

Table 3. Comparison of some published analytical methods for the determination of AC in water.	129
--	-----

Table 4. Analytical results for the determination of recoveries of AC spiked in tap and river water samples using L-cys-CdSe/ZnS QDs.	133
---	-----

Table S1. Elemental compositions of L-cys-CdSe and L-cys-CdSe/ZnS QDs by using EDS.	144
---	-----

Table S2. IR absorption bands of the L-cys-CdSe and L-cys-CdSe/ZnS QDs.	144
---	-----

Table S3. Chemical structures of potentially interfering analytes.	145
--	-----

Paper 5

Table 1. Spiked recovery results for the determination of AC in water samples using 2 mL of 0.8 mg of MIP@QDs in 3 mL of Millipore water and 200 μ L of AC standard solution (n=3).	158
---	-----

Table 2. Comparison of the proposed fluorescence method with other recently reported methods for AC determination in water samples.	159
---	-----

Table S1. Chemical structures of potential interfering analytes.	165
--	-----

Appendices

Appendix B

Table 1. Water: methanol percentage gradient elution.	176
---	-----

Appendix C

Paper 2

Table 1. Summary of the photophysical properties of the different-sized CdS core and CdS/AgZnSe QDs.	195
--	-----

List of Schemes

Chapter 2

Scheme 1. Schematic of the synthesis of (A) QDs by the organometallic approach and (B) surface modification by thiol ligands..... 23

Scheme 2. Formation process of (A) conventional MIPs through in-situ polymerization and (B) luminescent MIP nanocomposites (MIP-NCs) through copolymerization..... 31

Chapter 3

Paper 2

Scheme 1. Schematic illustration of AC treatment in wastewater by H₂O₂/UV.86

Scheme 2. Schematic illustration of acetaminophen metabolism in humans.87

Paper 4

Scheme 1. Fluorescence resonance energy transfer from AC to the L-cys-CdSe/ZnS QDs.131

Paper 5

Scheme 1. Schematic illustration of the preparation of MIP@QDs and the sensing mechanism for AC.150

Scheme 2. Schematic illustration of the molecular imprinting mechanism of AC in a silica matrix through hydrogen bond interactions (the third H-bond is between the amine group of AC and a hydroxyl group of L-cys associated with the QDs – not shown).151

Scheme 3. (A) Schematic representation of the MIP@QDs fluorescence quenching mechanism based on electron transfer-induced energy transfer and (B) schematic of the fluorescence quenching of MIP@QDs according to molecular orbital theory (B).158

Scheme S1. Molecular orbital diagram of AC. The molecular orbital diagram of acetaminophen was generated with a gas phase single point calculation in the Gaussian 09 program package [1] from the crystal structure (COTZAN02) in the CCDC database.164

Appendices

Appendix C

Paper 1

Scheme 1. Conjugation of GO (A) to alloyed L-cysteine-capped CdSeTeS/ZnS QDs (B) to form the QD-GO nanocomposite (C).180

Scheme 2. Schematic representation of the π - π induced PAH adsorption on GO which triggers the fluorescence enhancement of the conjugated QDs.184

List of Symbols

The symbols in the articles in Chapters 3, 4 and Appendices are not listed here.

A	Absorbance of the sample at the excitation wavelength
A_{std}	Absorbance of the reference at the excitation wavelength
β	Full width at maxima of the reflection peak
C	Molar concentration of the quantum dots
c	Speed of light
D	Size of the semiconductor nanocrystal
d	Space of atomic planes
E	Band gap energy
ε	Extinction coefficient
F	Fluorescence intensity
H	Planks constant
K	Scherrer constant
K_{sv}	Stern–Volmer quenching constant
λ	Wavelength of reflected X-ray
λ_1	First excitonic absorption peak of the corresponding sample
λ_{max}	Max emission wavelength
L	Path length (cm) of the radiation beam
n	Refractive indices of solvents used for the sample
n_{std}	Refractive indices of solvents used for the reference
Q	Quencher
r	Donor-acceptor distance
R_0	Förster distance
ΔE	Energy of the first excitonic peak
Θ	Angle of diffraction
Φ_{F}	Quantum yield

List of Abbreviations

The abbreviations in the articles in Chapters 3, 4 and Appendices are not listed here.

AC	Acetaminophen
AEE	Aminoethoxyethanol
APS	Aminopropyltris (methoxy) silane
APTES	3-aminopropyltriethoxysilane
APTMS	(3-aminopropyl) trimethoxysilane
AuNP	Gold nanoparticle
Cd(Ac) ₂	Cadmium acetate
Ce6	Chlorin e6
CNP	Carbon nanoparticle
DMAET	2-(dimethylamino) ethanethiol
EC	Effective concentration
ECP	Emerging chemical pollutant
EDAC	1-ethyl-3-(3-dimethylaminopropyl) carbodiimide hydrochloride
EDS	Energy-dispersive X-ray spectroscopy
ELS	Early life stage
FRET	Förster resonance energy transfer
FT-IR	Fourier-transform infrared spectroscopy analysis
FW	Freshwater
GSH	Glutathione
GSI	Gonadosomatic index.
HAD	Hexadecylamine
HRSEM	High resolution scanning electron microscopy
HRTEM	High resolution transmission electron microscopy
HIS	Hepatosomatic index
IC	Inhibition concentration
Invert.	Invertebrates
LC	Lethal concentration
L-cys	L-cysteine
LDH	Lactate dehydrogenase
LOEC	Lowest-observed-effect concentration
ME	Mercaptoethanol
Me ₂ Cd	Dimethyl cadmium
Me ₂ Zn	Dimethyl zinc

MDH	Minnesota Department of Health
MIC	Minimum inhibitory concentration
MIP	Molecularly imprinted polymer
MIP@QDs	Molecularly imprinted polymer capped quantum dots
MIP-NCs	MIP nanocomposites
MPA	Mercaptoacetic acid
MPS	Mercaptopropyltris (methoxy) silane
MSA	Mercaptosuccinic acid
MTBE	Methyl-t-butyl ether
MUA	Mercaptoundecanoic acid
NAC	N-acetyl-L-cysteine
NIH	National Institutes of Health
NIP@QDs	Non-imprinted polymer capped quantum dots
NOEC	No-observed effects concentration
NSAID	Non-steroidal anti-inflammatory drug
OA	Oleic acid
ODA	Octadecylamine
ODE	Octadec-1-ene
PAHs	Polycyclic aromatic hydrocarbons
PBDEs	Polybrominated diphenyl ethers
PBT	Persistence, bioaccumulation and ecotoxicity
PCBs	Polychlorinated biphenyls
PEC	Predicted environmental concentration
PEG	Polyethylene glycol
PFCs	Perfluorinated compounds
PLQY	Photoluminescence quantum yield
PMMA	Polymethylmethacrylate
PNEC	Predicted no effect concentration
PPCPs	Pharmaceutical and personal care products
PVP	Poly (vinylpyrrolidone)
QDs	Quantum dots
QSAR	Quantitative structure-activity relationship
QY	Quantum yield
RSD	Relative standard deviation
SPTMS	(3-sulfanyl propyl) trimethoxysilane
SSD	Species sensitivity distribution
STP	Sewage treatment plant

SW	Surface water
TBP	Tributylphosphine
TCS	Triclosan
TDPA	Tetradecyl phosphonic acid
TEOS	Tetraethyl orthosilicate
TGA	Thermogravimetric analysis
TMAH	Tetramethylammonium hydroxide
(TMS) ₂ S	Bis(trimethylsilyl) sulfide
TOPO	Trioctylphosphine oxide
TOP	Trioctylphosphine
U.S. FDA	The United States Food and Drug Agency
VTG	Vitellogenin
WWTP	Wastewater treatment plant
XRD	X-ray diffraction
ZnEt ₂	Diethyl zinc

Chapter 1 Background and Motivation

In this chapter an overview of the problem which motivated this study is given. In addition, aims and objectives together with the context of the thesis are presented.

1.1 Problem statement and motivation

Environmental contaminants which have been produced by industries as well as anthropogenic and agricultural activities put unprecedented strain on the environment and human health. Emerging chemical pollutants (ECPs) comprise a wide variety of compounds including endocrine disruptors, hormones, toxins, pharmaceuticals and personal care products (PPCPs) (Gavrilescu *et al.*, 2015; Thomaidis *et al.*, 2012). Triclosan, and acetaminophen as PPCPs are of particular concern as regulatory and/or analytical standards have yet to be developed for these compounds. In addition, there is a paucity of accurate and precise data concerning the concentration, biodegradation, resistance and their risks in the environment. The analysis of water is also vitally important as the ECPs drastically affect water quality and potentially impact the ecosystem and human health (Bolong *et al.*, 2009; Gomes *et al.*, 2003). Therefore, in order to prevent and manage the detrimental effects of these pollutants, the development of robust methods for selective removal and determination thereof is of great importance.

Effective screening methods are necessary to facilitate regular monitoring of the environment for pollution. It may serve as a warning system for the community to take preventive measurements in minimizing contact with the pollutants. The data recorded from the monitoring produces a broad overview into the dynamic interaction between the environment and the stressors. Such information is worthwhile to foresee potential environmental influences in the future and early policies and management programs can be installed to avoid the impacts so as to build a more sustainable future (Lovett *et al.*, 2007). However, data relating to the occurrence of ECPs, particularly in developing countries, is severely restricted due to the prohibitive expense of analysis and lack of expertise. Fortunately, with the aid of screening methods, large sample sets can be analysed.

The analysis of ECPs is challenging for a number of reasons. Firstly, the concentration of these pollutant chemicals is extremely low and also there is a lot of possible isomers and analogues which may interfere with the target analyses. Hence, high-quality and stable nanomaterials with high purity are desirable for the development of sensitive and selective screening methods in this regard. Furthermore, the complexity of environmental matrices must be considered as an obstacle hindering the wide analysis of ECPs. As a result, stable nanomaterials such as quantum dots (QDs) with improved selectivity should be developed for the target analytes (Liu *et al.*, 2014).

1.2 Aims and objectives of the thesis

1.2.1 General aim of the thesis

The primary aim of this research was to develop fluorescence sensor materials based on nanomaterials, with particular reference to quantum dots and molecularly imprinted polymers, for the detection of two pharmaceutical and personal care products (PPCPs), namely, acetaminophen (AC) and triclosan (TCS).

1.2.2 Objectives

- i. To synthesize semiconductor core/shell quantum dots with different precursors that can be used for ligand exchange reaction.
- ii. To convert hydrophobic quantum dots to water soluble quantum dots via different thiol ligands including L-cysteine, N-acetyl-L-cysteine and glutathione.
- iii. Characterization of the synthesized water soluble core/shell quantum dots.
- iv. Optimisation of the optical properties and application of the resultant quantum dots in the detection of triclosan and acetaminophen in standard solutions and real water samples in the presence of potential interfering compounds.
- v. To entrap the synthesized L-cys-CdSe/ZnS QDs in a molecularly imprinted polymer (MIP) and fabricate MIP@QDs in order to improve the selectivity of the quantum dots towards acetaminophen.
- vi. Characterization of the resultant polymers.
- vii. Optimisation of the optical properties of the synthesized MIP@QDs to be applied for the determination of acetaminophen in standard solutions followed by real water samples in the presence of structurally related compounds.

1.3 Context of the thesis

Paper 1 focused on the worldwide concentration of triclosan in aquatic systems and its stability and toxicity. Moreover, various analytical techniques for the determination of triclosan in different environmental compartments were presented including chromatography-mass spectrometry, electrochemistry, capillary zone electrophoresis and spectrophotometry. The removal efficiencies of triclosan via wastewater treatment processes were then investigated in this paper. Further to this, green analytical chemistry together with future outlook are examined.

In **Paper 2**, analytical techniques for the determination of acetaminophen are reviewed, mainly chromatographic methods for the aquatic environment and voltammetric methods for

pharmaceuticals and biological fluids, as well as environmental samples. Further to this, spectroscopic and capillary electrophoresis approaches for the quantification of acetaminophen are summarized. Moreover, future perspectives regarding the utilization of new materials are highlighted.

Paper 3 described the synthesis and characterization of glutathione (GSH)-capped CdSe/ZnS QDs for application in the determination of triclosan in standard solutions, tap and river water samples. The paper investigated the optimum conditions for sensing, including QD concentration and incubation time for triclosan detection. In addition, a turn-on mechanism between QDs and triclosan was proposed. Selectivity of the developed sensor was then evaluated with similar structures to triclosan.

Paper 4 reported on testing three different water-soluble core/shell QDs with different capping agents of L-cysteine (L-cys), N-acetyl-L-cysteine (NAC) and glutathione (GSH) respectively, for the fluorescence detection of acetaminophen which is an environmental contaminant. This work utilised the one-pot approach to synthesize the thiol-capped QDs. L-cys-CdSe/ZnS QDs showed the highest sensitivity which were thus chosen as a turn-on probe for the determination of acetaminophen. Different characterization techniques were performed to confirm the passivation of the CdSe and CdSe/ZnS QDs with L-cysteine. Furthermore, this work fulfilled the applicability of the method for acetaminophen detection in standard solutions and real water samples in the presence of structurally related compounds.

In order to improve the selectivity of L-cysteine (L-cys)-capped CdSe/ZnS QD-AC system, which was developed in Paper 4, molecularly imprinted polymer capped quantum dots (MIP@QDs) were fabricated and characterized. Therefore, **Paper 5** was dedicated to the application of L-cys-CdSe/ZnS QDs entrapped in a molecularly imprinted polymer for the detection of acetaminophen in standard solutions and real water samples in the presence of potential interferences.

1.4 References

- Bolong, N., Ismail, A.F., Salim, M.R., & Matsuura, T. (2009). A review of the effects of emerging contaminants in wastewater and options for their removal. *Desalination*, 239(1-3), 229-246.
- Gavrilescu, M., Demnerová, K., Aamand, J., Agathos, S., & Fava, F. (2015). Emerging pollutants in the environment: present and future challenges in biomonitoring, ecological risks and bioremediation. *New Biotechnology*, 32(1), 147-156.
- Gomes, R.L., & Lester, J.N. (2003). *Endocrine disruptors in wastewater and sludge treatment processes*, Chapter 6, (pp. 177-218). Florida: CRC Press, Boca Raton.
- Liu, Q., Zhou, Q., & Jiang, G. (2014). Nanomaterials for analysis and monitoring of emerging chemical pollutants. *TrAC Trends in Analytical Chemistry*, 58, 10-22.
- Lovett, G.M., Burns, D.A., Driscoll, C.T., Jenkins, J.C., Mitchell, M.J., Rustad, L., Shanley, J.B., Likens, G.E., & Haeuber, R. (2007). Who needs environmental monitoring? *Frontiers in Ecology and the Environment*, 5(5), 253-260.
- Thomaidis, N.S., Asimakopoulos, A.G., & Bletsou, A. (2012). Emerging contaminants: a tutorial mini-review. *Global NEST Journal*, 14(1), 72-79.

Chapter 2 Introduction

This chapter provides a general overview of terms and definitions concerning semiconductor quantum dots and molecularly imprinted polymers. In addition, synthetic and surface ligand exchange reactions and polymerisation approaches for quantum dots and molecularly imprinted polymers together with the principal of sensing are reviewed. The synthesized quantum dots and molecularly imprinted polymers which were utilized are also highlighted. Furthermore, analytical tools for the characterization of quantum dots and molecularly imprinted polymers are described. Finally, toxicity of the two target analytes, namely triclosan and acetaminophen, which were quantified in this thesis are briefly presented.

2.1 Background

Emerging chemical pollutants (ECPs) comprise a wide spectrum of chemicals for which no legislative limits are currently in place, but which may have an impact on the environment and human health (Liu *et al.*, 2014). ECP compound classes include pesticides, polycyclic aromatic hydrocarbons (PAHs), pharmaceutical and personal care products (PPCPs), flame retardants, perfluorinated compounds (PFCs) and industrial additives (Liu *et al.*, 2014), as shown in Table 1. ECPs are of particular environmental concern as regulatory and/or standard analytical methods have yet to be developed for them and they may impact water quality, ecosystems and human health. Therefore, they have become a new area of concern in environmental science.

Generally, environmental monitoring is a process that involves the identification of selected variables of the environment and subsequently quantifying them (Gupta, 2011). Simple analytical probes are often utilized in environmental monitoring since they are cheaper, cater for on-site real time monitoring, and are easier to handle compared to laboratory measurements using conventional instruments. Different working mechanisms are adopted in these probes depending on the detection principle. Optical measurement methods have gained attention due to advantages including small size, high sensitivity, ease of implementation, and generally fast response times (Hung, 1982; Lee, 2003). Fluorescence measurement techniques are a popular subset of optical methods, which use a fluorophore material as a sensing receptor to detect a specific analyte. The type of fluorophore can be chosen from a vast selection of nanomaterials including carbon nanoparticles (CNPs), gold nanoparticles (AuNPs), magnetic nanoparticles and semiconductor quantum dots (QDs) (Liu *et al.*, 2014).

Table 1. Examples of emerging compound classes (Lopez de Alda *et al.*, 2003).

Compound class	Examples
Veterinary and human antibiotics	Trimethoprim, Erythromycine, Lincomycin, Sulfamethoxazole
Analgesics and anti-inflammatory drugs	Acetaminophen , Codeine, Ibuprofen, Acetylsalicylic acid, Diclofenac, Fenoprofen
Psychiatric drugs	Diazepam
Lipid regulators	Bezafibrate, Clofibrac acid, Fenofibrac acid
β -Blockers	Metoprolol, Propranolol, Timolol
X-ray contrasts	Iopromide, Iopamidol, Diatrizoate
Steroids and hormones (contraceptives)	Estradiol, Estrone, Estriol, Diethylstilbestrol
Personal care products:	
Fragrances	Nitro, polycyclic and macrocyclic musks
Sun-screen agents	Benzophenone, Methylbenzylidene camphor
Insect repellants	<i>N,N</i> -Diethyltoluamide
Antiseptics	Triclosan , Chlorophene
Surfactants and surfactant metabolites	Alkylphenol ethoxylates, Alkylphenols (nonylphenol and octylphenol), Alkylphenol carboxylates
Flame retardants	Polybrominated diphenyl ethers (PBDEs), Tris (2-chloroethyl)phosphate
Industrial additives and agents	Chelating agents (EDTA), Aromatic sulfonates
Gasoline additives	Dialkyl ethers, Methyl-t-butyl ether (MTBE)
Disinfection byproducts	Iodotrihalomethanes, Bromoacids, Bromoacetonitriles, Bromoaldehydes, Cyanoformaldehyde, Bromate
PAHs	Pyrene, Phenanthrene, Benzo[a]pyrene
Pesticides	Atrazine, Terbutylazine, Glyphosate

2.2 Quantum dots (QDs)

A quantum dot (QD) is a semiconductor nanocrystal with physical dimensions smaller than the exciton Bohr radius (Noh *et al.*, 2010). Quantum dots were first discovered by Alexey Ekimov in 1981 (Ekimov *et al.*, 1985; Ekimov *et al.*, 1982) in a glass matrix and then in colloidal solutions by Louis E. Brus in 1985 (Allwine *et al.*, 2002). The term "quantum dot" was coined by Mark Reed (Reed *et al.*, 1988).

In semiconductor QDs, the excitation of an electron from valence band to the conduction band leaves an orbital hole in the valence band. The photo-generated electron-hole pair is known as an exciton which upon recombination, can produce fluorescence emission of the QDs (Burda *et al.*, 2005). The presence of coordinative unsaturation can result in localized electronic states which are known as defect states or surface states. These states generate from the nature of the ligand or synthesis which determine fluorescence efficiency of the QDs (Murray *et al.*, 1993).

The cores are typically made from elements from group III and V (gallium arsenate (GaAs), indium arsenate (InAs), indium phosphate (InP), and gallium nitride (GaN) metalloid cores) or groups II-VI such as zinc sulfide (ZnS), cadmium-selenide (CdSe), zinc-selenide (ZnSe) and cadmium telluride (CdTe) (Hines *et al.*, 1996). These QD cores are small enough to exhibit quantum mechanical properties due to confinement of the excitons in all three spatial dimensions. The electronic properties of these materials are intermediate between those of bulk semiconductors and of discrete molecules (Figure 1) (Brus, 2007; Murray *et al.*, 2000; Norris, 1995; Smith *et al.*, 2009).

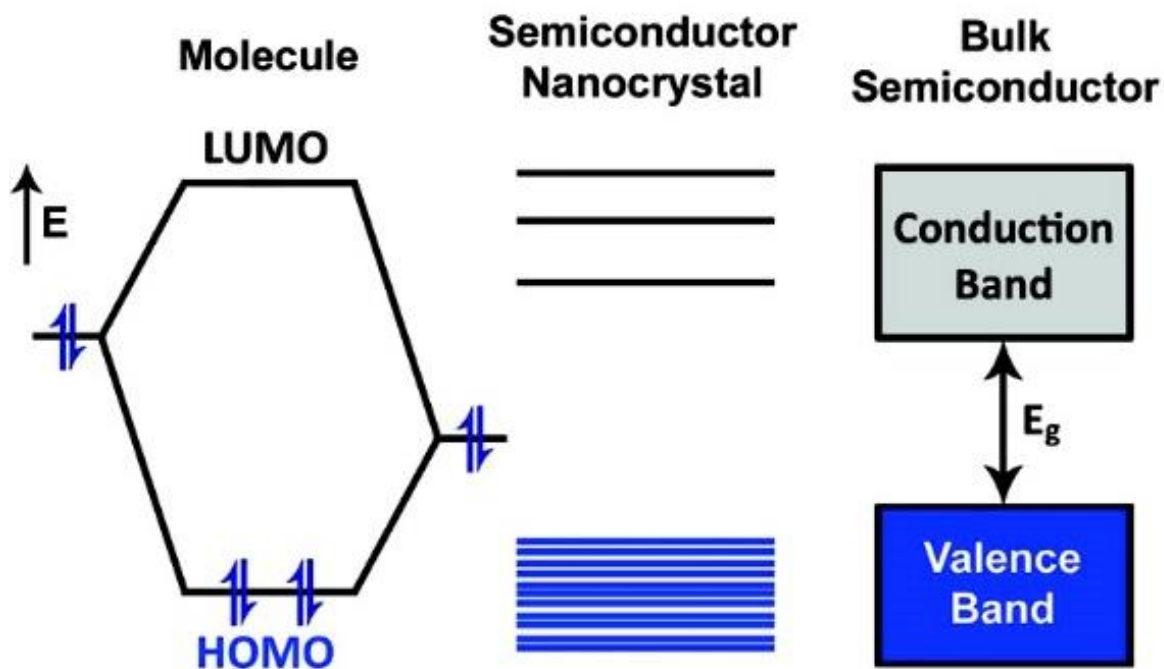


Figure 1. Electronic energy states of a semiconductor in the transition from discrete molecules to nanosized crystals and bulk crystals (Smith *et al.*, 2009).

QDs have unique chemical and physical properties which includes size-dependent fluorescence, high fluorescence quantum yields, independence of emission on the excitation wavelength, narrow spectral line widths, and stability against photobleaching (William *et al.*, 2006). Furthermore, because of their large surface to volume ratios, their surface activity, and their strong adsorption affinity to other nanoparticles, their utilization can be advantageous over larger particles. QDs have size-dependent optical properties, which means their absorption and emission properties can be tuned by changing the particle size, shape and surface structure (Zhang *et al.*, 2003). Figure 2 (a) illustrates how the emission wavelength of QDs varies with particle size.

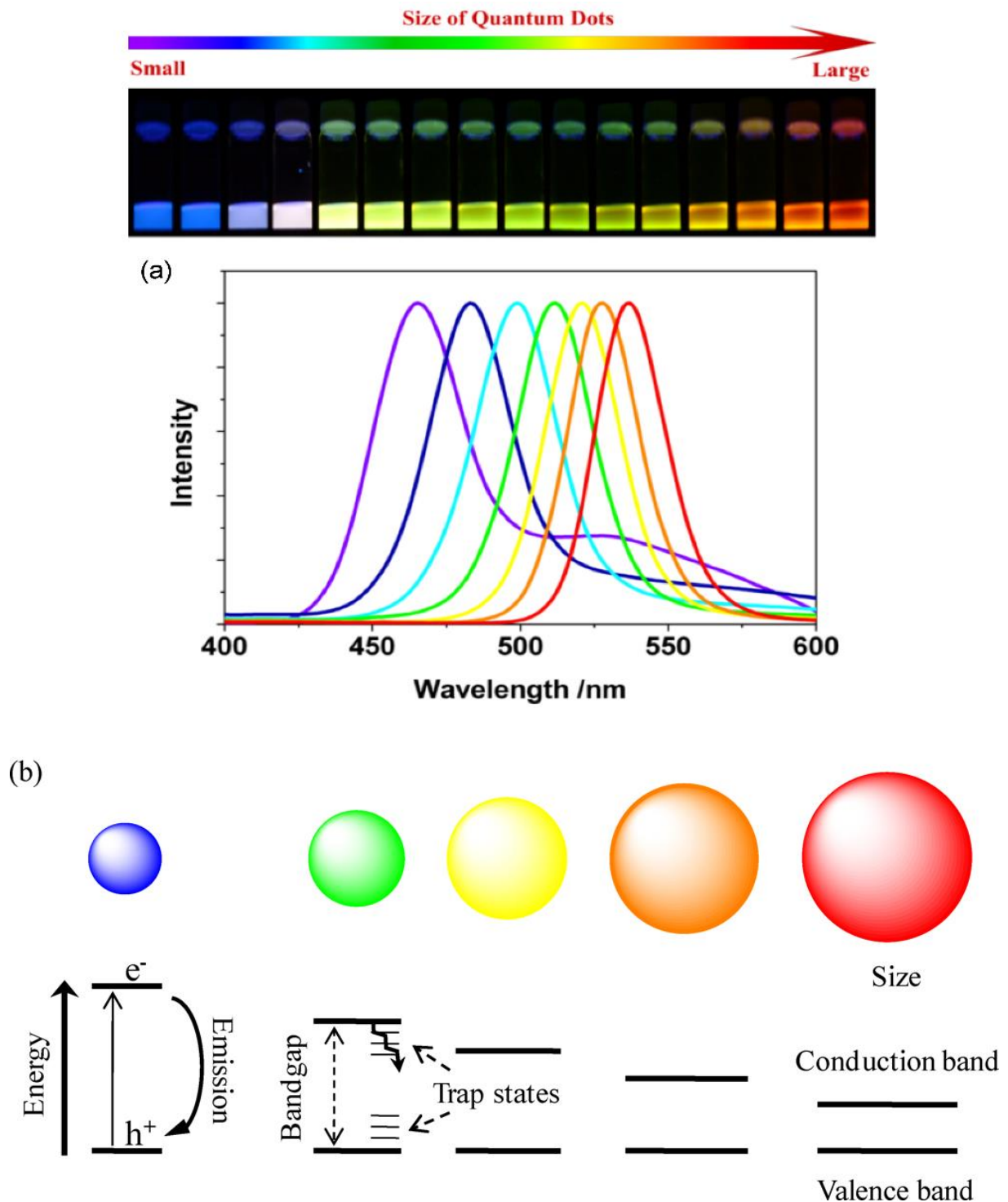


Figure 2. (a) Sixteen emission colors from small (blue) to large (red) QDs excited by a near-ultraviolet lamp; size of QDs can be from ~ 1 nm to ~ 10 nm. (b) Creation of an exciton upon photon absorption followed by fluorescence emission or relaxation through trap states (Bera *et al.*, 2010; Frasco *et al.*, 2009; Jaiswal *et al.*, 2003).

QDs possess intrinsic physicochemical properties that pertain to the combination of their crystalline metalloid core structure/composition and quantum-size confinement (Hardman, 2006). In addition, when the size of the exciton, indicated by the exciton Bohr radius, (r_{Bohr}

(~ 1-5 nm)), exceeds the physical size of the semiconductor nanocrystal (D), the quantum confinement effect of QDs occurs which provides size-dependent emission (Wilson *et al.*, 1993). Semiconductor nanocrystals exhibit particularly interesting properties when the exciton is strongly confined ($D < 2 \text{ rBohr}$) (Martienssen *et al.*, 2005). Moreover, QDs are photo electrochemically active and they have potential to be applied in (photo) electrochemical sensors (Gill *et al.*, 2008). These properties enable the use of QDs as reliable optical labels in environmental analysis.

When an electron absorbs a photon with an energy greater than the band gap energy of the material, it is excited from the valence band to the conduction band and an orbital hole is formed in the valence band. When the electron relaxes back to the valence band to recombine with the hole, a photon is emitted which has an energy proportional to the band gap of the material. This mechanism shows why QDs can absorb all wavelengths more than their band gap and then emit specific wavelength (Smyder *et al.*, 2011). The influence of the QD surface on photoluminescence can be described by "trap states" which can be caused by surface defects such as local lattice mismatches, atomic vacancies, dangling bonds or adsorbates at the surface (Figure 2 (b)). When electron and hole recombine, it is likely that the presence of trap states trap either the electron or the hole resulting in nonradiative recombination (Murphy, 2002).

QD-based sensors have gained great popularity in different scientific areas such as medicine, agriculture, food safety, biology and environmental protection (Stanisavljevic *et al.*, 2015).

2.3 Core/shell nanoparticles

The concept of a multilayer semiconductor particle was first developed by Eychmüller *et al.* (Eychmüller *et al.*, 1993). The terminology "core/shell" (Zhou *et al.*, 1994) was established when researchers realized that heterogeneous composite or sandwich colloidal semiconductor particles have better efficiency compared to their corresponding single semiconductor particles (Youn *et al.*, 1988). They can be widely defined as a core (inner material) and a shell (outer layer material) (Ghosh Chaudhuri *et al.*, 2012) which comprise of a wide range of different combinations in close interaction (Figure 3). The purpose of the coating on the core particle is manifold, such as controlled release of the core, the ability to increase the dispersibility functionality and stability, surface modification and reduction in consumption of precious materials, and so forth (Ghosh Chaudhuri *et al.*, 2012). The spectroscopic characterization of the core/shell particles shows that with increasing shell thickness the intensity of the UV absorbance increases and the reflectance shifts towards the higher wavelength region (Ye *et al.*, 2008). Due to the shell material coating, the properties of

the core particle, such as reactivity, decreases or the thermal stability can be modified. Therefore the overall particle dispersibility and stability of the core particle increases.

Inorganic/inorganic core/shell nanoparticles are the most prominent class of core/shell nanoparticles. These types of particles are broadly applied for the improvement of semiconductor efficiency, optical bio-imaging, biological labelling, catalysis, optoelectronics and information storage. The distinct advantages of multilayer semiconductor nanoparticles are improved optical properties, higher quantum yield, increased half-life times, higher photoluminescence efficiency and easy detection of emission spectra, because they are shifted towards longer wavelengths in the visible range. Moreover, due to their improved electronic properties (band gap and band alignment), they possess better structural (lattice mismatch) properties than core QDs. More importantly, an inorganic shell is added to the surface of QDs in order to reduce surface defects which arise from coordinative unsaturation (Galian *et al.*, 2009).

It is important to point out that the term lattice mismatch refers to “the situation where two materials having different lattice constants are brought together by deposition of one material on top of another”. The advantage of lattice mismatch between the core and shell material is that the shell can grow to a significant thickness without losing its luminescence properties (Ghosh Chaudhuri *et al.*, 2012).

In order to render synthesized core/shell QDs water soluble, they can be functionalized or given secondary coatings to improve QD core durability, water solubility and suspension characteristics. Functionalization may be conducted via covalent bonding, electrostatic interactions, adsorption or multivalent chelation (Hardman, 2006).

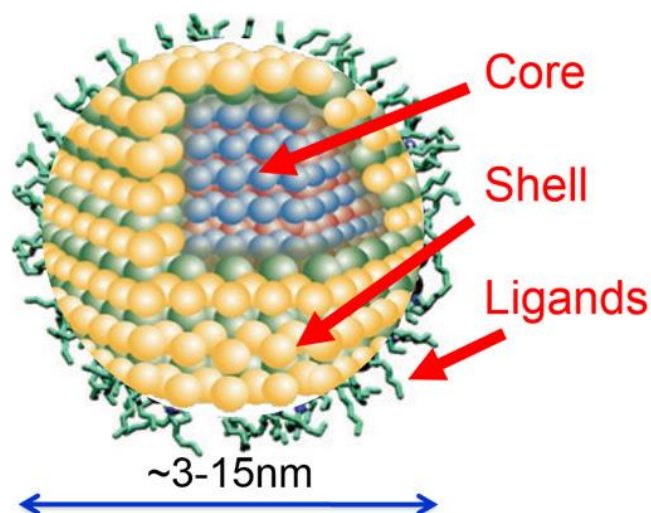


Figure 3. The structure of a quantum dot showing its three main features: core, shell and ligands (Greenwood, 2007).

2.4 Toxicity considerations

Despite the important properties of QDs and their invaluable social benefits such as drug targeting and *in vivo* biomedical imaging (Gao *et al.*, 2004; Michalet *et al.*, 2005), their potential toxicity has restricted their application. QD toxicity depends on multiple factors resulting from individual QD physicochemical properties and environmental conditions including outer coating bioactivity (capping material and functional groups), concentration, QD size, charge, mechanical stability, as well as oxidative and photolytic stabilities (Hardman, 2006). They may also pose a threat to the environment and human health, due to their very small size and strong adsorption ability, they can penetrate through the skin and result in significant adverse health effects (Liu *et al.*, 2014). Therefore, it is critically important to develop a stable sensor from which the chemical components do not leach. The main concern for their toxicity is the release of heavy metals (e.g. Cd^{2+}) from the core of QDs (Chen *et al.*, 2012), due to the fact that the cores of QDs are mostly synthesized from heavy metals. However, stabilization of the core QD with an inorganic shell such as ZnS and also surface coating with a capping agent (e.g. mercaptoacetic acid (MPA), L-cysteine or glutathione (GSH)) can reduce ion leakage thereby reducing toxicity in use (Tiwari *et al.*, 2011; Zhang *et al.*, 2006) and additionally protect the core from air oxidation (Su *et al.*, 2009).

As reported in Nsibandé *et al.*, (2016), studies have been done to investigate the toxicity of different QDs in different living systems like cell cultures and mice (Valizadeh *et al.*, 2012). It has thus been shown that passivating the core with nontoxic shell layers greatly reduces leakage of cadmium, thereby reducing potential toxic effects. For example, Kuzyniak *et al.*, (2014) spiked living cells with increasing concentrations of CdSe and the release of a cytoplasmic enzyme (LDH) was used as a measure of toxicity. Their study showed that capping the QDs with the ligand glutathione (GSH) and encapsulating with a nontoxic ZnS shell to form GSH-CdSe/ZnS nanoparticles, greatly reduced the toxicity of QDs in the living cells.

2.5 Synthesis of QDs

QD synthesis was first achieved by precipitation from a solution containing the metal ion such as Cd, Zn, Hg, In, Ag or Pb by addition of a hydroxide solution of Se, S or Te. Homogeneity, surface structure, shape and size of the QDs may be controlled to prepare QDs with unique properties (Farkhani *et al.*, 2014). Two approaches have been employed to synthesize crystalline QD nanoparticles.

2.5.1 Organometallic synthesis of QDs

This method was invented by Steigerwald *et al.* (Steigerwald *et al.*, 1990) and it is a widely used approach. It involves preparation of QDs in high-temperature organic solvents. The reaction mixture is comprised of three components: precursors, organic surfactants and solvents, although occasionally, surfactants can act as solvents (Yin *et al.*, 2005). Different sized QDs can be manufactured by changing the amount of precursors and growth time. An important part of synthesis is finding the appropriate precursor molecules to serve as organometallic reagents, as they are needed to decompose and produce reactive atomic or molecular species (monomers) that influence nanocrystal nucleation and growth. In the synthesis of chalcogenide QDs, cadmium precursors are organometallics (Hambrock *et al.*, 2001) like CdO or Cd(CH₃)₂ whereas Se, S and Te precursors are usually from elemental sources. The use of CdO as a Cd²⁺ source, for example, produces safer and more environmentally friendly procedure compared with Cd(CH₃)₂ (Peng *et al.*, 2001).

Organic solvents include trioctylphosphine oxide (TOPO) (Murray *et al.*, 1993), hexadecylamine (HDA) (Talpin *et al.*, 2004) and octadecene (Bullen *et al.*, 2004) which may be used at high temperature (200 – 400 °C). They are chemically bonded to the precursors by Van der Waals interactions. In this process, organometallic precursors in hot coordinating solvents are pyrolysed to produce monodispersed QDs with <5% size-distribution (Murray *et al.*, 2000). Reactive species known as monomers are manufactured by dissolving and decomposing precursors in the solvent. The best precursors contain "leaving groups" that quickly depart to leave the favourable reactive species (Yin *et al.*, 2005).

Two phenomena should occur in this procedure: (i) decomposition or reaction of precursors at high temperature to generate a supersaturated solution of monomer followed by a burst of nucleation of nanocrystals, and (ii) the growth of nuclei from molecular precursors. The reaction typically is performed under an inert gas such as Ar since some nanocrystals are sensitive to air and also reactant molecules may be pyrophoric (Farkhani *et al.*, 2014). Organometallic precursors produce CdSe, CdS or CdTe QDs but they have a low quantum yield (QY) (<10%) and the bare QDs can be easily oxidised which results in the release of toxic ions. These QDs must therefore be passivated or covered with a shell of a higher band-gap material such as ZnS, which is grown epitaxially (ordered growth on top of the crystallite substrate) around the core to eliminate all energy levels inside the gap and to increase the QY by removing surface trap sites and confining the exciton (electron-hole pair) (Galian *et al.*, 2009; Pong *et al.*, 2008). It is important to point out that photostability and biocompatibility have been dramatically improved via epitaxial growth (Hines *et al.*, 1996; Li *et al.*, 2003).

The high reaction temperature for the synthesis of QDs has considerable advantages: it can facilitate the removal of crystalline defects and allow photoluminescence improvement (Cingarapu *et al.*, 2012). Moreover, QDs synthesized by this method have high quantum yields and size distribution can be easily controlled by changing the reaction time (Bakar *et al.*, 2008) and temperature. More importantly, QDs with a narrower particle size distribution can be manufactured (Gaponik *et al.*, 2002). These QDs comprise of 100 to 100,000 atoms within the volume of the QDs with a diameter of 10-50 atoms which corresponds to 2-10 nm. Hence, approximately 3 million QDs could be lined up end to end in 10 nm diameter and fit within the width of a human thumb (Modani *et al.*, 2013; Pandurangan *et al.*, 2012).

2.5.1.1 *Water-solubilisation of QDs*

QDs synthesized by organometallic methods are soluble in non-polar organic solvents (Smith *et al.*, 2008). Hence, they must be modified to be soluble in water and be compatible with environmental analysis. Three strategies have been established for this purpose: (i) ligand exchange by replacing the hydrophobic ligands with new ligands containing thiol groups and aminated polymers; and (ii) the surface can be modified by encapsulation within block polymer shells and (iii) phospholipid micelles. In encapsulation, amphiphilic molecules (Smith *et al.*, 2008) have been utilized such as β -cyclodextrine and polymer microspheres (Cassette *et al.*, 2013; Mattoussi *et al.*, 2012).

2.5.2 **Wet chemistry**

The application of direct aqueous synthesis of QDs such as CdSe (Rogach *et al.*, 1999) and CdTe (Gaponik *et al.*, 2002) by utilization of thiol groups as stabilizers can provide an alternative route instead of using high boiling organic solvents. In this procedure, exchange processes are needed and the ligands which are used during the synthesis become surface ligands (Zhang *et al.*, 2011). In aqueous routes, first a metal salt and a thiol compound are dissolved in water and heating of the reaction mixture allows particle growth to commence, similar to organometallic synthesis (Eychmüller *et al.*, 2000).

2.6. **Comparison of aqueous and organometallic synthetic approaches**

In spite of the fact that the wet chemistry approach is environmentally friendly and cheap, it is suitable for large-scale synthesis (Li *et al.*, 2011), some serious drawbacks have restricted the use of these QDs. First, they are apt to degradation and aggregation in solution because of weakly bound thiol ligands. Secondly, they suffer from relatively poor photostability (Law *et*

al., 2009). In addition, the salt tolerance of prepared QDs in the aqueous phase is lower than QDs prepared in an organic phase (Liu *et al.*, 2010). Therefore, the organometallic route is preferable and was applied in this work to synthesis the QDs due to the following reasons (Bakar *et al.*, 2008; Farkhani *et al.*, 2014; Gaponik *et al.*, 2002):

- i. Synthesized QDs by this method possess a high degree of crystallinity.
- ii. QDs have high photoluminescence quantum yield (PLQY).
- iii. Particle size distribution of QDs can be well controlled by reaction time and temperature.
- iv. It is feasible to synthesis QDs with narrower particle size distribution.

2.7 Characterization techniques

2.7.1 Ultraviolet-visible absorption spectroscopy (UV/Vis)

A UV-Vis spectrophotometer is a very straightforward device which can be used for quantification of different samples. It also provides quick and easy analysis. The best solvents for UV/Vis should be transparent in a particular region and those that do not have absorption at the measuring wavelength in order not to interfere with the quantitative analysis of the sample.

In this study, UV-Vis spectra were recorded in a quartz cuvette with 1 cm path length in the range of 200 nm to 800 nm with a bandwidth of 1.0 nm using a Cary Eclipse (Varian) spectrophotometer. Millipore water was used as blank and all QDs were dissolved in it. All measurements were carried out at room temperature. In order to measure PLQY, the absorbance of the QDs was set in the range of 0.02-0.05 (Lakowicz, 1999).

The average size of the QDs can be estimated by an empirical formula (Yu *et al.*, 2003) which is shown in Eq. 1.

$$D = (1.6122 \times 10^{-9})\lambda_1^4 - (2.6575 \times 10^{-6})\lambda_1^3 + (1.6242 \times 10^{-3})\lambda_1^2 - (0.4277)\lambda_1 + (41.57) \quad \text{Eq. 1}$$

Where D (nm) is the size of the QDs, and λ_1 (nm) is the wavelength of the first excitonic absorption peak of the corresponding sample.

The extinction coefficient of the synthesized QDs can be obtained by Eq. 2 or Eq. 3 (Yu *et al.*, 2003), where D is the diameter or size of the QDs and ΔE is the energy of the first excitonic peak in units of eV and ϵ is the extinction coefficient per mole of the QDs ($\text{L mol}^{-1} \text{ cm}^{-1}$).

$$\varepsilon = 5857 (D)^{2.65} \quad \text{Eq. 2}$$

$$\varepsilon = 1600 \Delta E (D)^3 \quad \text{Eq. 3}$$

If the absorption spectrum is obtained for a low-concentration sample to avoid reabsorption, and the distribution of the nanoparticle diameters is not broad, the concentration of the QDs in the solution can be directly found from the Beer-Lambert-equation (Eq. 4) (Yu *et al.*, 2003).

$$A = \varepsilon CL \quad \text{Eq. 4}$$

Here, A is the intensity of the absorbance, ε is the extinction coefficient per mole of the QDs ($\text{L mol}^{-1} \text{ cm}^{-1}$), C is the molar concentration (mol L^{-1}) of the QDs, L is the path length (cm) of the radiation beam used for recording the absorption spectrum, which was fixed at 1 cm in our research experiments.

2.7.2 Fluorescence spectroscopy

Generally, spectrofluorimetry is more sensitive than spectrophotometry since the intensity of fluorescence can be measured by emission spectroscopy whereas, absorption spectroscopy measures the ratio of the intensity of two beams. Therefore, the fluorescence signal is proportional to the intensity of excitation source (Skoog *et al.*, 2017). The emission spectra were recorded at different excitation wavelengths by a Horiba Jobin Yvon Fluoromax-4 spectrofluorometer using a 1 cm path quartz cuvette. The full width at half maxima (FWHM) and photostability of the QDs were also measured by a spectrofluorometer.

Some information regarding the emission wavelength, size distribution, presence of surface traps, and the bandgap energy value of the QDs can be gathered from fluorescence spectrum (Lakowicz, 1999). The emission band gap energy values of the QDs can be estimated according to Eq. 5.

$$E = \frac{h*c}{\lambda_{max}} \quad \text{Eq. 5}$$

Where E is band gap energy, h is Planks constant (6.63×10^{-34} J.s), c is the speed of light (3.0×10^8 m s⁻¹) and λ is the max emission wavelength (m).

The influence of the ligand exchange on the optical properties of QDs can be scrutinized using spectroscopic techniques. Moreover, any changes in the ligand environment or solvent

composition are accompanied by spectral shifts in the absorption and emission spectra of QDs which are traceable by spectroscopic methods.

2.7.3 Powder X-ray diffraction (XRD)

XRD is a non-destructive analytical technique which can provide a unique fingerprint of Bragg reflection relating to the crystalline structure as well as chemical composition and physical properties of materials. This technique can also be applied for the characterization of nanomaterials (Sharma *et al.*, 2012). Powder X-ray diffraction (XRD) patterns were analysed using a PANalytical X'Pert Pro powder diffractometer in θ - θ configuration with a X'Celerator detector, variable divergence and receiving slits with Fe filtered Co-K α radiation ($\lambda=1.789\text{\AA}$).

Bragg's law can relate the wavelength of reflected X-ray (λ) to the angle of diffraction (θ) and the space of atomic planes (d) which is shown in Eq. 6. For the first order diffraction, $n=1$.

$$2d \sin \theta = n\lambda \quad \text{Eq. 6}$$

The average size of crystallites can also be measured by Scherrer formula (Eq. 7).

$$D = \frac{K\lambda}{\beta \cos \theta} \quad \text{Eq. 7}$$

Here, λ is the wavelength of the radiation, β is the full width at maxima of reflection peak, θ is the angle corresponding to the peak and K is the Scherrer constant which is equal to 0.9 (Jensen *et al.*, 2006).

Semiconductor materials from group II-VI and III-V, including ZnS, crystallize in the form of either hexagonal wurtzite or cubic zinc blende (Figure 4) (Rogach, 2008). The zinc blende structure is more thermodynamically favoured. However, because of the slow construction of wurtzite structures, both forms of ZnS can be found (Ma *et al.*, 2003; Yu *et al.*, 2002). They have 1:1 stoichiometry ratio of zinc to sulphur. Wurtzite has a hexagonal structure, while zinc blende is cubic. The difference between wurtzite and zinc blende lies in the different arrangements of layers of ions (Huheey *et al.*, 1993).

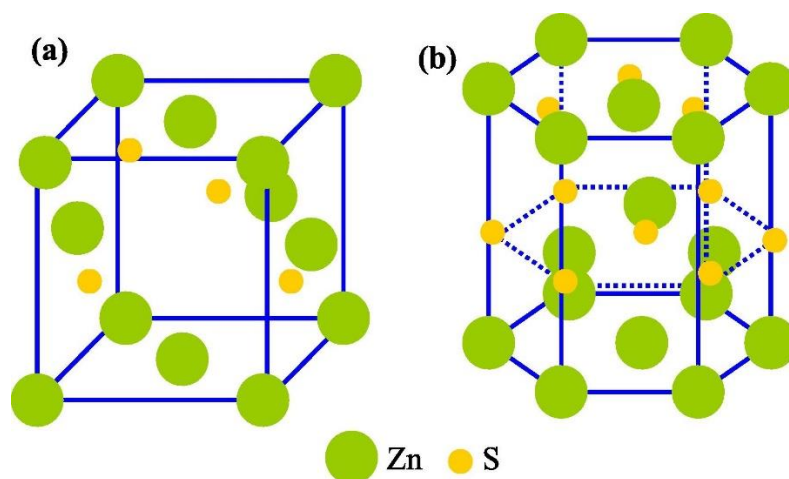


Figure 4. (a) Zinc blende and (b) wurtzite crystal structures of ZnS (Moore *et al.*, 2006).

2.7.4 Fourier-transform infrared spectroscopy analysis (FT-IR)

FTIR spectra were recorded using a Spectrum RXI FT-IR System from Perkin Elmer in the range of 4000-400 cm^{-1} . FTIR can be used to determine the structures of molecules by changing the dipole moment of molecules. A KBr pellet was used as the background and also to prepare the samples for FTIR measurements because this alkali halide is transparent and has a larger transmission window in the infrared region. KBr is also able to eliminate moisture of the samples.

2.7.5 High resolution transmission electron microscopy analysis (HRTEM)

HRTEM analysis was employed to determine the size and shape of the QDs, the synthesized MIP@QDs and NIP@QDs. This tool is very time-intensive and due to the small analyzed area, it can only provide qualitative information (Ray *et al.*, 2003). Two different concentrations were prepared in Millipore water for spotting of the samples. A drop of each sample was mounted onto a holey carbon support film followed by drying under ambient atmosphere. The grids were examined with a JEOL JEM 2100F TEM operated at 200 kV. ImageJ software was also utilized to determine the estimated particle size distribution (<http://imagej.nih.gov/ij/>, U.S. National Institutes of Health (NIH), Bethesda, Maryland, USA).

2.7.6 High resolution scanning electron microscopy analysis (HRSEM)

HRSEM can produce information about morphology, topography, crystallographic nature and composition of analyzed materials. Although electron and optical microscopes enjoy the same principles, HRSEM analysis can outweigh the limitation of optical microscopy such as providing chemical composition information. Sample preparation is the most important step for accurate analysis and the sample must be electrically conductive otherwise the surface of

the sample must be covered by a very thin layer of carbon or gold or gold/palladium alloy or platinum thin film (Girão *et al.*, 2017). HRSEM measurements were carried out using an FE-SEM Zeiss Ultra Plus in this research study.

2.7.7 Raman analysis

This characterization tool is employed in order to describe bulk homogenous materials and nano-sized crystals with a structural disorder at nanoscale like nanocomposites, nanoceramics and glassy materials. Raman spectroscopy is also non-destructive characterization method which can be used for probing and mapping of nanophases dispersed in a matrix (Gouadec *et al.*, 2007). Raman spectra were taken using a WITec Alpha 300 micro-Raman imaging system with 488 nm excitation laser and CCD detector at room temperature with laser power below 2 mW in order to minimize heating effects.

2.7.8 Energy-dispersive X-ray spectroscopy analysis (EDS)

X-rays are high energetic photons which are associated with the electronic transitions of atoms by the incident accelerated electron beam. Analytical X-rays enable qualitative and semi-quantitative analysis of the specimens which can be used for identification of existing constituent and the amount of each element. The combination of SEM or TEM with EDS is an indispensable tool in the characterization of micro- and nanomaterials. Moreover, a minimum amount of sample is required for analysis. Thus, characterization of several polymers with different sizes and morphology present in the same trial is feasible (Girão *et al.*, 2017). For accurate analysis in SEM-EDS, the sample needs to be polished to a flat surface. Therefore, the samples are embedded in a resin followed by polishing with silicon carbide paper with different grids until the surface of the specimen is exposed (Girão *et al.*, 2017). Energy dispersive X-ray spectroscopy analysis of the synthesized QDs was performed using a HRSEM integrated EDS Zeiss Crossbeam 540 with software AZtech version 3 by Oxford Instruments, while HRTEM integrated EDS (Oxford INCAx-sight, 20 keV range and 150 s acquisition) was utilized for the characterization of the polymers.

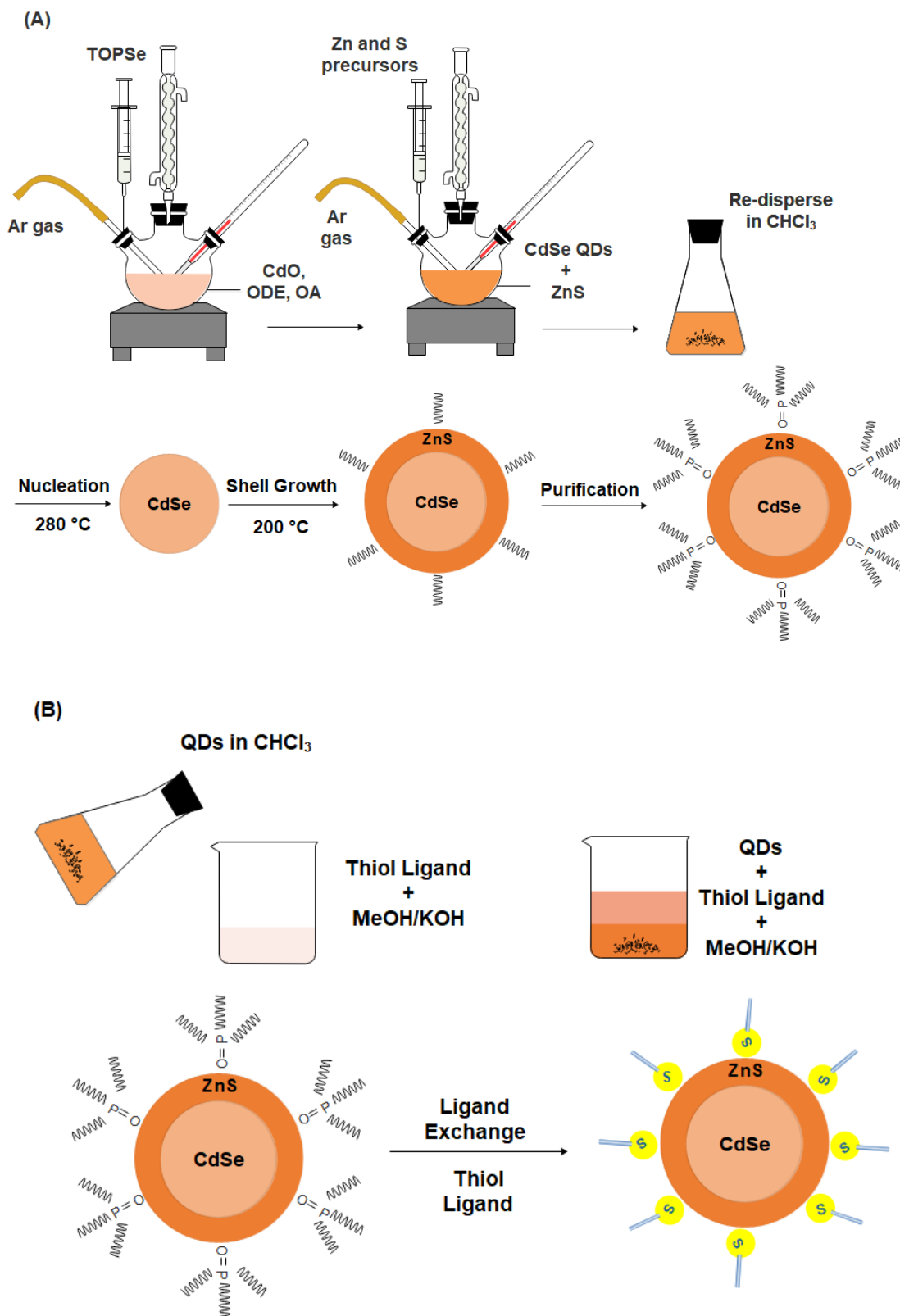
2.7.9 Thermogravimetric analysis (TGA)

Thermal analysis (TA) is a practical tool to gain in-depth insight into the structure of materials including polymer nanocomposites, even at nanoscale. TGA has been widely utilized to investigate thermal stability and degradation of the polymers (Corcione *et al.*, 2012). In this study, thermal analysis was carried out for the synthesized polymers using a TA Instruments SDT Q600 thermogravimetric analyzer (TGA) using a heating rate of 10 °C min⁻¹ from 25 to 1200 °C, under nitrogen atmosphere at a rate of 100 mL min⁻¹. 5.0 mg of the polymers was weighed out and placed into an alumina pan for TGA analysis.

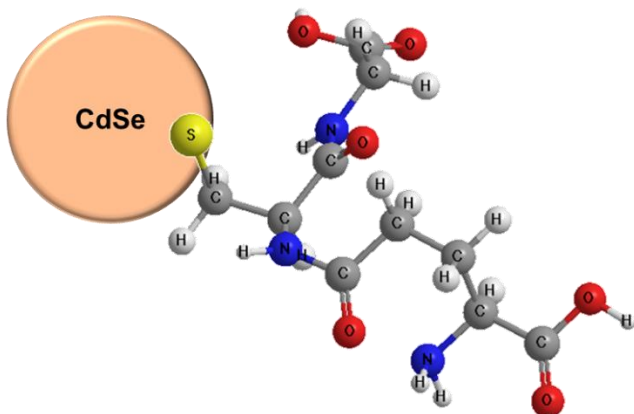
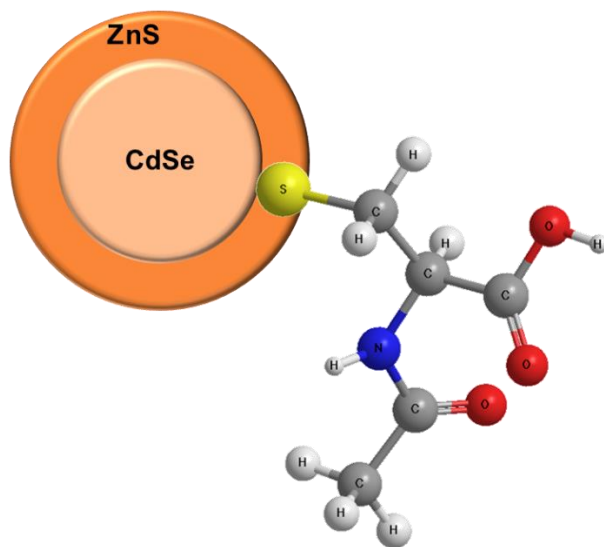
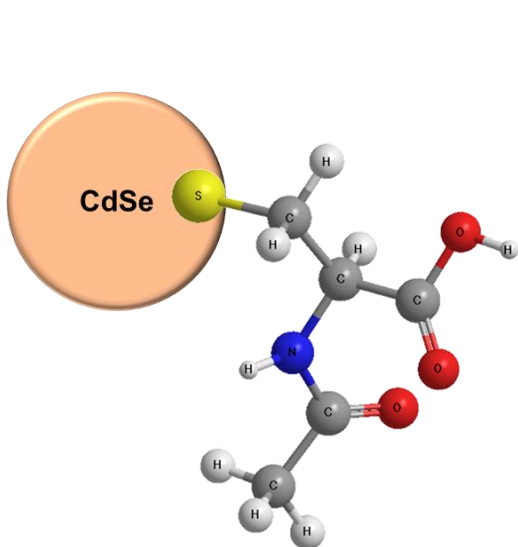
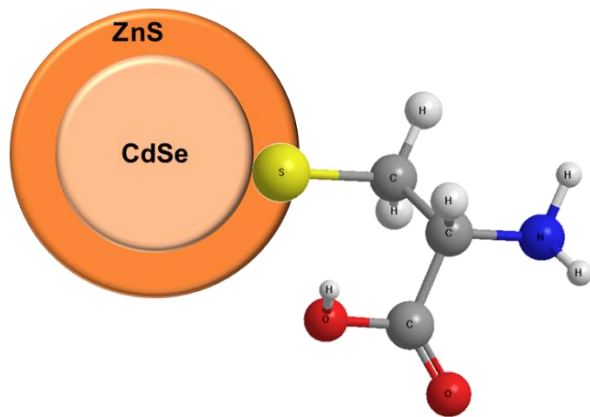
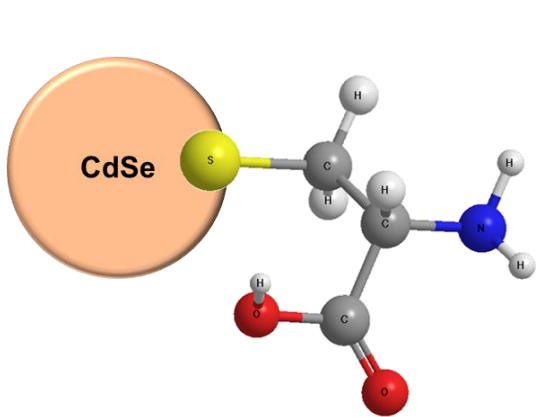
2.8 QDs utilized in this work

In this work, cadmium-based QDs were employed since they are highly functional materials with modifiable properties for various applications. Furthermore, they have shown high fluorescence quantum yields and stability. A one pot organometallic approach (Scheme 1 A) with some modifications was selected to synthesise core and core/shell QDs as this method provides more stable QDs compared to the wet chemistry approach. The core in this work was CdSe which was over-coated with ZnS to prepare CdSe/ZnS core/shell QDs. Ligand exchange reactions (Scheme 1 B) with different thiol capping agents, including L-cysteine (L-cys), N-acetyl-L-cysteine (NAC) and glutathione (GSH), were then performed to make the hydrophobic core and core/shell QDs water dispersible for use in water testing (Figure 5 A-E). It is important to emphasize that n-alkyl amines (thiol derivatives) produce great affinity towards the surface of QDs compared to the addition of a silica layer because they contain a thiol moiety with high affinity to the surface of QDs, an alkyl chain and another functional group of carboxylate moiety. In addition, different properties like capping density electron donation, chain length and stereochemical effect play a pivotal role in the fluorescence properties of QDs (Galian *et al.*, 2009).

Three core/shell QD-ligand systems namely L-cys-CdSe/ZnS QDs (Figure 5 D), NAC-CdSe/ZnS QDs (Figure 5 E) and GSH-CdSe/ZnS QDs (Figure 5 F) were tested as fluorescence probes for the determination of AC while NAC-CdSe/ZnS QDs and GSH-CdSe/ZnS QDs were compared for the determination of TCS. With respect to sensitivity, L-cys-CdSe/ZnS QDs and GSH-CdSe/ZnS QDs showed higher sensitivity relative to NAC-CdSe/ZnS QDs towards AC and TCS, respectively. Therefore, L-cys-CdSe/ZnS QDs were chosen for further analysis of AC and GSH-CdSe/ZnS QDs for TCS detection. The synthesized core and core/shell QDs which were utilized in this work are shown under UV irradiation in Figure 6.



Scheme 1. Schematic of the synthesis of (A) QDs by the organometallic approach and (B) surface modification by thiol ligands.



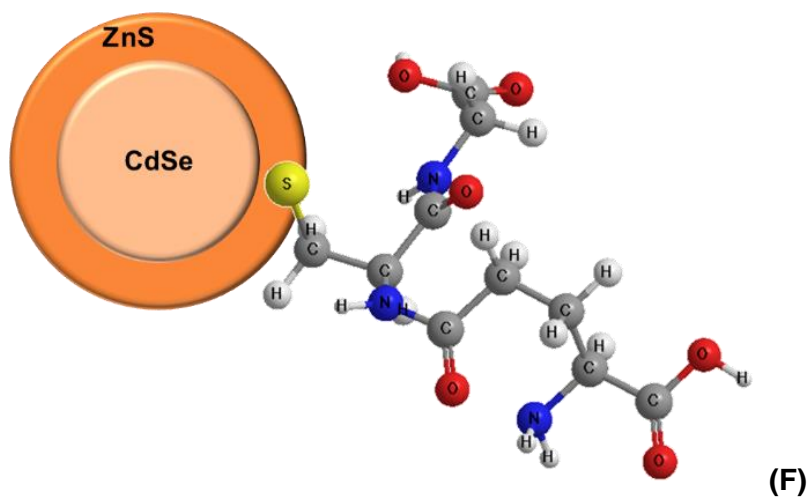


Figure 5. QDs utilized in this work: (A) L-cys-CdSe QDs, (B) NAC-CdSe QDs, (C) GSH-CdSe QDs, (D) L-cys-CdSe/ZnS QDs, (E) NAC-CdSe/ZnS QDs, (F) GSH-CdSe/ZnS QDs.

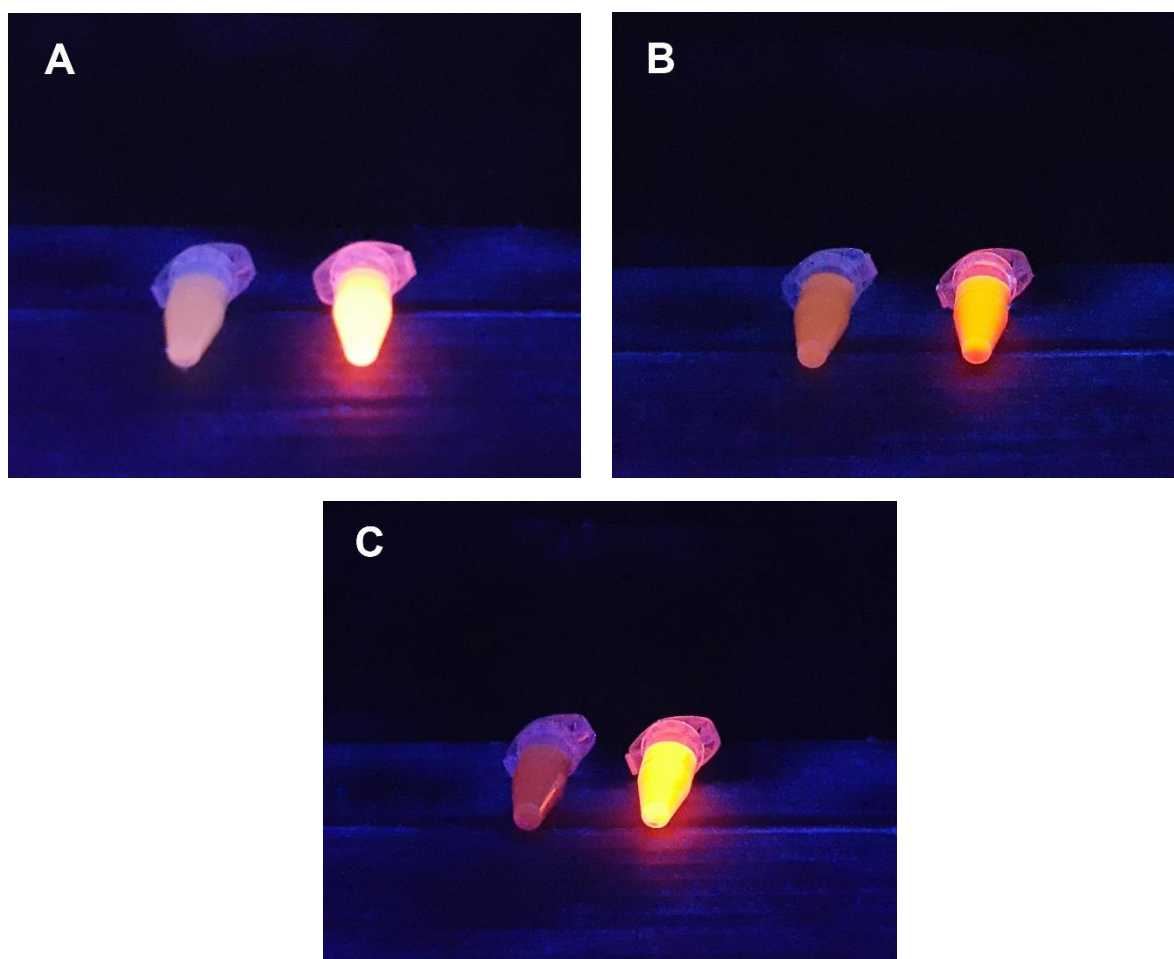


Figure 6. Synthesized QDs under UV irradiation with an excitation wavelength 365 nm, (A) L-cys-CdSe QDs (left), L-cys-CdSe/ZnS QDs (right); (B) NAC-CdSe QDs (left), NAC-CdSe/ZnS QDs (right); (C) GSH-CdSe QDs (left), GSH-CdSe/ZnS QDs (right).

2.9 Application of CdSe/ZnS QDs in fluorescence sensing

With respect to obtaining high quality semiconductor QDs suitable for a wide range of chemical and biological applications, the hot-injection organometallic synthetic route is the most effective. The reason is due to the flexibility involved in tuning the optical properties of the QDs to eliminate as much as possible the presence of surface defects that diminishes the optical properties of the QDs. Amongst the classes of conventional Cd-based QDs, CdSe/ZnS core/shell QDs are the most popular, due to their better optical properties than the parent core and their low toxicity in the presence of the non-toxic ZnS shell layer. They have been synthesized at high temperature in organic media and stabilized with hydrophobic capping agents including trioctylphosphine oxide (TOPO) and oleic acid (OA) (Scheme 1 A) (Dabbousi *et al.*, 1997; Hines *et al.*, 1996; Sapsford *et al.*, 2006b; Xie *et al.*, 2005).

A mixture of trioctylphosphine and trioctylphosphine oxide (TOP/TOPO) is the typical ligand system for most of the semiconductor QDs made from elements of groups II-VI and III-V such as CdSe and InP (Micic *et al.*, 1994; Murray *et al.*, 1993). These ligands not only provide all important solubility in common organic solvents such as hexane and toluene, but also they serve as agents for reducing the unwanted electronic defects associated with dangling bonds or surface defect states. Oleic acid-capped CdSe/ZnS QDs can be suspended in many non-polar solvents such as chloroform, hexane, toluene and dichloromethane.

As these QDs have no tendency to be soluble in aqueous media, three main techniques have been promoted to alter the surface of the QDs to enhance their water solubility. The first and most successful method for surface modification is ligand-exchange reactions to replace TOPO or OA with hetero-bi-functional ligands such as thiol terminated ligands and mercapto-carbonic acids, in which the mercapto or thiol end binds onto the QDs surface while the carboxyl moiety establishes water solubility (Chan *et al.*, 2002; Chan *et al.*, 1998). Pong *et al.* (2008) reported that free thiols are not capable of binding onto the ZnS surface. So, in order to enhance the reactivity of the thiol, the mixture must be dehydrogenated at the thiolic sulfur in basic environments (e.g. MeOH/KOH) which means that the bound state must be a thiolate.

In a second method, a cross-linked silica shell, which has been functionalized with polar groups, replaces the TOPO-shell (Bruchez *et al.*, 1998; Gerion *et al.*, 2001). The third approach refers to encapsulation of TOPO-capped QDs with amphiphilic copolymers or phospholipids (Pellegrino *et al.*, 2004; Wu *et al.*, 2003). Despite the fact that the silica shell or encapsulation by a polymer/phospholipid provide good water solubility and quantum yield, they significantly increase the QD particle size and shell thickness so they restrain the application of QDs in Förster resonance energy transfer (FRET) processes because of the limitation in terms of proximity of acceptor and QD core. Short-chain mercapto-carbonic

ligands are suitable for FRET and due to the thin barrier around the QDs they can be used in ion sensors based on fluorescence transduction changes (Chen *et al.*, 2002; Jin *et al.*, 2005).

As mentioned above, free thiols have no tendency to bind onto ZnS shells. Therefore, the reactivity of the thiol must be enhanced by removing the thiolic hydrogen. In an in-depth investigation by Pong *et al.* (2008), they showed that alkyl thiols cannot directly interact with the hexagonal wurtzite structure of the ZnS shell. So they improved procedures to functionalize CdSe/ZnS QDs with MPA and used mild reaction conditions (tetramethylammonium hydrogen) at room temperature to dehydrate thiolic hydrogen. Not only was the quantum yield of QDs increased, but also the colloidal stability was bolstered to four months. As a matter of fact, the bond strength of the Zn-S_{thiol} and S-S_{thiol} are 46.5 and 25.1 kcal mol⁻¹, respectively, which shows that the Zn-S bond is relatively strong while the S-S_{thiol} bond is weak which may have resulted in the low stability of thiol-ZnS sorption observed. The amount of thiol ligand for ligand exchange procedure was also investigated in this study, as it was found that it was crucially important to control the surface coverage of the ligands to preserve quantum yield.

It is worth noting that water molecules are responsible for quenching of the photoluminescence in aqueous media (Cordero *et al.*, 2000; Stsiapura *et al.*, 2006). As a result, the reactivity of the QDs can be preserved by removing thiolic hydrogen with a strong base medium because thiol ligands can make a compact coverage on the surface of the QDs to form a barrier against water molecules and to prevent the penetration of water molecules to the surface of the QDs. Moreover, as a ZnS shell may dissolve at low pH, the utilization of a strong base media can hinder the dissolution of the passivation of ZnS shell during the ligand exchange reaction (Pong *et al.*, 2008). A list of stabilizing agents, particle size, and precursors for the synthesis of CdSe/ZnS QDs reported in the literature and also target analytes which have been detected using these QDs are summarized in Table 2.

Table 2. List of the precursors, stabilizing agents and particle sizes for the synthesis of CdSe/ZnS QDs reported in the literature and target analytes which have been detected, where appropriate.

Particle size (nm)	Precursors ^a	Stabilizing agent	Target	Reference
1.2 ± 0.6	Me ₂ Cd, Se, TOPO, TOP, Me ₂ Zn, (TMS) ₂ S	-	NA	(Hines <i>et al.</i> , 1996)
2.3 – 5.5	CdMe ₂ , Se, TOPO, TOP, ZnEt ₂ , (TMS) ₂ S	-	NA	(Dabbousi <i>et al.</i> , 1997)
6 – 17 (Silica) 5 – 12 (MPA)	TOPO, MPS, APS, TMAH	Silica, MPA	NA	(Gerion <i>et al.</i> , 2001)
5 ± 0.2	Commercial	Histidine and <i>N</i> -acetyl-cysteine	NA	(Ai <i>et al.</i> , 2007)
<10	Cd(Ac) ₂ , HDA, TOPO, TOP, Se, Zinc ethylxanthate, TBP	MPA, ME, AEE, L-cys, cys-dipeptide	NA	(Murcia <i>et al.</i> , 2008)
-	CdO, TOPO, TOP, Se, ZnEt ₂ , (TMS) ₂ S	L-cysteine, D-cysteine	Carnitine enantiomers	(Carrillo-Carrion <i>et al.</i> , 2009)
5	CdO, Se, ODE, OA, S, ZnO, ODA	PMMA	Paeonol	(Dong <i>et al.</i> , 2011)
2.9 ± 0.3 5.6 ± 0.6	Commercial	Methyl ester <i>N</i> -acetyl-L-cysteine (CysP)	Aryl propionic acids, Ketoprofen, Naproxen, Flurbiprofen, Ibuprofen	(Delgado-Perez <i>et al.</i> , 2013)
~5.5	TOPO, cysteamine, DMAET, EDAC	L-cysteine, PEG then Ce6	NA	(Martynenko <i>et al.</i> , 2013)
10 – 12	CdO, ODE, OA, TOP, Se, Me ₂ Zn, (TMS) ₂ S	L-cys, TGA, MPA, MSA, MUA	NA	(Rahman <i>et al.</i> , 2014)
2 – 3.5	Se, NaBH ₄ , CdCl ₂ •2.5H ₂ O, L-cys, ZnCl ₂	GSH	Biomedical use on chicken embryo	(Kuzyniak <i>et al.</i> , 2014)
10	TOPO, HAD, TDPA, Cd(Ac) ₂ , TOP, Se, ODE, ZnO, OA, S powder	-	NA	(Gupta <i>et al.</i> , 2017)

^a The abbreviations are explained in the list of abbreviations.

NA: Not applicable (no application investigated).

2.10 Fluorescence quantum yield

One of the unique intrinsic properties of QDs is their high fluorescence quantum yield (PLQY) and molar extinction coefficient which is 10 to 100 times higher than that of organic dyes (Sapsford *et al.*, 2006a). PLQY relates the number of emitted photons to the number of absorbed photons. Larger PLQY approaching a value of one indicates bright emission and when more photons are emitted from the donor the better the energy transfer (Stanisavljevic *et al.*, 2015).

Fluorescence quantum yields (Φ_F) can be determined by the comparative method (Fery-Forgues *et al.*, 1999) (Eq. 8).

$$\Phi_F = \Phi_{F(Std)} \frac{F \cdot A_{Std} \cdot n^2}{F_{Std} \cdot A \cdot n_{Std}^2} \quad \text{Eq. 8}$$

Here F and F_{Std} represent the integrated fluorescence intensity of the QDs and the reference standard, whilst A and A_{Std} refer to the absorbance of the sample and reference standard at the excitation wavelength, respectively, and n and n_{Std} are the refractive indices of solvents used for the sample and standard.

For the determination of the PLQY of QDs in water ($n=1.333$) in this study, rhodamine 6G in ethanol ($\Phi_F=0.95$ and $n=1.36$) was employed as a standard (Kubin *et al.*, 1982; Lakowicz, 1999).

2.11 Principle of optical sensing using QDs

Interaction of analytes with the QDs, which takes place at the surface of the QDs, affects the efficiency of the radiative recombination inducing photoluminescence (PL) activation or quenching (Frasco *et al.*, 2010). In theory, Förster resonance energy transfer (FRET) is a non-radiative process and if the emission spectrum of the donor overlaps with the absorption spectrum of the acceptor, energy transfer from the donor to the acceptor could occur through long-range dipole-dipole interaction, leading to enhanced or quenched QD fluorescence signals which usually occurs at distances from 10 to 100 Å (Sapsford *et al.*, 2006a). The rate of energy transfer depends on the relative orientation of the transition dipoles, spectral overlap and most importantly the distance between donor and acceptor (Duong *et al.*, 2011).

Steady state FRET efficiency (Eff_{ss}) can be related to the donor-acceptor distance (r (Å)) by Eq. 9.

$$Eff_{ss} = \frac{R_0^6}{R_0^6 + r^6} \quad \text{Eq. 9}$$

Where r represents the center-to-center separation distance (Å) between the donor and the acceptor, R_0 is the Förster distance (Å), i.e. the distance between donor-acceptor molecules when the efficiency of energy transfer is 50% and depends on the quantum yield of the donor (Förster, 1959; Lakowicz, 1999). The PhotochemCAD software program (Du *et al.*, 1998) was used in this study for the calculation of FRET parameters which are shown in Appendix A. In this program, the relative orientation of the transition dipoles of the donor and acceptor was assumed to be $2/3$ because the donor-acceptor pairs were in a liquid medium and their dipole moments are deemed to be isotropically oriented during the excited state lifetimes (Chidawanyika *et al.*, 2010).

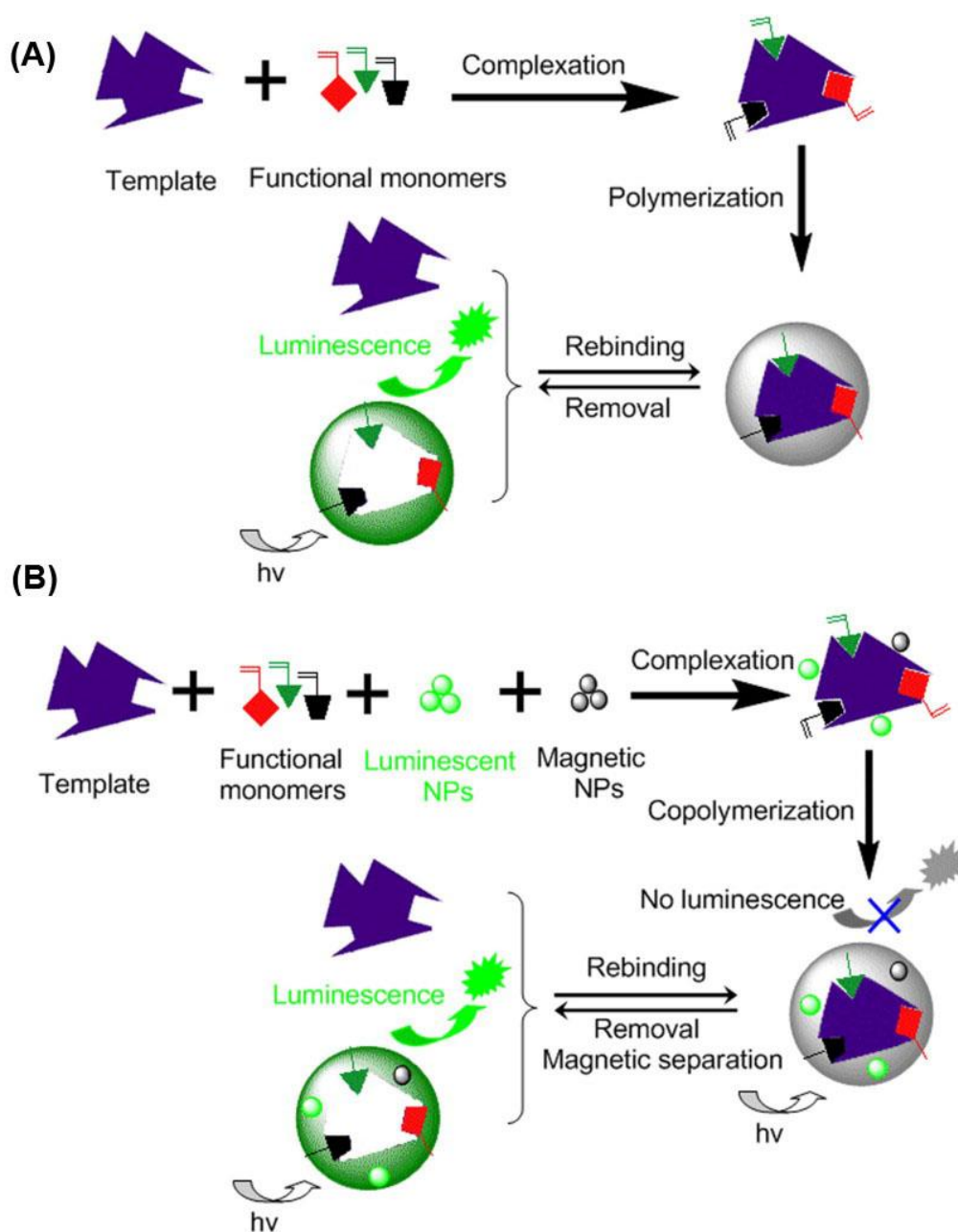
2.12 Molecularly imprinted polymers (MIPs)

Molecularly imprinted polymers (MIPs) are synthetic polymeric materials possessing specific recognition sites complementary in size, shape and functional groups to the template molecule (Holthoff *et al.*, 2011; Yang *et al.*, 2011). MIPs have been considered as alternatives for natural receptors (Reddy *et al.*, 2013; Yuan *et al.*, 2011) in chemical assays or sensors and this is due to their low cost, long lifetime, tailor-made recognition sites for target analytes and intrinsic robustness. In Scheme 2 (A) the conventional route to synthesis molecularly imprinted polymers via *in-situ* polymerisation is illustrated.

In molecular imprinting, functional monomers are located around the template molecules by non-covalent interaction or reversible covalent interaction, followed by polymerization and template removal. Consequently a molecular 'memory' within the imprinted polymer matrix is created, and then the target molecule can be selectively distinguished based on the molecular 'memory' (Fang *et al.*, 2009). In covalent molecularly imprinting, the functional monomer is attached to the template by reversible covalent bond during polymerisation (Kempe *et al.*, 1995) while in non-covalent interactions, the functional monomer associates to the template via an intermolecular interaction such as hydrogen bonding or ion-pairing (Yu *et al.*, 1997).

Although conventional μm particle sized MIPs can be prepared at low cost, they may possess some limitations such as incomplete template removal due to the high cross linking nature of MIPs, low binding capacity (due to the low surface area to volume ratio) and slow mass transfer which reduces the number of recognition sites for rebinding of template molecule (Schirhagl, 2014). In order to circumvent this issue, imprinting techniques have been combined with nanomaterials via surface imprinting.

Among various polymerisation techniques, surface imprinting has drawn considerable attention. This approach can be used in diverse applications such as sensing, separation and medical uses (Yan *et al.*, 2006). Due to the small size of these particles below 100 nm, the surface area to volume ratios are markedly improved having higher binding capacity, sensitivity and faster rebinding kinetics (Figueiredo *et al.*, 2016; Ma *et al.*, 2015). Many particles have been utilized as supports in the surface imprinting approach including luminescent nanomaterials (Scheme 2 (B)) in particular quantum dots (Diltemiz *et al.*, 2008; Wang *et al.*, 2009b). They can provide great photostability, readily tunable spectral properties and good chemical stability (Deng *et al.*, 2011; Wang *et al.*, 2010).



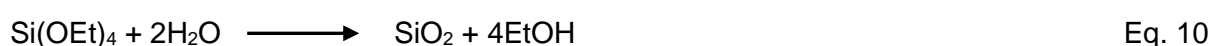
Scheme 2. Formation process of (A) conventional MIPs through *in-situ* polymerization and (B) luminescent MIP nanocomposites (MIP-NCs) through copolymerization (Ma *et al.*, 2015).

2.13 Mechanisms involved in MIP preparation

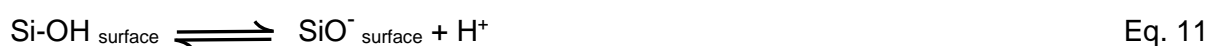
The mechanisms of MIP preparation include free-radical polymerization and sol-gel processes. In the sol-gel process (Stöber process), tetraalkoxysilane precursors, such as tetramethoxysilane and tetraethoxysilane, first hydrolyze to form a colloidal solution (a sol), and then they polycondense to form highly cross-linked silica materials (or gels) (Lofgreen *et al.*, 2014). The sol-gel technique has many advantages over other polymerization techniques, including simple preparation at room temperature as well as preventing problems associated with thermal and chemical decomposition. Furthermore, environmentally friendly solvents such as Millipore water or ethanol can be used instead of toluene, acetonitrile or chloroform required for radical polymerisation (Chen *et al.*, 2016; Chen *et al.*, 2011). It is important to note that due to solvent memory in the MIPs prepared in organic solvents via free-radical polymerization, they work poorly in aqueous media (Chen *et al.*, 2011).

Generally, the Stöber process (Stöber *et al.*, 1968) is carried out by the addition of tetraethyl orthosilicate (TEOS) to colloiddally stable seed particles (or QDs) in the presence of an EtOH/H₂O/NH₃ mixture. Hence, the surface of the QDs has to be exchanged with more polar ligands in order to enable solubility in ethanol. Furthermore nucleation sites are provided for the control growth of a homogenous silica coating by using 3-sulfanyl propyltrimethoxysilane (SPTMS), 3-aminopropyltrimethoxysilane (APTMS) or 3-aminopropyltriethoxysilane (APTES) (Liz-Marzán *et al.*, 1996; Mulvaney *et al.*, 2000) as well as the polymer of poly (vinyl pyrrolidone) (PVP) (Graf *et al.*, 2003).

The effect of water and ammonia on the hydrolysis of TEOS is described in Eq. 10.



As a matter of fact, water catalyzes the hydrolysis of TEOS and consequently increases the nucleation rate of silica particles. In addition, solvents with higher dielectric constants provide colloidal stability for the silica-coated QDs which thus favors ionization of silanol groups through the Eq. 11 as well as enhancing electrostatic repulsion between particles (Nann *et al.*, 2004).



Ammonia can be also applied as a catalyst for TEOS hydrolysis. It was found that the rate of spontaneous nucleation increases as the amount of ammonia decreases (Nann *et al.*, 2004).

The Stöber process based approach is difficult to employ when nanoparticles are insoluble in alcohol-water solution while for hydrophilic QDs this method can be directly applied. The size of particles can be controlled by the thickness of the silica and can range from a few nanometers to several micrometers (Wang *et al.*, 2009a).

In this research study, the advantages of surface molecular imprinting and nano techniques were merged, where a surface molecularly imprinted shell and a nanocomposite core can enable the template-imprinting sites to be placed at the surface of the material to provide favourable selectivity, high capacity and fast association/dissociation kinetics. Therefore, silica layers were anchored on the surface of L-cys-CdSe/ZnS QDs by the sol-gel and surface imprinting techniques to prepare MIP-capped L-cys CdSe/ZnS QDs (MIP@QDs).

2.14 Polymers utilized in this work

In this research, molecularly imprinted polymer capped L-cys CdSe/ZnS QDs (MIP@QDs) were synthesized via a surface molecular imprinting process with a functional monomer, cross linker, a template and a proper solvent in the presence of a catalyst (Figure 7 A and B). Non imprinted polymer capped QDs (NIP@QDs) were also prepared in parallel without the addition of template in order to compare the affinity of the analyte towards the polymers (Figure 7 C). The synthesized MIP@QDs and NIP@QDs, under UV irradiation, which were utilized in this work are shown in Figure 8.

The synthesized NIP@QDs had the same chemical properties as the MIP@QDs but without specific recognition sites. As a result, the nature of interactions between the MIP@QDs with the template is similar to those between NIP@QDs and the template. The only difference originates from the strength of the interactions. If well-defined recognition cavities are produced during polymerisation, the strength of interactions with the MIP@QDs is higher than those of the NIP@QDs because of the spatial complementary nature of the template with cavities (Pichon *et al.*, 2008).

In a common approach, complexation of the template in a solution containing a functional monomer takes place through covalent or non-covalent interactions (e.g. ionic, hydrophobic and hydrogen bonding), followed by the polymerisation of the monomer around the template with the aid of a cross linker. Templates are then extracted after polymerisation by an excess amount of a solvent (an acid, a base, methanol or ethanol) in order to disrupt template-functional monomer assemblies and providing cavities complementary to the template in shape, size and the position of functional groups (Pichon *et al.*, 2008). Although covalent interactions produce polymers with higher stability (Wulff *et al.*, 2001), a non-covalent

approach is more favorable to generate molecular binding sites due to the following reasons (Pichon *et al.*, 2008; Yan *et al.*, 2006):

- i. The removal of the template is much easier for non-covalent self-assemblies which can be achieved by extensive washing steps.
- ii. Non-covalent interactions can be simply carried out to avoid the synthesis of a prepolymerization complex.
- iii. A non-covalent approach can produce higher affinity binding sites.

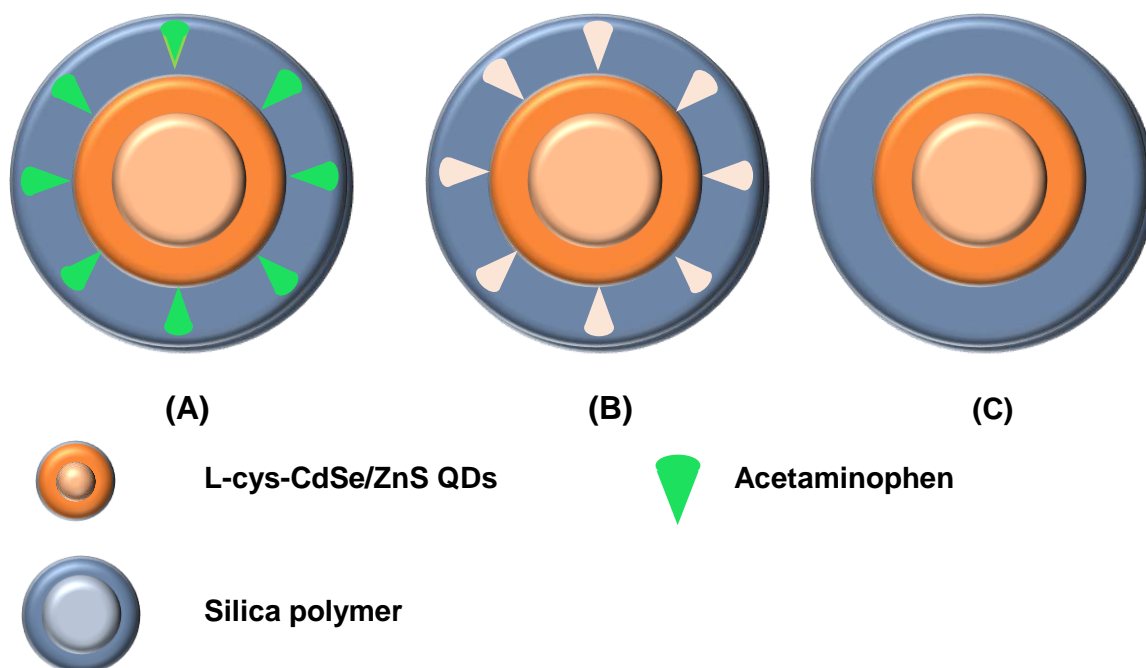


Figure 7. Polymers utilized in this work: (A) MIP@QDs without template removed, (B) MIP@QDs with template removed and (C) NIP@QDs polymer.



Figure 8. Synthesized polymers with template removed under UV irradiation with an excitation wavelength 365 nm; MIP@QDs (left), NIP@QDs (right).

In bringing this information together in a useful fashion for synthetic purposes, it is constructive to highlight the importance of functional monomers, cross linkers, solvents and the template for non-covalent interactions, and in this study hydrogen bonding.

2.14.1 Functional monomers

In the world of molecular imprinting, functional monomers can be used for the binding interactions in the imprinting recognition sites. It is of great importance to match the functionality of the functional monomer with the functionality of the template such as H-bond donor with H-bond acceptor so as to increase the imprinting factor and complex formation. Furthermore, a template to functional monomer ratio of 1:4 is common for non-covalent imprinting (Cormack *et al.*, 2004).

In the current study, an organically modified silica namely 3-aminopropyltriethoxysilane (APTES) (Figure 9) was applied as a functional monomer as its amine groups are available to form hydrogen bonds with the carboxylic groups of acetaminophen.

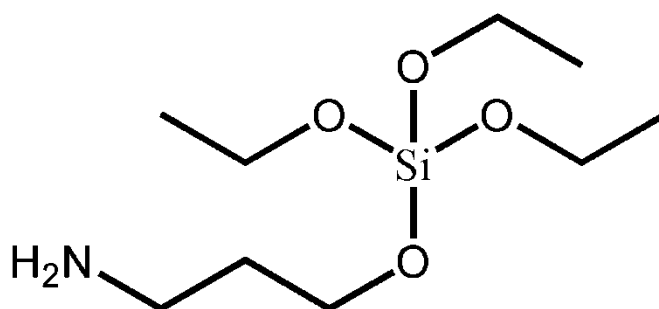


Figure 9. Structure of 3-aminopropyltriethoxysilane.

2.14.2 Cross linkers

Cross linkers are responsible for stabilizing the imprinting sites, providing mechanical stability and controlling the morphology of the polymer matrix whether it is gel-type, macroporous or a microgel powder (Cormack *et al.*, 2004; Yan *et al.*, 2006). Furthermore, cross linkers play a pivotal role to fix the functional groups of monomer around the template and to form a highly cross-linked polymer (Chen *et al.*, 2011).

Tetraethyl orthosilicate (TEOS), an organically modified silica, was employed as a cross linker in this study to synthesize a molecularly imprinted polymer (Figure 10).

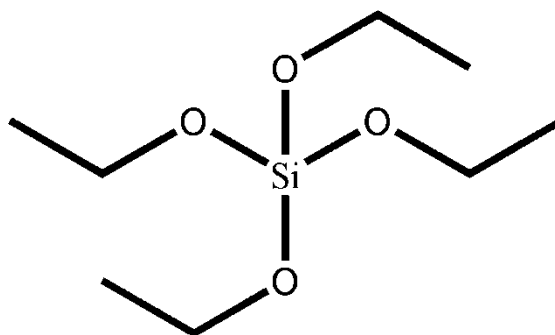


Figure 10. Structure of tetraethyl orthosilicate.

2.14.3 Template

In the molecular imprinting process, the template is of central importance as the functionality and structure of this molecule defines its ability to strongly interact with monomers as well as the properties of the binding sites. Although molecular imprinting process can be applied for a large number analytes, not all templates are amenable for imprinting. Most MIPs are using small templates since not only are larger molecules such as proteins less rigid, but also they cannot facilitate the creation of well-defined cavities during imprinting process (Yan *et al.*, 2006).

It should also be borne in mind that chemical stability, functionalities, cost and availability are the main factors in selecting a molecule as a template (Chen *et al.*, 2011; Pichon *et al.*, 2008). In non-covalent binding, the template should have multiple functional groups to reinforce template-monomer interactions. In the case of expensive, poorly available templates or low soluble target analytes, a structural analogue or a dummy molecule can be used which has similar shape and structure to the template (Pichon *et al.*, 2008).

In this research work, acetaminophen was used to synthesize the MIP since it possessed functional sites which favored the formation of template-functional monomer assemblies by hydrogen bonding.

2.14.4 Solvents

From the polymerisation point of view, the solvent has a substantial role in determining the efficiency of the recognition sites because the accuracy of template-functional monomer assembly depends on the physical and chemical properties of the solvent (Pichon *et al.*, 2008). The main purpose of using a solvent is to bring all components including template, functional monomer and cross linker into one phase. In addition, the solvent in non-covalent imprinting polymerisation maximizes the probability of template-functional monomer complex formation (Cormack *et al.*, 2004). Non-polar to moderately polar and aprotic solvents can be used as

solvent to render strong polar interactions such as hydrogen bonds and electrostatic interactions. Recently, ethanol, methanol and water are being utilized as polar and protic solvents for the synthesis of MIPs to develop hydrogen bonds and electrostatic interactions (Pichon *et al.*, 2008).

2.15 Principle of optical sensing using MIP-capped QDs (MIP@QDs)

Generally, fluorescence quenching hinges on the adsorptive affinity of the analyte and particles which includes two types of quenching, i.e. dynamic (collisional) quenching and static quenching. Fluorescence lifetime measurements, temperature-varying experiments and absorption spectrum measurements are often used to identify the kind of quenching and its mechanism (Cheng *et al.*, 2006). In static quenching, the absorption spectrum of the polymer changes in the presence of the quencher while the fluorescence lifetime of the polymer, before and after the addition of the quencher, does not change (Lakowicz, 1999; Rahman *et al.*, 2006).

In the system of MIP@QDs-AC, fluorescence quenching was achieved by the affinity of the MIP@QDs recognition cavities for AC molecules due to specific interactions according to Stern–Volmer equation (Xu *et al.*, 2013). The Stern–Volmer equation for static quenching is shown in Eq. 12 (Rahman *et al.*, 2006).

$$\frac{F_0}{F} = 1 + K_{sv} [Q] \quad \text{Eq. 12}$$

Here, F_0 and F are the steady state fluorescence intensities in the absence and presence of the quencher, respectively, $[Q]$ is the total analyte concentration and K_{sv} represents the Stern–Volmer quenching constant.

2.16 Toxicity of triclosan

Triclosan (TCS), or 5-chloro-2-(2,4-dichlorophenoxy) phenol (Figure 11) with the commercial name Irgasan DP300, has been used in a variety of consumer products (Bhargava *et al.*, 1996; Jones *et al.*, 2000). The chemical structure of TCS is similar to bisphenol A, dioxins, polybrominated diphenyl ethers (PBDEs), polychlorinated biphenyls (PCBs) and thyroid hormones molecules with two aromatic rings (Allmyr *et al.*, 2008; Crofton *et al.*, 2007).

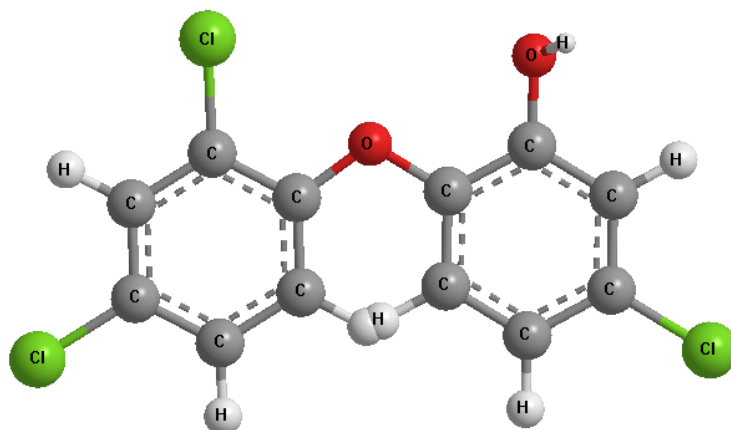


Figure 11. Chemical structure of triclosan.

TCS is a fairly small molecule, with a molecular weight of $289.54 \text{ g mol}^{-1}$ and a diameter of about 7.4 \AA (Rossner *et al.*, 2009) and has a solubility of $<10^{-6} \text{ g mL}^{-1}$ in water (Du Preez *et al.*, 2003). The partition coefficient of TCS ($\log P_{ow} = 4.76$), suggests that it is lipophilic, where the partition coefficient is a ratio of solubility between two liquids, in this case octanol and water. Values of the pK_a for TCS have been reported in the range of 7.9–8.1 (Son *et al.*, 2009). The soil organic carbon coefficient (K_{oc}) of TCS has been calculated to equal 13,400 at pH 7; 6,020 at pH 8; and 934 at pH 9 (Chalew *et al.*, 2009).

Typical environmental concentration ranges for TCS in water systems are shown in Figure 12, which relates these to toxicological threshold values for various aquatic species.

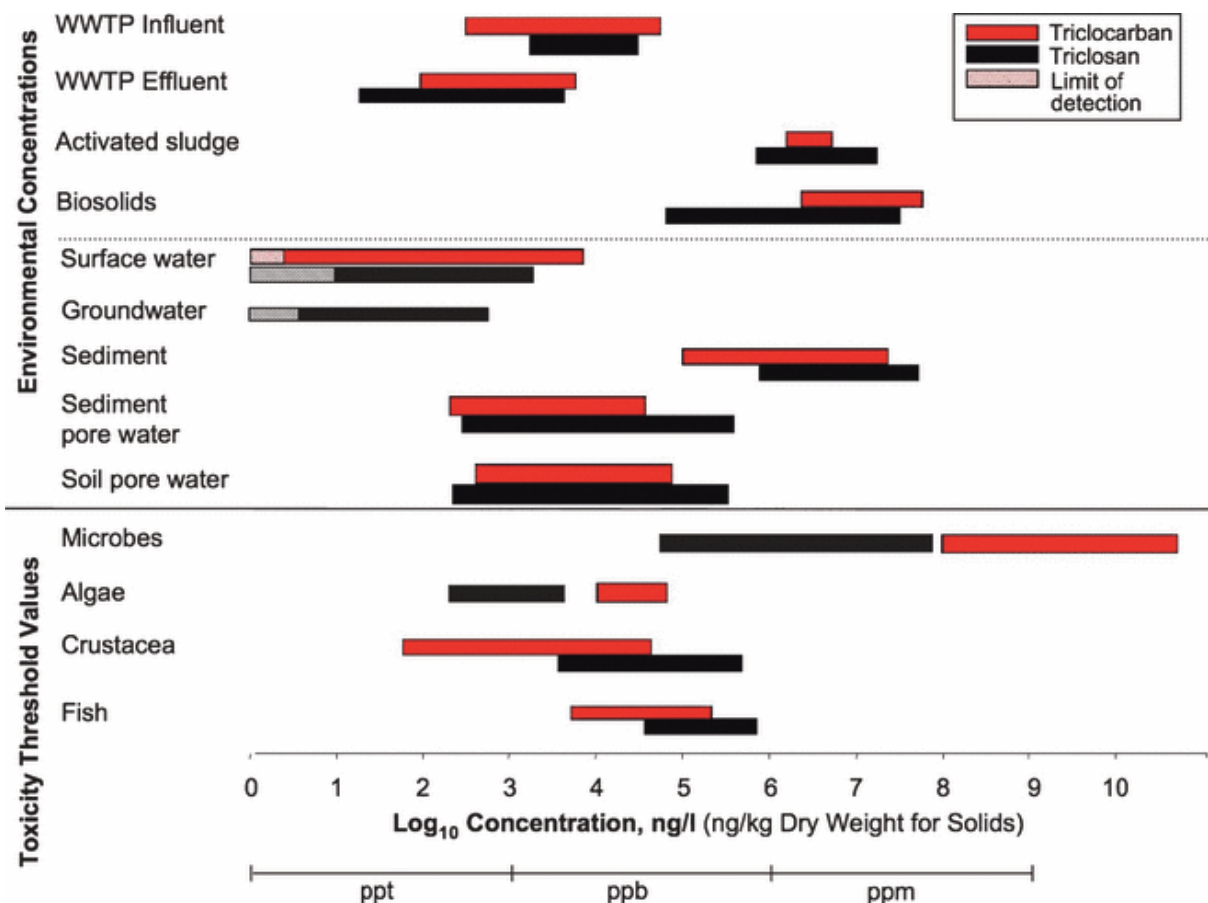


Figure 12. Comparison of environmental occurrence data of triclosan and toxicity threshold values for different organisms (Chalew *et al.*, 2009).

As it is obvious from the black bars in Figure 12, fish, algae and crustaceans may be affected by high levels of TCS in surface waters. Minimum inhibitory concentration (MIC) threshold values for microbes with respect to TCS may be exceeded in activated sludge and biosolids which is a vital implication for the fertility of agricultural soils treated with biosolids. Fish may be affected by environmental TCS exposures in surface waters heavily influenced by raw and treated sewage. Moreover, algae and crustaceans are highly sensitive indicator organisms that may be influenced by TCS occurrences in surface waters receiving raw and treated sewage. Importantly, TCS has been detected in surface waters at concentrations exceeding the no-observed effects concentration (NOEC) of algae, whilst crustaceans can be adversely affected by TCS levels in sediment pore water (Chalew *et al.*, 2009).

2.16.1 Toxicity threshold of triclosan

Ecotoxicity data are indispensable for the elucidation of biocide occurrences in the environment. Acute and chronic effects can be considered as common measures of toxicity. Threshold values for acute toxicity of TCS in fish have been determined to range from 260,000

to 602,000 ng L⁻¹ (Ishibashi *et al.*, 2004; Orvos *et al.*, 2002) whereas chronic effect thresholds were in the range of 71,300 – 290,000 ng L⁻¹ (Orvos *et al.*, 2002; Tatarazako *et al.*, 2004). Acute toxicity threshold values in crustaceans were determined to range from 390,000 ng L⁻¹-125,000,000 and chronic toxicity was observed at levels as low as 6,000 – 440,000 ng L⁻¹ (Mimmert, 2006; Orvos *et al.*, 2002). Toxic concentrations of TCS to algae were also in the parts-per-billion range, with values of 200 – 2,800 ng L⁻¹ (Samsøe-Petersen *et al.*, 2003; Yang *et al.*, 2008). Inhibitory effects on microorganisms were shown to begin at levels ranging from 25,000 – 80,000,000 ng L⁻¹ for TCS (Farré *et al.*, 2008; Stasinakis *et al.*, 2007; Stickler *et al.*, 2008).

In one study, a chronic predicted no-effect concentration (PNEC) of 1,550 ng L⁻¹ was determined for TCS by the species sensitivity distribution (SSD) approach which was based on toxicity data for 14 aquatic species. This study then suggested that TCS concentrations could be between 850 ng L⁻¹ without in-stream removal and 250 ng L⁻¹ with in-stream removal in U.S. surface waters (Capdevielle *et al.*, 2008). Moreover, as the concentration of TCS increases, there is a possibility of adaption of bacterial strains by developing resistance (Stickler *et al.*, 2008).

Researchers in Spain conducted another environmental risk assessment for 26 PPCPs (de García *et al.*, 2014). They employed Microtox acute ecotoxicity tests and activated sludge respirometry assays. The quantitative structure-activity relationship (QSAR) program was also utilized to predict the estimated ecotoxicological effects. Based on the results of ecotoxicity tests, TCS was found to be very toxic to different species. Furthermore, evaluation of persistence, bioaccumulation and ecotoxicity (PBT) revealed that TCS is persistent and toxic but not bioaccumulative (de García *et al.*, 2011).

Triclosan has been shown to exert deleterious effects towards different somatic and reproductive mammalian cells at extracellular concentrations of <1,000,000–5,000,000 ng L⁻¹. It also had adverse effects on cells that are non-renewable (pancreatic β-cells). TCS is a mitochondrial toxic chemical which may cause unexpected long-term toxic effects depending on its tissue distribution and elimination (Ajao *et al.*, 2015).

Therefore it is evident that aquatic species such as algae, invertebrates and certain types of fish are much more sensitive to TCS than mammals. Specifically, algae is highly sensitive indicator organism that may be impacted by TCS occurrences in surface waters at levels of 200 – 2,800 ng L⁻¹, where the worldwide concentration has been found to range from 1.4 – 40,000 ng L⁻¹ (Dhillon *et al.*, 2015; SCCS, 2010). Reported toxicity of TCS to aquatic organisms is summarized in Table 3. Acute and chronic toxicity data relating to TCS are also provided in Table 4 and Table 5.

Table 3. Effects of TCS on freshwater (FW) and marine (SW) organisms (Dann *et al.*, 2011).

Test species	Life stage	System type	Route of exposure	Test duration	TCS exposure	Endpoint	Reference
Algae Phytoplankton (<i>Dunaliella tertiolecta</i>)	-	SW	Water (static)	Acute (96 h)	3,500 ng L ⁻¹	EC50 (population density)	(Delorenzo <i>et al.</i> , 2008a)
Invertebrates (<i>Chironomus tentans</i>)	-	FW	Water (renewal)	10 days	400,000 ng L ⁻¹	LC50	(Dussault <i>et al.</i> , 2008)
Invertebrates (<i>Hyalella Azteca</i>)	Embryo				200,000 ng L ⁻¹		
					651,000 ng L ⁻¹		
Grass shrimp (<i>Palaemonetes pugio</i>)	Larvae	SW	Water (renewal)	Acute (96 h)	154,000 ng L ⁻¹	LC50	(Delorenzo <i>et al.</i> , 2008b)
	Adult				305,000 ng L ⁻¹		
Crustacean (<i>Thamnocephalus platyurus</i>)	-	FW	Water (static)	Acute (24 h)	470,000 ng L ⁻¹	LC50	(Kim <i>et al.</i> , 2009)
Bivalve (<i>Mytilus galloprovincialis</i>)	Hemocytes		<i>In vitro</i>	Acute (30 min)	1 µM	↓lysosomal membrane stability	(Canesi <i>et al.</i> , 2007)
	Whole animal	SW	Injection	Acute (24 h)	2.9 µg kg ⁻¹	Altered hemocyte and digestive gland function	
Zebra mussel (<i>Dreissena polymorpha</i>)	Hemocytes	FW	<i>In vitro</i>	Acute (60 min)	0.1 µM	Geno toxicity	(Binelli <i>et al.</i> , 2009a; Binelli <i>et al.</i> , 2009b)
			<i>In vivo</i>	Acute (96 h)	1 M		

Medaka (<i>Oryzias latipes</i>)	Eggs	SW	In ovo injection	1 day post fertilization	4.2 ng egg ⁻¹	EC50 (survival)	(Nassef <i>et al.</i> , 2010)
Medaka (<i>Oryzias latipes</i>)	Adult	SW	Water (renewal)	Acute (96 h)	1700,000 ng L ⁻¹	LC50	(Nassef <i>et al.</i> , 2009)
Medaka (<i>Oryzias latipes</i>)	Larvae	FW	Water (static)	Acute (96 h)	600,000 ng L ⁻¹	LC50	(Kim <i>et al.</i> , 2009)
Fathead minnow (<i>Pimephales promelas</i>)	Full life cycle	FW	Water (TCS in mixture)	-	100 and 300 ng L ⁻¹ mixture of products	No effects F ₀ ; ↑ larval deformities in F ₁	(Parrott <i>et al.</i> , 2009)
Zebrafish (<i>Danio rerio</i>)	Embryo	FW	24-Well microplates	Acute (96 h)	420,000 ng L ⁻¹	LC50; teratogenic effects	(Oliveira <i>et al.</i> , 2009)
	Adult		Semi-static		340,000 ng L ⁻¹		
Amphibians Bullfrog (<i>Acris crepitans Blanchardii</i>)	Larvae				367,000 ng L ⁻¹		
Amphibians Bullfrog (<i>Bufo woodhousii Woodhousii</i>)	Stage 30	FW	Water	Acute (96 h)	152,000 ng L ⁻¹	LC50	(Palenske <i>et al.</i> , 2010)
Amphibians Bullfrog (<i>Rana sphenoccephala</i>)	-				562,000 ng L ⁻¹		
Amphibians Bullfrog (<i>Xenopus laevis</i>)	Stage 41				343,000 ng L ⁻¹		

Table 4. Acute toxicity data of triclosan.

Species	Trophic group	Endpoint/duration	LC50 (ng L ⁻¹)	Reference
<i>Daphnia magna</i>	Invertebrate	48 h	390,000	(Orvos <i>et al.</i> , 2002)
<i>Ceriodaphnia dubia</i>	Invertebrate	24, 48 h (pH = 7.0)	200,000, ~125,000,000	(Orvos <i>et al.</i> , 2002)
<i>Pimephales promelas</i>	Fish	24 h	360,000	(Orvos <i>et al.</i> , 2002)
		48 h	270,000	
		72 h	270,000	
		96 h	260,000	
		24h	440,000	
<i>Lepomis macrochirus</i>	Fish	48 h	410,000	(Orvos <i>et al.</i> , 2002)
		96 h	370,000	
<i>Oryzias latipes</i>	Fish	96 h	602,000 (larvae), 399,000 (embryos)	(Ishibashi <i>et al.</i> , 2004)
<i>Xenopus laevis</i>	Amphibian	96 h	259,000	(Palenske <i>et al.</i> , 2010)
<i>Acris blanchardii</i>	Amphibian	96 h	367,000	(Palenske <i>et al.</i> , 2010)
<i>Bufo woodhousii</i>	Amphibian	96 h	152,000	(Palenske <i>et al.</i> , 2010)
<i>Rana sphenoccephala</i>	Amphibian	96 h	562,000	(Palenske <i>et al.</i> , 2010)
<i>Pseudokirch-neriella subcapitata</i>	Algae	72 h growth	530	(Yang <i>et al.</i> , 2008)

Table 5. Chronic toxicity data of triclosan*.

Species	Trophic group	Endpoint/duration	LOEC (ng L ⁻¹)	NOEC (ng L ⁻¹)	Reference
<i>Daphnia magna</i>	Invertebrate	21 d survival, reproduction	Repro.= 200,000	Surv. = 200,000	(Orvos <i>et al.</i> , 2002)
<i>Ceriodaphnia dubia</i>	Invertebrate	7 d survival	-	50,000-339,000	

		7 d reproduction		6,000-182,000	(Orvos <i>et al.</i> , 2002)
<i>Ceriodaphnia dubia</i>	Invertebrate	7 d survival, reproduction	IC25 = 170,000	-	(Tatarazako <i>et al.</i> , 2004)
<i>Chironomus riparius</i>	Invertebrate	28 d survival, emergence	-	440,000	(Mommert, 2006)
<i>Chironomus tentans</i>	Invertebrate	10 d survival, growth	LC25= 100,000	-	(Dussault <i>et al.</i> , 2008)
<i>Hyalella azteca</i>	Invertebrate	10 d survival, growth	LC25= 60,000		(Dussault <i>et al.</i> , 2008)
<i>Oncorhynchus mykiss</i>	Fish	96 d ELS hatching	No Effect	-	(Orvos <i>et al.</i> , 2002)
		Survival	71,300		
<i>Oryzias latipes</i>	Fish	14 d hatching	213,000	-	(Ishibashi <i>et al.</i> , 2004)
		21 d growth	200,000		
		Fecundity	No effect		
<i>Oryzias latipes</i>	Fish	HSI and GSI,	200,000	-	(Ishibashi <i>et al.</i> , 2004)
		VTG	20,000		
<i>Oryzias latipes</i>	Fish	14 d hatchability	LC25= 290,000	-	(Tatarazako <i>et al.</i> , 2004)
<i>Gambusia affinis</i>	Fish	35 d sperm count, VTG	101,300	-	(Raut <i>et al.</i> , 2010)
<i>Danio rerio</i>	Fish	9 d hatchability	LC25= 160,000		(Tatarazako <i>et al.</i> , 2004)
<i>Xenopus laevis</i>	Amphibian	21 d metamorphosis	No effect (200,000)	-	(Fort <i>et al.</i> , 2009)
<i>Rana catesbeiana</i>	Amphibian	18 d development	300,000	-	(Veldhoen <i>et al.</i> , 2006)
<i>Rana pipiens</i>	Amphibian	24 d survival	230,000	-	(Fraker <i>et al.</i> , 2004)
		Growth	2,300		
<i>Bufo americanus</i>	Amphibian	14 d survival, growth	No effect (230,000)	-	(Smith <i>et al.</i> , 2005)
<i>Selenastrum capricornutum</i>	Algae	96 h growth	EC50 = 4,460	EC25 = 2,440	(Orvos <i>et al.</i> , 2002)
<i>Scenedesmus subspicatus</i>	Algae	96 h biomass	EC50 = 1,200	EC50 = 500	(Orvos <i>et al.</i> , 2002)

		Growth rate	EC50 = 1,400	EC50 = 690	
<i>Skeletonema costatum</i>	Algae	96 h growth rate	EC50 ≥ 66,000	EC25 > 66,000	(Orvos <i>et al.</i> , 2002)
<i>Aphanizomenon flos-aquae</i>	Algae	96 h biomass	EC50 = 970	EC25 = 670	(Orvos <i>et al.</i> , 2002)
<i>Pseudokirch-neriella subcapitata</i>	Algae	72 h growth	400	200	(Yang <i>et al.</i> , 2008)
<i>N. pelliculosa</i>	Algae	96 h growth rate	EC50 = 19,100	EC25 = 10,700	(Orvos <i>et al.</i> , 2002)
<i>Natural algal assemblage</i>	Algae	96 h biomass	120	-	(Wilson <i>et al.</i> , 2003)
<i>Closterium ehrenbergii</i>	Algae	96 h growth	-	250,000	(Ciniglia <i>et al.</i> , 2005)
<i>Dunaliella tertiolecta</i>	Algae	96 h growth	-	1,600	(Delorenzo <i>et al.</i> , 2008a)
<i>Lemna gibba</i>	Plant	7 d growth	EC50 ≥ 62,500	EC25 ≥ 62,500	(Orvos <i>et al.</i> , 2002)
<i>Sesbania herbacea</i>	Plant	28 d seed germination	100,000 germination	-	(Stevens <i>et al.</i> , 2009)
		Morphology	10,000 morphology		
<i>Eclipta prostrata</i>	Plant	28 d seed germination	No effect	-	(Stevens <i>et al.</i> , 2009)
		Morphology	1000,000		
<i>Bidens frondosa</i>	Plant	28 d seed germination	100,000	-	(Stevens <i>et al.</i> , 2009)
		Morphology	10,000		

* The abbreviations are explained in the list of abbreviations.

2.16.2 Legal limit of triclosan

Triclosan is an anti-microbial and preservative agent added to personal care products (soap, lotions, toothpaste, detergent and skin care creams) at a typical concentration in the range of 0.1 – 0.3% (w/w) which is regulated by the European Community Cosmetic Directive or the US Food and Drug Agency (U.S. FDA) in Europe and the USA, respectively (Rodricks *et al.*, 2010; Sabaliunas *et al.*, 2003). The content of TCS in household products should not exceed

0.3% (w/w) (Allmyr *et al.*, 2006). The Minnesota Department of Health (MDH) developed a guidance value of 50 ppb for triclosan in drinking water. A person drinking water at or below this level, would have little or no risk of any health effects from triclosan ("Toxicological Summary: Triclosan," 2010). The Canadian Federal Water Quality Guideline for the protection of aquatic life from adverse effects of triclosan is 380 ng L⁻¹ (Canadian Environmental Protection Act, 2017).

2.17 Toxicity of acetaminophen

Acetaminophen (AC) or paracetamol (N-acetyl-p-aminophenol, Figure 13) with log K_{ow} 0.46 (Westerhoff *et al.*, 2005) is an acylated aromatic amide that was first introduced by Von Mering in 1893 as an antipyretic/analgesic medicine used for fever, headaches, and other minor pains (Wu *et al.*, 2012). It has a pK_a of 9.46 with a solubility of 1.4×10⁴ mg L⁻¹ in water at 25 °C (Achilleos *et al.*, 2008; Ishihama *et al.*, 2002). The high solubility and hydrophilicity of AC result in its accumulation in the aquatic environment. It has been detected in surface waters, drinking water and wastewater throughout the world (Thomas *et al.*, 2007).

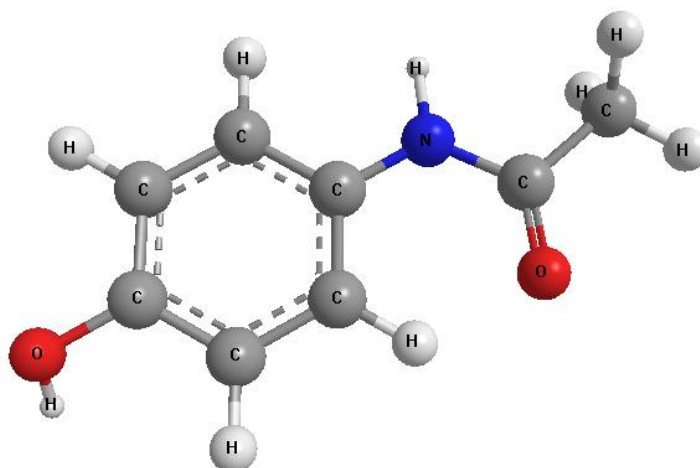


Figure 13. Structure of acetaminophen.

Acute overdoses of AC can cause potentially fatal liver damage, and in some individuals, a normal dose can cause the same, the risk of which can be heightened by alcohol consumption. Recent studies have suggested that excessive doses and/or excessively high blood plasma concentrations of AC may be associated with hepatotoxicity (Barker *et al.*, 1977). It has been demonstrated that 58–68% of AC and its metabolites are excreted from the body during therapeutic use (Muir *et al.*, 1997). Hu *et al.*, (2012) reported that microorganisms play a pivotal role in acetaminophen degradation in the environment under various conditions. Although the detected concentrations of pharmaceuticals are typically in the nanogram to microgram-per-liter range (Huber *et al.*, 2005), a variety of potential adverse effects, including

acute and chronic damage, accumulation in tissues, reproductive damage, inhibition of cell proliferation and behavioral changes, have been documented at these low levels (Escher *et al.*, 2011; Phillips *et al.*, 2010).

Figure 14 shows environmental concentration ranges for AC in water systems which relates these to toxicological threshold values for various aquatic species. Some authors reported the presence of AC in effluents at concentrations below to 20 ng L⁻¹ (Roberts & Thomas, 2006) to 4,300 ng L⁻¹ (Gómez *et al.*, 2007), although in surface waters values can reach 78,170 ng L⁻¹ (Grujić *et al.*, 2009), which are higher than the predicted no-effect concentration (PNEC) of 9,200 ng L⁻¹ (Carlsson *et al.*, 2006). Hence, AC might represent a threat to non-target organisms.

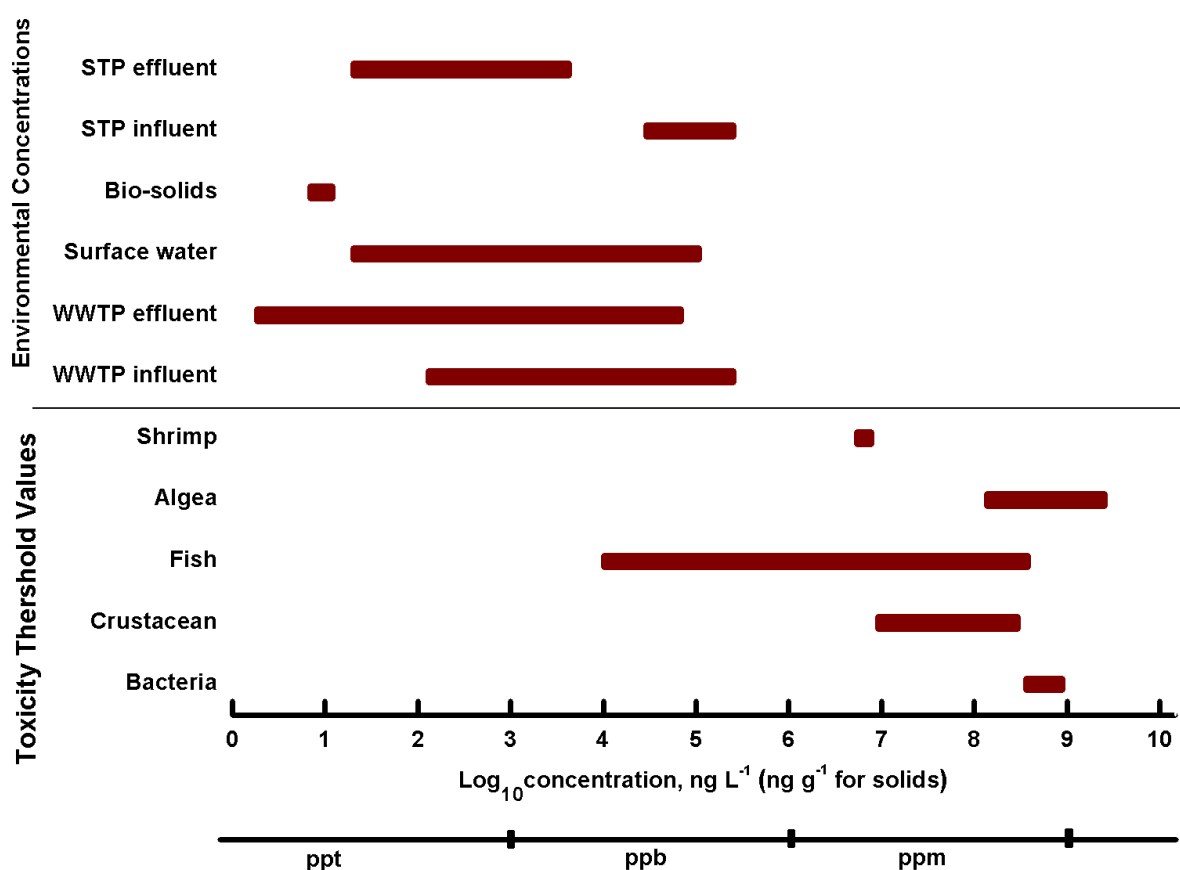


Figure 14. Environmental occurrence data for acetaminophen in comparison to available toxicity threshold values for various indicator organisms.

2.17.1 Toxicity threshold of acetaminophen

Although acetaminophen induces proliferation of cultured breast cancer cells via estrogen receptors without binding to them, it does not have estrogenic activity in rodents (Harnagea-Theophilus *et al.*, 1999). The mode of action of acetaminophen is not yet fully elucidated. It seems that this drug acts mainly by inhibiting the cyclooxygenase of the central nervous

system and it does not have anti-inflammatory effects, because of the lack of inhibition of peripheral cyclooxygenase involved in inflammatory processes. Adverse effects of acetaminophen are mainly due to the formation of hepatotoxic metabolites, primarily *N*-acetyl-*p*-benzoquinone imine, synthesized when the availability of glutathione is decreased in liver cells (Fent *et al.*, 2006; Harnagea-Theophilus *et al.*, 1999).

Acetaminophen has detrimental effects especially in over dosage related to the formation of toxic metabolites by oxidative pathways. Toxicity of acetaminophen is usually caused by reactive oxygen species which can result in protein denaturation to lipid peroxidation and DNA damage (Antunes *et al.*, 2013). The effects of AC on different organisms are shown in Table 6.

A separate study (Galus *et al.*, 2013) exposed adult zebrafish (*Danio rerio*) to a pharmaceutical mixture including acetaminophen and to diluted wastewater effluent over a six week period. They observed that chronic exposure of zebrafish to 10,000 ng L⁻¹ acetaminophen markedly decreased fecundity. Liver histology was altered and acetaminophen exposure significantly increased developmental abnormalities.

Acetaminophen has shown toxic effects on the development, growth, behavior and survival of *D. rerio* larvae of zebrafish embryos. It induces anomalies at different levels of development in a dose-dependent manner (0, 1×10⁶, 5×10⁶, 10×10⁶, 50×10⁶ and 100×10⁶ ng L⁻¹), causing impairment in (i) tail and tail-fin formation, (ii) larval behavior and survival, (iii) hatching, (iv) the early development, (v) organogenesis (by altering the rate of apoptosis), (vi) larval growth and morphometry and (vii) pigmentation (David *et al.*, 2009).

Acute aquatic toxicity of acetaminophen and some other pharmaceuticals was examined on a freshwater invertebrate (*Daphnia magna*), the Japanese medaka fish (*Oryzias latipes*) and a marine bacterium (*Vibrio fischeri*) in Korea (Kim *et al.*, 2007). The acute toxicity results were predicted by a quantitative structure activity relationship model using molecular orbital energy parameters and pH-dependent distribution coefficient of the test pharmaceuticals. The 48 hr EC50 values for *D magna* and *O. latipes* were 30,100,000 ng L⁻¹ and >160,000,000 ng L⁻¹ respectively while the 15 min EC50 for *V. fischeri* was 567,500,000 ng L⁻¹. The highest predicted environmental concentration (PEC) was also expected for acetaminophen (16,500 ng L⁻¹) due to the highest volume production of AC regarding pharmaceuticals in Korea (1,068,921 kg in 2003). The hazard quotient which was derived from the PEC and predicted no-effect concentration (PNEC) for acetaminophen was 1.8 showing potential environmental concerns of this medicine, as hazard quotients exceeding 1 indicate potential effects (Brausch *et al.*, 2011).

The effect of several environmental factors such as water pH (7.4, 8.3, and 9.2), temperature (15, 21, and 25 °C) and ultraviolet light (continuous irradiation of 15.0 $\mu\text{W cm}^{-2}$) on the toxicity of some pharmaceutical compounds including acetaminophen in water, has been evaluated by Kim *et al.*, (2010) using the freshwater invertebrate *Daphnia magna*. They showed that lower water pH caused greater acute lethal toxicity of acetaminophen due to the higher unionized fraction thereof. AC was more markedly toxic at pH 8.3 compared to pH 9.2 in terms of 48 hr EC50 ($P < 0.05$). Moreover, enhancement in the temperature of the water led to an increase in the acute toxicity of AC which was attributed to the alteration in toxicokinetics of the chemical, as well as the impact on the physiological mechanisms of the test organism. In the presence of UVB light, the toxicity of acetaminophen also tended to increase.

The acute toxicity (median lethal concentration, LC50, for a 96 h exposure) of acetaminophen and ibuprofen alone and different mixtures thereof was investigated in green neon shrimp (*Neocaridina denticulata*) (Sung *et al.*, 2014). They revealed that the LC50 value after 96 h exposure for acetaminophen was 6,070,000 ng L⁻¹. Furthermore, the LC50 value of 96 h exposure for mixtures with high acetaminophen concentration and low ibuprofen concentration indicated enhanced toxicity in *N. denticulate* (LC50 = 4,780,000 ng L⁻¹) compared to acetaminophen and ibuprofen alone.

Morasch and Perazzolo (Morasch *et al.*, 2010; Perazzolo *et al.*, 2010) evaluated wastewater treatment plant influent and effluent, and raw drinking water samples in Switzerland, for 37 pharmaceuticals including acetaminophen, four hormones and a number of other micropollutants. All pharmaceuticals were detected in at least one sample of influent or effluent from the wastewater treatment plants. Predicted no-effect concentrations of acetaminophen were exceeded in raw drinking water samples and therefore presented a potential risk to the ecosystem.

Table 6. Effects of acetaminophen on different organisms.

Taxon	Species	Toxicological endpoint	Ecotoxicity data (ng L ⁻¹)	Reference
Bacteria	<i>Vibrio fischeri</i>	EC50 (5 min)	549,700,000 (534,000,000–565,900,000)	(Kim <i>et al.</i> , 2007)
		EC50 (15 min)	567,500,000 (358,600,000–898,100,000)	
Bacteria	<i>Vibrio fischeri</i>	EC50 (30 min)	650,000,000	(Henschel <i>et al.</i> , 1997)
Crustacean	<i>Daphnia magna</i>	EC50 (24 h) (immobilization)	293,000,000	(Henschel <i>et al.</i> , 1997)

		EC50 (48 h) (immobilization)	50,000,000	
Crustacean	<i>Daphnia magna</i>	EC50 (48 h) (immobilization)	9,200,000	(Kühn <i>et al.</i> , 1989)
Crustacean	<i>Daphnia magna</i>	EC50 (48 h) (immobilization)	30,100,000 (23,200,000– 39,000,000)	(Kim <i>et al.</i> , 2007)
		EC50 (96 h) (immobilization)	26,600,000 (19,600,000– 33,600,000)	
Fish	<i>Oryzias latipes</i>	LC50 (48 h)	>160,000,000	(Kim <i>et al.</i> , 2007)
		LC50 (96 h)	>160,000,000	
Fish	<i>Brachydanio rerio</i> (zebra fish)	LC50 (48 h)	378,000,000	(Henschel <i>et al.</i> , 1997)
Algae	<i>Scenedesmus subspicatus</i>	EC50 (72 h)	134,000,000	(Henschel <i>et al.</i> , 1997)
Ciliates	<i>Tetrahymena pyriformis</i>	EC50 (48 h) (growth inhibition)	112,000,000	(Henschel <i>et al.</i> , 1997)
Green neon shrimp	<i>Neocaridina denticulata</i>	LC50 (96 h) (exposure)	6,070,000 (5,330,000– 7,840,000)	(Sung <i>et al.</i> , 2014)

2.17.2 Legal limits of acetaminophen

Based on available information, the Minnesota Department of Health (MDH) developed a guidance value of 200 ppb for acetaminophen in drinking water. The MDH considers the liver to be the organ most sensitive to acetaminophen exposure ("Toxicological Summary for: Acetaminophen," 2010).

2.18 References

Achilleos, A., Ines Vasquez Hadjilyra, M., Hapeshi, E., Michael, C., Monou, S.M., M., & Fatta Kassinos, D. (2008). *Predicted environmental concentration of selected pharmaceutical active ingredients in urban wastewater in Cyprus*. Paper presented at the International Conference on the Protection and Restoration of the Environment IX, Kefalonia, Greece.

- Ai, X., Xu, Q., Jones, M., Song, Q., Ding, S.Y., Ellingson, R.J., Himmel, M., & Rumbles, G. (2007). Photophysics of (CdSe)ZnS colloidal quantum dots in an aqueous environment stabilized with amino acids and genetically-modified proteins. *Photochemical & Photobiological Sciences*, 6(9), 1027-1033.
- Ajao, C., Andersson, M.A., Teplova, V.V., Nagy, S., Gahmberg, C.G., Andersson, L.C., Hautaniemi, M., Kakasi, B., Roivainen, M., & Salkinoja-Salonen, M. (2015). Mitochondrial toxicity of triclosan on mammalian cells. *Toxicology Reports*, 2, 624-637.
- Allmyr, M., Harden, F., Toms, L.-M.L., Mueller, J.F., McLachlan, M.S., Adolfsson-Erici, M., & Sandborgh-Englund, G. (2008). The influence of age and gender on triclosan concentrations in Australian human blood serum. *Science of the Total Environment*, 393(1), 162-167.
- Allmyr, M., McLachlan, M.S., Sandborgh-Englund, G., & Adolfsson-Erici, M. (2006). Determination of triclosan as its pentafluorobenzoyl ester in human plasma and milk using electron capture negative ionization mass spectrometry. *Analytical Chemistry*, 78, 6542-6546.
- Allwine, K.J., Thistle, H.W., Teske, M.E., & Anhold, J. (2002). The agricultural dispersal-valley drift spray drift modeling system compared with pesticide drift data. *Environmental Toxicology and Chemistry*, 21(5), 1085-1090.
- Antunes, S.C., Freitas, R., Figueira, E., Goncalves, F., & Nunes, B. (2013). Biochemical effects of acetaminophen in aquatic species: edible clams *Venerupis decussata* and *Venerupis philippinarum*. *Environmental Science and Pollution Research*, 20(9), 6658-6666.
- Bakar, N.A., Umar, A.A., Aziz, T.T., Abdullah, S.H., Salleh, M.M., Yahaya, M., & Majlis, B.Y. (2008, 25-27 November). *Synthesis of CdSe quantum dots: Effect of surfactant on the photoluminescence property*. Paper presented at the IEEE International Conference on Semiconductor Electronics, Johor Bahru.
- Barker, J.D., de Carle, D.J., & Anuras, S. (1977). Chronic excessive acetaminophen use and liver damage. *Annals of Internal Medicine*, 87(3), 299-301.
- Bera, D., Qian, L., Tseng, T.-K., & Holloway, P.H. (2010). Quantum dots and their multimodal applications: A review. *Materials*, 3, 2260-2345.
- Bhargava, H.N., & Leonard, P.A. (1996). Triclosan: applications and safety. *American Journal of Infection Control*, 24(3), 209-218.
- Binelli, A., Cogni, D., Parolini, M., Riva, C., & Provini, A. (2009a). Cytotoxic and genotoxic effects of in vitro exposure to triclosan and trimethoprim on zebra mussel (*Dreissena polymorpha*) hemocytes. *Comparative Biochemistry and Physiology Part C: Toxicology & Pharmacology*, 150(1), 50-56.

- Binelli, A., Cogni, D., Parolini, M., Riva, C., & Provini, A. (2009b). In vivo experiments for the evaluation of genotoxic and cytotoxic effects of Triclosan in Zebra mussel hemocytes. *Aquatic Toxicology*, *91*(3), 238-244.
- Brausch, J.M., & Rand, G.M. (2011). A review of personal care products in the aquatic environment: environmental concentrations and toxicity. *Chemosphere*, *82*(11), 1518-1532.
- Bruchez, M., Moronne, M., Gin, P., Weiss, S., & Alivisatos, A.P. (1998). Semiconductor nanocrystals as fluorescent biological labels. *Science*, *281*(5385), 2013-2016.
- Brus, L.E. (2007). *Chemistry and physics of semiconductor nanocrystals*. Columbia University. Retrieved from http://www.columbia.edu/cu/chemistry/fac-bios/brus/group/pdf-files/semi_nano_website_2007.pdf. Date of access: January 2018.
- Bullen, C.R., & Mulvaney, P. (2004). Nucleation and growth kinetics of CdSe nanocrystals in octadecene. *Nano Letters*, *4*(12), 2303-2307.
- Burda, C., Chen, X., Narayanan, R., & El-Sayed, M.A. (2005). Chemistry and properties of nanocrystals of different shapes. *Chemical Reviews*, *105*(4), 1025-1102.
- Canadian Environmental Protection Act, 1999. *Draft Federal Environmental Quality Guidelines, Triclosan*. Retrieved from https://www.google.co.za/url?sa=t&rct=j&q=&esrc=s&source=web&cd=1&ved=0ahUKEwit3cvxx4HWAhVnJMAKHZzXAKoQFggmMAA&url=http%3A%2F%2Fwww.ec.gc.ca%2Fese-ees%2FF6CF7AA4-1403-4ED1-8DE8-0B42BC1AA852%2FTriclosan%2520Factsheet_En.pdf&usq=AFQjCNHr7FfON1_Caz8IS0Q-KvdJczqzA. Date of access: February 2018.
- Canesi, L., Ciacci, C., Lorusso, L.C., Betti, M., Gallo, G., Pojana, G., & Marcomini, A. (2007). Effects of triclosan on mytilus galloprovincialis hemocyte function and digestive gland enzyme activities: possible modes of action on non target organisms. *Comparative Biochemistry and Physiology Part C: Toxicology & Pharmacology*, *145*(3), 464-472.
- Capdevielle, M., Van Egmond, R., Whelan, M., Versteeg, D., Hofmann-Kamensky, M., Inauen, J., Cunningham, V., & Woltering, D. (2008). Consideration of exposure and species sensitivity of triclosan in the freshwater environment. *Integrated Environmental Assessment and Management*, *4*(1), 15-23.
- Carlsson, C., Johansson, A.K., Alvan, G., Bergman, K., & Kühler, T. (2006). Are pharmaceuticals potent environmental pollutants?: Part I: Environmental risk assessments of selected active pharmaceutical ingredients. *Science of the Total Environment*, *364*(1), 67-87.
- Carrillo-Carrion, C., Cardenas, S., Simonet, B.M., & Valcarcel, M. (2009). Selective quantification of carnitine enantiomers using chiral cysteine-capped CdSe(ZnS) quantum dots. *Analytical Chemistry*, *81*(12), 4730-4733.

- Cassette, E., Helle, M., Bezdetsnaya, L., Marchal, F., Dubertret, B., & Pons, T. (2013). Design of new quantum dot materials for deep tissue infrared imaging. *Advanced Drug Delivery Reviews*, 65(5), 719-731.
- Chalew, T.E., & Halden, R.U. (2009). Environmental exposure of aquatic and terrestrial biota to triclosan and triclocarban. *Journal of the American Water Resources Association*, 45(1), 4-13.
- Chan, W.C., Maxwell, D.J., Gao, X., Bailey, R.E., Han, M., & Nie, S. (2002). Luminescent quantum dots for multiplexed biological detection and imaging. *Current Opinion in Biotechnology*, 13(1), 40-46.
- Chan, W.C.W., & Nie, S. (1998). Quantum dot bioconjugates for ultrasensitive nonisotopic detection. *Science*, 281(5385), 2016-2018.
- Chen, L., Wang, X., Lu, W., Wu, X., & Li, J. (2016). Molecular imprinting: perspectives and applications. *Chemical Society Reviews*, 45(8), 2137-2211.
- Chen, L., Xu, S., & Li, J. (2011). Recent advances in molecular imprinting technology: current status, challenges and highlighted applications. *Chemical Society Reviews*, 40(5), 2922-2942.
- Chen, N., He, Y., Su, Y., Li, X., Huang, Q., Wang, H., Zhang, X., Tai, R., & Fan, C. (2012). The cytotoxicity of cadmium-based quantum dots. *Biomaterials*, 33(5), 1238-1244.
- Chen, Y., & Rosenzweig, Z. (2002). Luminescent CdS quantum dots as selective ion probes. *Analytical Chemistry*, 74(19), 5132-5138.
- Cheng, P.P.H., Silvester, D., Wang, G., Kalyuzhny, G., Douglas, A., & Murray, R.W. (2006). Dynamic and static quenching of fluorescence by 1-4 nm diameter gold monolayer-protected clusters. *The Journal of Physical Chemistry B*, 110(10), 4637-4644.
- Chidawanyika, W., Litwinski, C., Antunes, E., & Nyokong, T. (2010). Photophysical study of a covalently linked quantum dot-low symmetry phthalocyanine conjugate. *Journal of Photochemistry and Photobiology A: Chemistry*, 212(1), 27-35.
- Cingarapu, S., Yang, Z., Sorensen, C.M., & Klabunde, K.J. (2012). Synthesis of CdSe/ZnS and CdTe/ZnS quantum dots: refined digestive ripening. *Journal of Nanomaterials*, 2012, 1-12.
- Ciniglia, C., Cascone, C., Giudice, R.L., Pinto, G., & Pollio, A. (2005). Application of methods for assessing the geno-and cytotoxicity of triclosan to *C. ehrenbergii*. *Journal of Hazardous Materials*, 122(3), 227-232.
- Corcione, C.E., & Frigione, M. (2012). Characterization of nanocomposites by thermal analysis. *Materials*, 5(12), 2960-2980.
- Cordero, S., Carson, P., Estabrook, R., Strouse, G., & Buratto, S. (2000). Photo-activated luminescence of CdSe quantum dot monolayers. *The Journal of Physical Chemistry B*, 104(51), 12137-12142.

- Cormack, P.A., & Elorza, A.Z. (2004). Molecularly imprinted polymers: synthesis and characterisation. *Journal of Chromatography B*, 804(1), 173-182.
- Crofton, K.M., Paul, K.B., DeVito, M.J., & Hedge, J.M. (2007). Short-term in vivo exposure to the water contaminant triclosan: evidence for disruption of thyroxine. *Environmental Toxicology and Pharmacology*, 24(2), 194-197.
- Dabbousi, B., Rodriguez-Viejo, J., Mikulec, F.V., Heine, J., Mattoussi, H., Ober, R., Jensen, K., & Bawendi, M. (1997). (CdSe) ZnS core-shell quantum dots: synthesis and characterization of a size series of highly luminescent nanocrystallites. *The Journal of Physical Chemistry B*, 101(46), 9463-9475.
- Dann, A.B., & Hontela, A. (2011). Triclosan: environmental exposure, toxicity and mechanisms of action. *Journal of Applied Toxicology*, 31(4), 285-311.
- David, A., & Pancharatna, K. (2009). Effects of acetaminophen (paracetamol) in the embryonic development of zebrafish, *Danio rerio*. *Journal of Applied Toxicology*, 29(7), 597-602.
- de García, S.A.O., Pinto, G.P., García-Encina, P.A., & Irusta-Mata, R. (2014). Ecotoxicity and environmental risk assessment of pharmaceuticals and personal care products in aquatic environments and wastewater treatment plants. *Ecotoxicology*, 23(8), 1517-1533.
- de García, S.O., García-Encina, P., & Irusta-Mata, R. (2011). Environmental risk assessment (ERA) of pharmaceuticals and personal care products (PPCPs) using ecotoxicity tests. *Ecotoxicology*, 23(8), 1-8.
- Delgado-Perez, T., Bouchet, L.M., de la Guardia, M., Galian, R.E., & Perez-Prieto, J. (2013). Sensing chiral drugs by using CdSe/ZnS nanoparticles capped with N-acetyl-L-cysteine methyl ester. *A European Journal of Chemistry*, 19(33), 11068-11076.
- Delorenzo, M.E., & Fleming, J. (2008a). Individual and mixture effects of selected pharmaceuticals and personal care products on the marine phytoplankton species *Dunaliella tertiolecta*. *Archives of Environmental Contamination and Toxicology*, 54(2), 203-210.
- Delorenzo, M.E., Keller, J.M., Arthur, C.D., Finnegan, M.C., Harper, H.E., Winder, V.L., & Zdankiewicz, D.L. (2008b). Toxicity of the antimicrobial compound triclosan and formation of the metabolite methyl-triclosan in estuarine systems. *Environmental Toxicology*, 23(2), 224-232.
- Deng, M., Ma, Y., Huang, S., Hu, G., & Wang, L. (2011). Monodisperse upconversion NaYF₄ nanocrystals: syntheses and bioapplications. *Nano Research*, 4(7), 685-694.
- Dhillon, G.S., Kaur, S., Pulicharla, R., Brar, S.K., Cledón, M., Verma, M., & Surampalli, R.Y. (2015). Triclosan: current status, occurrence, environmental risks and bioaccumulation potential. *International Journal of Environmental Research and Public Health*, 12(5), 5657-5684.

- Diltemiz, S.E., Say, R., Büyüktiryaki, S., Hür, D., Denizli, A., & Ersöz, A. (2008). Quantum dot nanocrystals having guanosine imprinted nanoshell for DNA recognition. *Talanta*, 75(4), 890-896.
- Dong, W., Shen, H.-B., Liu, X.-H., Li, M.-J., & Li, L.-S. (2011). CdSe/ZnS quantum dots based fluorescence quenching method for determination of paeonol. *Spectrochimica Acta Part A: Molecular and Biomolecular Spectroscopy*, 78(1), 537-542.
- Du, H., Fuh, R.C.A., Li, J., Corkan, L.A., & Lindsey, J.S. (1998). PhotochemCAD: A computer-aided design and research tool in photochemistry. *Photochemistry and Photobiology*, 68(2), 141-142.
- Du Preez, J., & Yang, W. (2003). Improving the aqueous solubility of triclosan by solubilization, complexation, and in situ salt formation. *Journal of Cosmetic Science*, 54, 537-550.
- Duong, H.D., Reddy, C.V.G., Rhee, J.I., & Vo-Dinh, T. (2011). Amplification of fluorescence emission of CdSe/ZnS QDs entrapped in a sol-gel matrix, a new approach for detection of trace level of PAHs. *Sensors and Actuators B: Chemical*, 157(1), 139-145.
- Dussault, E.B., Balakrishnan, V.K., Sverko, E., Solomon, K.R., & Sibley, P.K. (2008). Toxicity of human pharmaceuticals and personal care products to benthic invertebrates. *Environmental Toxicology and Chemistry*, 27(2), 425-432.
- Ekimov, A., Efros, A.L., & Onushchenko, A. (1985). Quantum size effect in semiconductor microcrystals. *Solid State Communications*, 56(11), 921-924.
- Ekimov, A., & Onushchenko, A. (1982). Quantum size effect in the optical-spectra of semiconductor micro-crystals. *Soviet Physics Semiconductors-Ussr*, 16(7), 775-778.
- Escher, B.I., Baumgartner, R., Koller, M., Treyer, K., Lienert, J., & McArdell, C.S. (2011). Environmental toxicology and risk assessment of pharmaceuticals from hospital wastewater. *Water Research*, 45(1), 75-92.
- Eychmüller, A., Mews, A., & Weller, H. (1993). A quantum dot quantum well: CdS/HgS/CdS. *Chemical Physics Letters*, 208(1), 59-62.
- Eychmüller, A., & Rogach, A.L. (2000). Chemistry and photophysics of thiol-stabilized II-VI semiconductor nanocrystals. *Pure and Applied Chemistry*, 72(1-2), 179-188.
- Fang, C., Yi, C., Wang, Y., Cao, Y., & Liu, X. (2009). Electrochemical sensor based on molecular imprinting by photo-sensitive polymers. *Biosensors and Bioelectronics*, 24(10), 3164-3169.
- Farkhani, S.M., & Valizadeh, A. (2014). Review: three synthesis methods of CdX (X = Se, S or Te) quantum dots. *IET Nanobiotechnology*, 8(2), 59-76.
- Farré, M., Asperger, D., Kantiani, L., González, S., Petrovic, M., & Barceló, D. (2008). Assessment of the acute toxicity of triclosan and methyl triclosan in wastewater based on the bioluminescence inhibition of *Vibrio fischeri*. *Analytical and Bioanalytical Chemistry*, 390(8), 1999-2007.

- Fent, K., Weston, A.A., & Caminada, D. (2006). Ecotoxicology of human pharmaceuticals. *Aquatic Toxicology*, 76(2), 122-159.
- Fery-Forgues, S., & Lavabre, D. (1999). Are fluorescence quantum yields so tricky to measure? A demonstration using familiar stationery products. *Journal of Chemical Education*, 76(9), 1260.
- Figueiredo, L., Erny, G.L., Santos, L., & Alves, A. (2016). Applications of molecularly imprinted polymers to the analysis and removal of personal care products: A review. *Talanta*, 146, 754-765.
- Förster, T. (1959). 10th Spiers Memorial Lecture. Transfer mechanisms of electronic excitation. *Discussions of the Faraday Society*, 27, 7-17.
- Fort, D.J., Rogers, R.L., Gorsuch, J.W., Navarro, L.T., Peter, R., & Plautz, J.R. (2009). Triclosan and anuran metamorphosis: no effect on thyroid-mediated metamorphosis in *xenopus laevis*. *Toxicological Sciences*, 113(2), 392-400.
- Fraker, S.L., & Smith, G.R. (2004). Direct and interactive effects of ecologically relevant concentrations of organic wastewater contaminants on *rana pipiens* tadpoles. *Environmental Toxicology*, 19(3), 250-256.
- Frasco, M.F., & Chaniotakis, N. (2009). Semiconductor quantum dots in chemical sensors and biosensors. *Sensors*, 9(9), 7266-7286.
- Frasco, M.F., & Chaniotakis, N. (2010). Bioconjugated quantum dots as fluorescent probes for bioanalytical applications. *Analytical and Bioanalytical Chemistry*, 396(1), 229-240.
- Galian, R.E., & de la Guardia, M. (2009). The use of quantum dots in organic chemistry. *TrAC Trends in Analytical Chemistry*, 28(3), 279-291.
- Galus, M., Jeyaranjan, J., Smith, E., Li, H., Metcalfe, C., & Wilson, J.Y. (2013). Chronic effects of exposure to a pharmaceutical mixture and municipal wastewater in zebrafish. *Aquatic Toxicology*, 132, 212-222.
- Gao, X., Cui, Y., Levenson, R.M., Chung, L.W., & Nie, S. (2004). In vivo cancer targeting and imaging with semiconductor quantum dots. *Nature Biotechnology*, 22(8), 969-976.
- Gaponik, N., Talapin, D.V., Rogach, A.L., Hoppe, K., Shevchenko, E.V., Kornowski, A., Eychmueller, A., & Weller, H. (2002). Thiol-capping of CdTe nanocrystals: an alternative to organometallic synthetic routes. *Journal of Physical Chemistry B*, 106(29), 7177-7185.
- Gerion, D., Pinaud, F., Williams, S.C., Parak, W.J., Zanchet, D., Weiss, S., & Alivisatos, A.P. (2001). Synthesis and properties of biocompatible water-soluble silica-coated CdSe/ZnS semiconductor quantum dots. *The Journal of Physical Chemistry B*, 105(37), 8861-8871.

- Ghosh Chaudhuri, R., & Paria, S. (2012). Core/shell nanoparticles: classes, properties, synthesis mechanisms, characterization, and applications. *Chemical Reviews*, 112(4), 2373-2433.
- Gill, R., Zayats, M., & Willner, I. (2008). Semiconductor quantum dots for bioanalysis. *Angewandte Chemie International Edition*, 47(40), 7602-7625.
- Girão, A.V., Caputo, G., & Ferro, M.C. (2017). Application of scanning electron microscopy–energy dispersive X-ray spectroscopy (SEM-EDS). *Comprehensive Analytical Chemistry*, 75, 153-168.
- Gómez, M.J., Bueno, M.J.M., Lacorte, S., Fernández-Alba, A.R., & Agüera, A. (2007). Pilot survey monitoring pharmaceuticals and related compounds in a sewage treatment plant located on the Mediterranean coast. *Chemosphere*, 66(6), 993-1002.
- Gouadec, G., & Colombari, P. (2007). Raman spectroscopy of nanomaterials: how spectra relate to disorder, particle size and mechanical properties. *Progress in Crystal Growth and Characterization of Materials*, 53(1), 1-56.
- Graf, C., Vossen, D.L., Imhof, A., & van Blaaderen, A. (2003). A general method to coat colloidal particles with silica. *Langmuir*, 19(17), 6693-6700.
- Greenwood, M. A. (2007). Are Quantum Dots on the Brink of Their Big Break? *Photonics Spectra*, 41(5), 60-66.
- Grujić, S., Vasiljević, T., & Laušević, M. (2009). Determination of multiple pharmaceutical classes in surface and ground waters by liquid chromatography–ion trap–tandem mass spectrometry. *Journal of Chromatography A*, 1216(25), 4989-5000.
- Gupta, D.K., Verma, M., Sharma, K., & Saxena, N.S. (2017). Synthesis, characterization and optical properties of CdSe/CdS and CdSe/ZnS core-shell nanoparticles. *Indian Journal of Pure & Applied Physics*, 55(2), 113-121.
- Gupta, T. (2011). Exposure science: monitoring environmental contaminants. In J. O. Nriagu (Ed.), *Encyclopedia of Environmental Health*, Elsevier (pp. 675). Burlington.
- Hambrock, J., Birkner, A., & Fischer, R.A. (2001). Synthesis of CdSe nanoparticles using various organometallic cadmium precursors. *Journal of Materials Chemistry*, 11(12), 3197-3201.
- Hardman, R. (2006). A Toxicologic Review of Quantum Dots: Toxicity Depends on Physicochemical and Environmental Factors. *Environmental Health Perspectives*, 114(2), 165-172.
- Harnagea-Theophilus, E., Gadd, S.L., Knight-Trent, A.H., DeGeorge, G.L., & Miller, M.R. (1999). Acetaminophen-induced proliferation of breast cancer cells involves estrogen receptors. *Toxicology and Applied Pharmacology*, 155(3), 273-279.

- Henschel, K.-P., Wenzel, A., Diedrich, M., & Fliedner, A. (1997). Environmental hazard assessment of pharmaceuticals. *Regulatory Toxicology and Pharmacology*, 25(3), 220-225.
- Hines, M.A., & Guyot-Sionnest, P. (1996). Synthesis and characterization of strongly luminescing ZnS-capped CdSe nanocrystals. *The Journal of Physical Chemistry*, 100(2), 468-471.
- Holthoff, E.L., Stratis-Cullum, D.N., & Hankus, M.E. (2011). A nanosensor for TNT detection based on molecularly imprinted polymers and surface enhanced Raman scattering. *Sensors*, 11(3), 2700-2714.
- Hu, J., Zhou, L., Zhou, Q.W., Wei, F., Zhang, L.L., & Chen, J.M. (2012). *Biodegradation of paracetamol by aerobic granules in a sequencing batch reactor (SBR)*. Paper presented at the Advanced Materials Research.
- Huber, M.M., Göbel, A., Joss, A., Hermann, N., Löffler, D., McArdell, C.S., Ried, A., Siegrist, H., Ternes, T.A., & von Gunten, U. (2005). Oxidation of pharmaceuticals during ozonation of municipal wastewater effluents: a pilot study. *Environmental Science & Technology*, 39(11), 4290-4299.
- Huheey, J.E., Keiter, E., & Keiter, R. (1993). *Inorganic Chemistry-Principles of Structure and Reactivity*, Harper Collins College Publishers, New York.
- Hung, Y.Y. (1982). Shearography: a new optical method for strain measurement and nondestructive testing. *Optical Engineering*, 21(3), 391-395.
- Ishibashi, H., Matsumura, N., Hirano, M., Matsuoka, M., Shiratsuchi, H., Ishibashi, Y., Takao, Y., & Arizono, K. (2004). Effects of triclosan on the early life stages and reproduction of medaka *Oryzias latipes* and induction of hepatic vitellogenin. *Aquatic Toxicology*, 67(2), 167-179.
- Ishihama, Y., Nakamura, M., Miwa, T., Kajima, T., & Asakawa, N. (2002). A rapid method for pKa determination of drugs using pressure-assisted capillary electrophoresis with photodiode array detection in drug discovery. *Journal of Pharmaceutical Sciences*, 91(4), 933-942.
- Jaiswal, J.K., Mattoussi, H., Mauro, J.M., & Simon, S.M. (2003). Long-term multiple color imaging of live cells using quantum dot bioconjugates. *Nature Biotechnology*, 21(1), 47-51.
- Jensen, H., Pedersen, J.H., Jorgensen, J., Pedersen, J.S., Joensen, K.D., Iversen, S.B., & Sogaard, E. (2006). Determination of size distributions in nanosized powders by TEM, XRD, and SAXS. *Journal of Experimental Nanoscience*, 1(3), 355-373.
- Jin, W.J., Fernández-Argüelles, M.T., Costa-Fernández, J.M., Pereiro, R., & Sanz-Medel, A. (2005). Photoactivated luminescent CdSe quantum dots as sensitive cyanide probes in aqueous solutions. *Chemical Communications*, 7, 883-885.

- Jones, R.D., Jampani, H.B., Newman, J.L., & Lee, A.S. (2000). Triclosan: a review of effectiveness and safety in health care settings. *American Journal of Infection Control*, 28(2), 184-196.
- Kempe, M., & Mosbach, K. (1995). Molecular imprinting used for chiral separations. *Journal of Chromatography A*, 694(1), 3-13.
- Kim, J.-W., Ishibashi, H., Yamauchi, R., Ichikawa, N., Takao, Y., Hirano, M., Koga, M., & Arizono, K. (2009). Acute toxicity of pharmaceutical and personal care products on freshwater crustacean (*Thamnocephalus platyurus*) and fish (*Oryzias latipes*). *The Journal of Toxicological Sciences*, 34(2), 227-232.
- Kim, J., Park, J., Kim, P.-G., Lee, C., Choi, K., & Choi, K. (2010). Implication of global environmental changes on chemical toxicity-effect of water temperature, pH, and ultraviolet B irradiation on acute toxicity of several pharmaceuticals in *Daphnia magna*. *Ecotoxicology*, 19(4), 662-669.
- Kim, Y., Choi, K., Jung, J., Park, S., Kim, P.G., & Park, J. (2007). Aquatic toxicity of acetaminophen, carbamazepine, cimetidine, diltiazem and six major sulfonamides, and their potential ecological risks in Korea. *Environment International*, 33(3), 370-375.
- Kubin, R.F., & Fletcher, A.N. (1982). Fluorescence quantum yields of some rhodamine dyes. *Journal of Luminescence*, 27(4), 455-462.
- Kühn, R., Pattard, M., Pernak, K.-D., & Winter, A. (1989). Results of the harmful effects of selected water pollutants (anilines, phenols, aliphatic compounds) to *Daphnia magna*. *Water Research*, 23(4), 495-499.
- Kuzyniak, W., Adegoke, O., Sekhosana, K., D'Souza, S., Tshangana, S.C., Hoffmann, B., Ermilov, E.A., Nyokong, T., & Höpfner, M. (2014). Synthesis and characterization of quantum dots designed for biomedical use. *International Journal of Pharmaceutics*, 466(1), 382-389.
- Lakowicz, J. (1999). *Principles of Fluorescence Spectroscopy*, Kluwer Academic Plenum Press (2nd ed.). New York.
- Law, W.C., Yong, K.T., Roy, I., Ding, H., Hu, R., Zhao, W., & Prasad, P.N. (2009). Aqueous-Phase Synthesis of Highly Luminescent CdTe/ZnTe Core/Shell Quantum Dots Optimized for Targeted Bioimaging. *Small*, 5(11), 1302-1310.
- Lee, B. (2003). Review of the present status of optical fiber sensors. *Optical Fiber Technology*, 9(2), 57-79.
- Li, J.J., Wang, Y.A., Guo, W., Keay, J.C., Mishima, T.D., Johnson, M.B., & Peng, X. (2003). Large-scale synthesis of nearly monodisperse CdSe/CdS core/shell nanocrystals using air-stable reagents via successive ion layer adsorption and reaction. *Journal of the American Chemical Society*, 125(41), 12567-12575.

- Li, Z., Dong, C., Tang, L., Zhu, X., Chen, H., & Ren, J. (2011). Aqueous synthesis of CdTe/CdS/ZnS quantum dots and their optical and chemical properties. *Luminescence*, 26(6), 439-448.
- Liu, L., Guo, X., Li, Y., & Zhong, X. (2010). Bifunctional multidentate ligand modified highly stable water-soluble quantum dots. *Inorganic Chemistry*, 49(8), 3768-3775.
- Liu, Q., Zhou, Q., & Jiang, G. (2014). Nanomaterials for analysis and monitoring of emerging chemical pollutants. *TrAC Trends in Analytical Chemistry*, 58, 10-22.
- Liz-Marzán, L.M., Giersig, M., & Mulvaney, P. (1996). Synthesis of nanosized gold– silica core– shell particles. *Langmuir*, 12(18), 4329-4335.
- Lofgreen, J.E., & Ozin, G.A. (2014). Controlling morphology and porosity to improve performance of molecularly imprinted sol–gel silica. *Chemical Society Reviews*, 43(3), 911-933.
- Lopez de Alda, M.a.J., Díaz-Cruz, S., Petrovic, M., & Barceló, D. (2003). Liquid chromatography–(tandem) mass spectrometry of selected emerging pollutants (steroid sex hormones, drugs and alkylphenolic surfactants) in the aquatic environment. *Journal of Chromatography A*, 1000(1-2), 503-526.
- Ma, C., Moore, D., Li, J., & Wang, Z.L. (2003). Nanobelts, nanocombs, and nanowindmills of wurtzite ZnS. *Advanced Materials*, 15(3), 228-231.
- Ma, Y., Xu, S., Wang, S., & Wang, L. (2015). Luminescent molecularly-imprinted polymer nanocomposites for sensitive detection. *TrAC Trends in Analytical Chemistry*, 67, 209-216.
- Martienssen, W., & Warlimont, H. (2005). *Handbook of Condensed Mater and Materials Data*, (Vol. 18, pp. 1120): Springer, Heidelberg.
- Martynenko, I.V., Orlova, A.O., Maslov, V.G., Baranov, A.V., Fedorov, A.V., & Artemyev, M. (2013). Energy transfer in complexes of water-soluble quantum dots and chlorin e6 molecules in different environments. *Beilstein Journal of Nanotechnology*, 4, 895-902.
- Mattoussi, H., Palui, G., & Na, H.B. (2012). Luminescent quantum dots as platforms for probing in vitro and in vivo biological processes. *Advanced Drug Delivery Reviews*, 64(2), 138-166.
- Memmert, U. (2006). Triclosan: effects on the development of sediment-dwelling larvae of *chironomus riparius* in a water-sediment system with spiked sediment. *RCC Ltd., Itingen, Switzerland*.
- Michalet, X., Pinaud, F.F., Bentolila, L.A., Tsay, J.M., Doose, S., Li, J.J., Sundaresan, G., Wu, A.M., Gambhir, S.S., & Weiss, S. (2005). Quantum dots for live cells, in vivo imaging, and diagnostics. *Science*, 307(5709), 538-544.

- Micic, O.I., Curtis, C.J., Jones, K.M., Sprague, J.R., & Nozik, A.J. (1994). Synthesis and characterization of InP quantum dots. *The Journal of Physical Chemistry*, 98(19), 4966-4969.
- Modani, S., Kharwade, M., & Nijhawan, M. (2013). Quantum dots: a novelty of medical field with multiple applications. *International Journal of Current Pharmaceutical Research*, 5(4), 55-59.
- Moore, D., & Wang, Z.L. (2006). Growth of anisotropic one-dimensional ZnS nanostructures. *Journal of Materials Chemistry*, 16(40), 3898-3905.
- Morasch, B., Bonvin, F., Reiser, H., Grandjean, D., De Alencastro, L.F., Perazzolo, C., Chèvre, N., & Kohn, T. (2010). Occurrence and fate of micropollutants in the vidy bay of lake Geneva, Switzerland. Part II: micropollutant removal between wastewater and raw drinking water. *Environmental Toxicology and Chemistry*, 29(8), 1658-1668.
- Muir, N., Nichols, J., Stillings, M., & Sykes, J. (1997). Comparative bioavailability of aspirin and paracetamol following single dose administration of soluble and plain tablets. *Current Medical Research and Opinion*, 13(9), 491-500.
- Mulvaney, P., Liz-Marzan, L., Giersig, M., & Ung, T. (2000). Silica encapsulation of quantum dots and metal clusters. *Journal of Materials Chemistry*, 10(6), 1259-1270.
- Murcia, M.J., Shaw, D.L., Long, E.C., & Naumann, C.A. (2008). Fluorescence correlation spectroscopy of CdSe/ZnS quantum dot optical bioimaging probes with ultra-thin biocompatible coatings. *Optics Communications*, 281(7), 1771-1780.
- Murphy, C. J. (2002). Optical sensing with quantum dots. *Analytical Chemistry*, 74, 520A–526A.
- Murray, C., Norris, D.J., & Bawendi, M.G. (1993). Synthesis and characterization of nearly monodisperse CdE (E= sulfur, selenium, tellurium) semiconductor nanocrystallites. *Journal of the American Chemical Society*, 115(19), 8706-8715.
- Murray, C.B., Kagan, C., & Bawendi, M. (2000). Synthesis and characterization of monodisperse nanocrystals and close-packed nanocrystal assemblies. *Annual Review of Materials Science*, 30(1), 545-610.
- Nann, T., & Mulvaney, P. (2004). Single quantum dots in spherical silica particles. *Angewandte Chemie International Edition*, 43(40), 5393-5396.
- Nassef, M., Kim, S.G., Seki, M., Kang, I.J., Hano, T., Shimasaki, Y., & Oshima, Y. (2010). In ovo nanoinjection of triclosan, diclofenac and carbamazepine affects embryonic development of medaka fish (*Oryzias latipes*). *Chemosphere*, 79(9), 966-973.
- Nassef, M., Matsumoto, S., Seki, M., Kang, I.J., Moroishi, J., Shimasaki, Y., & Oshima, Y. (2009). Pharmaceuticals and personal care products toxicity to Japanese medaka fish (*Oryzias latipes*). *Journal of the Faculty of Agriculture Kyushu University*, 54(2), 407-411.

- Noh, M., Kim, T., Lee, H., Kim, C.-K., Joo, S.-W., & Lee, K. (2010). Fluorescence quenching caused by aggregation of water-soluble CdSe quantum dots. *Colloids and Surfaces A: Physicochemical and Engineering Aspects*, 359(1), 39-44.
- Norris, D.J. (1995). *Measurement and assignment of the size-dependent optical spectrum in cadmium selenide (CdSe) quantum dots*. Massachusetts Institute of Technology.
- Nsibande, S., & Forbes, P. (2016). Fluorescence detection of pesticides using quantum dot materials—a review. *Analytica Chimica Acta*, 945, 9-22.
- Oliveira, R., Domingues, I., Koppe Grisolia, C., & Soares, A.M. (2009). Effects of triclosan on zebrafish early-life stages and adults. *Environmental Science and Pollution Research*, 16(6), 679-688.
- Orvos, D.R., Versteeg, D.J., Inauen, J., Capdevielle, M., Rothenstein, A., & Cunningham, V. (2002). Aquatic toxicity of triclosan. *Environmental Toxicology and Chemistry*, 21(7), 1338-1349.
- Palenske, N.M., Nallani, G.C., & Dzialowski, E.M. (2010). Physiological effects and bioconcentration of triclosan on amphibian larvae. *Comparative Biochemistry and Physiology Part C: Toxicology & Pharmacology*, 152(2), 232-240.
- Pandurangan, D.K., & Mounika, K. (2012). Quantum dot aptamers-an emerging technology with wide scope in pharmacy. *International Journal of Pharmacy and Pharmaceutical Sciences*, 4(3), 24-31.
- Parrott, J., & Bennie, D. (2009). Life-cycle exposure of fathead minnows to a mixture of six common pharmaceuticals and triclosan. *Journal of Toxicology and Environmental Health, Part A*, 72(10), 633-641.
- Pellegrino, T., Manna, L., Kudera, S., Liedl, T., Koktysh, D., Rogach, A.L., Keller, S., Rädler, J., Natile, G., & Parak, W.J. (2004). Hydrophobic nanocrystals coated with an amphiphilic polymer shell: a general route to water soluble nanocrystals. *Nano Letters*, 4(4), 703-707.
- Peng, Z.A., & Peng, X. (2001). Formation of high-quality CdTe, CdSe, and CdS nanocrystals using CdO as precursor. *Journal of the American Chemical Society*, 123(1), 183-184.
- Perazzolo, C., Morasch, B., Kohn, T., Magnet, A., Thonney, D., & Chèvre, N. (2010). Occurrence and fate of micropollutants in the Vidy Bay of Lake Geneva, Switzerland. Part I: priority list for environmental risk assessment of pharmaceuticals. *Environmental Toxicology and Chemistry*, 29(8), 1649-1657.
- Phillips, P.J., Smith, S.G., Kolpin, D.W., Zaugg, S.D., Buxton, H.T., Furlong, E.T., Esposito, K., & Stinson, B. (2010). Pharmaceutical formulation facilities as sources of opioids and other pharmaceuticals to wastewater treatment plant effluents. *Environmental Science & Technology*, 44(13), 4910-4916.

- Pichon, V., & Chapuis-Hugon, F. (2008). Role of molecularly imprinted polymers for selective determination of environmental pollutants—A review. *Analytica Chimica Acta*, 622(1), 48-61.
- Pong, B.K., Trout, B.L., & Lee, J.Y. (2008). Modified ligand-exchange for efficient solubilization of CdSe/ZnS quantum dots in water: a procedure guided by computational studies. *Langmuir*, 24(10), 5270-5276.
- Rahman, M., & Harmon, H.J. (2006). Absorbance change and static quenching of fluorescence of meso-tetra (4-sulfonatophenyl) porphyrin (TPPS) by trinitrotoluene (TNT). *Spectrochimica Acta Part A: Molecular and Biomolecular Spectroscopy*, 65(3-4), 901-906.
- Rahman, S.A., Ariffin, N., Yusof, N.A., Abdullah, J., Zubir, Z.A., Aziz, N.M.A.N.A., Azmi, N.E., Sidek, H., & Ramli, N.I. (2014). Synthesis and surface modification of biocompatible water soluble core-shell quantum dots. *Advanced Materials Research*, 879, 184-190.
- Raut, S.A., & Angus, R.A. (2010). Triclosan has endocrine-disrupting effects in male western mosquitofish, *Gambusia affinis*. *Environmental Toxicology and Chemistry*, 29(6), 1287-1291.
- Ray, S.S., & Okamoto, M. (2003). Polymer/layered silicate nanocomposites: a review from preparation to processing. *Progress in Polymer Science*, 28(11), 1539-1641.
- Reddy, S.M., Hawkins, D.M., Phan, Q.T., Stevenson, D., & Warriner, K. (2013). Protein detection using hydrogel-based molecularly imprinted polymers integrated with dual polarisation interferometry. *Sensors and Actuators B: Chemical*, 176, 190-197.
- Reed, M., Randall, J., Aggarwal, R., Matyi, R., Moore, T., & Wetsel, A. (1988). Observation of discrete electronic states in a zero-dimensional semiconductor nanostructure. *Physical Review Letters*, 60(6), 535.
- Rodricks, J.V., Swenberg, J.A., Borzelleca, J.F., Maronpot, R.R., & Shipp, A.M. (2010). Triclosan: a critical review of the experimental data and development of margins of safety for consumer products. *Critical Reviews in Toxicology*, 40(5), 422-484.
- Rogach, A.L. (2008). *Semiconductor nanocrystal quantum dots*. Wien-New York: Springer.
- Rogach, A.L., Kornowski, A., Gao, M., Eychmüller, A., & Weller, H. (1999). Synthesis and characterization of a size series of extremely small thiol-stabilized CdSe nanocrystals. *The Journal of Physical Chemistry B*, 103(16), 3065-3069.
- Rossner, A., Snyder, S.A., & Knappe, D.R. (2009). Removal of emerging contaminants of concern by alternative adsorbents. *Water Research*, 43(15), 3787-3796.
- Sabaliunas, D., Webb, S.F., Hauk, A., Jacob, M., & Eckhoff, W.S. (2003). Environmental fate of triclosan in the River Aire Basin, UK. *Water Research*, 37(13), 3145-3154.
- Samsøe-Petersen, L., Winther-Nielsen, M., & Madsen, T. (2003). *Fate and effects of triclosan*. Danish Environmental Protection Agency, No. 861, 1-47.

- Sapsford, K.E., Berti, L., & Medintz, I.L. (2006a). Materials for fluorescence resonance energy transfer analysis: beyond traditional donor–acceptor combinations. *Angewandte Chemie International Edition*, 45(28), 4562-4589.
- Sapsford, K.E., Pons, T., Medintz, I.L., & Mattoussi, H. (2006b). Biosensing with luminescent semiconductor quantum dots. *Sensors*, 6(8), 925-953.
- SCCS. (2010) *Opinion on triclosan – antimicrobial resistance*. Retrieved from http://ec.europa.eu/health/scientific_committees/consumer_safety/index_en.htm. Date of access: January 2018.
- Schirhagl, R. (2014). Bioapplications for molecularly imprinted polymers. *Analytical Chemistry*, 86(1), 250-261.
- Sharma, R., Bisen, D., Shukla, U., & Sharma, B. (2012). X-ray diffraction: a powerful method of characterizing nanomaterials. *Recent Research in Science and Technology*, 4(8), 77-79.
- Skoog, D.A., Holler, F.J., & Crouch, S.R. (2017). *Principles of instrumental analysis* (7th ed.): Cengage learning.
- Smith, A.M., Duan, H., Mohs, A.M., & Nie, S. (2008). Bioconjugated quantum dots for in vivo molecular and cellular imaging. *Advanced Drug Delivery Reviews*, 60(11), 1226-1240.
- Smith, A.M., & Nie, S. (2009). Semiconductor nanocrystals: structure, properties, and band gap engineering. *Accounts of Chemical Research*, 43(2), 190-200.
- Smith, G.R., & Burgett, A.A. (2005). Effects of three organic wastewater contaminants on American toad, *Bufo americanus*, tadpoles. *Ecotoxicology*, 14(4), 477-482.
- Smyder, J.A., & Krauss, T.D. (2011). Coming attractions for semiconductor quantum dots. *Materials Today*, 14(9), 382-387.
- Son, H.-S., Ko, G., & Zoh, K.-D. (2009). Kinetics and mechanism of photolysis and TiO₂ photocatalysis of triclosan. *Journal of Hazardous Materials*, 166(2), 954-960.
- Stanisavljevic, M., Krizkova, S., Vaculovicova, M., Kizek, R., & Adam, V. (2015). Quantum dots-fluorescence resonance energy transfer-based nanosensors and their application. *Biosensors and Bioelectronics*, 74, 562-574.
- Stasinakis, A.S., Petalas, A.V., Mamais, D., Thomaidis, N.S., Gatidou, G., & Lekkas, T.D. (2007). Investigation of triclosan fate and toxicity in continuous-flow activated sludge systems. *Chemosphere*, 68(2), 375-381.
- Steigerwald, M.L., & Brus, L.E. (1990). Semiconductor crystallites: a class of large molecules. *Accounts of Chemical Research*, 23(6), 183-188.
- Stevens, K.J., Kim, S.Y., Adhikari, S., Vadapalli, V., & Venables, B.J. (2009). Effects of triclosan on seed germination and seedling development of three wetland plants: *Sesbania herbacea*, *Eclipta prostrata*, and *Bidens frondosa*. *Environmental Toxicology and Chemistry*, 28(12), 2598-2609.

- Stickler, D.J., & Jones, G.L. (2008). Reduced susceptibility of *Proteus mirabilis* to triclosan. *Antimicrobial Agents and Chemotherapy*, 52(3), 991-994.
- Stöber, W., Fink, A., & Bohn, E. (1968). Controlled growth of monodisperse silica spheres in the micron size range. *Journal of Colloid and Interface Science*, 26(1), 62-69.
- Stsiapura, V., Sukhanova, A., Baranov, A., Artemyev, M., Kulakovich, O., Oleinikov, V., Pluot, M., Cohen, J.H., & Nabiev, I. (2006). DNA-assisted formation of quasi-nanowires from fluorescent CdSe/ZnS nanocrystals. *Nanotechnology*, 17(2), 581.
- Su, Y., He, Y., Lu, H., Sai, L., Li, Q., Li, W., Wang, L., Shen, P., Huang, Q., & Fan, C. (2009). The cytotoxicity of cadmium based, aqueous phase-synthesized, quantum dots and its modulation by surface coating. *Biomaterials*, 30(1), 19-25.
- Sung, H.H., Chiu, Y.W., Wang, S.Y., Chen, C.M., & Huang, D.J. (2014). Acute toxicity of mixture of acetaminophen and ibuprofen to Green Neon Shrimp, *Neocaridina denticulate*. *Environmental Toxicology Pharmacology*, 38(1), 8-13.
- Talpin, D.V., Mekis, I., Götzinger, S., Kornowski, A., Benson, O., & Weller, H. (2004). CdSe/CdS/ZnS and CdSe/ZnSe/ZnS core-shell-shell nanocrystals. *The Journal of Physical Chemistry B*, 108(49), 18826-18831.
- Tatarazako, N., Ishibashi, H., Teshima, K., Kishi, K., & Arizono, K. (2004). Effects of triclosan on various aquatic organisms. *Environmental Sciences: an International Journal of Environmental Physiology and Toxicology*, 11(2), 133-140.
- Thomas, K.V., Dye, C., Schlabach, M., & Langford, K.H. (2007). Source to sink tracking of selected human pharmaceuticals from two Oslo city hospitals and a wastewater treatment works. *Journal of Environmental Monitoring*, 9(12), 1410-1418.
- Tiwari, D.K., Jin, T., & Behari, J. (2011). Bio-distribution and toxicity assessment of intravenously injected anti-HER2 antibody conjugated CdSe/ZnS quantum dots in Wistar rats. *International Journal of Nanomedicine*, 6, 463-475.
- Toxicological Summary for: Acetaminophen. (2010). Retrieved from www.health.state.mn.us/divs/eh/risk/guidance/dwec/sumacetamin.pdf. Date of access: February 2018.
- Toxicological Summary for: Triclosan. (2010). Retrieved from www.health.state.mn.us/divs/eh/risk/guidance/gw/triclosan.pdf. Date of access: February 2018.
- Valizadeh, A., Mikaeili, H., Samiei, M., Farkhani, S., Zarghami, N., kouhi, M., Akbarzadeh, A., & Davaran, S. (2012). Quantum dots: synthesis, bioapplications, and toxicity. *Nanoscale Research Letters*, 7(1), 480.
- Veldhoen, N., Skirrow, R.C., Osachoff, H., Wigmore, H., Clapson, D.J., Gunderson, M.P., Van Aggelen, G., & Helbing, C.C. (2006). The bactericidal agent triclosan modulates thyroid

- hormone-associated gene expression and disrupts postembryonic anuran development. *Aquatic Toxicology*, 80(3), 217-227.
- Wang, C., Ma, Q., Dou, W., Kanwal, S., Wang, G., Yuan, P., & Su, X. (2009a). Synthesis of aqueous CdTe quantum dots embedded silica nanoparticles and their applications as fluorescence probes. *Talanta*, 77(4), 1358-1364.
- Wang, H.-F., He, Y., Ji, T.-R., & Yan, X.-P. (2009b). Surface molecular imprinting on Mn-doped ZnS quantum dots for room-temperature phosphorescence optosensing of pentachlorophenol in water. *Analytical Chemistry*, 81(4), 1615-1621.
- Wang, L., Zhang, Y., & Zhu, Y. (2010). One-pot synthesis and strong near-infrared upconversion luminescence of poly (acrylic acid)-functionalized YF₃:Yb³⁺/Er³⁺ nanocrystals. *Nano Research*, 3(5), 317-325.
- Westerhoff, P., Yoon, Y., Snyder, S., & Wert, E.C. (2005). Fate of endocrine-disruptor, pharmaceutical, and personal care product chemicals during simulated drinking water treatment processes. *Environmental Science & Technology*, 39(17), 6649-6663.
- William, W.Y., Chang, E., Drezek, R., & Colvin, V.L. (2006). Water-soluble quantum dots for biomedical applications. *Biochemical and Biophysical Research Communications*, 348(3), 781-786.
- Wilson, B.A., Smith, V.H., deNoyelles, F., & Larive, C.K. (2003). Effects of three pharmaceutical and personal care products on natural freshwater algal assemblages. *Environmental Science & Technology*, 37(9), 1713-1719.
- Wilson, W.L., Szajowski, P., & Brus, L. (1993). Quantum confinement in size-selected, surface-oxidized silicon nanocrystals. *Science (New York, NY)*, 262(5137), 1242-1244.
- Wu, S., Zhang, L., & Chen, J. (2012). Paracetamol in the environment and its degradation by microorganisms. *Applied Microbiology and Biotechnology*, 96(4), 875-884.
- Wu, X., Liu, H., Liu, J., Haley, K.N., Treadway, J.A., Larson, J.P., Ge, N., Peale, F., & Bruchez, M.P. (2003). Immunofluorescent labeling of cancer marker Her2 and other cellular targets with semiconductor quantum dots. *Nature Biotechnology*, 21(1), 41-46.
- Wulff, G., & Biffis, A. (2001). *Molecularly imprinted polymers: Man-made mimics of antibodies and their applications in analytical chemistry*. (B. Sellergren Ed. 1st ed.). Amsterdam: Elsevier.
- Xie, R., Kolb, U., Li, J., Basché, T., & Mews, A. (2005). Synthesis and characterization of highly luminescent CdSe-Core CdS/Zn_{0.5}Cd_{0.5}S/ZnS multishell nanocrystals. *Journal of the American Chemical Society*, 127(20), 7480-7488.
- Xu, S., Lu, H., Li, J., Song, X., Wang, A., Chen, L., & Han, S. (2013). Dummy molecularly imprinted polymers-capped CdTe quantum dots for the fluorescent sensing of 2,4,6-trinitrotoluene. *ACS Applied Materials & Interfaces*, 5(16), 8146-8154.

- Yan, H., & Row, K.H. (2006). Characteristic and synthetic approach of molecularly imprinted polymer. *International Journal of Molecular Sciences*, 7(5), 155-178.
- Yang, L.H., Ying, G.G., Su, H.C., Stauber, J.L., Adams, M.S., & Binet, M.T. (2008). Growth-inhibiting effects of 12 antibacterial agents and their mixtures on the freshwater microalga *pseudokirchneriella subcapitata*. *Environmental Toxicology and Chemistry*, 27(5), 1201-1208.
- Yang, Y., Yi, C., Luo, J., Liu, R., Liu, J., Jiang, J., & Liu, X. (2011). Glucose sensors based on electrodeposition of molecularly imprinted polymeric micelles: A novel strategy for MIP sensors. *Biosensors and Bioelectronics*, 26(5), 2607-2612.
- Ye, J., Van de Broek, B., De Palma, R., Libaers, W., Clays, K., Van Roy, W., Borghs, G., & Maes, G. (2008). Surface morphology changes on silica-coated gold colloids. *Colloids and Surfaces A: Physicochemical and Engineering Aspects*, 322(1), 225-233.
- Yin, Y., & Alivisatos, A.P. (2005). Colloidal nanocrystal synthesis and the organic–inorganic interface. *Nature*, 437(7059), 664-670.
- Youn, H.C., Baral, S., & Fendler, J.H. (1988). Dihexadecyl phosphate, vesicle-stabilized and in situ generated mixed cadmium sulfide and zinc sulfide semiconductor particles: preparation and utilization for photosensitized charge separation and hydrogen generation. *The Journal of Physical Chemistry*, 92(22), 6320-6327.
- Yu, C., & Mosbach, K. (1997). Molecular imprinting utilizing an amide functional group for hydrogen bonding leading to highly efficient polymers. *The Journal of Organic Chemistry*, 62(12), 4057-4064.
- Yu, S.H., & Yoshimura, M. (2002). Shape and phase Control of ZnS nanocrystals: template fabrication of wurtzite ZnS single-crystal nanosheets and ZnO flake-like dendrites from a lamellar molecular precursor $ZnS \cdot (NH_2CH_2CH_2NH_2)_{0.5}$. *Advanced Materials*, 14(4), 296-300.
- Yu, W.W., Qu, L., Guo, W., & Peng, X. (2003). Experimental determination of the extinction coefficient of CdTe, CdSe, and CdS nanocrystals. *Chemistry of Materials*, 15(14), 2854-2860.
- Yuan, L., Zhang, J., Zhou, P., Chen, J., Wang, R., Wen, T., Li, Y., Zhou, X., & Jiang, H. (2011). Electrochemical sensor based on molecularly imprinted membranes at platinum nanoparticles-modified electrode for determination of 17 β -estradiol. *Biosensors and Bioelectronics*, 29(1), 29-33.
- Zhang, H., Wang, L.-P., Xiong, H., Hu, L., Yang, B., & Li, W. (2003). Hydrothermal synthesis for high-quality CdTe nanocrystals. *Advanced Materials*, 15(20), 1712-1715.
- Zhang, T., Stilwell, J.L., Gerion, D., Ding, L., Elboudwarej, O., Cooke, P.A., Gray, J.W., Alivisatos, A.P., & Chen, F.F. (2006). Cellular effect of high doses of silica-coated

quantum dot profiled with high throughput gene expression analysis and high content cellomics measurements. *Nano Letters*, 6(4), 800-808.

Zhang, Y., & Clapp, A. (2011). Overview of stabilizing ligands for biocompatible quantum dot nanocrystals. *Sensors*, 11(12), 11036-11055.

Zhou, H., Sasahara, H., Honma, I., Komiyama, H., & Haus, J.W. (1994). Coated semiconductor nanoparticles: the CdS/PbS system's photoluminescence properties. *Chemistry of Materials*, 6(9), 1534-1541.

Chapter 3 Literature Review

This chapter presents a review of monitoring techniques for the determination of TCS in the aquatic environment as well as TCS global environmental concentrations and its stability in water systems. In addition, developed analytical methods for the quantification of AC in the aquatic environment, pharmaceuticals and biological fluids together with the effect of water treatment processes on AC, as well as the toxicity of AC and its metabolites are reviewed.

3.1 Paper 1

This paper was formatted in accordance with the journal *TrAC Trends in Analytical Chemistry*, an Elsevier journal in which it has been published:

Montaseri, H., & Forbes, P.B.C. (2016). A review of monitoring methods for triclosan and its occurrence in aquatic environments. *TrAC Trends in Analytical Chemistry*, 85, 221-231.

Impact Factor 7.034. <https://doi.org/10.1016/j.trac.2016.09.010>



A review of monitoring methods for triclosan and its occurrence in aquatic environments



Hanieh Montaseri, Patricia B.C. Forbes *

Department of Chemistry, Faculty of Natural and Agricultural Sciences, University of Pretoria, Lynnwood Road, Pretoria 0002, South Africa

ARTICLE INFO

Keywords:

Triclosan
Personal care products
Electrochemistry
Capillary zone electrophoresis
Molecularly imprinted polymers
Chromatography-mass spectrometry
Spectrophotometry
Chemiluminescence

ABSTRACT

Triclosan is a phenyl ether with broad spectrum antimicrobial action which is employed in a great number of everyday household and personal care products including plastics, fabrics, soaps, deodorants, toothpaste, and cosmetics. There is serious concern, however, regarding this widespread use in terms of the potential environmental impacts of triclosan. Triclosan may enter the aquatic environment via numerous pathways including discharge of effluents from industries and wastewater treatment plants. To date, however, a comprehensive review of the determination of triclosan in aquatic environments has not been reported. Herein, we review the environmental concentration of triclosan in aquatic systems globally, as well as its stability and toxicity. The wide variety of monitoring methods utilized for the determination of triclosan are discussed, including those based on chromatography-mass spectrometry, electrochemistry, capillary zone electrophoresis and spectrophotometry over the last 10 years.

© 2016 Elsevier B.V. All rights reserved.

Contents

1. Introduction	222
1.1. Concentrations of triclosan in water resources.....	222
1.2. Stability of triclosan in the environment.....	222
1.3. Removal of triclosan via wastewater treatment processes.....	223
2. Green analytical chemistry	223

Abbreviations: APTES, 3-Aminopropyltriethoxysilane; AQA, Analytical Quality Assurance; AuNPs, Gold Nanoparticles; β -CD/GNP, β -Cyclodextrin/Graphene Nano Plate-lets; BRI, Biomarker Response Index; CE, Capillary Electrophoresis; CL, Chemiluminescence; CNP-PDDAC, Carbon Nanoparticles-Poly(Diallyl Dimethyl Ammonium Chloride); CNTs@SiO₂, Carbon Nanotubes Coated with Silica; CNTs@TCS-MIPs, Carbon Nanotubes@Triclosan – Molecularly Imprinted Polymer; CTAB, Cetyltrimethylammonium Bromide; CV, Cyclic Voltammetry; CZE-DAD, Capillary Zone Electrophoresis – Diode Array Detection; CZE-UV, Capillary Zone Electrophoresis with UV detection; 2,4-DCP, 2,4-Dichlorophenol; DLLME, Dispersive Liquid–Liquid Microextraction; DLLME-SFO, Dispersive Liquid–Liquid Microextraction Based on Solidification of Floating Organic droplet; DMBUA, 2,3-dimethyl-6-(undec-10-enamide)-6-deoxy- β -cyclodextrin; DPV, Differential Pulse Voltammetry; DVB/CAR/PDMS, Divinylbenzene/Carboxen/Polydimethylsiloxane; DW, Dry Weight; ECOSAR, Ecological Structure–Activity Relationships; EDCs, Endocrine Disrupting Chemicals; EPA, Environmental Protection Agency; GAC, Green Analytical Chemistry; GC/ECNI/MS, Gas Chromatography/Electron Capture Negative Ionization/Mass Spectrometry; GC-MS/MS, Gas Chromatography-Tandem Mass Spectrometry; HPLC-ESI-MS/MS, High Performance Liquid Chromatography-Electron Spray Ionization-Tandem Mass Spectrometry; HPLC-UV, High Performance Liquid Chromatography – Ultraviolet Detection; IC₅₀, The inhibiting concentration at which a reduction of 50% in survival or reproduction was observed; IL-DLPME, Ionic Liquid – Dispersive Liquid Phase Microextraction; IPR, Initial Precision and Recovery; IT-USA-SI-LLME, In-Tube based Ultra-Sound-Assisted Salt-Induced Liquid-Liquid Microextraction; K_{oc}, Soil Organic Carbon-Water Partitioning Coefficient; LC-DAD, Liquid Chromatography-Diode Array Detection; LC-ESI-MS/MS, Liquid Chromatography-Electron Spray Ionization – Tandem Mass Spectrometry; LC-MS/MS, Liquid Chromatography-Tandem Mass Spectrometry; LVI-GC-MS, Large Volume Injection-Gas Chromatography–Mass Spectrometry; MALLE, Membrane-Assisted Liquid–Liquid Extraction; MEPS, Microextraction by Packed Sorbent; MIC, Minimum Inhibitory Concentration; MIP, Molecularly Imprinted Polymer; MWCNTs, Multiwall Carbon Nanotubes; NOEC, No-Observed-Effects Concentration; nZnO-MWCNT/GCE, Nano-Zinc Oxide-Multiwalled Carbon Nanotube/Glassy Carbon Elec-trode; o-PD/GCE, o-Phenylene Diamine/Glassy Carbon Electrode; OPR, Ongoing Precision and Recovery standard; PA, Polyacrylate; PBDEs, Poly Brominated Diphenyl Ethers; PBT, Persistence, Bioaccumulation and Ecotoxicity; PDDAC, Poly-(Diallyl Dimethyl Ammonium Chloride); PDMS-DVB, Poly (dimethylsiloxane-divinylbenzene); p(HEMAGA), Poly(2-Hydroxyethylmethacrylate–Methacryloylamidoglutamic Acid); PLE, Pressurized Liquid Extraction; POM, Polyoxyometalate; PPCPs, Pharmaceutical and Personal Care Products; QA/QC, Quality Assurance/Quality Control; QSAR, Quantitative structure–activity relationship; RDSE, Rotating Disk Sorptive Extraction; rGO, Reduced Graphene Oxide; RP-HPLC, Reverse Phase-High Performance Liquid Chromatography; RSD, Relative Standard Deviation; SBSE, Stir Bar Sorptive Extraction; SBSE-LD, Stir Bar Sorptive Extraction and Liquid Desorption; SPCEs, Screen-Printed Carbon Electrodes; SPME, Solid Phase Microextraction; SPR, Surface Plasmon Resonance; SWV, Square Wave Voltammetry; 2,4,6-TCP, 2,4,6-Trichlorophenol; TCS, Triclosan; TD-GC-MS, Thermal Desorption–Gas Chromatography–Mass Spectrometry; TEOS, Tetraethyl orthosilicate; TIL-DLME, Temperature-Controlled Ionic Liquid-Dispersive Liquid Phase Microextraction; UHPLC, Ultra-High-Pressure Liquid Chromatography; UHPLC-TUV, Ultra-High Pressure Liquid Chromatography-Tunable Ultraviolet Detection; UPLC, Ultra Performance Liquid Chromatography; USAEME, Ultrasound-Assisted Emulsification–Microextraction; USFDA, US Food and Drug Agency; VER, Calibration Verification; WLRS, White Light Reflectance Spectroscopy; WWTPs, Wastewater Treatment Plants.

* Corresponding author. Tel.: +27 12 420 5426; fax: +27 12 420 4687.
E-mail address: patricia.forbes@up.ac.za (P.B.C. Forbes).

3.	Quality assurance/quality control	224
4.	Monitoring methods for triclosan	224
4.1.	Chromatography-mass spectrometry.....	224
4.2.	Electrochemical methods	224
4.3.	Capillary zone electrophoresis methods.....	227
4.4.	Optical methods	228
5.	Conclusion and future outlook	228
	Acknowledgements	229
	References	229

1. Introduction

Triclosan, or 5-chloro-2-(2,4-dichlorophenoxy) phenol (Fig. 1), with the commercial name Irgasan DP300, is a white powder with a slight phenolic odor which has been used in a variety of consumer products [1,2]. It is an antimicrobial and preservative agent used in personal care products (such as toothpaste, detergent, soap, shampoos, skin care creams and lotions) with a typical concentration in the range of 0.1–0.3% of product weight. The content of triclosan (TCS) should not exceed 0.3% (w/w) which is regulated by the European Community Cosmetic Directive or the US Food and Drug Agency (USFDA) in Europe and the USA, respectively [3,4].

The solubility of triclosan in water is $<10^{-6}$ g mL⁻¹, although its solubility increases when the pH becomes more alkaline [5]. The partition coefficient of triclosan ($\log P_{ow} = 5.4$), suggests that it is lipophilic [6]. The halogenated biphenyl ether structure of triclosan is similar to that of bisphenol A, dioxins, polybrominated diphenyl ethers (PBDEs) and thyroid hormones, therefore concern has been raised over triclosan as a potential endocrine disruptor, specifically regarding disruption of thyroid hormone homeostasis [7,8].

The ubiquitous use of triclosan has resulted in its release into wastewater and many water sources [9] where it may affect ecosystems and human health. In particular, triclosan can cause death of algae with a reported IC₅₀ (the inhibiting concentration at which a reduction of 50% in survival or reproduction was observed) of 4700 ng L⁻¹ [10]. There have also been several other health concerns attributed to triclosan, as it can accumulate in the human body over time and may result in long-term health risks [11]. In addition, toxic and persistent compounds such as methyl triclosan, chlorinated phenols and biphenyl ethers may be formed after biological methylation or chlorination of triclosan [12–14]. Some surveys have revealed that methyl triclosan is more lipophilic than its parent compound, contributing to its persistence and bioaccumulation potential in wildlife and humans [15,16].

1.1. Concentrations of triclosan in water resources

Several recent studies have clearly demonstrated the widespread presence of triclosan in the environment, especially in wastewater, wastewater treatment plant effluents, rivers and in sediments in various countries.

A study in the United States identified triclosan as one of the top seven contaminants in surface water, with a maximum concentration of 2300 ng L⁻¹ [17]. The worldwide concentration range of

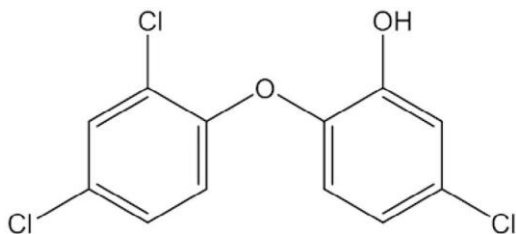


Fig. 1. Chemical structure of triclosan.

triclosan in water has been found to range from 1.4–40,000 ng L⁻¹ in surface waters, 20–86,161 ng L⁻¹ in wastewater influent, 23–5370 ng L⁻¹ wastewater effluent, <0.001–100 ng L⁻¹ in sea water, sediment (lake/ river/other surface water) <100–53,000 µgkg⁻¹ dry weight (dw); sediment (marine) 0.02–35 µg kg⁻¹ dw, biosolids from WWTP 20–133,000 µgkg⁻¹ dw, activated/digested sludge 580–15,600 µg kg⁻¹ dw; and pore water 0.201–328.8 µg L⁻¹ [18,19].

Triclosan is a frequent contaminant of aquatic and terrestrial environments and it is detected at a concentration ranging from parts-per-trillion in surface water to parts-per-million in biosolids. The elevated concentration of triclosan in biosolids and aquatic sediments may be attributed to the high usage, strong sorption to organic matter and environmental persistence of this compound [20]. Regarding the half-life, this depends on the environmental compartment and prevailing conditions [21].

Fish, algae, and crustaceans may be affected by elevated levels of biocides in surface waters, the concentrations of which are influenced by raw and treated sewage. It is important to note that triclosan has been detected in surface waters at levels higher than the no-observed-effects concentration (NOEC) of algae [20]. Micro-organisms are generally not as sensitive to triclosan compared to non-target species, and the minimum inhibitory concentration (MIC) threshold values for microbes may be increased by the environmental levels of triclosan [20].

A study examined the toxicity ranking of five pharmaceutical and personal care products (PPCPs) including triclosan. Bivalve *Dreissena polymorpha* in fresh water were exposed to different environmentally relevant concentrations of the PPCPs over 96 hrs and the biological response of eight biomarkers was integrated into a simple biomarker response index (BRI). It was found that triclosan demonstrated dramatic effects. The relative toxicities of the compounds were found to be triclosan > trimethoprim > ibuprofen > diclofenac = paracetamol [22].

Researchers in Spain conducted another environment risk assessment for 26 PPCPs [23]. They employed Microtox acute ecotoxicity tests and activated sludge respirometry assays. The US EPA Ecological Structure–Activity Relationships (ECOSAR™) QSAR program was also utilized to predict the estimated ecotoxicological effects. Based on the results of ecotoxicity tests, triclosan is very toxic to different species. Furthermore, evaluation of persistence, bioaccumulation and ecotoxicity (PBT) showed that triclosan is persistent and toxic but not bioaccumulative [24].

1.2. Stability of triclosan in the environment

The US EPA has reported that triclosan is hydrolytically stable under abiotic and buffered conditions over the pH range of 4–9. It degrades with calculated non-linear half-lives of 1.3–1.4 days in water, 53.7–60.3 days in sediment, and 39.8–55.9 days in aerobic water-sediment systems maintained in darkness, whilst the calculated aqueous photolytic half-life is 41 min [19,25].

Triclosan has a pK_a of 7.9 [26] which means that it exists partially in the dissociated form in the environment, which is of relevance as anions do not generally adsorb as strongly to organic carbon and clay as their neutral counterparts [27], although an estimated K_{oc} (Soil Organic Carbon–Water Partitioning Coefficient) value of 9200 has been

reported [28]. In aquatic environments, triclosan is expected to adsorb to suspended solids and sediments (K_{ow} 4.76) [28,29], posing a potential threat to aquatic organisms. Triclosan has an estimated Henry's Law constant of 1.5×10^{-7} atm.m³/mol [19,29], thus it is not anticipated to volatilize readily from soil or water surfaces.

1.3. Removal of triclosan via wastewater treatment processes

Triclosan is susceptible to oxidative degradation by ozone and chlorine in the presence of sunlight, and to biodegradation by microorganisms [19]. It has been found that biodegradation is an efficient mechanism for triclosan removal from wastewater and also that biodegradation under aerobic conditions provides higher removal efficiency in comparison with anaerobic media [30].

Wastewater treatment achieves average triclosan removal efficiencies in the range of 58–99% [31], depending on the technical capabilities of the sewage treatment systems [30,32–39]. Approximately 50% of the incoming mass of triclosan, which is produced by activated sludge treatment together with aerobic biosolid digestion in conventional WWTPs, persists and becomes sequestered in biosolids. As a result, major pathways of biocide release into the environment are WWTP effluent discharge into surface waters and the application of biosolids to land [20].

Cleavage of the ether bond and chlorination of the phenolic bond were identified as the main degradation pathways for triclosan during wastewater treatment [40]. Five main products were found in the reaction of triclosan with free chlorine including 2,4-dichlorophenol (2,4-DCP), 2,4,6-trichlorophenol (2,4,6-TCP) and tetra- and penta-chlorinated species. 2,4,6-TCP is a known endocrine disruptor, and may cause cancer, birth defects and developmental disorders in offspring, whilst 2,4-DCP may be fatal if large amounts are absorbed by the body [40].

Treatment with ozone during municipal sewage treatment was efficient in the removal of triclosan [41–43]. Although chloramines can be employed, chlorine is a stronger oxidant and has been shown to be more effective at oxidizing pharmaceuticals and endocrine disrupting chemicals (EDCs) in a comparative study where phenolic compounds including triclosan exhibited greater than 95% removal by chlorination under the conditions tested [44]. The reaction mechanisms of phenolic compounds with free chlorine proceeds via an electrophilic substitution pathway, with a mixture of substituted products at the ortho and para positions. Further chlorine addition results in cleavage of the aromatic ring [44,45]. It is noteworthy to mention that photo transformation can also remove triclosan from wastewaters [46].

Based on the widespread use of triclosan, its known presence in aquatic systems, as well as the potential environmental impacts it can incur, it is crucial that analytical methods for triclosan are sensitive and robust to allow for the reliable detection and quantification thereof in water systems. Moreover, quality assurance/quality control is needed to ensure reliable analytical information and green analytical chemistry approaches should be considered.

This review discusses the cycling and concentration of triclosan in different environmental compartments and focuses on the development of analytical methods for the determination of triclosan over the last 10 years (2006–2016). It should be noted that although some of the methods discussed have been developed to analyse a class of pharmaceutical compounds, we have limited our discussion to triclosan in aquatic media. Reported analytical methods in this regard are thus reviewed in this paper to assist readers in the evaluation and comparison of the different options which have been tested.

2. Green analytical chemistry

The term “green analytical chemistry (GAC)” was proposed by J. Namieśnik [47] and has gained a great deal of attention in recent years. The main purposes of GAC are not only making laboratory practices more environmentally friendly, but also reducing the negative impact of chemical analyses on the environment and to enable implementation of sustainable development principles in analytical laboratories. One of the most important challenges for the future of GAC is to provide a compromise between increasing the quality of the results in terms of selectivity, sensitivity, reliability of analysis and reducing analysis time on one hand, and improving environmental friendliness of analytical methods on the other. In 2013, Namieśnik et al proposed the following 12 principles of GAC [48]:

1. Direct analytical techniques should be applied to avoid sample treatment.
2. Minimal sample size and minimal number of samples are goals.
3. *In situ* measurements should be performed.
4. Integration of analytical processes and operations to save energy and reduce the use of reagents.
5. Automated and miniaturized methods should be selected.
6. Derivatization should be avoided.
7. Generation of a large volume of analytical waste should be avoided and proper management of analytical waste should be provided.
8. Multi-analyte or multi-parameter methods are preferred versus methods for one analyte at a time.
9. The use of energy should be minimized.
10. Reagents obtained from renewable sources should be preferred.
11. Toxic reagents should be eliminated or replaced.
12. The safety of the operator should be increased.

In this way, the principles of green chemistry can be applied to the analytical field. However, a number of the 12 principles may cause a decrease in analytical performance parameters such as accuracy, precision and sensitivity.

Table 1 compares less green techniques used for determination of triclosan with their greener alternatives.

Table 1

Examples of green techniques compared to conventional analytical methods and their relative advantages and disadvantages

Analytical method	Potential advantages	Potential disadvantages	References
Less green analytical methods			
HPLC	Rapid, sensitive, accurate and selective, small sample volume,	Potentially poor repeatability, consumes reagents, produces wastes	[49,50]
GC-MS	Low detection limit, selective, sensitive, accurate, low sample volume	Requires the use of toxic reagents and derivatization, consumes reagents, produces wastes, time-consuming, multi-stage sample treatment often necessary	[51,52]
Spectrophotometry	Simple, rapid, inexpensive	High detection limit, consumes reagents, produces wastes, poor sensitivity and selectivity, uses toxic and corrosive reagents	[53]
Greener methods			
Electrochemical sensor	Simple and fast, low detection limits, sensitive, simple, rapid, reliable, inexpensive, low energy consumption	Sometimes poor reproducibility, needs monitoring of electrode stability, possible interferences from other analytes	[54–56]
Electrophoresis	Small sample volume, reduced reagent volumes, rapid, portable, uses little power	Often poor reproducibility and sensitivity	[57,58]

Selection of the greenest method from all available methods is based on the needs of the user such as accuracy, selectivity and detection limits. Typically direct, automated, miniaturized and portable analytical techniques are the greenest options [59]. In addition, multi-analyte or multi-parameter methods are of great importance for environmental monitoring, where information on a number of analytes can be obtained from a single analysis [48]. The majority of reagents to be replaced in analytical procedures are organic solvents [59] where ionic liquids and supercritical fluids are considered as alternative (green) solvents. These are finding application in chromatography, electrochemistry and spectroscopy [60]. Green aspects of the analytical methods discussed in this paper are provided to assist readers in evaluating the different options available and the areas where further improvements in this regard should be investigated.

3. Quality assurance/quality control

Green analytical chemistry entails performing reliable analysis while applying quality assurance/quality control (QA/QC) and simultaneously minimizing any environmental impacts resulting from the analysis [61]. The minimum requirements for QA/QC comprise of an initial demonstration of laboratory capability, analysis of samples spiked with labeled compounds to evaluate data quality, and analysis of standards and blanks as tests of continued performance [62]. QA activities may include participation in laboratory accreditation programs, external system audits, and inter-laboratory comparisons [63]. Analytical method validation forms the first level of QA in the laboratory. Moreover, analytical quality assurance (AQA) is the complete set of measures a laboratory must undertake to ensure that it can always achieve high-quality data [64].

The US EPA conducted research regarding the determination of pharmaceuticals and personal care products in water, soil, sediment and biosolids by HPLC-MS/MS [62]. Based on this study, relative standard deviation (RSD) and the average percent recovery (X) with the corresponding limits for each native and labeled compound were compared in order to investigate initial precision and recovery (IPR). The requirement is that if RSD and X for all compounds meet the acceptance criteria, system performance is acceptable and analysis of blanks and samples may begin. If, however, any individual RSD exceeds the precision limit or any individual X falls outside the range for recovery, system performance is unacceptable for that compound and requires correction. In addition, the recovery of each labeled compound must be within the limits to ensure method performance. If the recovery of any compound falls outside of these limits, additional cleanup procedures may be employed or the sample size should be adjusted. Proposed QC parameters for triclosan are given in Table 2 [62].

4. Monitoring methods for triclosan

A range of techniques have been employed in the monitoring of triclosan in different matrices. Although not all of the methods discussed in this section were developed specifically for the monitoring of triclosan in water samples, they have the potential to be used for this application. In addition, it should be noted that some

methods are for the simultaneous analysis of a range of pharmaceutical compounds, as indicated in Table 3.

4.1. Chromatography-mass spectrometry

Numerous chromatography methods coupled with mass spectrometry have been employed to selectively detect low levels of triclosan in aqueous systems, but these methods usually have disadvantages in terms of analytical running costs, complexity, environmentally unfriendly solvent use, expensive instrumentation, long analysis time, as well as the need for highly skilled technicians and laborious sample pre-treatment [55,87]. Rapid and sensitive screening methods may, therefore, provide desirable alternatives, as discussed in later sections of this paper. Table 3 shows a range of chromatography-based methods for triclosan (and in some cases additional pharmaceutical analytes) and compares the linear ranges and detection limits for triclosan. The sample extraction (pre-concentration) technique, derivatization reagent employed, and the detector employed are also included.

In addition to the extraction methods listed in Table 3, research has been conducted into the use of molecularly imprinted polymers (MIPs) as extraction media for triclosan. Gao and coworkers, for example, synthesized core-shell MIPs on silica-coated multi-walled carbon nanotubes (MWCNTs) via a sol-gel process for the determination of triclosan in environmental water samples with HPLC analysis (Fig. 2). The binding isotherms of TCS were determined in the concentration range of 3.0×10^6 – 1.2×10^{10} ng L⁻¹ [90].

Developments have been observed to make chromatography more environmentally friendly, such as the substitution of organic solvents with less toxic alternatives and there has been a shift towards miniaturization [91]. One of the main advantages of chromatographic procedures is that they facilitate the analysis of hundreds of pollutants in a single run [92], however sample preparation can have the most detrimental effect on the environment. In recent years the development of dispersive liquid–liquid microextraction (DLLME); liquid-phase microextraction (LPME), and single drop microextraction (SDME) has enabled greener sample preparation procedures due to the lower solvent volumes employed [93].

It is widely accepted that LC is less “green” than GC because LC mobile phases are usually solvents (unless water is used). One of the most commonly used toxic solvents in LC is acetonitrile thus one of the most common approaches to designing an appropriate green mobile phase in reversed-phase high performance liquid chromatography (RP–HPLC) is to add small volumes of modifiers to water [79].

4.2. Electrochemical methods

The application of electrochemical techniques has dramatically increased as a consequence of the development of more sophisticated instrumentation and novel electrode materials. Compared to other analytical techniques, the direct electrochemical analysis of triclosan is simple, rapid, sensitive and cost-effective and is based on the phenolic hydroxyl of triclosan which can undergo oxidation processes under optimal conditions. More importantly this

Table 2
Proposed QC acceptance criteria for triclosan [62]

Compound	(% Calibration Verification (VER)	Initial Precision and Recovery (IPR)		Ongoing Precision and Recovery standard (OPR)	Labeled compound recovery in samples (%)
		RSD (%)	X (%)		
Triclosan	70–130	30	55–108	50–120	
¹³ C ₁₂ -Triclosan	70–130	30	6–151	6–168	5–153

Table 3
Comparison of selected chromatography-based methods for triclosan determinations in water samples

Method	Extraction method	Analytes	Derivatization reagent	Linear range (ng L ⁻¹)	LOD (ng L ⁻¹)	LOQ (ng L ⁻¹)	Samples	Reference
GC-MS	SPE (GFF glass fiber filter)	Triclosan, Nonylphenol, Nonylphenol ethoxylates, and Bisphenol A	Bis(trimethylsilyl) trifluoroacetamide	1.0×10^6 – 1.0×10^7	130.3	434.3	Wastewater	[65]
GC-MS	Oasis HLB cartridge	Triclosan, Acidic pharmaceuticals, Phenols, Estrone, 17 β -estradiol, 17 α -ethinylestradiol	MTBSTFA, TBDMSCI, BSTFA, TMSCI	18.0– 2.3×10^4	0.1 10.1	–	Spring water Untreated wastewater	[51]
GC-MS	SBSE–LD	Triclosan, Methyl triclosan	MTBSTFA	20.0 – 2.0×10^4	5.0	–	River water	[66]
GC-MS	RDSE	Triclosan, Methyl triclosan	MTBSTFA	160.0–2,000.0	46.0	152.0	Untreated wastewater	[67]
GC-MS	Oasis HLB cartridge	Triclosan, Pharmaceuticals and Endocrine-disrupting substances	MTBSTFA	5.0–202.7	<58.0 <101.3	–	Drinking water Surface water	[52]
GC-MS GC-FID	In-drop derivatisation liquid-phase microextraction	Triclosan, 9 known phenolic endocrine disruptors	Ethyl chloroformate	$1,100$ – 28×10^3 55×10^3 – 72×10^4	400 18,300	–	Surface water, wastewater	[68]
TD–GC-MS	SBSE (PDMS)	Triclosan	NA	20.0 – 2.0×10^4	5.0	20.0	River water	[69]
TD–GC-MS	SBSE	Triclosan, Methyl triclosan, Paraben	Acetic anhydride in basic medium	–	1.39	4.65	Tap water, untreated and treated wastewater	[70]
LVI–GC–MS	MEPS	Triclosan, Methyl triclosan, Paraben	NA	100.0 – 1.0×10^4	1.0–15.0 20.0–590.0	3.3–49.5 66.0 – 2×10^3	Ultrapure water Raw wastewater	[71]
GC-MS/MS	C18 SPE cartridge	Triclosan	NA	145.0–211.4	0.26	–	Wastewater, river, sea water	[72]
GC-MS/MS	Oasis HLB sorbent	Triclosan, Neutral and acidic pharmaceuticals	NA	9.8–984.4	2.0	8.7	Hospital effluent	[73]
GC-MS/MS	SPE (C18 cartridge)	Triclosan	NA	4.1–115.8	20.3	–	River and coastal water	[74]
GC-MS/MS	SPME (DVB/CAR/PDMS)	Triclosan, Paraben, Related chlorophenols	Acetic anhydride	10.0–5,000	6.5	28	River water, wastewaters and swimming pool water	[75]
GC-MS/MS	DLLME	Triclosan, Methyl triclosan	MTBSTFA	10.0–2,000.0	6.0	2.0	Tap water, river water, treated wastewater and raw wastewater	[76]
GC-MS/MS	USAEME	Triclosan, phenolic preservatives	Acetic anhydride	1.0×10^3 – 1.4×10^6	5.84	–	Influent and effluent wastewaters, river waters and swimming pool water	[77]
GC-MS/MS	MALLE	Triclosan, Paraben	Acetic anhydride and Potassium hydrogenphosphate	10.0–5,000.0	1.1	3.6	Treated and raw wastewaters	[78]
RP-LC-DAD	SBSE-LD	Triclosan	NA	400.0 – 108.0×10^3	100.0	400.0	Urban wastewater,	[79]
HPLC-DAD	SPME (PDMS)	Triclosan, Triclocarban, and transformation products of triclocarban	NA	250.0 – 1.0×10^5	60.0 470.0	–	Deionized water River water	[80]
HPLC-DAD	SBSE	Triclosan, 4-n-nonylphenol, and di-n-butyl phthalate	NA	1.0×10^4 – 1.0×10^7	–	1.0×10^4	Bottled water	[81]
HPLC-UV	On-line solid-phase microextraction	Triclosan, 2,4-dichlorophenol, 2,4,6-trichlorophenol, 3-chlorophenol, Bisphenol A, Mefenamic acid and Gemfibrozil	NA	10.0 – 168.0×10^3	1.0	–	Tap water, river water and municipal wastewater	[49]
HPLC–UV LC-MS/MS	DLLME-SFO	Triclosan and 2,4-dichlorophenol	NA	500.0 – 5.0×10^5 20.0 – 1.0×10^4	100.0 2.0	–	Tap water, lake water and river water	[50]
LC-MS/MS	SPE-Strata-X 33U Polymeric Reversed Phase	Triclosan and 20 acidic pharmaceuticals and personal care products	NA	Ave = 0.0 Ave = 1.0 Ave = 2.3 Ave = 46.0	– – – –	1.0 3.0 5.0 5.0	Drinking water River water Wastewater influent Wastewater effluent	[82]

(continued on next page)

Table 3 (continued)

Method	Extraction method	Analytes	Derivatization reagent	Linear range (ng L ⁻¹)	LOD (ng L ⁻¹)	LOQ (ng L ⁻¹)	Samples	Reference
HPLC-MS/MS	SPME (PDMS)	Triclosan, Triclocarban, and transformation products of triclocarban	NA	0.5–100.0	1.28 1.37	4.22 4.52	Deionized water River water	[80]
HPLC-ESI-MS/MS	IL-DLPME	Triclosan and Triclocarban	NA	1.0×10^3 – 6.0×10^4	580.0	–	Tap water and wastewater	[83]
HPLC-ESI-MS/MS	Temperature-controlled ionic liquid dispersive liquid-phase microextraction	Triclosan and Triclocarban	NA	50.0 – 1.0×10^5	3.0×10^2	–	Lake water, river water, and tap water	[84]
HPLC-ESI-MS/MS	Ionic liquid/ionic liquid dispersive liquid liquid microextraction	Triclosan and Triclocarban	NA	2.5×10^3 – 5.0×10^5	3.5×10^2	–	Tap water, river water, snow water and lake water	[85]
HPLC-ESI/MS	Microporous bamboo-activated charcoal solid-phase extraction	Triclosan	NA	20.0 – 2.0×10^4	2.0	–	River waters	[86]
UHPLC	DLLME	Triclosan, Triclocarban, Methyl-triclosan	NA	50.0 – 1.0×10^5	134.0	–	River water, irrigating water, reclaimed water and domestic water	[87]
UHPLC-TUV	TIL-DLME	Triclosan, Triclocarban, Methyl-triclosan	NA	10.0 – 1.0×10^5	1.15	–	Reclaimed water, irrigating water, wastewater and domestic water	[88]
UHPLC-MS/MS	SPE (Oasis HLB and Bond Elut Plexa)	Triclosan, Triclocarban, 4 preservatives, 5 UV filters	NA	500.0 – 5.0×10^5	200.0	5.0	Surface and wastewaters	[89]

BSTFA, N,O-bis(trimethylsilyl)trifluoroacetamide; DLLME, Dispersive Liquid–Liquid Microextraction; DLLME-SFO, Dispersive Liquid–Liquid Microextraction Based on Solid-ification of Floating Organic droplet; DVB/CAR/PDMS, Divinylbenzene/Carboxen/Polydimethylsiloxane; GC/ECNI/MS, Gas Chromatography/Electron Capture Negative Ionization/ Mass Spectrometry; GC-MS/MS, Gas Chromatography – Tandem Mass Spectrometry; HPLC-ESI-MS/MS, High Performance Liquid Chromatography-Electron Spray Ionization– Tandem Mass Spectrometry; HPLC-UV, High Performance Liquid Chromatography – Ultraviolet Detection; IL-DLPME, Ionic Liquid – Dispersive Liquid Phase Microextraction; IT-USA-SI-LLME, In-Tube based Ultra-Sound-Assisted Salt-Induced Liquid-Liquid Microextraction; LC-DAD, Liquid Chromatography – Diode Array Detection; LC-ESI-MS/MS, Liquid Chromatography-Electron Spray Ionization – Tandem Mass Spectrometry; LC-MS/MS, Liquid Chromatography – Tandem Mass Spectrometry; LVI-GC-MS, Large Volume Injection-Gas Chromatography–Mass Spectrometry; MALLE, Membrane-Assisted Liquid–Liquid Extraction; MEPS, Microextraction by Packed Sorbent; MTBSTFA, N-tert-butyltrimethylsilyl-N-methyltrifluoroacetamide; NA, Not Applicable; PLE, Pressurized Liquid Extraction; RDSE, Rotating Disk Sorptive Extraction; RP-HPLC, Reverse Phase-High Performance Liquid Chromatography; SBSE, Stir Bar Sorptive Extraction; SBSE-LD, Stir Bar Sorptive Extraction and Liquid Desorption; SPE, Solid Phase Extraction; SPME, Solid Phase Microextraction; TBDMSCI, Tert-butyltrimethylsilylchlorane; TD-GC-MS, Thermal Desorption–Gas Chromatography–Mass Spectrometry; TIL-DLME, Temperature-Controlled Ionic Liquid – Dispersive Liquid Phase Microextraction; TMSCI, Trimethylsilylchlorane; UHPLC, Ultra-High-Pressure Liquid Chromatography; UHPLC-TUV, Ultra-High Pressure Liquid Chromatography-Tunable Ultraviolet Detection; UPLC, Ultra Performance Liquid Chromatography; USAEME, Ultrasound-Assisted Emulsification–Microextraction.

technique enjoys the advantage of a broad linear range [94]. The first direct electrochemical method for triclosan was proposed by Pemberton et al [26], which employed cyclic voltammetry and screen-printed carbon electrodes (SPCEs) which were disposable, could be mass produced at low cost, and had a wide linear range.

Although the detection of triclosan has been investigated using a mercury electrode [95], it suffers from a narrow linear range and is considered to be an environmentally unfriendly technique. High temperature-high mass transport conditions were later induced by focused microwaves at glassy carbon and boron doped diamond electrode surfaces in order to enhance the electrochemical oxidation of triclosan [96]. In spite of the fact that the hydrophobic nature of triclosan resulted in binding thereof onto the electrode surface, it provided a good detection limit compared to other electrochemical methods and this problem can be overcome by the utilization of surfactants [97].

Chemically modified electrodes, such as a composite nano zinc oxide-multiwalled carbon nanotube modified glassy carbon electrode, have been found to accelerate electron transfer for electro-oxidation of triclosan [98].

A study compared the electrochemical determination of triclosan based on (i) the extraction of triclosan onto carbon nanoparticles followed by deposition onto electrodes and (ii) the adsorption of

triclosan directly onto carbon nanoparticles immobilized at electrodes, where the extraction process was found to be highly effective [99].

Table 4 summarizes and compares the linear ranges and detection limits for the detection of triclosan achieved using a range of electrochemical methods. It is evident that in most cases extraction prior to analysis is not required and that typically triclosan alone is determined.

The performance of electrochemical measurements is strongly influenced by the material of the working electrode. For many years, mercury working electrodes such as the hanging mercury drop electrode and mercury film electrode were the electrodes of choice due to the highly reproducible, renewable, and smooth surface of mercury [103]. However, these electrodes become increasingly disfavoured and banned in some countries due to health and environmental considerations. Alternative, environmentally friendly electrodes and chemically modified electrodes have thus become the focus of substantial recent research studies and have received great attention in electroanalysis due to their low background current, wide potential window, chemical inertness, low cost, and suitability for various sensing and detection applications [104] where the most popular schemes used to substitute mercury electrodes include boron-doped diamond electrodes [96], carbon nanotube electrodes [98,105], and screen printed electrodes [26].

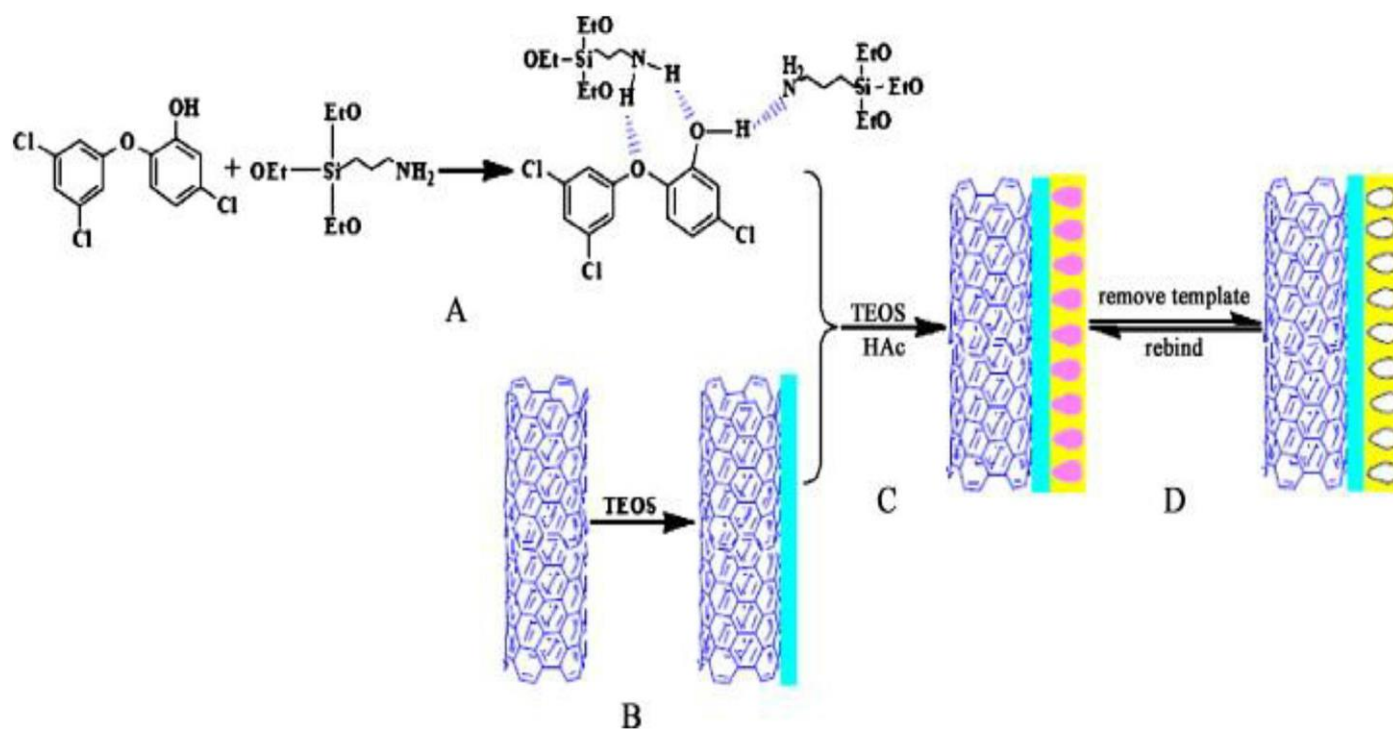


Fig. 2. Scheme for the synthesis of carbon nanotubes@triclosan – molecularly imprinted polymer (CNTs@TCS-MIPs): (a) formation of template triclosan (TCS)-aminosilica monomer 3-aminopropyltriethoxysilane (APTES) complex; (b) transformation of the surface of purified CNTs to silica shell by a sol-gel process using tetraethoxysilane (TEOS) and APTES in the presence of cetyltrimethylammonium bromide (CTAB) to obtain core@shell carbon nanotubes coated with silica (CNTs@SiO₂); (c) reaction of CNTs@SiO₂ with template silica monomer complex to produce silica surface functionalized with TCS-imprinted polymer; (d) removal of the TCS from polymer shells to obtain the CNTs@TCS-MIPs [90].

Electrochemical methods have advantages in that they generally minimize hazardous substance usage and waste generation during analyses.

4.3. Capillary zone electrophoresis methods

A number of sample extraction and pre-concentration methods for triclosan have been mentioned for the various analytical techniques discussed in this paper. Similarly a number of extraction methods have been used in conjunction with capillary zone electrophoresis for the determination of triclosan. The combined use of dispersive liquid-liquid microextraction with capillary zone electrophoresis-UV detection (CZE-UV), for example, can be applied

to detect trace amounts of triclosan in different matrices. This technique provides the considerable advantage of little matrix interference, good repeatability and recoveries within a short time and relatively high enrichment factors [57].

A rapid and convenient method was developed for the simultaneous determination of triclosan and bisphenol A (BPA) in water samples by dispersive liquid-liquid microextraction (DLLME) combined with capillary zone electrophoresis with UV detection (CZE-UV) [57]. Under optimized conditions, the calibration curve for triclosan was linear over the range of 2.0×10^4 – 2.0×10^6 ng L⁻¹ with a detection limit of 4.0×10^3 ng L⁻¹.

A sensitive method was also developed using capillary zone electrophoresis with UV-diode array detection (CZE-DAD) for

Table 4
Comparison of linear ranges and limits of detection (LODs) for triclosan obtained using a range of electrode based systems

Materials/Electrodes	Detection method	Extraction	Analyte	Linear range (ng L ⁻¹)	LOD (ng L ⁻¹)	Samples	Reference
CNP-PDDAC	CV	Yes	Triclosan	1.4×10^5 – 1.4×10^7	–	–	[54]
Carbon and diamond electrodes	CV	No	Triclosan	–	3.0×10^8	–	[96]
Cellulose-PDDAC film electrode	CV	Yes	Triclosan	3×10^5 – 3×10^8	–	–	[100]
Carbon nanoparticles	CV	Yes	Triclosan, benzophenone-3	3.0×10^6 – 3.0×10^7	5.8×10^6	–	[99]
o-PD/GCE	Amperometry	No	Triclosan	5.8×10^4 – 8.7×10^5	2.3×10^4	–	[56]
Polymeric micelles	DPV	No	Triclosan	1×10^4 – 6×10^5 1×10^6 – 8×10^6	5×10^3	Wastewater, Toothpaste, Hand gel, Liquid soap	[101]
β-CD/GNP	CV	No	Triclosan	5.8×10^5 – 3.5×10^7	1.7×10^5	Water samples	[102]
nZnO-MWCNT/GCE	CV, DPV and SWV	No	Triclosan	1.5×10^3 – 2.0×10^6	1.3×10^3	Tap water	[98]
MIP/AuNPs/POM/rGO/GC	CV	No	Triclosan	145.0 – 1.5×10^4	43.4	Wastewater and Lake water	[55]

AuNPs, Gold Nanoparticles; β-CD/GNP, β-Cyclodextrin/Graphene Nano Platelets; CNP-PDDAC, Carbon Nanoparticles-Poly(Diallyl Dimethyl Ammonium Chloride); CV, Cyclic Voltammetry; DPV, Differential Pulse Voltammetry; MIP, Molecularly Imprinted Polymer; MWCNTs, Multiwall Carbon Nanotubes; nZnO-MWCNT/GCE, Nano-Zinc Oxide-Multiwalled Carbon Nanotube/Glassy Carbon Electrode; o-PD/GCE, o-Phenylene Diamine/Glassy Carbon Electrode; PDDAC, Poly-(diallyldimethylammonium chloride); POM, Polyoxometalate; rGO, Reduced Graphene Oxide; SWV, Square Wave Voltammetry.

Table 5
Comparison of typical analytical parameters pertaining to liquid chromatography and capillary electrophoresis [111]

Parameter	HPLC	CE
Injected volume	1–100 μL	1–100 nL
Flow rate of the liquid phase	1–10 mL/min	1–100 nL/min
Analysis time	10–60 min	1–20 min
Separation technique	High pressure with complicated pumping system	Electrical field with stable high voltage source, no back pressure
Solvents	Different solvents for different columns	Different solvents in the same column

simultaneous determination of 19 pharmaceutical and personal care products, including triclosan, in wastewater. Solid phase extraction in combination with on-line pre-concentration methodology was applied. The proposed method provided the linear range of 1.0×10^5 – 1.0×10^6 ng L⁻¹ with a detection limit of 30.6 ng L⁻¹ for triclosan [106].

Another study was conducted for the determination of triclosan in untreated wastewater by capillary electrophoresis (CE) with UV detection. Instrument linear range, detection and quantification limits were 2.4×10^6 – 3.8×10^7 , 1.2×10^6 and 2.4×10^6 ng L⁻¹ respectively, with a method detection limit of 68.7 $\times 10^3$ ng L⁻¹ [58].

There are limited studies regarding the application of capillary zone electrophoresis for the determination of triclosan in water samples. Despite the advantages of CE, including reduced reagent consumption, low required sample volume, high separation efficiency and short analysis time; it provides low sensitivity in terms of solute concentration compared to other separation techniques, which is due to both the small optical path-length of the capillary (50–75 μm) used as a detection cell and the small volumes (usually a few nanoliters) that can be injected, which limit the application of CE [107,108]. Furthermore, the main drawbacks of CZE compared to other analytical methods are its relatively poor reproducibility and low sample tolerance [109].

The disadvantage of CE with regard to its inferior reproducibility as compared to HPLC is such an obstacle that HPLC is preferred for routine applications [110]. A certain amount of avoidance can be explained by the lack of familiarity with CE which can lead to the development of methods that are not robust, perform poorly and give CE a negative reputation [110]. Table 5 compares some analytical parameters of HPLC and CE.

4.4. Optical methods

An ultrasound-assisted emulsification–microextraction procedure for triclosan determination in wastewater samples was developed where a diazotation reaction was employed with microvolume UV–Vis spectrophotometry detection. A linear range of 5.8–52.1 ng L⁻¹ was obtained and the LOD was 1.45 ng L⁻¹ [112].

White light reflectance spectroscopy (WLRS) has also been used for the real-time monitoring of triclosan using synthesized 2,3-dimethyl-6-(undec-10-enamide)-6-deoxy- β -cyclodextrin (DMBUA) on a silicon wafer coated with a novolac resin, where the introduction of triclosan on the top of the DMBUA layer resulted in a peak wavelength shift [113].

Although spectrophotometric methods are comparatively cheap and fast, they are not as sensitive as the other methods described, hence they are generally not suitable for the direct monitoring of triclosan in environmental water samples, as analyte pre-concentration would be required. Alternative optical methods which are more sensitive, such as surface plasmon resonance based techniques have thus been developed.

In spite of the fact that chemiluminescence methods are convenient, fast and require less expensive instrumentation, pre-transformation is needed prior to triclosan analysis and the selectivity achieved is generally not good enough for direct application in water analysis [56]. Therefore there still remains a great need for a fast and user-friendly *in situ* monitoring device for triclosan.

A TCS-imprinted poly(2-hydroxyethylmethacrylate–methacryloylamidoglutamic acid) [p(HEMAGA)] surface plasmon resonance (SPR) nanosensor was developed as a novel molecularly imprinted SPR sensor for the sensitive and selective detection of triclosan in wastewater, using an allylmercaptane modified gold SPR chip and imprinted p(HEMAGA) nanofilm. The linearity range and detection limit of TCS were found to be 50 – 1.0×10^3 ng L⁻¹ and 17 ng L⁻¹, respectively with a LOQ of 50 ng L⁻¹ [114].

It is noteworthy to mention that, with the advent of mathematical data treatment (chemometrics), solvent-free methodologies based on direct spectroscopic measurements without any sample pretreatment have been developed for a range of analytes to provide quantitative as well as qualitative information [92]. These advances may result in interesting possibilities regarding the future establishment of both screening and quantitative spectroscopic methods.

5. Conclusion and future outlook

Triclosan is a synthetic, non-ionic, broad-spectrum antimicrobial agent that has been used extensively for more than 20 years. It is a relatively stable, lipophilic compound which has been detected in surface water systems. In general, due to the low concentration of triclosan in environmental matrices, it needs to be extracted and pre-concentrated before analysis. Traditional extraction techniques are not environmentally friendly and consumption of a large quantity of chemicals limits their application, therefore alternatives such as dispersive liquid-liquid microextraction has gained considerable attention, as it does not only provide better efficiency but is also a time-saving process because of the large contact surface involved and thus high speed of analyte mass transfer.

We have reviewed different approaches for the determination of triclosan and their linear ranges and detection limits have been compared. The determination of triclosan has predominately been performed by chromatography based methods and nanomaterial based electrode systems using voltammetric methods. Chromatography methods are sensitive and selective, however they are time consuming and they require bulky and expensive instrumentation, as well as high cost detectors such as MS and MS/MS. Triclosan can undergo oxidation at the surface of electrode materials, making it suitable for electrochemical detection. The combination of nanomaterials and electrochemical methods provide a fast, convenient and inexpensive approach for the determination of triclosan, however these methods suffer from strongly adsorbed oligomeric products of the oxidation of triclosan on the electrode surface.

Relatively few reports have been published recently on CE developments for the determination of triclosan. However, if reproducibility limitations of CE can be adequately addressed, green analytical chemistry requirements might lead to CE becoming a viable alternative to HPLC in the future in some applications [115].

Although spectrophotometric methods enjoy simplicity, and a wide linear range, they cannot be applied for direct application in water samples. The complexity of matrices also limits the application of spectroscopic methods in addition to their low sensitivity, which results in the need for clean-up and pre-concentration procedures. The relatively new development of employing molecularly imprinted polymers in the extraction and sensing of triclosan is a promising contribution for the determination of triclosan in water samples, due to the enhanced sensitivity and selectivity which can

result, as well as due to the low cost and mechanical stability of these materials.

Although GC or LC with MS is the method which is primarily used in routine applications, other techniques reported in this review are being developed and may see wider application once they become more widely known and tested. In many cases quality control needs further attention and analytical robustness needs to be proven following from the reporting of initial development results, to allow for the uptake of these methods for wider and routine applications. Due to the ubiquity of triclosan in the environment, we expect these developments to be realized for those methods showing promising selectivity and sensitivity, such as the application of MIPs.

Regarding GAC, online, miniaturized and automated sampling and analytical approaches are favourable, where solvent consumption is minimized. Some routine methods based on classical chromatographic analyses consume large amount of reagents or energy and they also generate large volumes of waste. These methods therefore require improvements so that they become more environmentally friendly.

As a result of the ubiquitous nature of triclosan in environmental water resources and due the concern regarding its potential environmental impacts, it is envisaged that future research efforts will focus on the development of novel methods which provide for the fast, simple, sensitive and selective determination of this analyte in a cost effective and environmentally responsible manner.

Acknowledgements

Funding from the University of Pretoria, the Water Research Commission (grant K5-2438), the Photonics Initiative of South Africa (grant PISA-15-DIR-06) and the National Research Foundation of South Africa (grants 90720 and 93394) is gratefully acknowledged.

References

- [1] H. Bhargava, P.A. Leonard, Triclosan: applications and safety, *Am. J. Infect. Control* 24 (1996) 209–218.
- [2] R.D. Jones, H.B. Jampani, J.L. Newman, A.S. Lee, Triclosan: a review of effectiveness and safety in health care settings, *Am. J. Infect. Control* 28 (2000) 184–196.
- [3] J.V. Rodricks, J.A. Swenberg, J.F. Borzelleca, R.R. Maronpot, A.M. Shipp, Triclosan: a critical review of the experimental data and development of margins of safety for consumer products, *Crit. Rev. Toxicol.* 40 (2010) 422–484.
- [4] EU, List of preservatives which cosmetic products may contain. *Cosmetics Directive 76/768/EEC, Annex VI, Part I, entry 25*, 2007.
- [5] J. Du Preez, W. Yang, Improving the aqueous solubility of triclosan by solubilization, complexation, and in situ salt formation, *J. Cosmet. Sci.* 54 (2003) 537–550.
- [6] H.-S. Son, G. Ko, K.-D. Zoh, Kinetics and mechanism of photolysis and TiO₂ photocatalysis of triclosan, *J. Hazard. Mater.* 166 (2009) 954–960.
- [7] M. Allmyr, F. Harden, L.-M.L. Toms, J.F. Mueller, M.S. McLachlan, M. Adolfsson-Erici, et al., The influence of age and gender on triclosan concentrations in Australian human blood serum, *Sci. Total Environ.* 393 (2008) 162–167.
- [8] N. Veldhoen, R.C. Skirrow, H. Osachoff, H. Wigmore, D.J. Clapson, M.P. Gunderson, et al., The bactericidal agent triclosan modulates thyroid hormone-associated gene expression and disrupts postembryonic anuran development, *Aquat. Toxicol.* 80 (2006) 217–227.
- [9] J.-L. Zhao, Q.-Q. Zhang, F. Chen, L. Wang, G.-G. Ying, Y.-S. Liu, et al., Evaluation of triclosan and triclocarban at river basin scale using monitoring and modeling tools: implications for controlling of urban domestic sewage discharge, *Water Res.* 47 (2013) 395–405.
- [10] N. Tatarazako, H. Ishibashi, K. Teshima, K. Kishi, K. Arizono, Effects of triclosan on various aquatic organisms, *Environ. Sci.* 11 (2004) 133–140.
- [11] M. Allmyr, M. Adolfsson-Erici, M.S. McLachlan, G. Sandborgh-Englund, Triclosan in plasma and milk from Swedish nursing mothers and their exposure via personal care products, *Sci. Total Environ.* 372 (2006) 87–93.
- [12] E.M. Fiss, K.L. Rule, P.J. Vikesland, Formation of chloroform and other chlorinated byproducts by chlorination of triclosan-containing antibacterial products, *Environ. Sci. Technol.* 41 (2007) 2387–2394.
- [13] K.L. Rule, V.R. Ebbett, P.J. Vikesland, Formation of chloroform and chlorinated organics by free-chlorine-mediated oxidation of triclosan, *Environ. Sci. Technol.* 39 (2005) 3176–3185.
- [14] A. Kanetoshi, H. Ogawa, E. Katsura, H. Kaneshima, Chlorination of Irgasan DP300 and formation of dioxins from its chlorinated derivatives, *J. Chromatogr. A* 389 (1987) 139–153.
- [15] A. Lindström, L.J. Buerge, T. Poiger, P.-A. Bergqvist, M.D. Müller, H.-R. Buser, Occurrence and environmental behavior of the bactericide triclosan and its methyl derivative in surface waters and in wastewater, *Environ. Sci. Technol.* 36 (2002) 2322–2329.
- [16] M.M. Häggblom, D. Janke, P.J. Middeldorp, M.S. Salkinoja-Salonen, O-methylation of chlorinated phenols in the genus *Rhodococcus*, *Arch. Microbiol.* 152 (1989) 6–9.
- [17] D.W. Kolpin, E.T. Furlong, M.T. Meyer, E.M. Thurman, S.D. Zaugg, L.B. Barber, et al., Pharmaceuticals, hormones, and other organic wastewater contaminants in US streams, 1999–2000: a national reconnaissance, *Environ. Sci. Technol.* 36 (2002) 1202–1211.
- [18] G.S. Dhillon, S. Kaur, R. Pulicharla, S.K. Brar, M. Cledón, M. Verma, et al., Triclosan: current status, occurrence, environmental risks and bioaccumulation potential, *Int. J. Environ. Res. Public Health* 12 (2015) 5657–5684.
- [19] SCCS, Opinion on Triclosan – Antimicrobial Resistance, Scientific Committee on Consumer Safety, 2010, pp. 1–56.
- [20] T.E. Chalew, R.U. Halden, Environmental exposure of aquatic and terrestrial biota to triclosan and triclocarban, *J. Am. Water Resour. Assoc.* 45 (2009) 4–13.
- [21] K. Bester, Fate of triclosan and triclosan-methyl in sewage treatment plants and surface waters, *Arch. Environ. Contam. Toxicol.* 49 (2005) 9–17.
- [22] M. Parolini, A. Pedriali, A. Binelli, Application of a biomarker response index for ranking the toxicity of five pharmaceutical and personal care products (PPCPs) to the bivalve *Dreissena polymorpha*, *Arch. Environ. Contam. Toxicol.* 64 (2013) 439–447.
- [23] S.A.O. de García, G.P. Pinto, P.A. García-Encina, R. Irusta-Mata, Ecotoxicity and environmental risk assessment of pharmaceuticals and personal care products in aquatic environments and wastewater treatment plants, *Ecotoxicology* 23 (2014) 1517–1533.
- [24] S.O. de García, P. García-Encina, R. Irusta-Mata, Environmental risk assessment (ERA) of pharmaceuticals and personal care products (PPCPs) using ecotoxicity tests, 2011.
- [25] USEPA, Targeted National Sewage Sludge Survey Sampling and Analysis Technical Report, United States Environmental Protection Agency, Washington, DC, 2009, pp. 1–10.
- [26] R.M. Pemberton, J.P. Hart, Electrochemical behaviour of triclosan at a screen-printed carbon electrode and its voltammetric determination in toothpaste and mouthrinse products, *Anal. Chim. Acta* 390 (1999) 107–115.
- [27] D. Mackay, R.S. Boethling, *Handbook of Property Estimation Methods for Chemicals: Environmental Health Sciences*, CRC Press, 2000.
- [28] Reregistration eligibility decision for triclosan, list B, 2008.
- [29] E. Aldous, L. Rockett, I. Johnson, Proposed EQS for Water Framework Directive Annex VIII Substances: Triclosan (for Consultation), Water Framework Directive-United Kingdom Technical Advisory Group, 2009.
- [30] D.C. McAvoy, B. Schatowitz, M. Jacob, A. Hauk, W.S. Eckhoff, Measurement of triclosan in wastewater treatment systems, *Environ. Toxicol. Chem.* 21 (2002) 1323–1329.
- [31] NICNAS, Triclosan, Priority Existing Chemical Assessment Report No. 30, National Industrial Chemicals Notification and Assessment, Sydney, Australia, 2009.
- [32] R. Kanda, P. Griffin, H.A. James, J. Fothergill, Pharmaceutical and personal care products in sewage treatment works, *J. Environ. Monit.* 5 (2003) 823–830.
- [33] K. Bester, Triclosan in a sewage treatment process—balances and monitoring data, *Water Res.* 37 (2003) 3891–3896.
- [34] H. Singer, S. Müller, C. Tixier, L. Pillonel, Triclosan: occurrence and fate of a widely used biocide in the aquatic environment: field measurements in wastewater treatment plants, surface waters, and lake sediments, *Environ. Sci. Technol.* 36 (2002) 4998–5004.
- [35] T.W. Federle, S.K. Kaiser, B.A. Nuck, Fate and effects of triclosan in activated sludge, *Environ. Toxicol. Chem.* 21 (2002) 1330–1337.
- [36] L. Lishman, S.A. Smyth, K. Sarafin, S. Kleywegt, J. Toito, T. Peart, et al., Occurrence and reductions of pharmaceuticals and personal care products and estrogens by municipal wastewater treatment plants in Ontario, Canada, *Sci. Total Environ.* 367 (2006) 544–558.
- [37] A. Lindström, L.J. Buerge, T. Poiger, P.-A. Bergqvist, M.D. Müller, H.-R. Buser, Occurrence and environmental behavior of the bactericide triclosan and its methyl derivative in surface waters and in wastewater, *Environ. Sci. Technol.* 36 (2002) 2322–2329.
- [38] V. Lopez-Avila, R.A. Hites, Organic compounds in an industrial wastewater. Their transport into sediments, *Environ. Sci. Technol.* 14 (1980) 1382–1390.
- [39] A. Thompson, P. Griffin, R. Stuetz, E. Cartmell, The fate and removal of triclosan during wastewater treatment, *Water Environ. Res.* 77 (2005) 63–67.
- [40] P. Canosa, S. Morales, I. Rodriguez, E. Rubi, R. Cela, M. Gomez, Aquatic degradation of triclosan and formation of toxic chlorophenols in presence of low concentrations of free chlorine, *Anal. Bioanal. Chem.* 383 (2005) 1119–1126.
- [41] S. Suarez, M.C. Dodd, F. Omil, U. von Gunten, Kinetics of triclosan oxidation by aqueous ozone and consequent loss of antibacterial activity: relevance to municipal wastewater ozonation, *Water Res.* 41 (2007) 2481–2490.
- [42] E.C. Wert, F.L. Rosario-Ortiz, S.A. Snyder, Effect of ozone exposure on the oxidation of trace organic contaminants in wastewater, *Water Res.* 43 (2009) 1005–1014.

- [43] M.C. Dodd, H.-P.E. Kohler, U. Von Gunten, Oxidation of antibacterial compounds by ozone and hydroxyl radical: elimination of biological activity during aqueous ozonation processes, *Environ. Sci. Technol.* 43 (2009) 2498–2504.
- [44] S. Snyder, E. Wert, H. Lei, P. Westerhoff, Y. Yoon, Removal of EDCs and Pharmaceuticals in Drinking and Reuse Treatment Processes (91188), American Water Works Association Research Foundation (AWWARF), Denver, CO, USA, 2007.
- [45] G.F. Lee, J.C. Morris, Kinetics of chlorination of phenol-chlorophenolic tastes and odors, *Int. J. Air Water Pollut.* 6 (1962) 419–431.
- [46] C. Tixier, H.P. Singer, S. Canonica, S.R. Müller, Phototransformation of triclosan in surface waters: a relevant elimination process for this widely used biocide laboratory studies, field measurements, and modeling, *Environ. Sci. Technol.* 36 (2002) 3482–3489.
- [47] J. Namies'nik, Green analytical chemistry – some remarks, *J. Sep. Sci.* 24 (2001) 151–153.
- [48] A. Gałuszka, Z. Migaszewski, J. Namies'nik, The 12 principles of green analytical chemistry and the SIGNIFICANCE mnemonic of green analytical practices, *Trends Analyt. Chem.* 50 (2013) 78–84.
- [49] D. Kim, J. Han, Y. Choi, On-line solid-phase microextraction of triclosan, bisphenol A, chlorophenols, and selected pharmaceuticals in environmental water samples by high-performance liquid chromatography–ultraviolet detection, *Anal. Bioanal. Chem.* 405 (2013) 377–387.
- [50] C. Zheng, J. Zhao, P. Bao, J. Gao, J. He, Dispersive liquid–liquid microextraction based on solidification of floating organic droplet followed by high-performance liquid chromatography with ultraviolet detection and liquid chromatography–tandem mass spectrometry for the determination of triclosan and 2, 4-dichlorophenol in water samples, *J. Chromatogr. A* 1218 (2011) 3830–3836.
- [51] R. Gibson, E. Becerril-Bravo, V. Silva-Castro, B. Jiménez, Determination of acidic pharmaceuticals and potential endocrine disrupting compounds in wastewaters and spring waters by selective elution and analysis by gas chromatography–mass spectrometry, *J. Chromatogr. A* 1169 (2007) 31–39.
- [52] Z. Yu, S. Peldszus, P.M. Huck, Optimizing gas chromatographic–mass spectrometric analysis of selected pharmaceuticals and endocrine-disrupting substances in water using factorial experimental design, *J. Chromatogr. A* 1148 (2007) 65–77.
- [53] H. Lu, H. Ma, G. Tao, Spectrophotometric determination of triclosan in personal care products, *Spectrochim. Acta A. Mol. Biomol. Spectrosc.* 73 (2009) 854–857.
- [54] M. Amiri, S. Shahrokhan, E. Psillakis, F. Marken, Electrostatic accumulation and determination of triclosan in ultrathin carbon nanoparticle composite film electrodes, *Anal. Chim. Acta* 593 (2007) 117–122.
- [55] M.L. Yola, N. Atar, H. Karimi-Maleh, S. Wang, Sensitive and selective determination of aqueous triclosan based on gold nanoparticles on polyoxometalate/reduced graphene oxide nanohybrid, *RSC Adv.* 5 (2015) 65953–65962.
- [56] Y. Liu, Q.-J. Song, L. Wang, Development and characterization of an amperometric sensor for triclosan detection based on electropolymerized molecularly imprinted polymer, *Microchem. J.* 91 (2009) 222–226.
- [57] H. Wang, A. Zhang, W. Wang, M. Zhang, H. Liu, X. Wang, Separation and determination of triclosan and bisphenol A in water, beverage, and urine samples by dispersive liquid–liquid microextraction combined with capillary zone electrophoresis–UV detection, *J. AOAC Int.* 96 (2013) 459–465.
- [58] S.E. Gibbons, C. Wang, Y. Ma, Determination of pharmaceutical and personal care products in wastewater by capillary electrophoresis with UV detection, *Talanta* 84 (2011) 1163–1168.
- [59] M. de la Guardia, S. Armenta, Green solvents for analytical separation and analyses, *Encycl. Anal. Chem.* (2010) doi:10.1002/9780470027318.a9179.
- [60] P. Sun, D.W. Armstrong, Ionic liquids in analytical chemistry, *Anal. Chim. Acta* 661 (2010) 1–16.
- [61] M. Tobiszewski, J. Namiesnik, Developments in green chromatography, *LC GC Eur.* 27 (2014) 405–408.
- [62] U.S. EPA, Method 1694: Pharmaceuticals and Personal Care Products in Water, Soil, Sediment, and Biosolids by HPLC/MS/MS, 2007, pp. 1–77.
- [63] J.C. Chow, J.G. Watson, J. Robles, X. Wang, L.-W.A. Chen, D.L. Trimble, et al., Quality assurance and quality control for thermal/optical analysis of aerosol samples for organic and elemental carbon, *Anal. Bioanal. Chem.* 401 (2011) 3141–3152.
- [64] I. Taverniers, M. De Loose, E. Van Bockstaele, Trends in quality in the analytical laboratory. II. Analytical method validation and quality assurance, *Trends Analyt. Chem.* 23 (2004) 535–552.
- [65] G. Gatidou, N.S. Thomaidis, A.S. Stasinakis, T.D. Lekkas, Simultaneous determination of the endocrine disrupting compounds nonylphenol, nonylphenol ethoxylates, triclosan and bisphenol A in wastewater and sewage sludge by gas chromatography–mass spectrometry, *J. Chromatogr. A* 1138 (2007) 32–41.
- [66] M.G. Pintado-Herrera, E. González-Mazo, P.A. Lara-Martín, Determining the distribution of triclosan and methyl triclosan in estuarine settings, *Chemosphere* 95 (2014) 478–485.
- [67] L. Jachero, B. Sepúlveda, I. Ahumada, E. Fuentes, P. Richter, Rotating disk sorptive extraction of triclosan and methyl-triclosan from water samples, *Anal. Bioanal. Chem.* 405 (2013) 7711–7716.
- [68] Y.C. Fiamegos, C.D. Stalikas, In-drop derivatization liquid-phase microextraction assisted by ion-pairing transfer for the gas chromatographic determination of phenolic endocrine disruptors, *Anal. Chim. Acta* 597 (2007) 32–40.
- [69] M. Kawaguchi, R. Ito, H. Honda, N. Endo, N. Okanouchi, K. Saito, et al., Stir bar sorptive extraction and thermal desorption–gas chromatography–mass spectrometry for trace analysis of triclosan in water sample, *J. Chromatogr. A* 1206 (2008) 196–199.
- [70] A.M.C. Ferreira, M. Möder, M.E.F. Laespada, GC-MS determination of parabens, triclosan and methyl triclosan in water by in situ derivatization and stir-bar sorptive extraction, *Anal. Bioanal. Chem.* 399 (2011) 945–953.
- [71] I. González-Mariño, J.B. Quintana, I. Rodríguez, S. Schrader, M. Moeder, Fully automated determination of parabens, triclosan and methyl triclosan in wastewater by microextraction by packed sorbents and gas chromatography–mass spectrometry, *Anal. Chim. Acta* 684 (2011) 59–66.
- [72] J.-L. Wu, N.P. Lam, D. Martens, A. Kettrup, Z. Cai, Triclosan determination in water related to wastewater treatment, *Talanta* 72 (2007) 1650–1654.
- [73] M. Gómez, A. Agüera, M. Mezcuca, J. Hurtado, F. Mocholf, A. Fernández-Alba, Simultaneous analysis of neutral and acidic pharmaceuticals as well as related compounds by gas chromatography–tandem mass spectrometry in wastewater, *Talanta* 73 (2007) 314–320.
- [74] W.C. Chau, J.L. Wu, Z. Cai, Investigation of levels and fate of triclosan in environmental waters from the analysis of gas chromatography coupled with ion trap mass spectrometry, *Chemosphere* 73 (2008) S13–S17.
- [75] J. Regueiro, E. Becerril, C. Garcia-Jares, M. Llompart, Trace analysis of parabens, triclosan and related chlorophenols in water by headspace solid-phase microextraction with in situ derivatization and gas chromatography–tandem mass spectrometry, *J. Chromatogr. A* 1216 (2009) 4693–4702.
- [76] R. Montes, I. Rodríguez, E. Rubí, R. Cela, Dispersive liquid–liquid microextraction applied to the simultaneous derivatization and concentration of triclosan and methyltriclosan in water samples, *J. Chromatogr. A* 1216 (2009) 205–210.
- [77] J. Regueiro, M. Llompart, E. Psillakis, J.C. Garcia-Montegudo, C. Garcia-Jares, Ultrasound-assisted emulsification–microextraction of phenolic preservatives in water, *Talanta* 79 (2009) 1387–1397.
- [78] R. E. Villaverde-de-Sáa, I. González-Mariño, J.B. Quintana, R. Rodil, I. Rodríguez, Cela, In-sample acetylation-non-porous membrane-assisted liquid–liquid extraction for the determination of parabens and triclosan in water samples, *Anal. Bioanal. Chem.* 397 (2010) 2559–2568.
- [79] A.R.M. Silva, J. Nogueira, New approach on trace analysis of triclosan in personal care products, biological and environmental matrices, *Talanta* 74 (2008) 1498–1504.
- [80] J.Y. Shen, M.S. Chang, S.H. Yang, G.J. Wu, Simultaneous determination of triclosan, triclocarban, and transformation products of triclocarban in aqueous samples using solid-phase micro-extraction-HPLC-MS/MS, *J. Sep. Sci.* 35 (2012) 2544–2552.
- [81] M.S. Chang, J.Y. Shen, S.-H. Yang, G.J. Wu, Determination of three endocrine disrupting chemicals, triclosan, 4-n-nonylphenol, and di-n-butyl phthalate using stir bar sorptive extraction in samples of different matrices, *Toxicol. Environ. Chem.* 94 (2012) 1027–1033.
- [82] E. Carmona, V. Andreu, Y. Picó, Occurrence of acidic pharmaceuticals and personal care products in Turia River Basin: from waste to drinking water, *Sci. Total Environ.* 484 (2014) 53–63.
- [83] R.-S. Zhao, X. Wang, J. Sun, S.-S. Wang, J.-P. Yuan, X.-K. Wang, Trace determination of triclosan and triclocarban in environmental water samples with ionic liquid dispersive liquid-phase microextraction prior to HPLC–ESI-MS–MS, *Anal. Bioanal. Chem.* 397 (2010) 1627–1633.
- [84] R.S. Zhao, X. Wang, J. Sun, J.P. Yuan, S.S. Wang, X.K. Wang, Temperature-controlled ionic liquid dispersive liquid-phase microextraction for the sensitive determination of triclosan and triclocarban in environmental water samples prior to HPLC-ESI-MS/MS, *J. Sep. Sci.* 33 (2010) 1842–1848.
- [85] R.-S. Zhao, X. Wang, J. Sun, C. Hu, X.-K. Wang, Determination of triclosan and triclocarban in environmental water samples with ionic liquid/ionic liquid dispersive liquid-liquid microextraction prior to HPLC-ESI-MS/MS, *Mikrochim. Acta* 174 (2011) 145–151.
- [86] J. Sun, C.L. Yi, R.S. Zhao, X. Wang, W.Q. Jiang, X.K. Wang, Determination of trace triclosan in environmental water by microporous bamboo-activated charcoal solid-phase extraction combined with HPLC-ESI-MS, *J. Sep. Sci.* 35 (2012) 2781–2786.
- [87] J.-H. Guo, X.-H. Li, X.-L. Cao, Y. Li, X.-Z. Wang, X.-B. Xu, Determination of triclosan, triclocarban and methyl-triclosan in aqueous samples by dispersive liquid–liquid microextraction combined with rapid liquid chromatography, *Chromatogr. A* 1216 (2009) 3038–3043.
- [88] J. Guo, X. Li, X. Cao, L. Qu, D. Hou, X. Xu, Temperature-controlled ionic liquid dispersive liquid phase microextraction combined with ultra-high-pressure liquid chromatography for the rapid determination of triclosan, triclocarban and methyl-triclosan in aqueous samples, *Sci. China Chem.* 53 (2010) 2600–2607.
- [89] M. Pedrouzo, F. Borrull, R.M. Marcé, E. Pocurull, Ultra-high-performance liquid chromatography–tandem mass spectrometry for determining the presence of eleven personal care products in surface and wastewaters, *J. Chromatogr. A* 1216 (2009) 6994–7000.
- [90] R. Gao, X. Kong, F. Su, X. He, L. Chen, Y. Zhang, Synthesis and evaluation of molecularly imprinted core-shell carbon nanotubes for the determination of triclosan in environmental water samples, *J. Chromatogr. A* 1217 (2010) 8095–8102.
- [91] J. Plotka, M. Tobiszewski, A.M. Sulej, M. Kupka, T. Gorecki, J. Namies'nik, Green chromatography, *J. Chromatogr. A* 1307 (2013) 1–20.
- [92] S. Armenta, M. De la Guardia, Green spectroscopy: a scientometric picture, *Spectrosc. Lett.* 42 (2009) 277–283.
- [93] L. Kociřová, I.S. Balogh, V. Andruch, Solvent microextraction: a review of recent efforts at automation, *Microchem. J.* 110 (2013) 599–607.

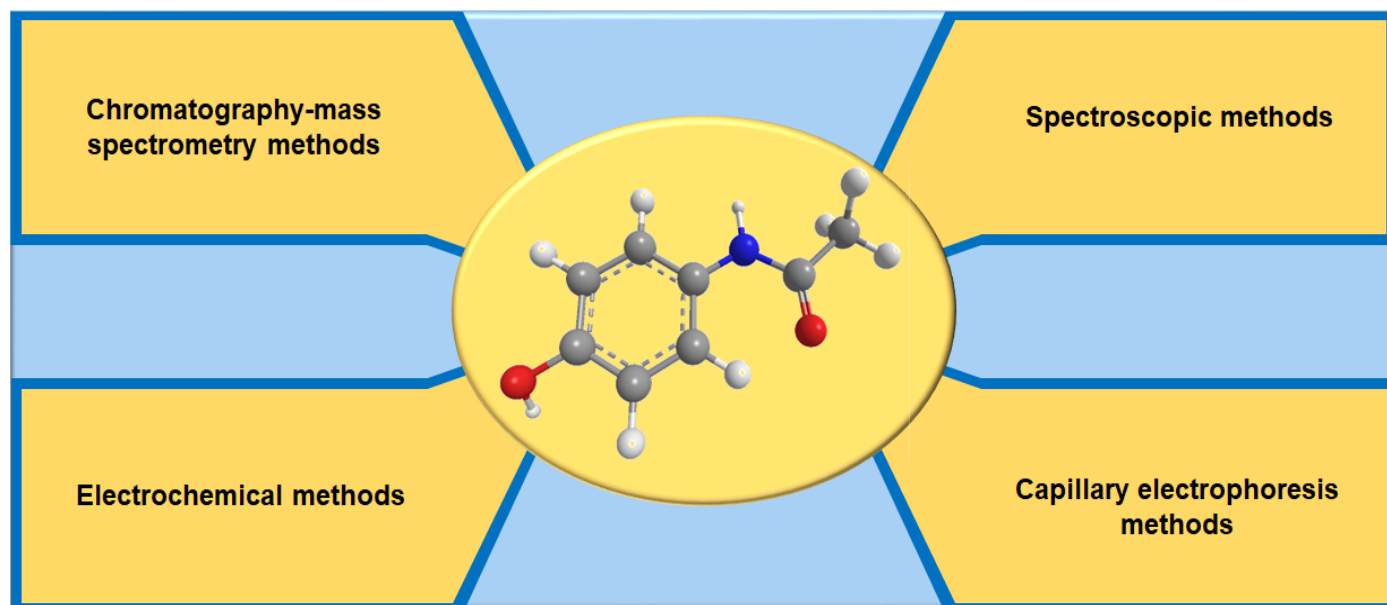
- [94] H. Dai, G. Xu, L. Gong, C. Yang, Y. Lin, Y. Tong, et al., Electrochemical detection of triclosan at a glassy carbon electrode modified with carbon nanodots and chitosan, *Electrochim. Acta* 80 (2012) 362–367.
- [95] A. Safavi, N. Maleki, H. Shahbaazi, Electrochemical determination of triclosan at a mercury electrode, *Anal. Chim. Acta* 494 (2003) 225–233.
- [96] M.A. Ghanem, R.G. Compton, B.A. Coles, E. Psillakis, M.A. Kulandainathan, F. Marken, Microwave activation of electrochemical processes: high temperature phenol and triclosan electro-oxidation at carbon and diamond electrodes, *Electrochim. Acta* 53 (2007) 1092–1099.
- [97] M.A. Ghanem, R.G. Compton, B.A. Coles, A. Canals, F. Marken, Microwave enhanced electroanalysis of formulations: processes in micellar media at glassy carbon and at platinum electrodes, *Analyst* 130 (2005) 1425–1431.
- [98] M. Moyo, L.R. Florence, J.O. Okonkwo, Improved electro-oxidation of triclosan at nano-zinc oxide-multiwalled carbon nanotube modified glassy carbon electrode, *Sens. Actuators B Chem.* 209 (2015) 898–905.
- [99] L. Vidal, A. Chisvert, A. Canals, E. Psillakis, A. Lapkin, F. Acosta, et al., Chemically surface-modified carbon nanoparticle carrier for phenolic pollutants: extraction and electrochemical determination of benzophenone-3 and triclosan, *Anal. Chim. Acta* 616 (2008) 28–35.
- [100] M.J. Bonne, K.J. Edler, J.G. Buchanan, D. Wolverson, E. Psillakis, M. Helton, et al., Thin-film modified electrodes with reconstituted cellulose-PDDAC films for the accumulation and detection of triclosan, *J. Phys. Chem. C* 112 (2008) 2660–2666.
- [101] L. Fotouhi, H.R. Shahbaazi, A. Fatehi, M.M. Heravi, Voltammetric determination of triclosan in waste water and personal care products, *Int. J. Electrochem. Sci.* 5 (2010) 1390–1398.
- [102] B. Li, Z. Qiu, Q. Wan, Y. Liu, N. Yang, β -cyclodextrin functionalized graphene nano platelets for electrochemical determination of triclosan, *Physica Status Solidi A Appl. Res.* 211 (2014) 2773–2777.
- [103] A.H. Alghamdi, Applications of stripping voltammetric techniques in food analysis, *Arabian J. Chem.* 3 (2010) 1–7.
- [104] J. Wang, Real-time electrochemical monitoring: toward green analytical chemistry, *Acc. Chem. Res.* 35 (2002) 811–816.
- [105] J. Yang, P. Wang, X. Zhang, K. Wu, Electrochemical sensor for rapid detection of Triclosan using a multiwall carbon nanotube film, *J. Agric. Food Chem.* 57 (2009) 9403–9407.
- [106] Z. Zhang, D. Zhang, X. Zhang, Simultaneous determination of pharmaceutical and personal care products in wastewater by capillary electrophoresis with head-column field-amplified sample stacking, *Anal. Methods* 6 (2014) 7978–7983.
- [107] F.J. Lara, D. Airado-Rodríguez, D. Moreno-González, J.F. Huertas-Pérez, A.M. García-Campaña, Applications of capillary electrophoresis with chemiluminescence detection in clinical, environmental and food analysis. A review, *Anal. Chim. Acta* 913 (2016) 22–40.
- [108] D.M. Osbourn, D.J. Weiss, C.E. Lunte, On-line preconcentration methods for capillary electrophoresis, *Electrophoresis* 21 (2000) 2768.
- [109] J. Frenz, S.-L. Wu, W.S. Hancock, Characterization of human growth hormone by capillary electrophoresis, *J. Chromatogr. A* 480 (1989) 379–391.
- [110] M. de la Guardia, S. Garrigues, *Handbook of Green Analytical Chemistry*, Wiley Online Library, 2012.
- [111] M. Koel, M. Kaljurand, Application of the principles of green chemistry in analytical chemistry, *Pure Appl. Chem.* 78 (2006) 1993–2002.
- [112] N. Cabaleiro, F. Pena-Pereira, I. de la Calle, C. Bendicho, I. Lavilla, Determination of triclosan by cuvetteless UV–vis micro-spectrophotometry following simultaneous ultrasound assisted emulsification–microextraction with derivatization: use of a micellar-ionic liquid as extractant, *Microchem. J.* 99 (2011) 246–251.
- [113] D. Maffeo, Z. Velkov, K. Misiakos, K. Mergia, A. Paulidou, M. Zavali, et al., Real-time monitoring of nanomolar binding to a cyclodextrin monolayer immobilized on a Si/SiO₂/novolac surface using white light reflectance spectroscopy: the case of triclosan, *J. Colloid Interface Sci.* 358 (2011) 369–375.
- [114] N. Atar, T. Eren, M.L. Yola, S. Wang, A sensitive molecular imprinted surface plasmon resonance nanosensor for selective determination of trace triclosan in wastewater, *Sens. Actuators B Chem.* 216 (2015) 638–644.
- [115] K.D. Altria, W. Ciccone, B. Nunnally, *Technology Forum: Capillary Electrophoresis, LC-GC*, 2009.

3.2 Paper 2

This paper was formatted in accordance with the journal *TrAC Trends in Analytical Chemistry*, an Elsevier journal in which it has been published:

Montaseri, H., & Forbes, P.B.C. (2018). Analytical techniques for the determination of acetaminophen: A review. *TrAC Trends in Analytical Chemistry*, 108, 122-134. Impact Factor 7.034. <https://doi.org/10.1016/j.trac.2018.08.023>

Graphical abstract





Analytical techniques for the determination of acetaminophen: A review



Hanieh Montaseri, Patricia B.C. Forbes*

Department of Chemistry, Faculty of Natural and Agricultural Sciences, University of Pretoria, Lynnwood Road, Pretoria, 0002, South Africa

ARTICLE INFO

Article history:
Available online 8 September 2018

Keywords:
Acetaminophen
Pharmaceuticals
Chromatography-mass spectrometry
Electrochemistry
Spectroscopy
Capillary electrophoresis

ABSTRACT

Acetaminophen is a very widely used pharmaceutical, consequently it has been detected in the water system. Reliable and robust analytical techniques are thus needed for the detection of acetaminophen, not only for quality control (of pharmaceuticals) and medical control (analysis in biological fluids), but also for environmental matrices. This review gives an overview of analytical methods for acetaminophen using chromatography-mass spectrometry for monitoring aquatic environments, and electrochemical methods for analysis of pharmaceuticals and biological fluids, as well as environmental samples. Other lesser utilized techniques, including spectroscopy and capillary zone electrophoresis, are also discussed. High sensitivity, speed, specificity and reproducibility allow for the utilization of conventional methods for the detection of acetaminophen in routine analysis. However, they are time consuming, expensive and labor intensive. It is envisioned that future research efforts will focus on the development of novel methods and sensor materials to address these limitations.

© 2018 Elsevier B.V. All rights reserved.

1. Introduction

Over the past few years, there has been widespread concern regarding the presence of pharmaceuticals in the environment, which can pose potential threats to living organisms. They are often considered as emerging chemical pollutants (ECPs) in waterbodies because they generally still remain unregulated or are currently undergoing a regularization process [1]. Emerging pollutants are comprised of human and veterinary pharmaceuticals, personal care products, surfactants, various industrial additives and plasticizers [2]. The ubiquity of pharmaceuticals in the environment can affect the quality of water and potentially negatively influence human health and ecosystem viability. Furthermore, the physio-chemical properties of acidic pharmaceuticals, such as high water solubility and poor degradability, may result in their passing through water treatment and filtration steps and they may consequently pose a risk to drinking water supplies [3].

Acetaminophen (paracetamol, refer to Scheme 1), which may be regarded as an ECP, is an acylated aromatic amide which is one of the most extensively used drugs for minor pain and fever treatment. According to the American College of Rheumatology (ACR)

guidelines for osteoarthritis, acetaminophen is considered as a first-line therapy because of its relative lack of adverse side effects, efficacy and low cost [4].

Acetaminophen (AC) is a subclass of organic contaminants that are continuously introduced into the aquatic environment from hospital waste, consumer use, disposal and manufacturing facilities. In spite of the fact that detected AC concentrations are in the ng L^{-1} to mg L^{-1} range in the environment, some potential deleterious effects, including acute and chronic damage to aquatic organisms and inhibition of cell proliferation in human cells [5] have been recorded at these low levels [6]. This contaminant does not need to be persistent in the environment, as the continuous introduction into the environment and high transformation rates can cause long term detrimental effects [2].

Some authors reported the presence of AC in effluents at concentrations below to 20 ng L^{-1} [7] to 4300 ng L^{-1} [8], although in surface waters values can reach $78,170 \text{ ng L}^{-1}$ [9], which are higher than the predicted no-effect concentration (PNEC) of 9200 ng L^{-1} [10]. Hence, AC might represent a threat to non-target organisms.

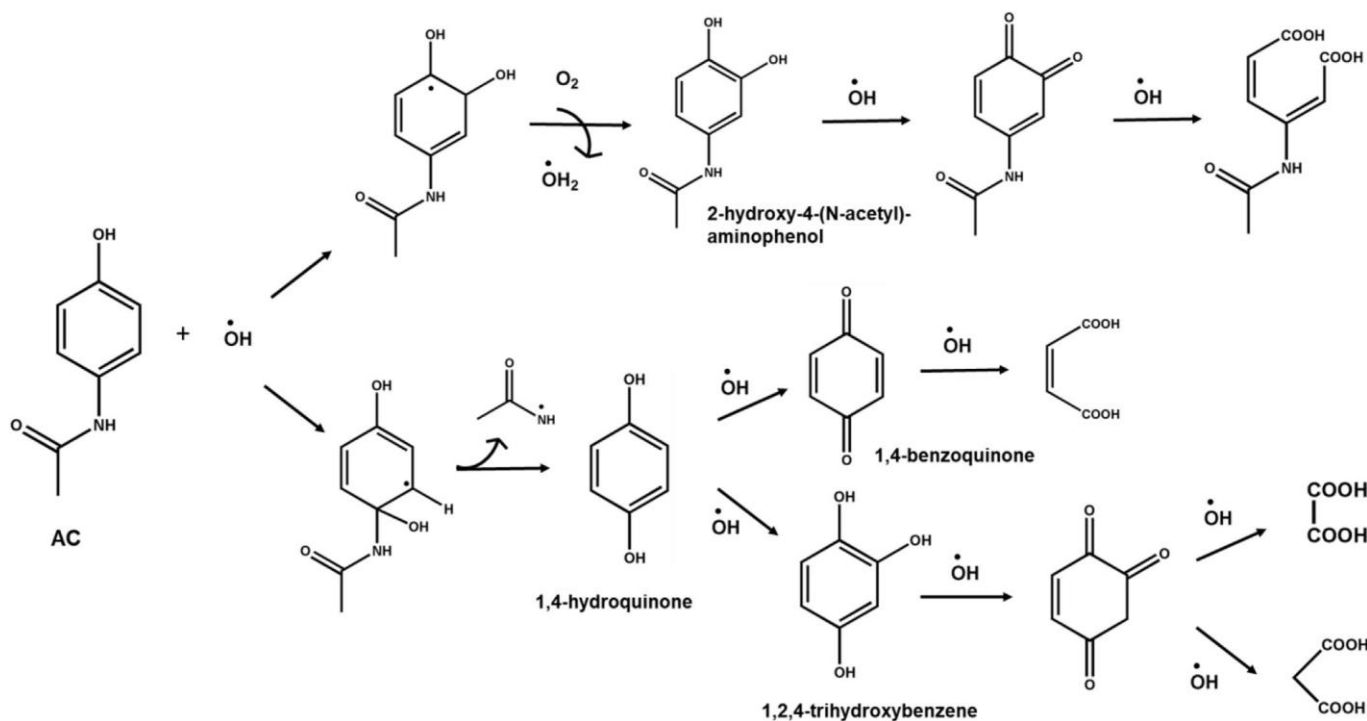
Based on available information, the Minnesota Department of Health (MDH) developed a guidance value of 200 ppb ($200,000 \text{ ng L}^{-1}$) for acetaminophen in drinking water. The MDH has considered the liver to be the most sensitive organ regarding acetaminophen exposure [11].

* Corresponding author.

E-mail address: patricia.forbes@up.ac.za (P.B.C. Forbes).

Abbreviations

AC	Acetaminophen	LLE	Liquid-liquid extraction
AC-Gluc	Acetaminophen-glucuronide	LOD	Limit of detection
ACR	American College of Rheumatology	LOQ	Limit of quantification
AC-3-OH	3-hydroxy-acetaminophen metabolite	LPME	Liquid-phase microextraction
amPA5-RGO	amphiphilic pillar [5] arene (amPA5) functionalized reduced graphene oxide	LTQ-Orbitrap	Linear trap quadrupole orbitrap
AC-Sulf	Acetaminophen-sulfate	MAA	Methacrylic acid
ANN	Artificial neural networks	MDH	Minnesota Department of Health
AO	Acridine orange	MDL	Method limit of detection
Au/PANI-cMWCNT/Bacillus subtilis/GA	Gold electrode based on Bacillus subtilis modified with carboxylated multiwall carbon nanotubes, polyaniline and cross-linking agent glutaraldehyde	MEKC	Micellar electrokinetic chromatography
Au-Pd/RGO/CPE	Au-Pd/reduced graphene oxide composite/ carbon paste electrode	MQL	Method quantification limit
BAW	Bio-mimetic bulk acoustic wave	MIPs	Molecularly imprinted polymers
BSTFA	N,O-Bis(trimethylsilyl)trifluoroacetamide	MWCNTs	Multi-walled carbon nanotubes
CE	Capillary electrophoresis	MWCNT/PE/surfactant	Multi-walled carbon nanotubes/paste electrode in the presence of surfactant
CGE	Capillary gel electrophoresis	MWCNTs/ZnCrFeO ₄ /CPE	Multi-walled carbon nanotubes/ZnCrFeO ₄ /carbon paste electrode
ChrA	Chronoamperometry	NA	Not applicable
CIEF	Capillary isoelectric focusing	ND	Not detected
CITP	Capillary isotachopheresis	NAPQI	N-acetyl-p-benzoquinone imine
CNTs	Carbon nanotubes	NR	Not reported
CPEs	Carbon paste electrodes	NPs	Nanoparticles
CPs	Conducting polymers	NSAIDs	Non-steroidal anti-inflammatory drugs
CS/CPE	Chitosan modified carbon paste electrode	PANI	Polyaniline
CV	Cyclic voltammetry	PCR	Principle component regression
CYP 450	Cytochrome P450	PLS	Partial least square
CZE	Capillary zone electrophoresis	PNBM/GCE	Poly(Nile blue)/glassy carbon electrode
DPV	Differential pulse voltammetry	PNEC	Predicted no-effect concentration
ECPs	Emerging chemical pollutants	Poly(L-Dopa)/MWCNTs/CPE	(L-Dopa) polymer and multi-walled carbon nanotubes complex modified carbon paste electrode
Fe(III)-NClino/CPE	Fe(III)-clinoptilolite nanoparticles/carbon paste electrode; Fe(III)-clinoptilolite nanoparticles/carbon paste electrode	QDs	Quantum dots
FI	Flow injection	QqQLIT	Triple quadrupole linear ion trap mass spectrometer
GCEs	Glassy carbon electrodes	QTOF	Quadrupole time of flight
GC-MS	Gas chromatography-mass spectrometry	SBSE	Stir bar sorptive extraction
HLB	Hydrophilic-lipophilic balance	SDME	Single-drop microextraction
HPLC	High performance liquid chromatography	SH-β-CD/AuNPs/rGO/GCE	SH-β-cyclodextrin functionalized gold nanoparticles/reduced-graphene oxide/glassy carbon electrode
HPLC-DAD	High-performance liquid chromatography-diode array detector	SPE	Solid phase extraction
HPLC-MS/MS	High pressure liquid chromatography-tandem mass spectrometry	SPE/CZE-DAD	Solid phase extraction/capillary zone electrophoresis with diode array detector
HPLC-MS-TOF	High performance liquid chromatography-mass spectrometry coupled to time-of-flight	SPME	Solid-phase microextraction
HPLC-Q-Orbitrap-HRMS	High performance liquid chromatography coupled to hybrid quadrupole-orbitrap high resolution mass spectrometry	STP	Sewage treatment plants
HRMS	High resolution mass spectrometry	SWV	Square wave voltammetry
LC-ESI-MS/MS	Liquid chromatography-electrospray ionization coupled with tandem mass spectrometry	TMCS	Trimethylchlorosilane
LC-MS/MS	Liquid chromatography coupled with tandem mass spectrometry	TOF	Time-of-flight
		UHPLC	High-pressure liquid chromatography
		UHPLC-QqLIT-MS/MS	Ultra-high-performance liquid chromatography quadrupole-linear ion trap analyzer tandem mass spectrometry
		UHPLC-LTQ-Orbitrap MS	Ultra-high performance liquid chromatography-linear trap quadrupole-orbitrap mass spectrometry
		4-VP	4-vinylpyridine
		WWTP	Wastewater treatment plant
		Y ₂ O ₃ NPs/CNTs/GCE	Yttrium (III) oxide nanoparticles/carbon nanotubes/glassy carbon electrode



Scheme 1. Schematic illustration of AC treatment in wastewater by $\text{H}_2\text{O}_2/\text{UV}$ (adopted from Ref. [16]).

In the world of pharmacokinetic studies, it is of great importance to thoroughly examine the active ingredient contents, impurities, drug formulations and metabolites as well as the degradation products of the pharmaceuticals prior to the launch of pharmaceuticals to the market. Analytical techniques including chromatographic, electrochemical, spectroscopic and electrophoresis methods have gained popularity in this regard. Stability assessment, quantification and identification of the impurities and selection of dosage can be performed with the assistance of these analytical techniques.

1.1. Effects of water treatment processes on acetaminophen

One of the most common processes for treatment of AC-contaminated waters is chlorination. Although this process can inactivate microorganisms, chlorine which is a strong electrophile, may also react with chemicals in water such as acetaminophen [12]. Eleven different chlorination products were observed during chlorination of acetaminophen, including the toxic substances N-acetyl-p-benzoquinone imine (NAPQI) and 1,4-benzoquinone. Although they are typically present at very low levels in drinking water and wastewater, their presence along with other pharmaceuticals may result in environmental impacts [13]. Acetaminophen has an LD_{50} of 500 mg kg^{-1} [14] whereas NAPQI and 1,4-benzoquinone have lower values of 20 mg kg^{-1} [14] and 8.5 mg kg^{-1} [15] respectively, which show that these metabolites are more toxic than AC.

Treatment of water can be also performed by oxidation processes including ozonation and $\text{H}_2\text{O}_2/\text{UV}$. Different degradation intermediates are formed during the ozone treatment while during the treatment with $\text{H}_2\text{O}_2/\text{UV}$, 1,4-hydroquinone and 1,4-benzoquinone are produced [16] which are shown in Scheme 1.

According to Xagorarakis et al. [12], acetaminophen can degrade and transform by free chlorine to form the toxic byproduct

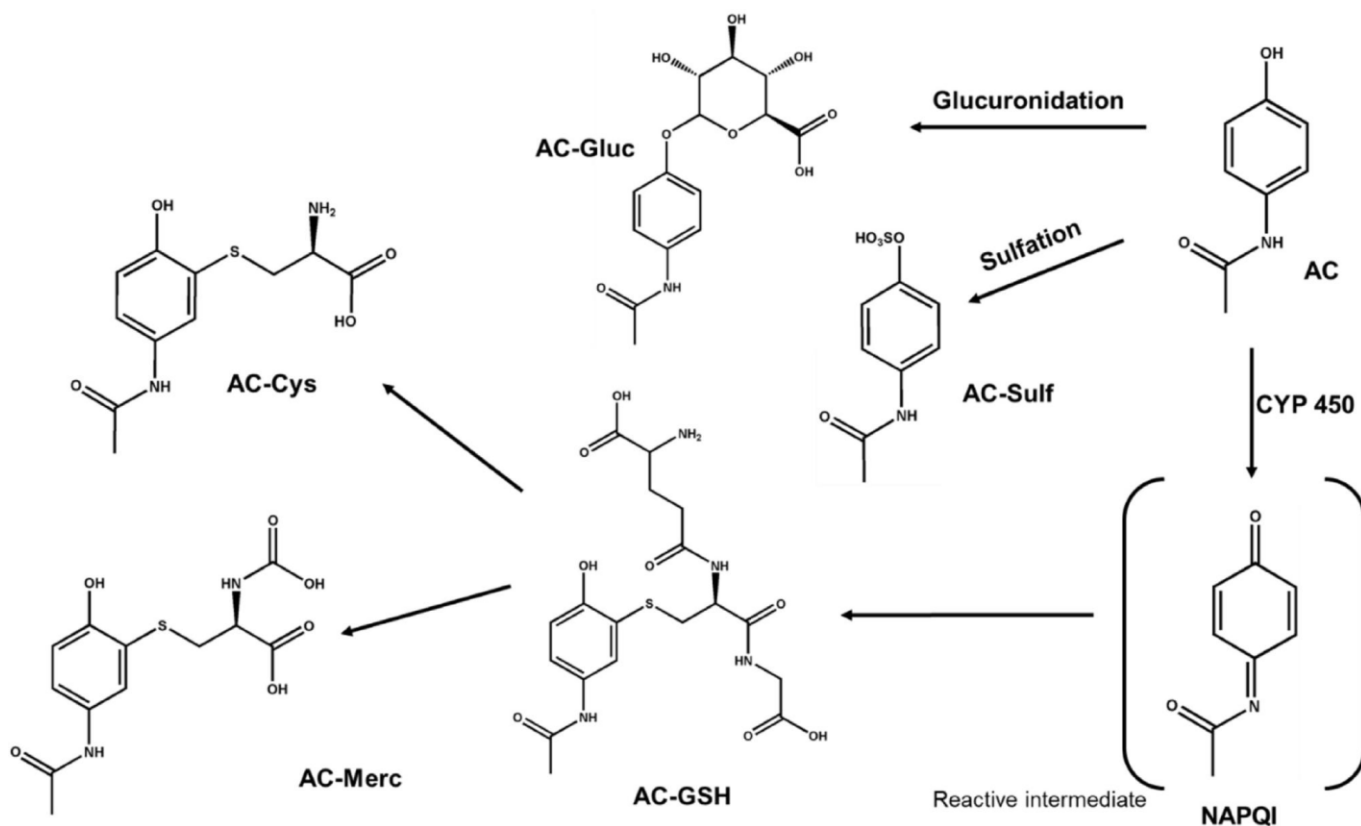
1,4-benzoquinone. They observed that the highest degradation rates were at pH 9.0 while the lowest rates occurred at pH 6.0.

1.2. Toxicity of acetaminophen and production of metabolites

Acetaminophen induces proliferation of cultured breast cancer cells via estrogen receptors without binding to them, but has no estrogenic activity in rodents. It seems that this drug acts mainly by inhibiting the cyclooxygenase of the central nervous system and it does not have anti-inflammatory effects, because of the lack of inhibition of peripheral cyclooxygenase involved in inflammatory processes [17].

Adverse effects of acetaminophen are mainly due to the formation of hepatotoxic metabolites, primarily N-acetyl-p-benzoquinone imine, which is synthesized when the availability of glutathione is diminished in liver cells [17]. It also has harmful effects in over dosage which is related to the formation of toxic metabolites by oxidative pathways. Toxicity of acetaminophen is usually caused by reactive oxygen species which consequently results in multiple effects, ranging from protein denaturation to lipid peroxidation and DNA damage [18].

The metabolism of acetaminophen in humans is illustrated in Scheme 2. This pathway is of great importance for toxicological purposes as it shows the production of the main reactive metabolites of AC [19]. Two main biotransformation products which circulate in plasma are AC-sulfate (AC-Sulf) and AC-glucuronide (AC-Gluc). The cytochrome P450 (CYP 450) oxidation can also produce 3-hydroxy AC metabolite (AC-3-OH) and NAPQI. A further decomposition of NAPQI is cysteine conjugated adduct (AC-Cys). NAPQI is known to react with glutathione leading to detoxification and has not been reported in human plasma, whilst AC-Gluc can be used to detect AC intake even after disappearance of AC in human plasma [20]. The long-term use of acetaminophen can induce depletion of glutathione and consequently results in disturbance of



Scheme 2. Schematic illustration of acetaminophen metabolism in humans (adapted from Ref. [19]).

the γ -glutamyl cycle and overproduction of 5-oxoproline which is the cause of metabolic acidosis [21].

Qualitative and quantitative information on AC and its metabolites in human plasma can be obtained by ultra-high performance liquid chromatography (UHPLC) coupled to a triple quadrupole linear ion trap mass spectrometer (QqQLIT) operating in selected reaction monitoring mode and to a high resolution quadrupole time-of-flight mass spectrometer as reported by Tonoli et al. [19]. HPLC coupled to a triple quadrupole tandem mass spectrometer can also be applied for the quantification of AC and its glucuronide conjugate in human plasma as well as in urine [22]. In addition other techniques such as LC-UV have been developed for the simultaneous determination of AC, AC-Sulf and AC-Gluc in human plasma [23]. The low limits of detection as well as the selectivity provided by these methods make them powerful analytical tools in this context.

This review aims to present various analytical methods for detecting acetaminophen in environmental matrices, pharmaceuticals and biological fluids and to evaluate the advantages and limitations of each analytical approach in terms of sensitivity, detection and quantification limits. Due to the numerous studies that have been published regarding the application of chromatographic, spectroscopic and capillary electrophoresis methods, this review is limited to recent publications over an 8 year period (2010-2017). In addition, this review provides an update of a previous review on electrochemical methods which was published in 2015 [24]. Comparable information is provided to assist researchers in the choice of an appropriate technique for the monitoring of acetaminophen for various applications.

The aim of this review is to collate information from published studies and present it in a useful fashion. Therefore this review is valuable for researchers in the pharmaceutical development and

manufacturing fields and for those in medical and environmental monitoring domains to assess the toxicological and environmental hazards of acetaminophen as well as to guide the design of new miniaturized devices for fast and reliable monitoring thereof in various matrices.

2. Monitoring methods for acetaminophen

2.1. Sample preparation

Generally, samples must be in the form of a liquid or finely divided solid to provide efficient extraction.

Fig. 1 shows the typical sample preparation procedure followed in the analysis of pharmaceuticals in aqueous matrices by chromatography-mass spectrometry, which applies to the analysis of AC. Sample pretreatment is vitally important in order to concentrate the analyte and to reduce the effect of matrix interferences. In addition, acidification of water samples is necessary especially for those pharmaceuticals which have acidic groups and are present in ionized form at neutral pH leading to poor retention in lipophilic sorbents [25]. Generally, 0.45 μ m or 0.2 μ m glass-fiber filters are utilized for the filtration of water samples because the presence of natural organic particles may lessen the efficiency of the extraction process [26]. Several sample preparation procedures have been developed including solid phase extraction (SPE), liquid-liquid extraction (LLE), solid-phase micro-extraction (SPME), liquid-phase micro-extraction (LPME), stir bar sorptive extraction (SBSE) and single-drop microextraction (SDME).

SPE is the most frequently used method for pre-concentration of emerging contaminants in water samples. In comparison with manual (off-line) SPE, automated approaches allow faster sample processing with a lower risk of sample contamination, lower

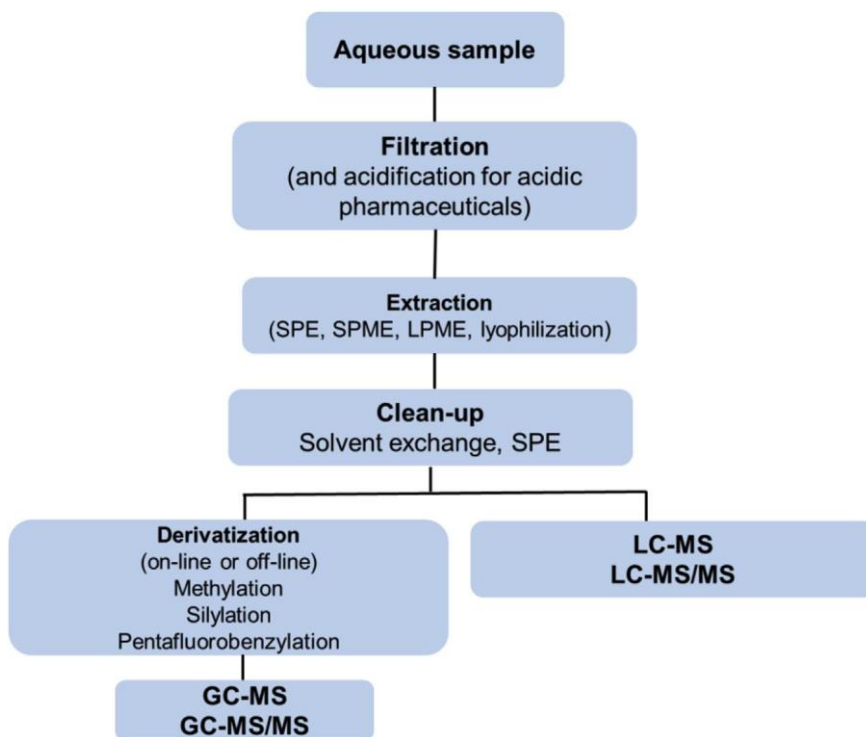


Fig. 1. The typical procedure followed for the analysis of pharmaceuticals in aqueous matrices by chromatography-mass spectrometry [26].

solvent consumption and greater reproducibility as well as good sensitivity. Some SPE sorbents enable the extraction of acidic, neutral and basic compounds at neutral pH. Examples of typically used SPE sorbents for AC extractions are given in Table 1.

LLE has also gained considerable attention in the pharmaceutical industry as it allows for the processing of heat-sensitive products [27]. Consumption of toxic solvents and expensive equipment for recycling thereof are seen as limitations of this method.

Alternative techniques such as SPME and LPME have been applied more recently due to several advantages they present over SPE in terms of minimizing solvent use, ease of sample handling and speed [26]. It has been reported that the fiber in SPME is fragile and has limited lifetime and in the case of SBSE and SDME, it is sometimes difficult to reach equilibrium even after a long extraction time. Moreover, the formation of air bubbles and breaking up of the organic solvent drop due to fast stirring may limit the application of SDME [28]. However, each pre-treatment process has its own advantages and drawbacks and particular care must therefore be exercised in selecting an appropriate pretreatment procedure.

For the quantification of AC from commercial formulations, tablets are accurately weighed and pulverized followed by dilution with deionized water [29], ethanol [30] or HCl: methanol (1:1) [31]. The resulting solution is sonicated and then filtered in order to remove any insoluble excipients prior to analysis.

2.2. Chromatography-mass spectrometry methods

The rapid, accurate and simultaneous determination of a wide range of pharmaceuticals in environmental matrices by chromatographic methods has allowed for the determination of emerging pollutants including pharmaceuticals at ng L^{-1} levels. It has been reported that multi-residue analytical methodologies are favorable tools relative to single group analysis of pharmaceuticals,

as they provide comprehensive knowledge regarding the occurrence of environmental contaminants [25]. In addition, in order to reduce matrix effects during GC-MS, GC-MS/MS, LC-MS or LC-MS/MS analysis, different methods and materials of extraction, derivatization, and clean-up have been investigated. High sensitivity of LC-MS based techniques provide better separation and detection of compounds with same molecular mass but different product ions compared with conventional LC with UV or fluorimetric detection. In addition, MS/MS detection can enhance selectivity and sensitivity in complex matrices such as wastewater [32]. It is noteworthy to emphasize that the ability of LC-MS/MS to analyze a broad range of compounds with minimal sample preparation and shorter analysis time has made it a favorable analytical method as compared with GC-MS, when a range of analytes are to be determined simultaneously [33].

GC-MS and LC-MS based methods have some limitations. Derivatization, for example, plays a pivotal role prior to GC-MS analysis of polar pharmaceuticals, which subsequently can affect the accuracy of the method. In addition, sample volatilization is not required for LC-MS methods, unlike GC-MS. Therefore problems associated with chemical degradation and the formation of new products under heated conditions are prevented [33]. There are also a great number of parameters in LC-MS which must be optimized. Furthermore, efficiency of ionization of the analyte in the ion source is difficult to control and the repeatability in terms of standard deviation of MS detectors may also be high [34].

LC-MS/MS offers specific advantages over LC-MS especially for complicated matrices. Although LC-MS has good sensitivity, it cannot always provide enough selectivity for quantification while LC-MS/MS can improve the selectivity of the method since not only is the compound characterized by the mass of the parent ion, but also by the masses of fragmentation ions from the parent ion. As a result, faster chromatographic techniques can be developed without issues of coelution [35]. The application of LC-MS with

Table 1
Selected chromatography based methods for the determination of acetaminophen in water and wastewater applications.

Analytical method	Analytes	Sample	Extraction method	Derivatization reagent	Linear range (ng L ⁻¹)	LOD (ng L ⁻¹)	LOQ (ng L ⁻¹)	Reference
GC-MS	Acetaminophen, 12 pharmaceuticals	Surface water	SPE (Oasis HLB cartridge)	BSTFA and TMCS	11-5000	3.6	10.5	[36]
LC-MS	Acetaminophen, 24 pharmaceuticals including antibiotic, anti(retro)viral, analgesic, anti-inflammatory and psychiatric drugs	River water WWTP influent	SPE (Oasis HLB cartridges)	NA	>107,000 160,000	NR	NR	[37]
LC-TOF-MS	Acetaminophen, 135 pharmaceuticals	Sewage sludge	Dispersive SPE	NA	<MQL-464 ng g ⁻¹	75 ng g ⁻¹	240 ng g ⁻¹	[38]
LC-MS/MS	Acetaminophen, 32 pharmaceuticals and 5 perfluorinated chemicals	Influent wastewater Effluent wastewater	SPE (Oasis HLB and Oasis MCX cartridges)	NA	1887-2143 2.6-104.3	0.1 0.1	NR	[39]
LC-MS/MS	Acetaminophen, 32 pharmaceuticals	Surface water	SPE (Chromabond HR-X cartridges)	NA	<LOQ-34.6	1.4	8.4	[40]
LC-ESI-MS/MS	Acetaminophen, 22 pharmaceuticals and synthetic hormones	River water STP effluent	SPE (Oasis [®] MCX cartridges)	NA	10 70	9.0 31	NR	[41]
LC-ESI-QTOF-MS	Acetaminophen, 121 pharmaceuticals, personal care products, pesticides and PAHs	Effluent wastewater	NR	NA	13-2557	25	83	[42]
HPLC-DAD	Acetaminophen 9 antibiotics 5 antipyretics, Atenolol, Bezafibrate Caffeine	Surface water Influent wastewater	SPE cartridges	NA	5800-59,000 59,000	NR NR	NR NR	[43]
HPLC-MS-TOF	Acetaminophen Salicylic acid Bisphenol-A Diclofenac	River water	SPE (Phenomenex Strata-X reverse phase cartridges)	NA	90-140	10	50	[44]
HPLC-Q-Orbitrap-HRMS	Acetaminophen, 23 pharmaceuticals	Wastewater	SPE (Strata-X and Strata C18 columns)	NA	1800-4200	NR	0.1	[45]
HPLC-MS/MS	Acetaminophen, Caffeine Carbamazepine Clozapine Erythromycin Metronidazole Ibuprofen Sulfamethoxazole Sulfamethazine Trimethoprim	Inlet wastewater Outlet wastewater Inlet bio-solid Outlet bio-solid	SPE (Oasis HLB cartridges)	NA	100-100,000	5800 <8.0 12.1 ng g ⁻¹ 7.0 ng g ⁻¹	NR NR	[46]
UPLC-MS/MS	Acetaminophen, 82 pharmaceutically active compounds	Coastal waters	SPE (Oasis HLB cartridges)	NA	0.6-75.6	0.5	1.8	[47]
UHPLC- ESI-MS/MS	Acetaminophen, 32 pharmaceutical and personal care products	River water	SPE (Oasis HLB cartridges)	NA	ND-3577	5.9	NR	[48]
UHPLC-QqLIT-MS/MS	Acetaminophen, 80 pharmaceuticals	Drinking water Reservoir water River water Sea water Influent wastewater Effluent wastewater	SPE (Oasis HLB and Oasis MCX cartridges)	NA	ND 21 <MQL-243 23 16,720-18,681 ND-338	0.8 2.5 9.2 3.0 12.9 6.0	1.0 8.3 20.0 10.1 43.0 20.0	[49]
UHPLC-LTQe Orbitrap MS	Acetaminophen, 7 pharmaceuticals,	Drinking water	C-18-based disposable solid-phase extraction cartridges	NA	100-10,000	NR	NR	[50]
UHPLC-MS/MS	Acetaminophen, 32 human and veterinary pharmaceuticals	Seawater River water Influent wastewater Effluent wastewater	SPE (Oasis MCX)	NA	53.2-269.7 <MDL-4.9 30,030-61,5135 736-2139	0.26 0.96 3.60 2.45	0.80 2.88 10.91 7.42	[51]

BSTFA, N,O-Bis(trimethylsilyl)trifluoroacetamide; GC-MS, Gas chromatography-mass spectrometry; HLB, Hydrophilic-lipophilic balance; HPLC-DAD, High-performance liquid chromatography-diode array detector; HPLC-MS/MS, High pressure liquid chromatography-tandem mass spectrometry; HPLC-MS-TOF, High performance liquid chromatography-mass spectrometry coupled to time-of-flight; HPLC-Q-Orbitrap-HRMS, High performance liquid chromatography coupled to hybrid quadrupole Orbitrap high resolution mass spectrometry; LC-ESI-MS/MS, Liquid chromatography-electrospray ionization coupled with tandem mass spectrometry; LC-MS/MS, Liquid chromatography coupled with tandem mass spectrometry; LOD, Limit of detection; LOQ, Limit of quantification; MDL, Method limit of detection; MQL, Method quantification limit; NA, Not applicable; ND, Not detected; NR, Not reported; SPE, Solid phase extraction; STP, Sewage treatment plant; TMCS, Trimethylchlorosilane; UHPLC-QqLIT-MS/MS, Ultra-high-performance liquid chromatography quadrupole-linear ion trap analyzer tandem mass spectrometry; WWTP, Wastewater treatment plant; UHPLC-LTQ-Orbitrap MS, Ultra-high performance liquid chromatography-linear trap quadrupole-orbitrap mass spectrometry.

HRMS analyzers can however enable the screening of a multitude of contaminants with high sensitivity in a single run.

Chromatographic separation techniques have been commonly used for the determination of acetaminophen in a wide variety of matrices. In this review, we have limited the scope of chromatographic techniques to their application in the analysis of AC in environmental water matrices (and related sediment or sludge samples where appropriate) for the period from 2010 to 2017 inclusive. As it can be seen in Table 1, LC-MS based methods are more common than GC-MS methods because acetaminophen is a non-volatile compound. It is also evident that modern chromatographic methods for AC rely greatly on MS and MS/MS detection and other detection methods such as the diode array detector (DAD) are currently rarely used.

AC has been detected at a concentration range spanning three orders of magnitude from parts-per-billion in river water (0.6 ppb) [47] to parts-per-million (160 ppm) [37] in wastewater influent by chromatography based methods with MS or MS/MS (Table 1).

Quantification of AC by LC/MS-MS achieved the lowest detection limit of 0.1 ng L⁻¹ [39] in wastewater while UHPLC-MS/MS was sensitive compared to other chromatography methods and was also capable of sub-ng L⁻¹ detection in sea and coastal water as evident from the limit of detection of 0.26 ng L⁻¹ [51] and 0.5 ng L⁻¹ [47] respectively. It was found that UHPLC based techniques can reduce the analytical run time and provide sufficient chromatographic resolution in order to prevent co-elution of compounds with close m/z values. Furthermore, improvement in detectability was achieved using this technique due to higher and narrower peaks [52].

The highest concentration of acetaminophen was found in wastewater influent (201,300 ng L⁻¹) due to the amount of acetaminophen consumed with or without prescription. Despite the high AC concentration in influent, it was sometimes absent in the effluent due to the high average removal rate of about 99% in wastewater treatment plants [8]. Acetaminophen probably undergoes biodegradation during wastewater treatment so the presence of this compound in surface water has been rarely reported [7].

Although some advantages including selectivity, versatility and specificity facilitate the detection of an analyte in the low ng L⁻¹ range and numerous pharmaceutical analytes can be analyzed in one run, matrix effects may limit the application of LC/MS-MS especially when working in electrospray ionization mode. These matrix effects can potentially cause suppression or enhancement of analyte signals, which consequently can cause inaccurate results. A comprehensive study to evaluate matrix effects should thus be included in the method validation to achieve reliable results.

LC-MS/MS has some limitations for multi-class analysis as the number of target analytes that can be monitored is restricted by the acquisition of each transition. Therefore, LC-MS/MS is insufficient to provide an extensive overview of pollutants presented in water samples because in targeted LC-MS/MS methods, compounds other than the selected targets are ignored even at high levels [52]. In order to overcome this constraint, high resolution mass spectrometry (HRMS) based on time-of-flight (TOF) and Orbitrap mass spectrometers are being used which provide high quality information due to high mass resolution and mass accuracy [53]. Moreover, additional information regarding confirmation of the structure of compounds can be achieved by hybrid instruments including quadrupole-TOF (QTOF) and linear trap quadrupole Orbitrap (LTQ-Orbitrap) [54]. The main advantage of HRMS is that reference standards are not necessarily required because tentative identification of the suspect analytes can be achieved based on the information provided by these methods [52].

Regarding the application of LC-MS/MS and LC-(Q)TOF-MS for the identification, quantification and confirmation of the pharmaceuticals in water samples, the most comprehensive, but costly, approach is to use complementary methods, LC-(Q)TOF-MS for screening and identification followed by quantification by LC/MS/MS as the QTOF can provide accurate mass measurements while LC-MS/MS has good precision and sensitivity [55].

Despite the fact that high performance liquid chromatography based methods are frequently used, in which basic drugs like AC can strongly interact with the column stationary phase, low separation efficiency and peak asymmetry may limit their applications. Moreover, disadvantages including high instrument cost, environmentally unfriendly toxic solvent use and time consuming analysis may hinder the utilization of thereof [56]. In addition, analytical complexity requires highly skilled analysts.

2.3. Electrochemical methods

In recent years, electrochemical techniques have received considerable research interest for the detection of pharmaceutical analytes and environmental pollutants. Voltammetry is a practical electrochemical analytical technique that may provide a wide linear range, as well as high precision, accuracy, sensitivity and selectivity. It utilizes low-cost instrumentation and has timesaving advantages [57].

Numerous reports have been published about the electroanalytical determination of acetaminophen based on its oxidation utilizing different electrodes such as nanotubes, gold electrodes, graphite electrodes, modified glassy carbon electrodes and screen printed electrodes [58,59]. The main reason that AC can be oxidized electrochemically is due to the presence of electroactive hydroxyl and acetamido groups [60].

A comprehensive review was previously published regarding AC detection using unmodified and chemically modified carbon nanotubes (CNTs) as well as graphene over the period 2010 to 2015 [24]. Here the application of a range of electrochemical sensors to the detection of AC in different matrices for the period from 2016 to 2017 is compared to provide an update to the previously published review.

Although there are limited studies regarding the utilization of electrochemical methods for the determination of AC in water samples, many reports have been published on the application of this method to AC in pharmaceuticals and human body fluids. The application of electrochemical sensors between 2016 and 2017 for the detection of AC in the aquatic environment is limited to two reports in which the high detection limits obtained (~10⁴-10⁵ ng L⁻¹) made them undesirable for routine analysis. Therefore, in this review, electrochemical sensors are reported for the determination of AC alone, as well as the simultaneous detection of this analyte in the presence of other compounds, in pharmaceutical and biological samples during the period from 2016 to 2017. Due to the vast number of publications, not all published articles are included, but rather relevant examples are provided.

Fig. 2 presents the number of publications and cumulative counts per year, which were identified by a key word search for "acetaminophen electrochemical sensors" from 2010 to 2017 inclusive. It is evident that there has been significant research interest in this field in recent years.

Selected electrochemical sensors which have favorable detection limits for AC are included in Table 2 which also compares the linear ranges of these methods.

It is known that poor electrochemical responses of AC in conventional working electrodes have restrained the application thereof. Consequently, various materials with excellent electro-catalytic activities have been developed in order to improve selectivity and sensitivity.

Amongst the different electrochemical detection methods, differential pulse voltammetry (DPV) is more sensitive than cyclic voltammetry (CV) [72]. In addition, high sensitivity and good resolution for the quantitative analysis of AC has also made DPV a popular choice. Acceptable recoveries provided evidence that matrix interferences for the analysis of complicated samples such as human body fluids by DPV were not significant [60].

Numerous electrochemical methods have used DPV and square wave voltammetry (SWV) in comparison with other electrochemical detection techniques. In addition, SWV showed more sensitivity with a low detection limit (approximately 150 ng L^{-1}) [66] relative to DPV (LOD of $1.0 \times 10^3 \text{ ng L}^{-1}$) [63] in the simultaneous detection of AC in pharmaceutical and human body fluids.

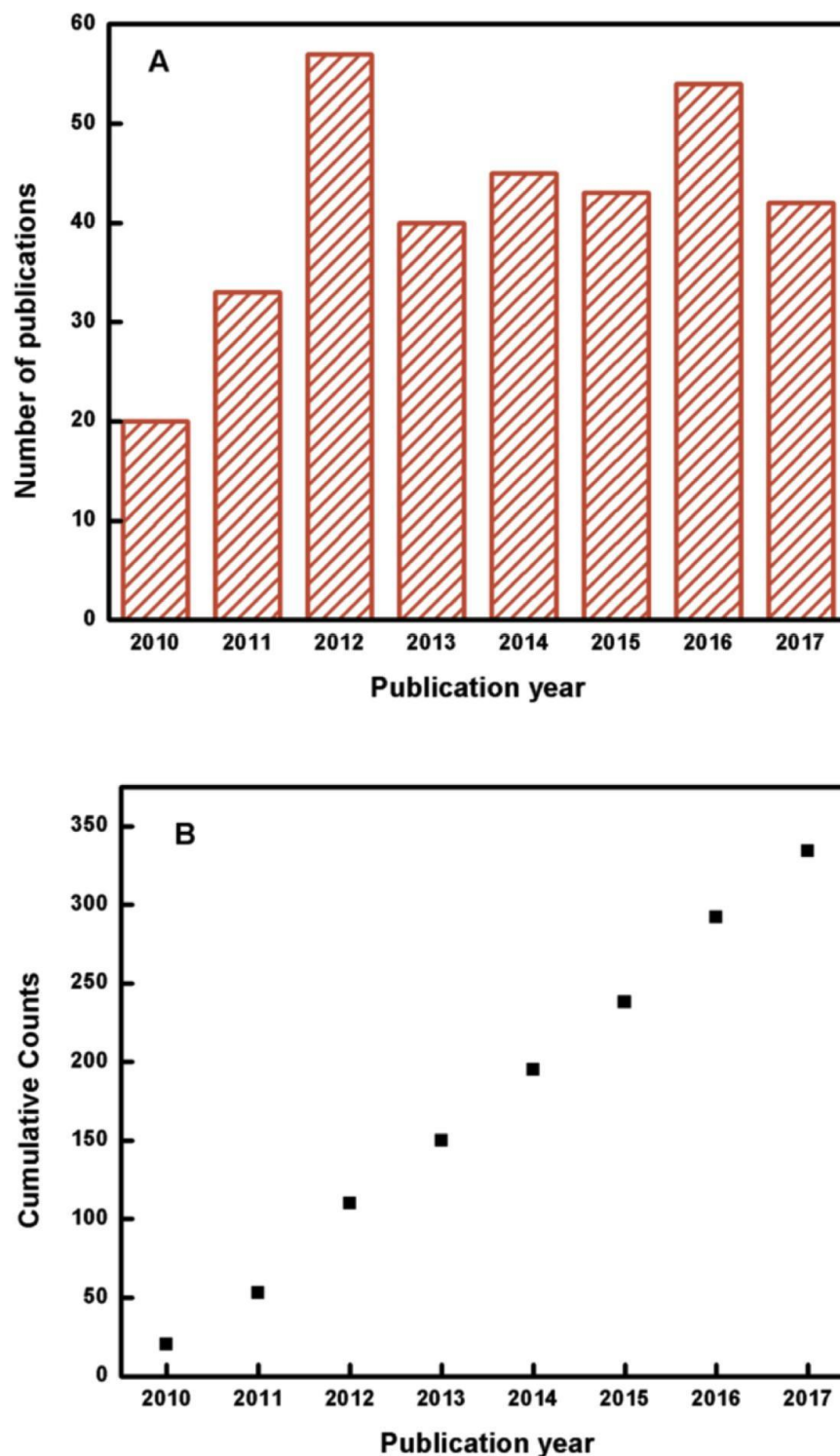


Fig. 2. Publications relating to acetaminophen electrochemical sensors applied to a range of matrices within the period of 2010-2017 inclusive, (A) number of publications per year and (B) cumulative counts (n=334).

Table 2
Comparison of the performance of selected electrochemical sensors and biosensors for acetaminophen sensing in date order for the two year period from 2016 to the end of 2017.

Electrode	Detection method	Analyte	Sample	Linear range (ng L ⁻¹)	Detection limit (ng L ⁻¹)	Reference
Y ₂ O ₃ NPs/CNTs/GCE	SWV	Acetaminophen	Pharmaceuticals	15.1-3.0×10 ³	4.5	[61]
CS/CPE	SWV	Acetaminophen	River water, sea water, commercial tablets and human urine	1.2×10 ⁵ -3.0×10 ⁷ 6.0×10 ⁷ -1.5×10 ⁸	7.7×10 ⁴	[62]
Au-Pd/RGO/CPE	DPV	Acetaminophen Ascorbic acid Tyrosine	Urine, serum and pharmaceutical sample	4.5×10 ³ -1.4×10 ⁶	1.1×10 ³	[63]
MWCNTs/ZnCrFeO ₄ /CPE	DPV	Acetaminophen Ascorbic acid Codeine	Pharmaceutical and biological samples	1.5×10 ⁴ -5.6×10 ⁷	1.4×10 ³	[64]
PNBM/GCE	CV	Acetaminophen Tramadol Caffeine	Pharmaceutical dosage forms	3.0×10 ⁴ -2.4×10 ⁶	1.2×10 ⁴	[65]
Fe(III)-NClino/CPE	SWV	Acetaminophen Ascorbic acid	Human serum, urine and tablets	1.5×10 ¹ -1.5×10 ⁹ 1.5×10 ³ -1.5×10 ¹⁰	150.0 3.8	[66]
MWCNT/PE/surfactant	DPV	Acetaminophen Hydroquinone Catechol	Tap and domestic wastewater	2.3×10 ⁶ -2.7×10 ⁷ 2.3×10 ⁶ -1.8×10 ⁷	4.4×10 ⁴ 6.7×10 ⁵	[67]
Au/PANI-cMWCNT/Bacillus subtilis/GA	Amperometric	Acetaminophen	Drug samples	7.6×10 ⁵ -9.5×10 ⁷	4.4×10 ⁵	[68]
Poly(L-Dopa)/MWCNTs/CPE	DPV	Acetaminophen	Serum	9.0×10 ³ -4.5×10 ⁶	3.0×10 ³	[69]
Nanorods-like Cd(OH) ₂ -rGO/GCE	DPV	Acetaminophen	Tablets	1.5×10 ⁴ -1.5×10 ⁷	1.2×10 ⁴	[70]
SH-β-CD/AuNPs/rGO/GCE	DPV	Acetaminophen Ofloxacin	Tablets and human urine	7.6×10 ³ -1.5×10 ⁷	4.5×10 ³	[71]

Au/PANI-cMWCNT/Bacillus subtilis/GA, Gold electrode based on Bacillus subtilis modified with carboxylated multiwall carbon nanotubes, polyaniline and cross-linking agent glutaraldehyde; Au-Pd/RGO/CPE, Au-Pd/reduced graphene oxide composite/carbon paste electrode; ChrA, Chronoamperometry; CS/CPE, Chitosan modified carbon paste electrode; CV, Cyclic voltammetry; DPV, Differential pulse voltammetry; Fe(III)-NClino/CPE, Fe(III)-clinoptilolite nanoparticles/carbon paste electrode; MWCNT/PE/surfactant, Multi-walled carbon nanotubes/paste electrode in the presence of surfactant; MWCNTs/ZnCrFeO₄/CPE, Multi-walled carbon nanotube/ZnCrFeO₄/carbon paste electrode; PNBm/GCE, Poly(Nile blue)/glassy carbon electrode; Poly(L-Dopa)/MWCNTs/CPE, (L-Dopa) polymer and multi-walled carbon nanotubes complex modified carbon paste electrode; SH-β-CD/AuNPs/rGO/GCE, SH-β-cyclodextrin functionalized gold nanoparticles/reduced-graphene oxide/glassy carbon electrode; SWV, Square wave voltammetry; Y₂O₃NPs/CNTs/GCE, Yttrium (III) oxide nanoparticles/carbon nanotubes/glassy carbon electrode.

SWV and chronoamperometry (ChrA) provided wider linear concentration ranges (more than seven orders of magnitude) for the simultaneous determination of acetaminophen with other compounds in pharmaceuticals and human body fluids with low detection limits of 150 ng L⁻¹ and 3.8 ng L⁻¹ respectively, as indicated in Table 2 [66].

Generally, a great number of the active drug compounds can be easily oxidized or reduced contrary to the excipients of pharmaceuticals. It has been shown that there are no electrochemical interferences from the excipients present in the pharmaceutical preparations with the analyte, therefore this method can be applied for the detection of AC in pharmaceutical formulations [73].

The investigation of various electrochemical electrodes using SWV and DPV for the determination of AC as a single analyte demonstrated that SWV was also more sensitive than DPV with a detection limit of 4.5 ng L⁻¹ [61].

It is widely accepted that voltammetric techniques provide the advantages of simplicity, low instrumental cost and convenience for simultaneous determinations. However, comprehensive strategies should be employed to design electrochemical sensors in order to avoid peak overlap and to enable multi-residue analysis [74]. Furthermore, although electrochemical sensors can be applied for in-situ and online measurements, the conditions of measuring such as chemical composition, pressure and temperature must be taken into consideration.

Multi-walled carbon nanotubes (MWCNTs) modified electrodes have captured worldwide research interest for the detection of AC due to their high surface to volume ratio, great biocompatibility and electrochemical conductivity [75]. Although these methods have been shown to provide good selectivity and sensitivity, the linear ranges achieved are rather limited, as is evident from Table 2. Therefore a new kind of material is required to fabricate fast and accurate electrodes with wider linear ranges for the determination of AC. It is also important to bear in mind that MWCNTs are

hydrophobic materials resulting in limitations for the application of these electrochemical sensors as shown by Hui et al. [75].

It is clear that chemically modified electrodes exhibit lower detection limits in comparison to unmodified electrodes. In addition, modified glassy carbon electrodes (GCEs) exhibit a well-defined redox couple with improved current response for AC determination relative to bare GCEs [61] while the modified carbon paste electrodes (CPEs) showed large surface area with good electro-catalytic activity and conductivity towards the electrochemical oxidation of AC [76]. However, there was much a less difference between detection limits of modified CPEs and GCEs.

The application of pure conducting polymers (CPs) such as polythiophene, polyaniline (PANI) and polypyrrole in electroanalytical approaches has some limitations including low selectivity and sensitivity and adsorption of intermediates which cause surface poisoning [77].

The advent of nanocomposites is a milestone in the field of material science which has allowed for improvement in the performance of the electrochemical sensors. Metal and metal oxide nanoparticles, carbon nanotubes, graphene and graphene oxide nanocomposites in various combinations and most recently molecularly imprinted polymers (MIPs), sol-gel and ionic liquids have been extensively used during the period 2016-2017 to prepare polymer nanocomposites for the determination of AC. It has been reported that carbon nanotubes are more favorable compared to other carbon electrodes in terms of electro-catalysis, selectivity and resistance to surface fouling [78]. Furthermore, modification of the electrodes with carbon nanotubes and metal oxide nanoparticles provide high sensitivity with low detection limits as well as decreased over-potential as shown by Baytak et al. [61]. The performance of zeolite-modified electrodes as low-cost and environmentally friendly electrodes also demonstrated low detection limits due to the combination of the merits of ion-exchange voltammetry with unique molecular-sieving properties of the zeolite [66].

Recently, the application of molecularly imprinted polymeric (MIP) films, which are formed in situ on the electrode surface, has decreased interferences of other analogous with similar oxidation potentials to AC such as aminophenol, uric acid, dopamine and ascorbic acid. The high selectivity and specificity of MIP sensors are due to the shape and spatial structure of the recognition cavities in the imprinted polymer matrix which enable binding of only the template [79].

Electrochemical biosensors have also received research interest in the analysis of AC as they provide low cost, sensitive and accurate measurements based on electrochemical techniques. These sensors integrate signal transduction processes with a specific biorecognition processes [76].

2.4. Spectroscopic methods

Spectrophotometric methods are based on the hydrolysis of acetaminophen to p-aminophenol followed by reaction with specific reagents to provide colored substances which can thus be detected by spectrophotometric methods [80]. These methods usually require sample pre-treatment steps (extraction, complex formation and derivatization). This, in addition to spectral overlap experienced in multicomponent pharmaceutical formulations and mixtures, limits the application of these methods. Chemometric approaches such as principle component regression (PCR), partial least squares (PLS) or artificial neural networks (ANN) can be applied in spectral analysis to remove the need for separation procedures. For example, a spectrophotometric study was reported for the simultaneous determination of acetaminophen and caffeine in tablets based on chemometric methods without any prior chemical separation [81].

Derivative spectrophotometry also provides significant advantages over classical absorption or difference spectrophotometry including better resolution, and the capability of revealing small peaks especially when broad, perturbing bands are present [82].

To the best of our knowledge, only one spectrophotometric study has been published for AC detection in water samples in the period of 2010-2017 which was based on a biocatalytic approach, while other studies have reported the application of spectrophotometric methods in pharmaceuticals and biological fluid applications [83,84]. The method was applied to monitor the degree of laccase inhibition during the oxidation of 2,20-azino-bis(3-ethylbenzothiazoline-6-sulphonic acid) in the presence of AC. The dynamic range was found to be 3.0×10^5 - 2.1×10^6 ng L⁻¹ with a detection limit of 8.3×10^4 ng L⁻¹. The method was then applied for AC detection in commercial potable bottled water, tap water and treated wastewater effluent [85].

In spite of a great number of reports which have been published regarding the determination of AC in pharmaceutical formulations and body fluids by spectrophotometry, their high detection limits indicate that they cannot be applied directly to AC detection in the environment due to the low concentrations thereof, necessitating pre-concentration and pre-extraction steps. Although spectrophotometric methods are rapid, simple and inexpensive, they have disadvantages including narrow linear ranges, high detection limits, use of corrosive and toxic reagents, waste production, as well as poor sensitivity and selectivity [86].

Spectrofluorimetric platforms have advantages of high sensitivity, selectivity and simplicity. Furthermore, in comparison with chromatography-mass spectrometry and electrochemical methods, fluorescence methods offer an alternative approach due to their significant merits of easy operation, fast and simple experimental processes, high sensitivity for different fluorescence emission wavelengths corresponding to different molecular structures, and low cost [87].

Spectrofluorimetric and spectrophotometric methods utilizing nanoparticles (NPs) have gained attention in analytical chemistry because of their unique properties which emanate from the quantum size effect [88]. The use of quantum dots (QDs) as a sub class of nanomaterials in optical probes in the analytical field has been exploited since the first application of QDs in biological systems for the recognition of specific antibodies or antigens [89] and on mouse fibroblasts in 1998 [90].

In 2012, a simple and sensitive assay of acetaminophen was proposed based on the quenching of the fluorescence intensity of L-cysteine capped CdTe NPs in aqueous solution (Fig. 3). Under optimal experimental conditions, the relative fluorescence intensity ($\Delta I = I_0/I$) of L-cysteine capped CdTe NPs versus the concentration of acetaminophen was linear over the range of 1.5×10^3 - 2.4×10^4 ng L⁻¹ with a detection limit of 635.0 ng L⁻¹. The applicability of the method was tested for the analysis of AC in pharmaceutical tablets [91].

In another study for the simultaneous spectrophotometric determination of acetaminophen and gentamicin in tablets, ampoules and blood serum samples, silver nanoparticles were synthesized and applied over the concentration range of 7.8×10^5 - 15.1×10^6 ng L⁻¹ with a detection limit of 1.8×10^4 ng L⁻¹ [88].

A bio-mimetic bulk acoustic wave (BAW) sensor was fabricated using a molecularly imprinted polymer with two functional monomers of 4-vinylpyridine (4-VP) and methacrylic acid (MAA) for the determination of acetaminophen over the linear range of 756 - 1.5×10^4 ng L⁻¹ with a detection limit of 756 ng L⁻¹. The biosensor was then applied for the determination of acetaminophen in human serum and urine samples [92].

Recently, amphiphilic pillar [5]arene (amPA5) functionalized reduced graphene oxide (amPA5-RGO) as a receptor has been applied as a 'turn on' fluorescence sensing platform for the determination of AC in serum samples. The mechanism was based on competitive host-guest interaction between acridine orange (AO) and acetaminophen which led to a change in fluorescence signal of the dye molecule. The prototype sensor gave a linear concentration range over 1.5×10^4 - 6.0×10^5 ng L⁻¹ and 6.0×10^5 - 5.0×10^6 ng L⁻¹ with a detection limit of 7.6×10^3 ng L⁻¹ [93].

A novel fluorescence "turn off-on" biosensor was designed based on polypyrrole/graphene quantum dots for the detection of acetaminophen and ascorbic acid in human serum samples. The quenching fluorescence of the sensor was proportional to the concentration of AC over the linear range of 67.0 - 233×10^3 ng L⁻¹ with a detection limit of 22.0 ng L⁻¹ [94].

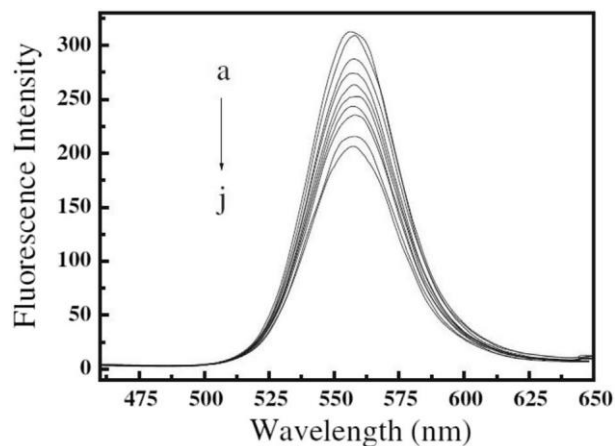


Fig. 3. Fluorescence quenching emission spectra of L-cysteine capped CdTe NPs in the absence and presence of acetaminophen in the concentration range 1.5×10^3 - 2.4×10^4 ng L⁻¹ [91] (reprinted with permission from Springer Nature).

Although there are few studies for the determination of AC achieved by nanoparticles and semiconductor QDs with the aid of fluorescence spectroscopy, due to the aforementioned advantages, this is expected to be an area of future research interest.

2.5. Capillary electrophoresis methods

Capillary electrophoresis (CE) is popular compared to conventional analytical methods like chromatography techniques in manufacturing processes and drug discovery, due to advantages including eco-friendly solvent use, high selectivity and high separation efficiency, short analysis time, minimal buffer (mobile phase) use and small sample volume requirements [95]. CE has also been reported as a powerful tool for a wide range of analyses, including many applications for the determination of drugs and drug related impurities [96]. In addition, the instrumentation required for CE is simple: it is comprised of electrodes, sample introduction systems, a capillary, a power supply, a detector and liquid-handling systems [95].

A main advantage of CE is the various operating modes possible including capillary zone electrophoresis (CZE), capillary isoelectric focusing (CIEF), micellar electrokinetic chromatography (MEKC), capillary isotachopheresis (CITP) and capillary gel electrophoresis (CGE), which permits the separation of different compounds. Among different modes CZE and MEKC are utilized as robust alternative techniques to HPLC for the simultaneous determination of acetaminophen with other drugs [95]. CE has the potential to be a powerful technique for the analysis of non-steroidal anti-inflammatory drugs, including acetaminophen, because of the high dissociation rate of this compound in water [97]. The application of CE in the field of environmental water sample analysis is, however, minimal.

The selectivity, sensitivity and flexibility of CE can be enhanced by the use of on-line sample pretreatment (flow injection, FI) and different detectors, such as fluorescence, chemiluminescence and contactless conductivity detectors, to enable the detection of new drugs [95].

Solid phase extraction followed by capillary zone electrophoresis with diode array detection (SPE/CZE-DAD) was performed for the simultaneous detection of the most frequently used non-steroidal anti-inflammatory drugs (NSAIDs), including AC, in the influent and effluent of a wastewater treatment plant. The concentration range for AC was found to be 1000-14,610 ng L⁻¹ in influent and 520-1650 ng L⁻¹ in effluent with a detection limit of 460 ng L⁻¹ [97], which is lower compared to capillary electrophoresis employing a diode array detector (LOD = 1.0 - 3.3 × 10⁶ ng L⁻¹) for the analysis of commercial formulations and biological fluids [98,99].

Although HPLC is accurate, sensitive and reproducible compared to CE, the numerous applications of CE in drug analysis clearly show its importance. These two methods thus complement each other in drug discovery in the pharmaceutical industry. It is expected that CE will continue to be applied in the future to facilitate quality control to ensure products have the highest efficiency and safety for patients.

3. Conclusion and future perspectives

The development of new methods for the identification and determination of acetaminophen in pharmaceuticals, biological fluids and environmental matrices are important in preventing and managing its potential detrimental effects. Taking into consideration the possible accumulation of acetaminophen in surface water,

drinking water and wastewater, efficient, sensitive and simple analytical techniques are of great importance for its determination. Although chemical oxidation processes are a popular methodology for the treatment of acetaminophen in wastewater, some disadvantages including harsh reaction conditions, high operational cost and the generation of secondary pollutants may restrain the utilization of thereof, leading to the release of this pharmaceutical into the environment.

The emergence of numerous publications on the analysis of acetaminophen in pharmaceuticals, human body fluids and environmental samples has been seen in recent years. The accelerated development of new methods for the determination of acetaminophen in these samples often focuses on the study of complex mixtures with other species of interest. For instance, chromatography-mass-spectrometry may be applied to the identification of acetaminophen with simultaneous determination of a range of pharmaceuticals in a single run. Moreover, new extraction methods not only allow for the study of complex samples without interferences from the matrix, but also the determination of acetaminophen at very low concentrations due to pre-concentration of the analyte. It is important to note that literature concerning the determination of acetaminophen in environmental samples is still relatively scarce, as most of these methods have been exclusively applied to the analysis of AC in pharmaceuticals and human body fluids.

Amongst chromatographic methods, LC-MS and LC-MS/MS are the most widely used techniques relative to GC-MS for the determination of acetaminophen due to its low volatility. LC-MS methods thus have the advantages of less complicated sample preparation as well as versatility to analyze a broader range of compounds in a single run, enabling a more comprehensive assessment of environmental contaminants. The advent of HRMS analyzers have allowed for high full scan selectivity and sensitivity with high resolution and sufficient fragmentation for qualitative and quantitative MS analysis. UHPLC coupled to HRMS analyzers has become a powerful technique which offers significant advantages of efficient separations, short analysis run times with good sensitivity [52].

In comparison with chromatographic techniques, electrochemical sensors can be directly applied to provide real-time sample information. Developments in electrode design by modification of the electrode materials have resulted in improved sensitivity and performance in the detection of analytes. Among various electrochemical techniques, cyclic voltammetry, differential pulse voltammetry and square wave voltammetry have been mostly employed for the determination of acetaminophen with high sensitivity. In spite of the simplicity of electrochemical methods, miniaturization of electrochemical sensors to fabricate in-field devices for in-situ monitoring and online operations is still challenging. Various biosensors incorporated into electrochemical electrodes have been explored for the determination of acetaminophen and there is scope for further research in this regard.

The use of pre-extraction and pre-concentration sample preparation steps, such as solid phase extraction, are of great importance for analytical methods of lower sensitivity, such as spectroscopic and capillary electrophoresis techniques, due to the expected low concentration levels (part per billion or part per trillion) of AC in the environment as well as the complexity of matrices like wastewater.

Regarding possible future developments, there is interest in the design of fast, simple, selective and sensitive screening methods for the determination of acetaminophen particularly in environmental media to allow for its more widespread analysis at a reasonable cost.

Acknowledgements

Funding from the University of Pretoria and the Water Research Commission (Grant K5/2438/1 and K5/2752) is gratefully acknowledged.

References

- Rivera-Utrilla, M. Sanchez-Polo, M.A. Ferro-García, G. Prados-Joya, R. Ocampo-Perez, Pharmaceuticals as emerging contaminants and their removal from water. A review, *Chemosphere* 93 (2013) 1268-1287.
- M. Petrovic, S. Gonzalez, D. Barcelo, Analysis and removal of emerging contaminants in wastewater and drinking water, *Trends Anal. Chem.* 22 (2003) 685-696.
- T. Knepper, F. Sacher, F.T. Lange, H. Brauch, F. Karrenbrock, O. Roerden, et al., Detection of polar organic substances relevant for drinking water, *Waste Manag.* 19 (1999) 77-99.
- A. Bertolini, A. Ferrari, A. Ottani, S. Guerzoni, R. Tacchi, S. Leone, Paracetamol: new vistas of an old drug, *CNS Drug Rev.* 12 (2006) 250-275.
- Y. Dai, A.I. Cederbaum, Cytotoxicity of acetaminophen in human cytochrome P450E1-transfected HepG2 cells, *J. Pharmacol. Exp. Ther.* 273 (1995) 1497-1505.
- P.J. Phillips, S.G. Smith, D.W. Kolpin, S.D. Zaugg, H.T. Buxton, E.T. Furlong, et al., Pharmaceutical formulation facilities as sources of opioids and other pharmaceuticals to wastewater treatment plant effluents, *Environ. Sci. Technol.* 44 (2010) 4910-4916.
- P.H. Roberts, K.V. Thomas, The occurrence of selected pharmaceuticals in wastewater effluent and surface waters of the lower Tyne catchment, *Sci. Total Environ.* 356 (2006) 143-153.
- M.J. Gomez, M.J.M. Bueno, S. Lacorte, A.R. Fernandez-Alba, A. Agüera, Pilot survey monitoring pharmaceuticals and related compounds in a sewage treatment plant located on the Mediterranean coast, *Chemosphere* 66 (2007) 993-1002.
- S. Grujic, T. Vasiljevic, M. Lausevic, Determination of multiple pharmaceutical classes in surface and ground waters by liquid chromatography-ion trap tandem mass spectrometry, *J. Chromatogr. A* 1216 (2009) 4989-5000.
- C. Carlsson, A.K. Johansson, G. Alvan, K. Bergman, T. Kühler, Are pharmaceuticals potent environmental pollutants?: Part I: environmental risk assessments of selected active pharmaceutical ingredients, *Sci. Total Environ.* 364 (2006) 67-87.
- Toxicological Summary for: Acetaminophen, 2010.** Retrieved from, www.health.state.mn.us/divs/eh/risk/guidance/dwec/sumacetamin.pdf.
- I. Xagorarakis, R. Hullman, W. Song, H. Li, T. Voice, Effect of pH on degradation of acetaminophen and production of 1, 4-benzoquinone in water chlorination, *J. Water Supply Res. Technol. AQUA* 57 (2008) 381-390.
- M. Bedner, W.A. MacCrehan, Transformation of acetaminophen by chlorination produces the toxicants 1, 4-benzoquinone and N-acetyl-p-benzoquinone imine, *Environ. Sci. Technol.* 40 (2006) 516-522.
- D.C. Dahlin, S.D. Nelson, Synthesis, decomposition kinetics, and preliminary toxicological studies of pure N-acetyl-p-benzoquinone imine, a proposed toxic metabolite of acetaminophen, *J. Med. Chem.* 25 (1982) 885-886.
- G.S. Serif, L.E. Seymour, Catabolism and excretion of the antithyroid substance, diacetyl-2, 6-diiodohydroquinone, *Biochem. Pharmacol.* 12 (1963) 885-891.
- R. Andreozzi, V. Caprio, R. Marotta, D. Vogna, Paracetamol oxidation from aqueous solutions by means of ozonation and H₂O₂/UV system, *Water Res.* 37 (2003) 993-1004.
- E. Harnagea-Theophilus, S.L. Gadd, A.H. Knight-Trent, G.L. DeGeorge, M.R. Miller, Acetaminophen-induced proliferation of breast cancer cells involves estrogen receptors, *Toxicol. Appl. Pharmacol.* 155 (1999) 273-279.
- S.C. Antunes, R. Freitas, E. Figueira, F. Goncalves, B. Nunes, Biochemical effects of acetaminophen in aquatic species: edible clams *Venerupis decussata* and *Venerupis philippinarum*, *Environ. Sci. Pollut. Res.* 20 (2013) 6658-6666.
- D. Tonoli, E. Varesio, G. Hopfgartner, Quantification of acetaminophen and two of its metabolites in human plasma by ultra-high performance liquid chromatography-low and high resolution tandem mass spectrometry, *Chromatogr. B* 904 (2012) 42-50.
- J.G.M. Bessems, N.P.E. Vermeulen, Paracetamol (acetaminophen)-induced toxicity: molecular and biochemical mechanisms, analogues and protective approaches, *Crit. Rev. Toxicol.* 31 (2001) 55-138.
- A.H. Wu, R. Gerona, P. Armenian, D. French, M. Petrie, K.L. Lynch, Role of liquid chromatography-high-resolution mass spectrometry (LC-HR/MS) in clinical toxicology, *Clin. Toxicol.* 50 (2012) 733-742.
- Q.-y. Tan, R.-h. Zhu, F. Wang, M. Yan, L.-b. Dai, Simultaneous quantitative determination of paracetamol and its glucuronide conjugate in human plasma and urine by liquid chromatography coupled to electrospray tandem mass spectrometry: application to a clinical pharmacokinetic study, *J. Chromatogr.* 893 (2012) 162-167.
- L.S. Jensen, J. Valentine, R.W. Milne, A.M. Evans, The quantification of paracetamol, paracetamol glucuronide and paracetamol sulphate in plasma and urine using a single high-performance liquid chromatography assay, *J. Pharm. Biomed. Anal.* 34 (2004) 585-593.
- A. Cernat, M. Tertis, R. Sandulescu, F. Bedioui, A. Cristea, C. Cristea, Electrochemical sensors based on carbon nanomaterials for acetaminophen detection: a review, *Anal. Chim. Acta.* 886 (2015) 16-28.
- M. Gros, M. Petrovic, D. Barcelo, Multi-residue analytical methods using LC-tandem MS for the determination of pharmaceuticals in environmental and wastewater samples: a review, *Anal. Bioanal. Chem.* 386 (2006) 941-952.
- D. Fatta, A. Achilleos, A. Nikolaou, S. Meriç, Analytical methods for tracing pharmaceutical residues in water and wastewater, *Trends Anal. Chem.* 26 (2007) 515-533.
- K.E. Crowell, in: E. Goldberg (Editor), *Pharmaceutical Applications of Liquid-liquid Extraction. Handbook of Downstream Processing*, Springer, Dordrecht, 1997.
- M. Pirsaeheb, T. Ahmadi-Jouibari, N. Fattahi, M. Shamsipur, Determination of fenvalerate in tomato by ultrasound-assisted solvent extraction combined with dispersive liquid-liquid microextraction, *J. Chromatogr. Sci.* 52 (2013) 944-949.
- B. Suchacz, M. Wesolowski, Voltammetric quantitation of acetaminophen in tablets using solid graphite electrodes, *Anal. Meth.* 8 (2016) 3307-3315.
- A. Pyka, M. Budzisz, M. Dolowy, Validation thin layer chromatography for the determination of acetaminophen in tablets and comparison with a pharmacopeial method, *BioMed. Res. Int.* 2013 (2013).
- G. Murtaza, I. Hussain, S.A. Khan, A. Shabbir, A. Mahmood, M.H.H.B. Asad, et al., Development of a UV-spectrophotometric method for the simultaneous determination of aspirin and paracetamol in tablets, *Sci. Res. Essays* 6 (2011) 417-421.
- M.S. Díaz-Cruz, D. Barcelo, LCeMS2 trace analysis of antimicrobials in water, sediment and soil, *Trends Anal. Chem.* 24 (2005) 645-657.
- E.R. Perez, J.A. Knapp, C.K. Horn, S.L. Stillman, J.E. Evans, D.P. Arfsten, Comparison of LC-MS-MS and GC-MS analysis of benzodiazepine compounds included in the drug demand reduction urinalysis program, *J. Anal. Toxicol.* 40 (2016) 201-207.
- A. Kruve, R. Rebane, K. Kipper, M.-L. Oldekop, H. Evard, K. Herodes, et al., Tutorial review on validation of liquid chromatography-mass spectrometry methods: Part I, *Anal. Chim. Acta* 870 (2015) 29-44.
- L. Tribalat, O. Paisse, G. Dessalces, M.-F. Grenier-Loustalot, Advantages of LC-MS-MS compared to LC-MS for the determination of nitrofurans residues in honey, *Anal. Bioanal. Chem.* 386 (2006) 2161-2168.
- N. Migowska, M. Caban, P. Stepnowski, J. Kumirska, Simultaneous analysis of non-steroidal anti-inflammatory drugs and estrogenic hormones in water and wastewater samples using gas chromatography-mass spectrometry and gas chromatography with electron capture detection, *Sci. Total Environ.* 441 (2012) 77-88.
- O. K'oreje K, L. Vergeynst, D. Ombaka, P. De Wispelaere, M. Okoth, H. Van Langenhove, et al., Occurrence patterns of pharmaceutical residues in wastewater, surface water and groundwater of Nairobi and Kisumu city, Kenya, *Chemosphere* 149 (2016) 238-244.
- W. Peysson, E. Vulliet, Determination of 136 pharmaceuticals and hormones in sewage sludge using quick, easy, cheap, effective, rugged and safe extraction followed by analysis with liquid chromatography-time-of-flight-mass spectrometry, *J. Chromatogr. A* 1290 (2013) 46-61.
- W.W.-P. Lai, Y.-C. Lin, H.-H. Tung, S.-L. Lo, A.Y.-C. Lin, Occurrence of pharmaceuticals and perfluorinated compounds and evaluation of the availability of reclaimed water in Kinmen, *Emerg. Contam.* 2 (2016) 135-144.
- C.D.S. Pereira, L.A. Maranhão, F.S. Cortez, F.H. Pusceddu, A.R. Santos, D.A. Ribeiro, et al., Occurrence of pharmaceuticals and cocaine in a Brazilian coastal zone, *Sci. Total Environ.* 548 (2016) 148-154.
- N.A. Al-Odaini, M.P. Zakaria, M.I. Yaziz, S. Surif, Multi-residue analytical method for human pharmaceuticals and synthetic hormones in river water and sewage effluents by solid-phase extraction and liquid chromatography-tandem mass spectrometry, *J. Chromatogr. A* 1217 (2010) 6791-6806.
- S.H. Lopez, M. Ulaszewska, M. Hernando, M.M. Bueno, M. Gomez, A. Fernandez-Alba, Post-acquisition data processing for the screening of transformation products of different organic contaminants. Two-year monitoring of river water using LC-ESI-QTOF-MS and GCxGC-EI-TOF-MS, *Environ. Sci. Pollut. Res.* 21 (2014) 12583-12604.
- F.O. Agunbiade, B. Moodley, Pharmaceuticals as emerging organic contaminants in Umgeni River water system, KwaZulu-Natal, South Africa, *Environ. Monit. Assess.* 186 (2014) 7273-7291.
- V.S.A. Lopes, R.R. Riente, A.A. da Silva, D.F. Torquillo, R. da Silva Carreira, M.R. da Costa Marques, Development of a solid-phase extraction system modified for preconcentration of emerging contaminants in large sample volumes from rivers of the lagoon system in the city of Rio de Janeiro, Brazil, *Mar. Pollut. Bull.* 110 (2016) 572-577.
- I. Pugajeva, J. Rusko, I. Perkons, E. Lundanes, V. Bartkevics, Determination of pharmaceutical residues in wastewater using high performance liquid chromatography coupled to quadrupole-Orbitrap mass spectrometry, *J. Pharm. Biomed. Anal.* 133 (2017) 64-74.
- S. Matongo, G. Birungi, B. Moodley, P. Ndungu, Pharmaceutical residues in water and sediment of Msunduzi River, kwazulu-natal, South Africa, *Chemosphere* 134 (2015) 133-140.
- R. María Baena-Nogueras, M.G. Pintado-Herrera, E. Gonzalez-Mazo, P.A. Lara-Martín, Determination of pharmaceuticals in coastal systems using solid phase extraction (SPE) followed by ultra performance liquid chromatography-tandem mass spectrometry (UPLC-MS/MS), *Curr. Anal. Chem.* 12 (2016) 183-201.
- R. Ma, B. Wang, L. Yin, Y. Zhang, S. Deng, J. Huang, et al., Characterization of pharmaceutically active compounds in Beijing, China: occurrence pattern, spatiotemporal distribution and its environmental implication, *J. Hazard Mater.* 323 (2017) 147-155.

- [49] M. Gros, S. Rodríguez-Mozaz, D. Barcelo, Fast and comprehensive multi-residue analysis of a broad range of human and veterinary pharmaceuticals and some of their metabolites in surface and treated waters by ultra-high-performance liquid chromatography coupled to quadrupole-linear ion trap tandem mass spectrometry, *J. Chromatogr. A* 1248 (2012) 104-121.
- [50] R. Pinhancos, S. Maass, D.M. Ramanathan, High-resolution mass spectrometry method for the detection, characterization and quantitation of pharmaceuticals in water, *J. Mass Spectrom.* 46 (2011) 1175-1181.
- [51] P. Paíga, L.H.M.L.M. Santos, C. Delerue-Matos, Development of a multi-residue method for the determination of human and veterinary pharmaceuticals and some of their metabolites in aqueous environmental matrices by SPE-UHPLC-MS/MS, *J. Pharm. Biomed. Anal.* 135 (2017) 75-86.
- [52] F. Hernandez, M. Ibanez, R. Bade, L. Bijlsma, J. Sancho, Investigation of pharmaceuticals and illicit drugs in waters by liquid chromatography-high-resolution mass spectrometry, *Trends Anal. Chem.* 63 (2014) 140-157.
- [53] M. Krauss, H. Singer, J. Hollender, LC/MS/MS high resolution MS in environmental analysis: from target screening to the identification of unknowns, *Anal. Bioanal. Chem.* 397 (2010) 943-951.
- [54] F. Hernandez, J. Sancho, M. Ibanez, E. Abad, T. Portoles, L. Mattioli, Current use of high-resolution mass spectrometry in the environmental sciences, *Anal. Bioanal. Chem.* 403 (2012) 1251-1264.
- [55] R. Lopez-Roldan, M.L. de Alda, M. Gros, M. Petrovic, J. Martín-Alonso, D. Barcelo, Advanced monitoring of pharmaceuticals and estrogens in the Llobregat River basin (Spain) by liquid chromatography-triple quadrupole-tandem mass spectrometry in combination with ultra performance liquid chromatography-mass spectrometry, *Chemosphere* 80 (2010) 1337-1344.
- [56] L. Suntornsuk, O. Pipitharome, P. Wilairat, Simultaneous determination of paracetamol and chlorpheniramine maleate by micellar electrokinetic chromatography, *J. Pharm. Biomed. Anal.* 33 (2003) 441-449.
- [57] C. Engin, S. Yilmaz, G. Saglikoglu, S. Yagmur, M. Sadikoglu, Electroanalytical investigation of paracetamol on glassy carbon electrode by voltammetry, *Int. J. Electrochem. Sci.* 10 (2015) 1916-1925.
- [58] S. Cheemalapati, S. Palanisamy, V. Mani, S.M. Chen, Simultaneous electrochemical determination of dopamine and paracetamol on multiwalled carbon nanotubes/graphene oxide nanocomposite-modified glassy carbon electrode, *Talanta* 117 (2013) 297-304.
- [59] W.Y. Su, S.H. Cheng, Electrochemical oxidation and sensitive determination of acetaminophen in pharmaceuticals at poly (3, 4-ethylenedioxythiophene)-modified screen-printed electrodes, *Electroanalysis* 22 (2010) 707-714.
- [60] J. Li, J. Liu, G. Tan, J. Jiang, S. Peng, M. Deng, et al., High-sensitivity paracetamol sensor based on Pd/graphene oxide nanocomposite as an enhanced electrochemical sensing platform, *Biosens. Bioelectron.* 54 (2014) 468-475.
- [61] A.K. Baytak, T. Teker, S. Duzmen, M. Aslanoglu, A composite material based on nanoparticles of yttrium (III) oxide for the selective and sensitive electrochemical determination of acetaminophen, *Mater. Sci. Eng. C* 66 (2016) 278-284.
- [62] Y.E.L. Bouabi, A. Farahi, N. Labjar, S. El Hajjaji, M. Bakasse, M.A. El Mhammedi, Square wave voltammetric determination of paracetamol at chitosan modified carbon paste electrode: application in natural water samples, commercial tablets and human urines, *Mater. Sci. Eng. C* 58 (2016) 70-77.
- [63] F. Tadayon, S. Vahed, H. Bagheri, Au-Pd/reduced graphene oxide composite as a new sensing layer for electrochemical determination of ascorbic acid, acetaminophen and tyrosine, *Mater. Sci. Eng. C* 68 (2016) 805-813.
- [64] M. Taei, H. Salavati, F. Hasanpour, S. Habibollahi, H. Baghlani, Simultaneous determination of ascorbic acid, acetaminophen and codeine based on multi-walled carbon nanotubes modified with magnetic nanoparticles paste electrode, *Mater. Sci. Eng. C* 69 (2016) 1-11.
- [65] S. Chitravathi, N. Munichandraiah, Voltammetric determination of paracetamol, tramadol and caffeine using poly (Nile blue) modified glassy carbon electrode, *J. Electroanal. Chem.* 764 (2016) 93-103.
- [66] S. Sharifian, A. Nezamzadeh-Ejehieh, Modification of carbon paste electrode with Fe (III)-clinoptilolite nano-particles for simultaneous voltammetric determination of acetaminophen and ascorbic acid, *Mater. Sci. Eng. C* 58 (2016) 510-520.
- [67] F.A. Gorla, E.H. Duarte, E.R. Sartori, C.R.T. Tarley, Electrochemical study for the simultaneous determination of phenolic compounds and emerging pollutant using an electroanalytical sensing system based on carbon nanotubes/surfactant and multivariate approach in the optimization, *Microchem. J.* 124 (2016) 65-75.
- [68] E. Bayram, E. Akyilmaz, Development of a new microbial biosensor based on conductive polymer/multiwalled carbon nanotube and its application to paracetamol determination, *Sens. Actuators B Chem.* 233 (2016) 409-418.
- [69] H. Yang, Z. Wei, S. He, T. Li, Y. Zhu, L. Duan, et al., Fabrication of electrochemical sensor for acetaminophen based on levodopa polymer and multi-walled carbon nanotubes complex, *Int. J. Electrochem. Sci.* 12 (2017) 11089-11101.
- [70] M. Sakthivel, M. Sivakumar, S.M. Chen, Y.S. Hou, V. Veeramani, R. Madhu, et al., A facile synthesis of Cd(OH)₂-rGO nanocomposites for the practical electrochemical detection of acetaminophen, *Electroanalysis* 29 (2017) 280-286.
- [71] Z.M. Jiang, G.Y. Li, M.X. Zhang, A novel electrochemical sensor Based on SH-beta-cyclodextrin functionalized gold nanoparticles/reduced-graphene oxide nanohybrids for ultrasensitive electrochemical sensing of acetaminophen and ofloxacin, *Int. J. Electrochem. Sci.* 12 (2017) 5157-5173.
- [72] F. Cao, Q. Dong, C. Li, J. Chen, X. Ma, Y. Huang, et al., Electrochemical sensor for detecting pain reliever/fever reducer drug acetaminophen based on electro-spun CeBiOx nanofibers modified screen-printed electrode, *Sens. Actuators B Chem.* 256 (2018) 143-150.
- [73] B. Uslu, S.A. Ozkan, Electroanalytical methods for the determination of pharmaceuticals: a review of recent trends and developments, *Anal. Lett.* 44 (2011) 2644-2702.
- [74] M.A. Prathap, B. Satpati, R. Srivastava, Facile preparation of polyaniline/MnO₂ nanofibers and its electrochemical application in the simultaneous determination of catechol, hydroquinone, and resorcinol, *Sens. Actuators B Chem.* 186 (2013) 67-77.
- [75] J. Hui, W. Li, Y. Guo, Z. Yang, Y. Wang, C. Yu, Electrochemical sensor for sensitive detection of paracetamol based on novel multi-walled carbon nanotubes-derived organiceinorganic material, *Bioproc. Biosyst. Eng.* 37 (2014) 461-468.
- [76] S. Shrivastava, N. Jadon, R. Jain, Next-generation polymer nanocomposite-based electrochemical sensors and biosensors: a review, *Trends Anal. Chem.* 82 (2016) 55-67.
- [77] S. Prakash, T. Chakrabarty, A.K. Singh, V.K. Shashi, Polymer thin films embedded with metal nanoparticles for electrochemical biosensors applications, *Biosens. Bioelectron.* 41 (2013) 43-53.
- [78] A. Kutluay, M. Aslanoglu, Modification of electrodes using conductive porous layers to confer selectivity for the voltammetric detection of paracetamol in the presence of ascorbic acid, dopamine and uric acid, *Sens. Actuators B Chem.* 185 (2013) 398-404.
- [79] J. Luo, C. Fan, X. Wang, R. Liu, X. Liu, A novel electrochemical sensor for paracetamol based on molecularly imprinted polymeric micelles, *Sens. Actuators B Chem.* 188 (2013) 909-916.
- [80] B.R. Shrestha, R.R. Pradhananga, Spectrophotometric method for the determination of paracetamol, *J. Nepal Chem. Soc.* 24 (2009) 39-44.
- [81] A.H. Aktas, F. Kitis, Spectrophotometric simultaneous determination of caffeine and paracetamol in commercial pharmaceutical by principal component regression, partial least squares and artificial neural networks chemometric methods, *Croat. Chem. Acta* 87 (2014) 69-74.
- [82] E. Pados, M. Dunach, A. Morros, M. Sabes, J. Manosa, Fourth-derivative spectrophotometry of proteins, *Trends Biochem. Sci.* 9 (1984) 508-510.
- [83] S. Behera, S. Ghanty, F. Ahmad, S. Santra, S. Banerjee, UV-visible spectrophotometric method development and validation of assay of paracetamol tablet formulation, *J. Anal. Bioanal. Tech.* 3 (2012) 151-157.
- [84] A.M. El-Kosasy, O. Abdel-Aziz, N. Magdy, N.M. El Zahar, Spectrophotometric and chemometric methods for determination of imipenem, ciprofloxacin hydrochloride, dexamethasone sodium phosphate, paracetamol and cilastatin sodium in human urine, *Spectrochim. Acta Part A Mol. Biomol. Spectrosc.* 157 (2016) 26-33.
- [85] A. Mendez-Albores, C. Tarín, G. Rebollar-Perez, L. Dominguez-Ramirez, E. Torres, Biocatalytic spectrophotometric method to detect paracetamol in water samples, *J. Environ. Sci. Health A* 50 (2015) 1046-1056.
- [86] F. Shamsa, H. Monsef, R. Ghamooshi, M. Verdian-rizi, Spectrophotometric determination of total alkaloids in some Iranian medicinal plants, *Thai J. Pharm. Sci.* 32 (2008) 17-20.
- [87] L. Li, R. Bian, Y. Ding, M. Yu, D. Yu, Application of functionalized ZnS nanoparticles to determinate uracil and thymine as a fluorescence probe, *Mater. Chem. Phys.* 113 (2009) 905-908.
- [88] M. Bahram, S. Alizadeh, T. Madrakian, Application of AgNPs for simple and rapid spectrophotometric determination of acetaminophen and gentamicin in real samples, *Sensor Lett.* 14 (2016) 127-133.
- [89] W.C. Chan, S. Nie, Quantum dot bioconjugates for ultrasensitive nonisotopic detection, *Science* 281 (1998) 2016e2018.
- [90] M. Bruchez, M. Moronne, P. Gin, S. Weiss, A.P. Alivisatos, Semiconductor nanocrystals as fluorescent biological labels, *Science* 281 (1998) 2013-2016.
- [91] L. Li, Y. Lu, Y. Ding, Y. Cheng, W. Xu, F. Zhang, Determination of paracetamol based on its quenching effect on the photoluminescence of CdTe fluorescence probes, *J. Fluoresc.* 22 (2012) 591-596.
- [92] Y. Tan, Z. Zhou, P. Wang, L. Nie, S. Yao, A study of a bio-mimetic recognition material for the BAW sensor by molecular imprinting and its application for the determination of paracetamol in the human serum and urine, *Talanta* 55 (2001) 337-347.
- [93] G. Zhao, L. Yang, S. Wu, H. Zhao, E. Tang, C.P. Li, The synthesis of amphiphilic pillar [5] arene functionalized reduced graphene oxide and its application as novel fluorescence sensing platform for the determination of acetaminophen, *Biosens. Bioelectron.* 91 (2017) 863-869.
- [94] X. Liu, W. Na, H. Liu, X. Su, Fluorescence turn-off-on probe based on polypyrrole/graphene quantum composites for selective and sensitive detection of paracetamol and ascorbic acid, *Biosens. Bioelectron.* 98 (2017) 222-226.
- [95] L. Suntornsuk, Recent advances of capillary electrophoresis in pharmaceutical analysis, *Anal. Bioanal. Chem.* 398 (2010) 29-52.
- [96] K.D. Altria, M.A. Kelly, B.J. Clark, Current applications in the analysis of pharmaceuticals by capillary electrophoresis. II, *Trends Anal. Chem.* 17 (1998) 214-226.
- [97] L. Capka, P. Lacina, M. Vavrova, Development and application of SPE/CZE method for detection and determination of selected non-steroidal anti-inflammatory drugs in wastewater, *Fresenius Environ. Bull.* 21 (2012) 3312-3317.
- [98] A. Solangi, S. Memon, A. Mallah, N. Memon, M.Y. Khuhawar, M.I. Bhangar, Determination of ceftriaxone, ceftizoxime, paracetamol, and diclofenac sodium by capillary zone electrophoresis in pharmaceutical formulations and in human blood serum, *Turkish J. Chem.* 34 (2010) 921-934.
- [99] M.A. Sultan, H.M. Maher, N.Z. Alzoman, M.M. Alshehri, M.S. Rizk, M.S. Elshahed, et al., Capillary electrophoretic determination of antimigraine formulations containing caffeine, ergotamine, paracetamol and domperidone or metoclopramide, *J. Chromatogr. Sci.* 51 (2012) 502-510.

Chapter 4 Experimental Methods, Results and Discussion

This chapter outlines the materials and experimental methods for the determination of triclosan and acetaminophen by quantum dots and quantum dots embedded in a molecularly imprinted polymer together with results and discussion based on three journal paper formats.

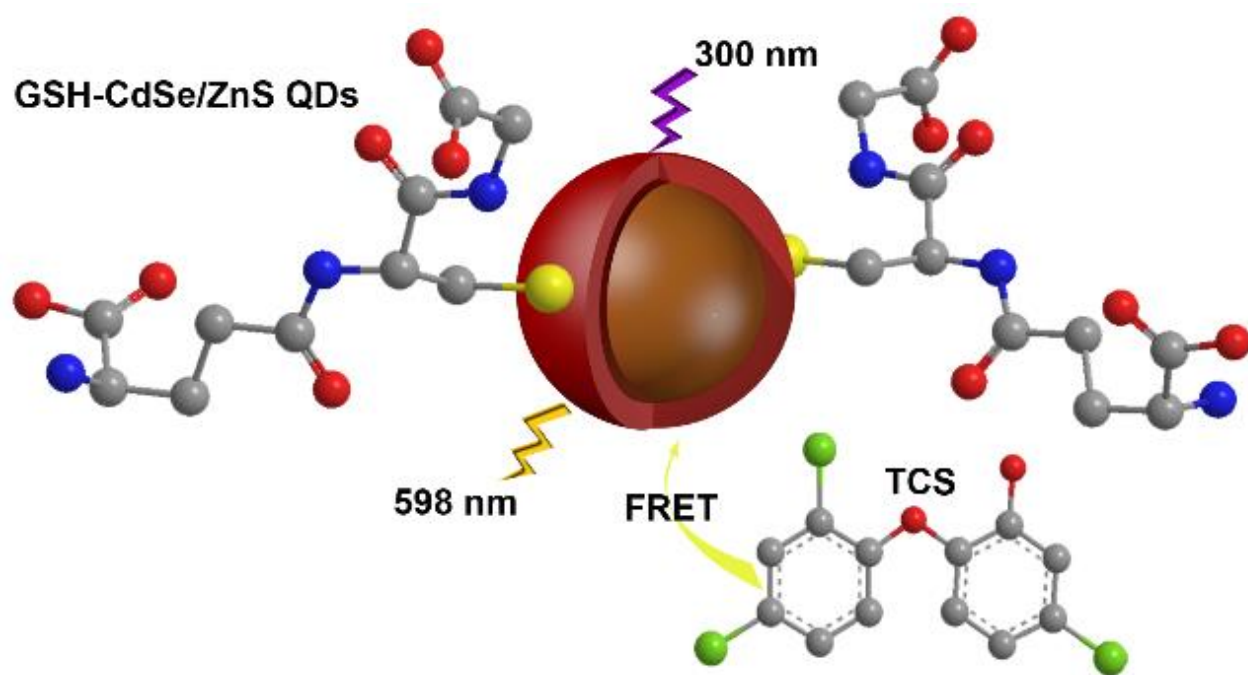
4.1 Paper 3

This paper was formatted in accordance with the journal *Spectrochimica Acta Part A: Molecular and Biomolecular Spectroscopy*, an Elsevier journal in which it has been published:

Montaseri, H., & Forbes, P.B.C. (2018). A triclosan turn-ON fluorescence sensor based on thiol-capped core/shell quantum dots. *Spectrochimica Acta Part A: Molecular and Biomolecular Spectroscopy*, 204, 370-379. Impact Factor 2.536.

<https://doi.org/10.1016/j.saa.2018.06.043>

Graphical abstract





Contents lists available at ScienceDirect

Spectrochimica Acta Part A: Molecular and Biomolecular Spectroscopy

journal homepage: www.elsevier.com/locate/saa

A triclosan turn-ON fluorescence sensor based on thiol-capped core/shell quantum dots

Hanieh Montaseri, Patricia B.C. Forbes*

Department of Chemistry, Faculty of Natural and Agricultural Sciences, University of Pretoria, Lynnwood Road, Pretoria 0002, South Africa



ARTICLE INFO

Article history:

Received 28 March 2018

Received in revised form 8 June 2018

Accepted 11 June 2018 Available online 15 June 2018

Keywords:

Triclosan

Personal care products

Quantum dots

FRET

Fluorescence spectroscopy

ABSTRACT

Triclosan (TCS) is a common antimicrobial found in many personal care products. A large amount of TCS thus enters the wastewater system leading to the accumulation thereof in water sources. In this work, core-shell structured GSH-CdSe/ZnS fluorescent quantum dots (QDs) were synthesized based on organometallic synthesis with a thiol ligand capping agent. The GSH-CdSe/ZnS QDs showed excellent photostability and a photoluminescence quantum yield of 89%. The fluorescence of the GSH-CdSe/ZnS QDs was enhanced by the introduction of TCS, likely owing to fluorescence resonance energy transfer from TCS to the QDs, allowing for its use as a “turn on” fluorescence probe for the detection and determination of TCS. A linear response was observed in the range of 10–300 nmol L⁻¹ with limits of detection and quantification of 3.7 and 12.4 nmol L⁻¹ respectively. The probe displayed good recoveries (94%–117.5%) for the determination of TCS in tap and river water samples which demonstrated the suitability of this novel sensor for a monitoring application of environmental relevance.

© 2018 Elsevier B.V. All rights reserved.

1. Introduction

Triclosan, 5-chloro-2-(2,4-dichlorophenoxy) phenol (Fig. 1) with the commercial name Irgasan DP300, has been used in a variety of consumer products [1, 2]. TCS is a fairly small molecule, with a molecular weight of 289.54 g mol⁻¹ and a diameter of about 7.4 Å [3] with a solubility of <10⁻⁶ g mL⁻¹ in water [4]. The partition coefficient of TCS (log P_{ow} = 4.76), suggests that it is lipophilic. Values of its pK_a have been reported in the range of 7.9–8.1 [5]. Triclosan is included in personal care products (such as shampoo, soap, toothpaste, detergent, lotion and skin care cream) due to its bactericide and antimicrobial properties at a typical concentration in the range of 0.1–0.3% (w/w), where the content of TCS in household products should not exceed the upper limit of this range [6].

However, its ubiquitous use has resulted in the presence of TCS in wastewater, sediments and many water sources [7] where its presence may affect ecosystems as it may kill algae for example [8]. There have also been several human health concerns associated with TCS, as it can accumulate in the human body over time leading to long-term health risks [9, 10]. TCS may degrade in the aquatic environment to more toxic products, the most concerning of which are dioxins, as these are known carcinogens and can mutate DNA and cause birth defects in offspring [11]. It is therefore of great importance that sensitive

methods be developed for the detection and quantification of TCS in the environment.

Instrumental techniques have been developed for the determination of TCS including those based on chromatography-mass spectrometry [12] electrochemical methods [13] and capillary zone electrophoresis methods [14]. The determination of triclosan relies mainly on chromatographic techniques or voltammetric methods, such as those employing nanomaterial based electrode systems. Advantages of chromatographic approaches include that they are selective and sensitive, however they are time consuming and they require large and expensive instrumentation, as well as high cost detectors such as MS or MS/MS. Although electrochemical methods provide a convenient, economical and fast approach, they suffer from strongly adsorbed oligomeric products of the oxidation of triclosan on the electrode surface. There is thus a need to develop a rapid, selective and sensitive method for triclosan determinations.

Fluorescence measurement techniques, as a subset of optical methods, have drawn a great deal of research interest, where a fluorophore material serves as a sensing receptor to detect the analyte(s).

Quantum dots (QDs) are fluorescent probes with unique chemical and physical properties such as size-dependent fluorescence, high fluorescence quantum yields, narrow spectral line widths, independence of emission on the excitation wavelength, and stability against photobleaching [15]. The application of quantum dots for analysis and sensing of various analytes such as organic compounds [16], ions [17, 18], biomolecules [19] and environmental pollutants [20, 21], as well

* Corresponding author.

E-mail address: Patricia.Forbes@up.ac.za (P.B.C. Forbes).<https://doi.org/10.1016/j.saa.2018.06.043>

1386-1425/© 2018 Elsevier B.V. All rights reserved.

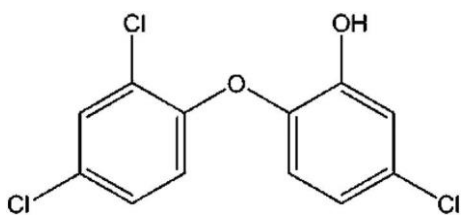


Fig. 1. Chemical structure of triclosan.

as for biological and medical use [22, 23], has increased significantly in recent years.

The mechanisms involved in QD-based sensing are energy transfer and charge transfer. Förster resonance energy transfer (FRET) is a non-radiative energy transfer between donor and acceptor fluorophores in which QDs may act as an energy donor by being size-tuned in order to provide overlap with the acceptor [24]. Although there are numerous applications reported where QDs serve as an energy donor, few publications report mechanisms related to QDs as acceptor [25]. In comparison with the photoluminescence (PL) quenching mode, the PL “turn-on” mode is generally more preferable, as a variety of factors other than the target analyte(s) can induce the ultimate PL “off” state. The PL “off-on” conversion in the “turn-on” mode can reduce the chance of false positives and is more amenable to multiplexing, like the simultaneous use of several detectors that uniquely respond to various analytes and which also provides lower detection limits [26].

To the best of our knowledge, until now there has been no report on detection of TCS in water samples based on the application of water soluble quantum dots. Only one research study has been performed on the use of molecularly imprinted polymers (MIPs) as extraction media for TCS, where molecularly imprinted core-shell nanotubes were synthesized on silica-coated multi-walled carbon nanotubes (MWCNTs) via a sol-gel process for the extraction of triclosan from environmental water samples with subsequent HPLC analysis. The binding isotherms of TCS were determined in the concentration range of $34.5\text{--}1.4 \times 10^5 \text{ nmol L}^{-1}$ [27].

The presence of TCS in environmental compartments, due to its partial elimination in wastewater systems, demands attention to ameliorate impacts on human and ecosystem health. In this work, we developed a simple and novel FRET based fluorescence sensor for the nanomolar determination of TCS in real water samples. Highly fluorescent CdSe/ZnS QDs were synthesized because simple QDs impose much less burden on the environment in terms of producing heavy metal wastes, and the ZnS shell protects against possible leaching of the Cd from the core.

2. Experimental

2.1. Reagents and Materials

Triethylphosphine oxide (TOPO), octadec-1-ene (ODE), zinc oxide, cadmium oxide, oleic acid (OA), sulfur powder, and 4-hydroxybenzoic acid (paraben) were purchased from Sigma Aldrich (St. Louis, MO, USA). 2,4,6-trichlorophenol was purchased from Fluka (Buchs, Switzerland). 2,4-dichlorophenol, 4-chlorophenol and 2,3,4-trichlorophenol were purchased from Riedel-de Haën (Seelze, Germany). Bisphenol A and triclocarban as potential interfering analytes were purchased from Dr. Ehrenstorfer GmbH (Augsburg, Germany). Hydrogen peroxide, sulfuric acid, methanol, chloroform, acetone, selenium powder, potassium hydroxide, glutathione (GSH) and triclosan (TCS) were purchased from Merck (Darmstadt, Germany). An ultrapure Milli-Q Water System ($18.0 \text{ M}\Omega\text{-cm}$ at 25°C) was used for sample preparation.

2.2. Apparatus

Fluorescence emission spectra were recorded on a Horiba Jobin Yvon Fluoromax-4 spectrofluorometer. Powder X-ray diffraction (XRD)

patterns were analyzed using a PANalytical X'Pert Pro powder diffractometer in $\theta\text{-}\theta$ configuration with a X'Celerator detector, variable divergence and receiving slits with Fe filtered Co-K α radiation ($\lambda = 1.789 \text{ \AA}$). IR measurements were taken using a Spectrum RXI FT-IR System from Perkin Elmer and UV–vis absorption spectra were recorded using a Cary Eclipse (Varian) spectrophotometer. High resolution transmission electron microscopy (HRTEM) images were taken using a JEOL JEM 2100F operated at 200 kV. The estimated particle size distribution QDs were determined using ImageJ software (<http://imagej.nih.gov/ij/>, U.S. National Institutes of Health [NIH], Bethesda, Maryland, USA). Energy dispersive x-ray spectroscopy (EDS) analysis was performed using a SEM integrated EDS Zeiss Crossbeam 540 with software AZtech version 3 by Oxford Instruments. The Förster distance was estimated using the program PhotochemCAD [28].

2.3. Fluorescence Studies

2.3.1. Fluorescence Quantum Yield

In order to determine the PL quantum yield (Φ_F) of the QDs, the integrated fluorescence intensities of the QDs (F) in Millipore water was compared to that of Rhodamine 6G in ethanol whilst taking into consideration the refractive indices (n) of the solvents and absorbance of both the QDs (A) and Rhodamine 6G (A_{Std}) at the excitation wavelength [24].

$$\Phi_F = \Phi_{F(\text{Std})} \frac{F \cdot A_{\text{Std}} \cdot n^2}{F_{\text{Std}} \cdot A \cdot n_{\text{Std}}^2} \quad \text{Eq. 1}$$

Here $\Phi_{F(\text{Std})} = 95\%$ [29], F and F_{Std} represent the integrated fluorescence intensity of the QDs and the reference standard, whilst A and A_{Std} refer to the absorbance of the sample and reference standard at the excitation wavelength, respectively and n and n_{Std} are the refractive indices of solvents used for the sample and standard.

The optical density of the first excitonic absorption peak of GSH-CdSe/ZnS QDs samples was set in the range of 0.02–0.05 in order to obtain a strong fluorescence signal with a good signal-to-noise ratio and to reduce the effect of self-absorption of nanoparticles on PL properties [30].

2.4. Synthesis of CdSe/ZnS Core/Shell QDs

2.4.1. Preparation of the Precursors

In order to prepare the Se precursor, 1.9 g of TOPO in 25 mL of ODE was heated up to 80°C to produce a clear solution then 0.3 g of Se powder was added and stirred continuously to generate the TOPSe solution. For the preparation of sulfur precursor, 1.9 g of TOPO in 30 mL of ODE, and 20 mL of OA was heated to 80°C and once a clear solution was formed, 0.16 g of S powder was added. Zinc precursor was prepared by dissolving 0.41 g of ZnO powder in 30 mL of ODE and 20 mL of OA.

2.4.2. Fabrication of the QDs

One pot synthesis was carried out for the preparation of the core/shell QDs according to published methods with some modifications [21, 31]. The one-pot approach can be realized only if both core and shell can grow controllably in the same reaction mixture. Briefly, in a three-necked flask fitted with a thermometer, refluxing condenser and septum, 1.3 g of CdO was added into a solution of 50 mL of ODE and 30 mL of OA and the solution was vigorously stirred to a temperature of $\sim 280^\circ\text{C}$ so as to form a colorless Cd-OA complex under inert atmosphere. Once the colorless complex solution was formed, a pre-mixed TOPSe solution was injected into the solution to allow for nucleation and growth of CdSe QDs. In order to passivate the alloyed core surface, ZnS shell was grown epitaxially on the core surface by adding zinc and sulfur precursors at a reduced temperature of $\sim 200^\circ\text{C}$. Aliquots of the sample were taken at different time intervals and used to record their PL spectra. The QDs were purified by methanol to completely remove unreacted precursors.

2.4.3. Water-Solubilization of the QDs with GSH

Water solubilization of the QDs was attained via ligand exchange reaction of the hydrophobic capping (OA and TOPO) with the hydrophilic thiol GSH ligand. Generally, GSH–KOH methanolic stock solution was prepared separately by adding 2 g of glutathione to 3.0 g of KOH in 40 mL methanol with dissolution followed by ultrasonication. The purified OA–TOPO-capped CdSe and CdSe/ZnS QDs were re-dispersed in chloroform and the GSH–KOH methanolic solution was subsequently added followed by the addition of Millipore water separately to each QD solution. The solutions were stirred for 1 h for effective separation of the organic phase from the aqueous phase. The water-soluble GSH–CdSe/ZnS QDs were purified repeatedly via centrifugation with acetone and chloroform to completely eradicate all unreacted organic substituents. The purified aqueous dispersible QDs were dried in a fume hood.

2.5. Determination of TCS with GSH Capped CdSe/ZnS QDs

All measurements were performed under the following conditions: the excitation and emission slit width was 5 nm and the fluorescence intensity was measured at an excitation wavelength of 300 nm. A typical procedure for the detection of TCS is described as follows: 1.5 mg of GSH–CdSe/ZnS QDs was dissolved in 3 mL Millipore water and a standard solution containing different amounts of TCS was added and the corresponding PL spectra were recorded after different periods of time. A TCS stock solution (7.8×10^{-4} mol L⁻¹) was prepared by dissolution of the solid in a mixture of HPLC grade methanol: Millipore water (1:2). Standard solutions were made by dilution with Millipore water. Sensing was carried out by placing 2 mL of QDs solution in a quartz cuvette followed by addition of 200 μ L of TCS solution standard solution. It took about 5 min for the stabilization of the PL profile and this PL intensity was set as F_0 . Moreover, the PL intensity of QDs in the presence of 200 μ L of water was set as F_0 . Through the variation of TCS concentration, a series of F/F_0 values were obtained.

Tap water samples for fluorescence measurements were collected from tap water in Pretoria, South Africa using pre-cleaned glass bottles. River water samples were also collected from LC de

Villiers sports grounds in Pretoria. The sample bottles were filled without headspace and immediately placed in coolers filled with icepacks and transferred to the laboratory for storage at 4 °C and were analyzed within one week. Before analysis, the collected tap water and river water samples were centrifuged at 4500 rpm for 5 min and filtered through filter paper (110 mm pore size).

3. Results and Discussion

3.1. Absorption and Photoluminescence Emission Characterization of Aqueous GSH–CdSe- and GSH–CdSe/ZnS QDs

Fig. 2 (A) illustrates the absorption spectra of water-soluble GSH-capped CdSe/ZnS QDs. A well pronounced and broad excitonic peak at 575 nm was obtained for the GSH–CdSe/ZnS QDs. The surface passivation with a ZnS shell resulted in fluorescence enhancement of the CdSe/ZnS QDs due to the effect of the larger band gap of the ZnS shell which effectively traps the electrons in the core.

Fig. 2 (B and C) shows a symmetric photoluminescence (PL) emission spectrum of water-soluble GSH-capped CdSe and CdSe/ZnS QDs with a peak at wavelength of 576 nm and 605 nm respectively, while the estimated full width at half maximum (FWHM) values were 39.0 and 32.7 nm for GSH–CdSe QDs and GSH–CdSe/ZnS QDs respectively. It can also be observed that the PL emission of GSH–CdSe/ZnS QDs had a red-shift of 29 nm compared to the GSH–CdSe QDs due to the increase in size of the QDs upon shell addition. The PL was also enhanced as the measured PL quantum yields of the GSH–CdSe and GSH–CdSe/ZnS QDs were 5.4% and 89%, respectively. The capping process thus led to a significant improvement in the optical properties of the QDs.

The particle size of the GSH–CdSe/ZnS QDs determined from the first excitonic absorption peak using Eq. (2) [32] was 3.7 nm, which agreed well with the size determined by HRTEM analysis.

$$D = (1.6122 \times 10^{-9})\lambda^4 - (2.6575 \times 10^{-6})\lambda^3 + (1.6242 \times 10^{-3})\lambda^2 - (0.4277)\lambda + (41.57) \quad \text{Eq. 2}$$

where D (nm) is the size of the QDs, and λ (nm) is the wavelength of the first excitonic absorption peak of the corresponding sample.

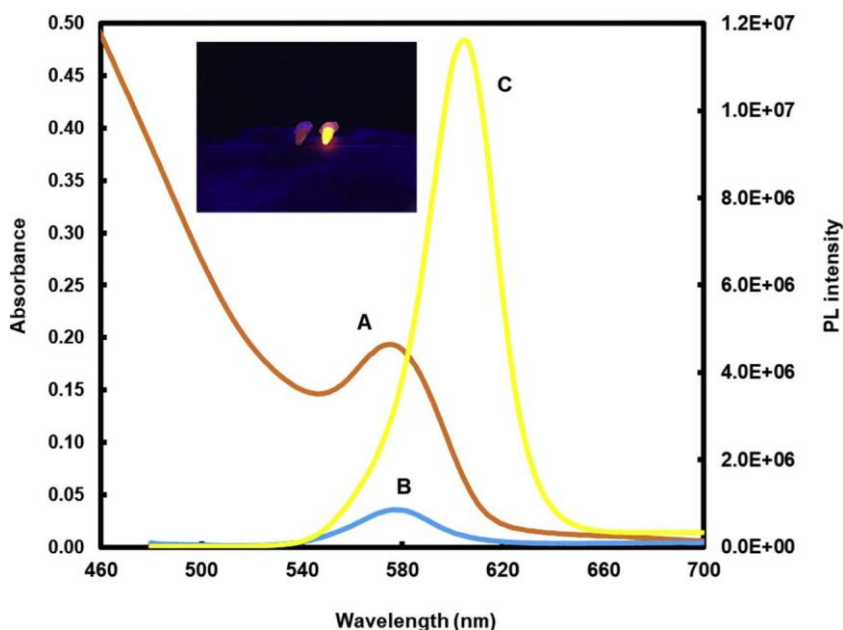


Fig. 2. Absorption spectra of the water-soluble GSH-capped CdSe/ZnS QDs in Millipore water (A) and PL emission spectra of the water-soluble GSH-capped CdSe QDs (B) and GSH-capped CdSe/ZnS QDs measured in Millipore water (C) at 470 nm. The inset shows GSH–CdSe QDs (left) and GSH–CdSe/ZnS QDs under UV irradiation with an excitation wavelength of 365 nm.

The extinction coefficient of GSH-CdSe/ZnS QDs was obtained by Eq. (3) [32] and was found to be $182,640 \text{ L mol}^{-1} \text{ cm}^{-1}$.

$$\varepsilon = 5857D^{2.65} \quad \text{Eq. 3}$$

where D is the diameter or size of the QDs.

Band gap energy values of GSH-CdSe and GSH-CdSe/ZnS QDs were also estimated to be 2.2 and 2.05 eV respectively according to Eq. (4).

$$E = h * C / \lambda \quad \text{Eq. 4}$$

where E is band gap energy, h is Planks constant ($6.63 \times 10^{-34} \text{ J}\cdot\text{s}$), C is the speed of light ($3.0 \times 10^8 \text{ ms}^{-1}$) and λ is cut off emission wavelength (m).

The band gap values for the synthesized QDs showed excellent correlation with other reported values obtained for the same QDs with the same sizes which were 2.2 eV and 2.009 eV for CdSe and CdSe/ZnS QDs respectively [33, 34].

3.2. Powder XRD

Fig. 3 compares the x-ray diffraction patterns of GSH-CdSe and GSH-CdSe/ZnS QDs. A typical zinc blende crystal structure with planes at {111}, {220} and {311} was obtained for CdSe/ZnS QDs with peaks at 31.65° , 52.71° and 60.18° according to the standard JCPDS (Card No. 5–566) crystalline ZnS with a zinc blende structure [35]. The results were also in complete agreement with other published reports [36, 37]. The peaks for CdSe QDs were at 31.64° , 52.66° and 59.44° also corresponding to a zinc blende crystalline structure. The diffraction peaks for alloyed CdSe/ZnS QDs are slightly shifted to higher Bragg angles in comparison to the alloyed CdSe core QDs. The sharp signals are spurious instrumental signals and are not related to x-rays. The broadening of the

diffraction peak is also associated with the nano-sized dimensions and small domains of the nanocrystals [38, 39].

From the XRD pattern, the average crystallite size of the GSH-CdSe and GSH-CdSe/ZnS QDs were determined using the Debye Scherrer equation [40].

$$D = \frac{0.9\lambda}{\beta \cos \theta} \quad \text{Eq. 5}$$

where D , λ , β and θ are the particle size of QDs, the wavelength of Co-K α radiation (1.789 Å), full width at half maximum (FWHM) and the angle corresponding to the peak, respectively. The average crystal sizes of GSH-CdSe and GSH-CdSe/ZnS QDs based on the width of the peak corresponding to the {111} plane were 3.2 nm and 3.3 nm respectively.

3.3. FT-IR Analysis

Confirmation of the attachment of GSH to the QDs was provided by FT-IR spectroscopy in Fig. 4. From this figure, it is clear that the IR spectra of the two QDs are similar which indicates that GSH binds on the surfaces of the two QDs in the same way. The most characteristic peak at 2524 cm^{-1} in the spectrum of pure GSH related to the stretching vibration of the –SH group. The symmetric stretching vibration of the carboxylic group is at 1396 cm^{-1} . Moreover, the peak at 550 cm^{-1} pertains to the bending vibration of the –SH group. More importantly, the absence of the band of the –SH group at $2550\text{--}2750 \text{ cm}^{-1}$ confirms the Cd-S bond formation in GSH-CdSe QDs and the formation of covalent bonds between thiols and the surface of ZnS in GSH-CdSe/ZnS QDs and successful attachment of GSH to the surface of QDs whilst the carboxyl group of GSH provides water solubility.

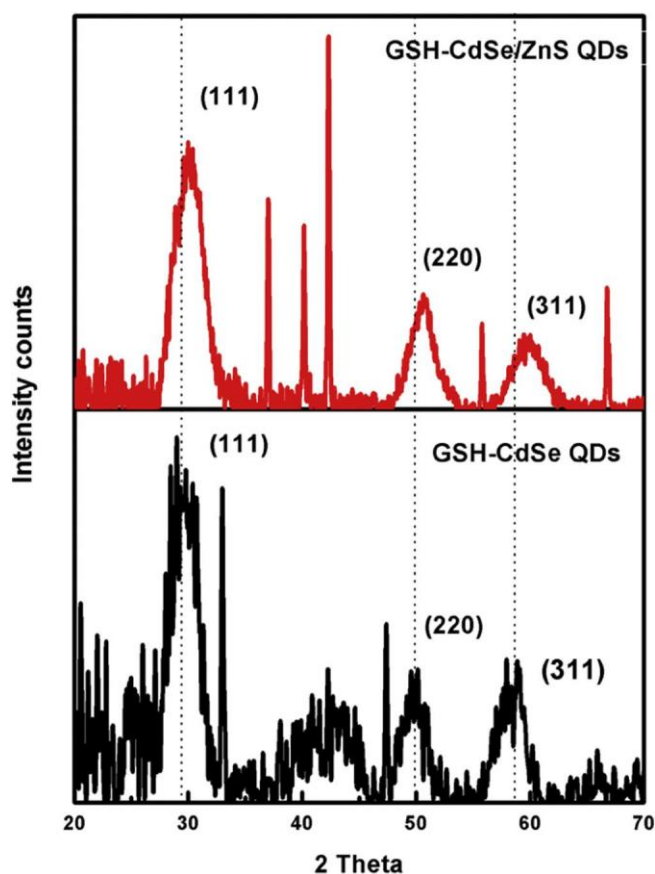


Fig. 3. Powder XRD pattern of the GSH-CdSe and GSH-CdSe/ZnS QDs.

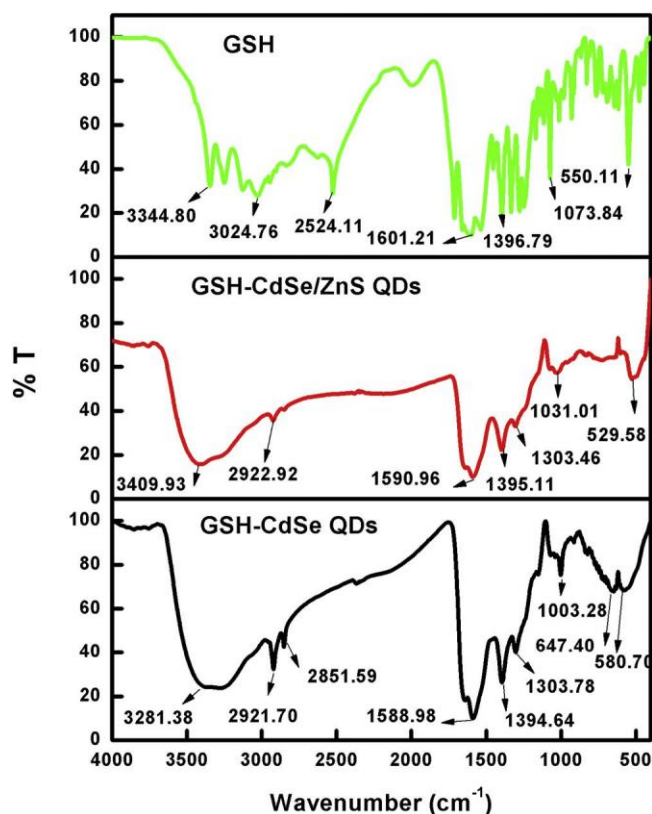


Fig. 4. The FT-IR spectra of GSH-CdSe QDs, GSH-CdSe/ZnS QDs, and GSH.

3.4. HRTEM Analysis

TEM analysis was carried out to determine the average particle size distribution and morphology of the QDs. The estimated particle size distribution of the QDs was determined using ImageJ software (<http://imagej.nih.gov/ij/>, U.S. National Institutes of Health [NIH], Bethesda, Maryland, USA). As shown in Fig. 5, it is evident that the QDs were monodispersed, spherical in shape and dispersed well in aqueous solution. The morphological display of the QDs also shows that they were almost homogenous in nature. The estimated average particle size

distribution (average particle size \pm standard deviation) of the GSH-CdSe QDs and GSH-CdSe/ZnS QDs were 2.5 ± 0.7 and 3.3 ± 1.3 nm respectively which were in accordance with the obtained sizes by XRD analysis. The particle size distributions of GSH-CdSe QDs and GSH-CdSe/ZnS QDs are shown in Fig. 5A1–B1.

3.5. EDS Analysis

EDS analysis was also carried out to confirm the existence of the metal components within the GSH-CdSe and GSH-CdSe/ZnS QD

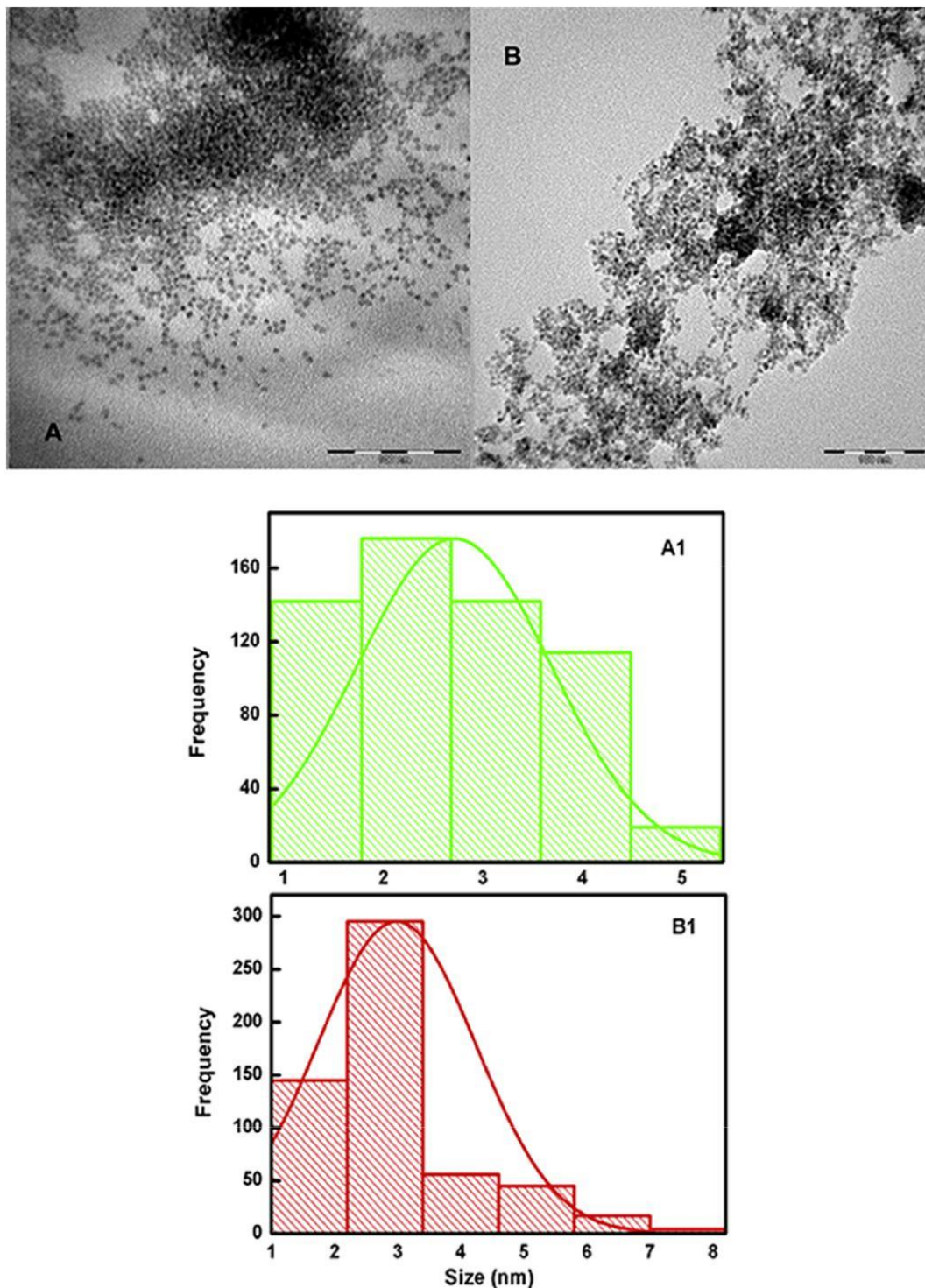


Fig. 5. TEM images of GSH-CdSe QDs (A) and GSH-CdSe/ZnS QDs (B) and particle size distribution of GSH-CdSe QDs (A1) and GSH-CdSe/ZnS QDs (B1).

structures (Fig. 6). The presence of Cd and Se were identified in the core while the additional signal of Zn and S were direct evidence of shell passivation onto the surface of the core. The approximate elemental composition for GSH-CdSe QDs were Cd (46.37%), Se (9.10%) and that of for the GSH-CdSe/ZnS core/shell QDs were Cd (53.81%), Se (7.05%), Zn (0.64%) and S (9.71%). In the EDS spectra, C, N, O and S also emanate from capping ligand GSH which were O (7.50%), N (0.73%) and C (26.65%), S (9.64%) for GSH-CdSe QDs and O (5.15%), N (0.15%) and C (23.48%) for GSH-CdSe/ZnS QDs.

3.6. Fluorescence Properties of TCS Standard Solution

The fluorescence behavior of TCS was recorded at different excitation wavelengths from 290 to 520 nm so as to investigate the possible effect on the PL spectra of GSH-CdSe/ZnS QDs. As shown in Fig. S1, the highest emission intensity was found at 407 nm at the excitation wavelength of 310 nm.

3.7. Optimization of the Determination of TCS

3.7.1. Effect of Aqueous GSH-CdSe/ZnS QDs Concentration

The concentration of GSH-CdSe/ZnS QDs influences the fluorescence intensity and sensitivity of the system. Thus different concentrations of GSH-CdSe/ZnS QDs (1.0, 1.5, 2.0, 2.5, 3.0 mg in 3.0 mL water) were prepared and 70 nmol L⁻¹ of TCS was added to each separately. F₀ was the fluorescence intensity of the QDs in the presence of water. It was found that high concentrations of aqueous GSH-CdSe/ZnS QDs decreased the

sensitivity of the system as self-quenching of QDs occurred (Fig. 7) therefore the optimum concentration was found to be 1.5 mg in 3.0 mL water.

3.7.2. Effect of Incubation Time

The effect of reaction time on the fluorescence intensity of the GSH capped CdSe/ZnS QDs-TCS system was investigated at different time intervals in the presence of 70 nmol L⁻¹ TCS (Fig. 8). The maximum fluorescence intensity was found after 5 min which indicated that the reaction was completed within 5 min at room temperature. Further studies were thus carried out after 5 min incubation.

3.8. Stabilization of Fluorescence Intensity

The fluorescence intensity of GSH-CdSe/ZnS QDs in Millipore water was slightly increased and became stable after one day compared to freshly prepared QDs solutions. The increase of fluorescence intensity of QDs can be attributed to the photo-activation of GSH-capped CdSe/ZnS QDs [41]. There were no remarkable changes in the fluorescence intensity of QDs even when stored for 5 days (Fig. S2). The slight red shift in the PL emission of the exposed GSH-CdSe/ZnS QDs was an indication that the band gap of the QDs decreased. Aggregation can also induce a red shift (1 nm) of the QD fluorescence which would be accompanied by PL quenching [42]. Consequently, all analytical measurements were carried out after the fluorescence intensity of QDs became stable.

3.9. Fluorescence Behavior of GSH Capped CdSe/ZnS QDs in the Presence of TCS

Under optimal conditions, the fluorescence spectra of GSH-CdSe/ZnS QDs with different concentrations of TCS were recorded. It was found that within the concentration range of 10–300 nmol L⁻¹, the intensity of aqueous GSH-CdSe/ZnS QDs enhanced with the introduction of TCS (Fig. 9). Förster resonance energy transfer (FRET) from analyte (donor) to QDs (acceptor) was deemed as the possible mechanism in this system. FRET is non-radiative transfer whereby energy transfers from an excited state of the donor (TCS) to a proximal ground state of the acceptor (QDs) through long-range dipole-dipole interactions which can be monitored by quenching or enhancement of acceptor [30]. In our experiments, the fluorescence intensity of the acceptor was enhanced while that of the donor was quenched. However, as the fluorescence of the donor (TCS) was of very weak intensity compared

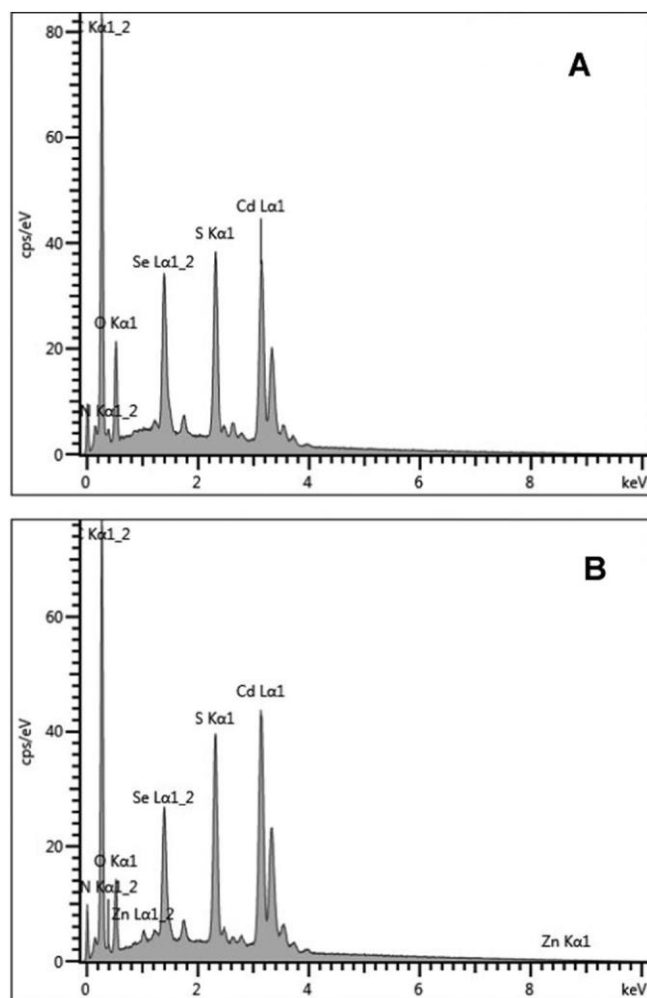


Fig. 6. EDS spectra of GSH-CdSe QDs (A) and GSH-CdSe/ZnS QDs (B).

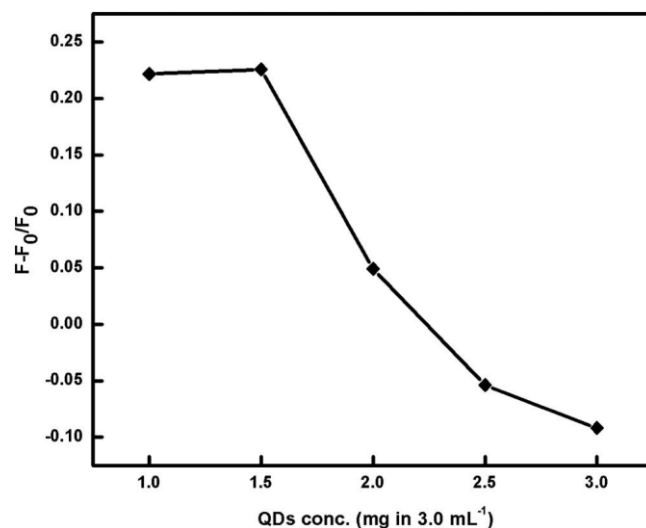


Fig. 7. Effect of the concentration of aqueous GSH-CdSe/ZnS QDs in the presence of 70 mol L⁻¹ TCS, fluorescence intensity without TCS (F₀), fluorescence intensity with TCS (F). The experimental conditions were excitation wavelength, 300 nm; slit widths of excitation and emission, 5 nm.

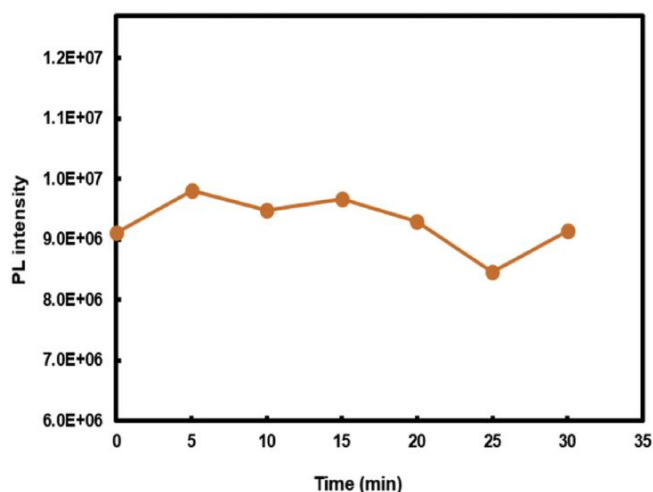


Fig. 8. Effect of reaction time on the fluorescence intensity of GSH capped CdSe/ZnS QDs in the presence of 70 nmol L^{-1} TCS. The experimental conditions were GSH-CdSe/ZnS QDs 1.5 mg in 3.0 mL Millipore water; excitation wavelength, 300 nm ; slit widths of excitation and emission, 5 nm .

to that of the acceptor (QDs), the quenching of the TCS fluorescence was not expected to be visible in Fig. 9.

3.10. Calibration Curve, Limit of Detection and Limit of Quantification

The fluorescence intensity of GSH capped CdSe/ZnS QDs increased linearly in the narrow concentration range of $10\text{--}300 \text{ nmol L}^{-1}$ of TCS ($r^2 = 0.98$) (Fig. 10). In comparison, the worldwide concentration range of TCS in water has been found to range from $0.005\text{--}140 \text{ nmol L}^{-1}$ in surface waters, $0.07\text{--}300 \text{ nmol L}^{-1}$ in wastewater influent, $0.08\text{--}18.0 \text{ nmol L}^{-1}$ wastewater effluent, and $<3.5 \times 10^{-6}\text{--}0.35 \text{ nmol L}^{-1}$ in sea water [43, 44]. The potential applicability of the fluorescence sensing method reported here for the monitoring of TCS in surface and wastewaters is thus evident. Moreover, the detection and quantification limits which were calculated using $3\delta/m$ and $10\delta/m$, where δ is the standard deviation of the blank signal ($n = 10$) and m is the slope of the linear range, were found to be 3.7 nmol L^{-1} and 12.4 nmol L^{-1} respectively. The LOD value is lower than the guidance value of 173 nmol L^{-1} (50 ppb) for triclosan in drinking water given by the Minnesota Department of Health (MDH) [45].

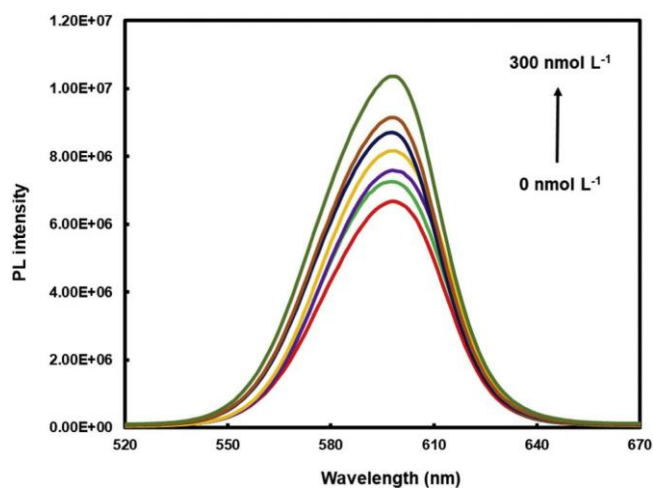


Fig. 9. The fluorescence spectra of GSH-CdSe/ZnS QDs in the presence of different concentrations of triclosan. The experimental conditions were GSH-CdSe/ZnS QDs 1.5 mg in 3.0 mL Millipore water; excitation wavelength, 300 nm ; slit widths of excitation and emission, 5 nm .

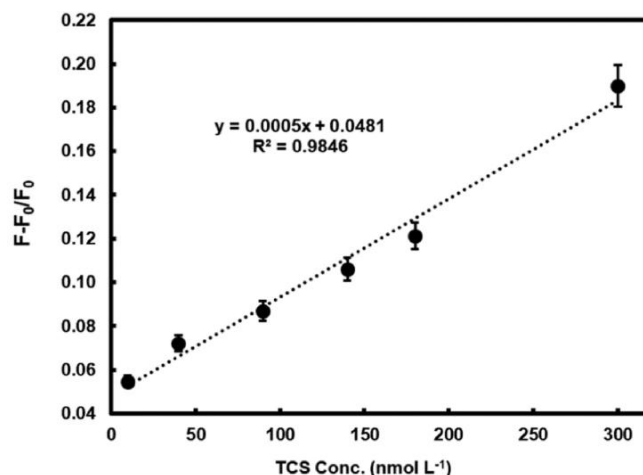


Fig. 10. Linear graph of $F-F_0/F_0$ versus TCS concentration. The experimental conditions were GSH-CdSe/ZnS QDs 1.5 mg in 3.0 mL Millipore water; excitation wavelength, 300 nm ; slit widths of excitation and emission, 5 nm .

For three replicate detections of TCS with three GSH-CdSe/ZnS QDs under optimum conditions, the precision was 4.0% (relative standard deviation).

The determination of TCS has mainly been carried out using voltammetry with nanomaterial based electrode systems and chromatography, respectively, as seen in Table 1. These methods have drawbacks in terms of environmentally unfriendly solvent use, complexity, analytical running costs, high-cost instrumentation, long analysis time, as well as the need for highly skilled technicians and time-consuming sample pre-treatment and are therefore not ideal for routine screening analysis [46].

3.11. Effect of Potential Interfering Analytes on GSH-CdSe/ZnS QDs

To further evaluate the applicability of the fluorescence probe, potential interfering compounds, as shown in Table S1, were investigated under the optimum conditions of 2 mL of $1.5 \text{ mg}/3.0 \text{ mL}$ GSH-CdSe/ZnS QDs in the presence of $200 \mu\text{L}$ of $180.0 \text{ nmol L}^{-1}$ of each analyte. 5 min was also employed as equilibrium time for each of the fluorescence measurements. Relative fluorescence intensity of GSH-CdSe/ZnS QDs was enhanced in the presence of each analyte (Fig. 11). The highest fluorescence intensity was achieved for TCS thus the probe is most sensitive to this target analyte. The prototype QD probe can also potentially be applied for the detection of a range of related compounds, particularly 2,3,4-TCP, 2,4-DCP, 4-CP, BPA and TCC for which significant fluorescence enhancement was observed.

The emission spectra of all compounds were also recorded in the range of 350 to 600 nm using a 300 nm excitation wavelength in order to investigate spectral overlap with the absorption spectrum of the QDs. The fluorescence emission of all compounds showed spectral overlap with the absorption spectra of the QDs. Therefore, the fluorescence turn-on probe can be utilized for the determination of this class of compounds, although the sensitivity of the sensor was shown to be greatest for TCS. If required, the selectivity of the sensor could be enhanced, for example by over-coating of the QDs with a molecularly imprinted polymer.

3.12. Analytical Application

The feasibility of the prototype sensor was evaluated in real water samples by the addition of different concentrations of TCS to tap and river water. The experimental results obtained using matrix matched standards are summarized in Table 2. The recoveries of different

Table 1
Comparison of some analytical methods for the determination of TCS in water samples.

Detection method	Linear range (nmol L ⁻¹)	Detection limit (nmol L ⁻¹)	pH of the sample	Reproducibility (%RSD)	Sample matrix	Reference
CNTs@TCS-MIPs/HPLC analysis	34.5–1.4 × 10 ⁵	–	9.5	8.9	River and lake water	[27]
GC-MS	0.07–70.0	0.02	NR	9.36	River water	[12]
HPLC-UV	0.03–580.2	0.003	3	7.0	Tap water, river water and municipal wastewater	[47]
HPLC-MS/MS	0.002–0.34	0.004 0.005	5.8	1.02–1.52	Deionized water River water	[48]
nZnO-MWCNT/GCE (CV, DPV and SWV)	5.2–7.0 × 10 ³	4.5	7	3.1	Tap water	[13]
β-CD/GNP (CV)	2 × 10 ³ –1.0 × 10 ⁵	6 × 10 ²	6	3.8	Water samples	[49]
DLLME-CZE-UV	70.0–7.0 × 10 ³	13.8	9.8	7.4	Tap and river water	[50]
Allylmercaptane modified gold SPR chip and imprinted p(HEMAGA) nanofilm	0.2–3.5	0.06	6	NR	Wastewater	[51]
Fluorescence: GSH-CdSe/ZnS QDs	10.0–300.0	3.7	7	4.0	Tap and river water	This work

β-CD/GNP, β-Cyclodextrin/graphene nano platelets; CNTs@TCS-MIPs, Carbon nanotubes@tricolosan-imprinted polymers; CV, Cyclic voltammetry; DLLME-CZE-UV, Dispersive liquid-liquid microextraction- capillary zone electrophoresis with UV detection; DPV, Differential pulse voltammetry; GC-MS, Gas chromatography – mass spectrometry; HPLC-UV, High performance liquid chromatography–ultraviolet detection; HPLC-MS/MS, High performance liquid chromatography–electron spray ionization–tandem mass spectrometry; NR, Not reported; nZnO-MWCNT/GCE, Nano zinc oxide-multi-walled carbon nanotube/glassy carbon electrode; [p(HEMAGA)], poly(2-hydroxyethylmethacrylate–methacryloylamidoglutaric acid); SPR, Surface plasmon resonance; SWV, Square wave voltammetry.

known amounts of TCS spiked in tap water and river water were very good and ranged from 94 to 115% and 98 to 117.5%, respectively, indicating the applicability of the sensor for quantitative determination of TCS in real water samples. It is also clear that typical metal ions and anions which were present in (and thus of relevance to) the matrix of interest did not impact on the fluorescence sensing of TCS.

The average triplicate pH value of GSH-CdSe/ZnS QDs in Millipore water was 7.0 while after injecting 200 μL of river or tap water into 2 mL of GSH-CdSe/ZnS QDs solution (containing 1.0 mg of GSH-CdSe/ZnS QDs), the pH values changed to 7.2 and 7.4 respectively. Therefore no significant pH changes occurred to the GSH-CdSe/ZnS QDs solution upon addition of real water samples and the effect of sample pH can thus be considered negligible. Regarding the salt concentration (ionic strength); considering the very large dilution effect (200 μL of tricolosan is injected into 2 mL of the QDs solution) the impact of the ionic strength of the sample on the GSH-CdSe/ZnS QDs-TCS system would be insignificant.

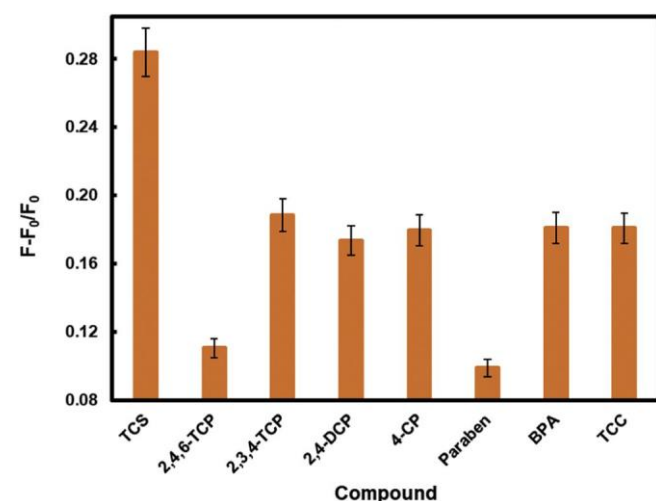


Fig. 11. Effect of other analytes on the fluorescence emission intensity of the GSH-CdSe/ZnS QDs probe at an emission wavelength of 598 nm. The concentration of TCS and each of the other analytes was 180 nmol L⁻¹ and GSH-CdSe/ZnS QDs was 1.5 mg in 3.0 mL Millipore water. F-F₀/F₀ relates to the fluorescence intensity of the QDs in the presence and absence of the analytes. Excitation wavelength was 300 nm. Analytes were 2,4,6-trichlorophenol (2,4,6-TCP), 2,3,4-trichlorophenol (2,3,4-TCP), 2,4-dichlorophenol (2,4-DCP), 4-chlorophenol (4-CP), 4-hydroxybenzoic acid (Paraben), Bisphenol A (BPA), and Triclocarban (TCC).

HPLC-MS/MS analysis was performed as a comparative method which confirmed that the background concentration of TCS in the tap and river water samples was below the detection limit.

3.13. Proposed Mechanism

The fluorescence behavior of TCS was recorded at different excitation wavelengths. As previously mentioned, the highest emission intensity was found at 407 nm at an excitation wavelength of 310 nm (Figs S1 and 12A).

Energy transfer is a possible mechanism for the fluorescence enhancement because there is overlap between the absorption spectrum of the core/shell QDs (500–600 nm) and the emission spectrum of TCS in the range 350–600 nm (Fig. 12B).

In general, Förster resonance energy transfer (FRET) is a specific mechanism of non-radiative energy transfer among donor and acceptor fluorophore molecules which are also called FRET pairs [24]. Energy transfer between a FRET pair may be owing to long-range dipole-dipole interaction [24]. FRET usually occurs when overlap of the emission spectrum of the donor and adsorption spectrum of the acceptor is bigger than 30% and the distance between them is <10 nm [52]. The more photons which are emitted from the donor, the better energy transfer will take place [24]. In this case, the QDs can absorb the emission energy from TCS leading to the enhancement of the PL emission of QDs, as was observed experimentally.

The energy transfer between a donor and acceptor pair relies on the distance between them which can be expressed by the Förster distance. It is the distance at which 50% of the excited donor molecules decay by energy transfer while the remainder decay through other radiative or non-radiative channels [25]. The Förster distance in the system of GSH-CdSe/ZnS QDs-TCS was found to be approximately 4.0 nm using the program PhotochemCAD which meets the distance required (<10 nm) for FRET to occur. This Förster distance is also similar to that

Table 2

Analytical results for the determination of TCS in tap and river water samples using GSH-capped CdSe/ZnS QDs.

	Spiked TCS (nmol L ⁻¹)	Determined TCS (mean ± SD; n = 3, nmol L ⁻¹)	Recovery (%)
Tap water	20	23 ± 0.3	115
	100	94 ± 0.6	94
	180	183 ± 0.3	102
River water	20	24 ± 0.4	117.5
	100	107 ± 2.4	107
	180	177 ± 1.2	98

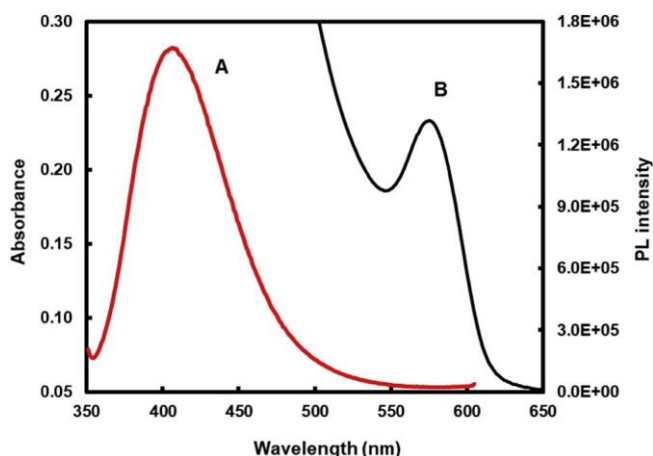


Fig. 12. Fluorescence spectrum of TCS (1.4×10^{-5} mol L⁻¹) at excitation wavelength 310 nm (A) and UV-Vis absorption spectrum of GSH-CdSe/ZnS QDs (B).

found in another study of 4.3–4.4 nm for the system of the same QDs (i.e. GSH-CdSe/ZnS), but in this case coordinated to gallium octacarboxy phthalocyanine (ClGaPc(COOH)₈) [53].

4. Conclusion

In summary, we designed and synthesized core-shell structured GSH-CdSe/ZnS QDs with a high photoluminescence quantum yield of 89%, via a one pot organometallic synthesis method. High resolution transmission electron microscopy images, FTIR spectra and fluorescence spectra confirmed the successful synthesis of QDs and the formation of a GSH coating thereon. The fluorescence of QDs was effectively enhanced by TCS at an emission wavelength of 598 nm over the concentration range of 10–300 nmol L⁻¹ with detection and quantification limits of 3.7 and 12.4 nmol L⁻¹ respectively, which confirmed the applicability of the method to detect TCS at nanomolar levels. The turn-on mechanism of the sensing process is likely associated with energy transfer from TCS to the QDs. Furthermore, the selectivity investigation of the prototype probe demonstrated the potential application of the sensor for the detection of 2,3,4-TCP, 2,4-DCP, 4-CP, BPA and TCC. The good response of this novel probe to TCS facilitates its application in the detection and determination of TCS in real water samples in the field of environmental monitoring for the first time.

Acknowledgements

Funding from the University of Pretoria and the Water Research Commission (Grant K5/2438/1 and K5/2752) is gratefully acknowledged. We also thank the Laboratory for Microscopy and Microanalysis, University of Pretoria, for assistance with the TEM measurements and Wiebke Grote of UP for the XRD measurements.

Appendix A. Supplementary data

Supplementary data to this article can be found online at <https://doi.org/10.1016/j.saa.2018.06.043>.

References

- [1] H.N. Bhargava, P.A. Leonard, Triclosan: applications and safety, *Am. J. Infect. Control* 24 (1996) 209–218.
- [2] R.D. Jones, H.B. Jampani, J.L. Newman, A.S. Lee, Triclosan: a review of effectiveness and safety in health care settings, *Am. J. Infect. Control* 28 (2000) 184–196.
- [3] A. Rossner, S.A. Snyder, D.R. Knappe, Removal of emerging contaminants of concern by alternative adsorbents, *Water Res.* 43 (2009) 3787–3796.
- [4] J. Du Preez, W. Yang, Improving the aqueous solubility of triclosan by solubilization, complexation, and in situ salt formation, *J. Cosmet. Sci.* 54 (2003) 537–550.

- [5] H.-S. Son, G. Ko, K.-D. Zoh, Kinetics and mechanism of photolysis and TiO₂ photocatalysis of triclosan, *J. Hazard. Mater.* 166 (2009) 954–960.
- [6] M. Allmyr, M.S. McLachlan, G. Sandborgh-Englund, M. Adolfsson-Erici, Determination of triclosan as its pentafluorobenzoyl ester in human plasma and milk using electron capture negative ionization mass spectrometry, *Anal. Chem.* 78 (2006) 6542–6546.
- [7] J.-L. Zhao, Q.-Q. Zhang, F. Chen, L. Wang, G.-G. Ying, Y.-S. Liu, B. Yang, L.-J. Zhou, S. Liu, H.-C. Su, Evaluation of triclosan and triclocarban at river basin scale using monitoring and modeling tools: implications for controlling of urban domestic sewage discharge, *Water Res.* 47 (2013) 395–405.
- [8] N. Tatarazako, H. Ishibashi, K. Teshima, K. Kishi, K. Arizono, Effects of triclosan on various aquatic organisms, *Environ. Sci.* 11 (2004) 133–140.
- [9] M. Allmyr, M. Adolfsson-Erici, M.S. McLachlan, G. Sandborgh-Englund, Triclosan in plasma and milk from Swedish nursing mothers and their exposure via personal care products, *Sci. Total Environ.* 372 (2006) 87–93.
- [10] A.M. Calafat, X. Ye, L.-Y. Wong, J.A. Reidy, L.L. Needham, Urinary concentrations of triclosan in the US population: 2003–2004, *Environ. Health Perspect.* 116 (2008) 303–307.
- [11] H.J. Geyer, K.-W. Schramm, E.A. Feicht, A. Behecti, C. Steinberg, R. Brüggemann, H. Poiger, B. Henkelmann, A. Ketttrup, Half-lives of tetra-, penta-, hexa-, hepta-, and octachlorodibenzo-p-dioxin in rats, monkeys, and humans—a critical review, *Chemosphere* 48 (2002) 631–644.
- [12] M.G. Pintado-Herrera, E. González-Mazo, P.A. Lara-Martín, Determining the distribution of triclosan and methyl triclosan in estuarine settings, *Chemosphere* 95 (2014) 478–485.
- [13] M. Moyo, L.R. Florence, J.O. Okonkwo, Improved electro-oxidation of triclosan at nano-zinc oxide-multiwalled carbon nanotube modified glassy carbon electrode, *Sensors Actuators B Chem.* 209 (2015) 898–905.
- [14] Z. Zhang, D. Zhang, X. Zhang, Simultaneous determination of pharmaceutical and personal care products in wastewater by capillary electrophoresis with head-column field-amplified sample stacking, *Anal. Methods* 6 (2014) 7978–7983.
- [15] W.Y. William, E. Chang, R. Drezek, V.L. Colvin, Water-soluble quantum dots for biomedical applications, *Biochem. Biophys. Res. Commun.* 348 (2006) 781–786.
- [16] W. Dong, H.-B. Shen, X.-H. Liu, M.-J. Li, L.-S. Li, CdSe/ZnS quantum dots based fluorescence quenching method for determination of paeonol, *Spectrochim. Acta A Mol. Biomol. Spectrosc.* 78 (2011) 537–542.
- [17] M. Shamsipur, H.R. Rajabi, Pure zinc sulfide quantum dot as highly selective luminescent probe for determination of hazardous cyanide ion, *Mater. Sci. Eng. C* 36 (2014) 139–145.
- [18] H.R. Rajabi, M. Shamsipur, A.A. Khosravi, O. Khani, M.H. Yousefi, Selective spectrofluorimetric determination of sulfide ion using manganese doped ZnS quantum dots as luminescent probe, *Spectrochim. Acta A Mol. Biomol. Spectrosc.* 107 (2013) 256–262.
- [19] D. Cui, B. Pan, H. Zhang, F. Gao, R. Wu, J. Wang, R. He, T. Asahi, Self-assembly of quantum dots and carbon nanotubes for ultrasensitive DNA and antigen detection, *Anal. Chem.* 80 (2008) 7996–8001.
- [20] O. Adegoke, H. Montaseri, S.A. Nsibande, P.B. Forbes, Alloyed quaternary/binary core/shell quantum dot-graphene oxide nanocomposite: preparation, characterization and application as a fluorescence “switch ON” probe for environmental pollutants, *J. Alloys Compd.* 720 (2017) 70–78.
- [21] O. Adegoke, P.B.C. Forbes, L-cysteine-capped core/shell quantum dot– graphene oxide nanocomposite fluorescence probe for polycyclic aromatic hydro-carbon detection, *Talanta* 146 (2016) 780–788.
- [22] Y.-P. Gu, R. Cui, Z.-L. Zhang, Z.-X. Xie, D.-W. Pang, Ultrasmall near-infrared Ag₂Se quantum dots with tunable fluorescence for in vivo imaging, *J. Am. Chem. Soc.* 134 (2011) 79–82.
- [23] W. Kuzyniak, O. Adegoke, K. Sekhosana, S. D’Souza, S.C. Tshangana, B. Hoffmann, E.A. Ermilov, T. Nyokong, M. Höpfner, Synthesis and characterization of quantum dots designed for biomedical use, *Int. J. Pharm.* 466 (2014) 382–389.
- [24] M. Stanisavljevic, S. Krizkova, M. Vaculovicova, R. Kizek, V. Adam, Quantum dots-fluorescence resonance energy transfer-based nanosensors and their application, *Biosens. Bioelectron.* 74 (2015) 562–574.
- [25] K.E. Sapsford, L. Berti, I.L. Medintz, Materials for fluorescence resonance energy transfer analysis: beyond traditional donor–acceptor combinations, *Angew. Chem. Int. Ed.* 45 (2006) 4562–4589.
- [26] H. Xu, R. Miao, Z. Fang, X. Zhong, Quantum dot-based “turn-on” fluorescent probe for detection of zinc and cadmium ions in aqueous media, *Anal. Chim. Acta* 687 (2011) 82–88.
- [27] R. Gao, X. Kong, F. Su, X. He, L. Chen, Y. Zhang, Synthesis and evaluation of molecularly imprinted core-shell carbon nanotubes for the determination of triclosan in environmental water samples, *J. Chromatogr. A* 1217 (2010) 8095–8102.
- [28] H. Du, R.C.A. Fuh, J. Li, L.A. Corkan, J.S. Lindsey, PhotochemCAD: a computer-aided design and research tool in photochemistry, *Photochem. Photobiol.* 68 (1998) 141–142.
- [29] D. Magde, R. Wong, P.G. Seybold, Fluorescence quantum yields and their relation to lifetimes of rhodamine 6G and fluorescein in nine solvents: improved absolute standards for quantum yields, *Photochem. Photobiol.* 75 (2002) 327–334.
- [30] J. Lakowicz, Principles of Fluorescence Spectroscopy, 2nd ed. Kluwer Academic Plenum Press, New York, 1999.
- [31] I. Mekis, D.V. Talapin, A. Kornowski, M. Haase, H. Weller, One-pot synthesis of highly luminescent CdSe/CdS core-shell nanocrystals via organometallic and “greener” chemical approaches, *J. Phys. Chem. B* 107 (2003) 7454–7462.
- [32] W.W. Yu, L. Qu, W. Guo, X. Peng, Experimental determination of the extinction coefficient of CdTe, CdSe, and CdS nanocrystals, *Chem. Mater.* 15 (2003) 2854–2860.
- [33] C. Cheng, H. Yan, Bandgap of the core–shell CdSe/ZnS nanocrystal within the temperature range 300–373 K, *Physica E* 41 (2009) 828–832.

- [34] X. Ai, Q. Xu, M. Jones, Q. Song, S.Y. Ding, R.J. Ellingson, M. Himmel, G. Rumbles, Photophysics of (CdSe)ZnS colloidal quantum dots in an aqueous environment stabilized with amino acids and genetically-modified proteins, *Photochem. Photobiol. Sci.* 6 (2007) 1027–1033.
- [35] P.T. Nga, N.H. Yen, D.H. Cuong, N.N. Hai, N.X. Nghia, V.T.H. Hanh, L.V. Vu, L. Coolen, Study on the fabrication of CdZnSe/ZnSeS ternary alloy quantum dots, *Int. J. Nanotechnol.* 12 (2015) 525–537.
- [36] H.R. Rajabi, F. Karimi, H. Kazemdehdashti, L. Kavoshi, Fast sonochemically assisted synthesis of pure and doped zinc sulfide quantum dots and their applicability in organic dye removal from aqueous media, *J. Photochem. Photobiol. B Biol.* 181 (2018) 98–105.
- [37] H.R. Rajabi, M. Farsi, Study of capping agent effect on the structural, optical and photocatalytic properties of zinc sulfide quantum dots, *Mater. Sci. Semicond. Process.* 48 (2016) 14–22.
- [38] O. Adegoke, M.-W. Seo, T. Kato, S. Kawahito, E.Y. Park, Gradient band gap engineered alloyed quaternary/ternary CdZnSeS/ZnSeS quantum dots: an ultrasensitive fluorescence reporter in a conjugated molecular beacon system for the biosensing of influenza virus RNA, *J. Mater. Chem. B* 4 (2016) 1489–1498.
- [39] H.R. Rajabi, F. Shahrezaei, M. Farsi, Zinc sulfide quantum dots as powerful and efficient nanophotocatalysts for the removal of industrial pollutant, *J. Mater. Sci. Mater. Electron.* 27 (2016) 9297–9305.
- [40] D.K. Gupta, M. Verma, K. Sharma, N.S. Saxena, Synthesis, characterization and optical properties of CdSe/CdS and CdSe/ZnS core-shell nanoparticles, *Indian J. Pure Appl. Phys.* 55 (2017) 113–121.
- [41] M. Koneswaran, R. Narayanaswamy, L-cysteine-capped ZnS quantum dots based fluorescence sensor for Cu²⁺ ion, *Sensors Actuators B Chem.* 139 (2009) 104–109.
- [42] O. Adegoke, T. Nyokong, P.B. Forbes, Photophysical properties of a series of alloyed and non-alloyed water-soluble L-cysteine-capped core quantum dots, *J. Alloys Compd.* 695 (2017) 1354–1361.
- [43] G.S. Dhillon, S. Kaur, R. Pulicharla, S.K. Brar, M. Cledón, M. Verma, R.Y. Surampalli, Triclosan: current status, occurrence, environmental risks and bioaccumulation potential, *Int. J. Environ. Res. Public Health* 12 (2015) 5657–5684.
- [44] SCCS, Opinion on triclosan – antimicrobial resistance, http://ec.europa.eu/health/scientific_committees/consumer_safety/index_en.htm 2010 1–56.
- [45] Toxicological Summary: Triclosan, Retrieved from www.health.state.mn.us/divs/eh/risk/guidance/gw/triclosan.pdf 2010.
- [46] J.-H. Guo, X.-H. Li, X.-L. Cao, Y. Li, X.-Z. Wang, X.-B. Xu, Determination of triclosan, triclocarban and methyl-triclosan in aqueous samples by dispersive liquid–liquid microextraction combined with rapid liquid chromatography, *J. Chromatogr. A* 1216 (2009) 3038–3043.
- [47] D. Kim, J. Han, Y. Choi, On-line solid-phase microextraction of triclosan, bisphenol A, chlorophenols, and selected pharmaceuticals in environmental water samples by high-performance liquid chromatography–ultraviolet detection, *Anal. Bioanal. Chem.* 405 (2013) 377–387.
- [48] J.Y. Shen, M.S. Chang, S.H. Yang, G.J. Wu, Simultaneous determination of triclosan, triclocarban, and transformation products of triclocarban in aqueous samples using solid-phase micro-extraction-HPLC-MS/MS, *J. Sep. Sci.* 35 (2012) 2544–2552.
- [49] B. Li, Z. Qiu, Q. Wan, Y. Liu, N. Yang, β -cyclodextrin functionalized graphene nano platelets for electrochemical determination of triclosan, *Phys. Status Solidi A* 211 (2014) 2773–2777.
- [50] H. Wang, A. Zhang, W. Wang, M. Zhang, H. Liu, X. Wang, Separation and determination of triclosan and bisphenol A in water, beverage, and urine samples by dispersive liquid–liquid microextraction combined with capillary zone electrophoresis–UV detection, *J. AOAC Int.* 96 (2013) 459–465.
- [51] N. Atar, T. Eren, M.L. Yola, S. Wang, A sensitive molecular imprinted surface plasmon resonance nanosensor for selective determination of trace triclosan in wastewater, *Sensors Actuators B Chem.* 216 (2015) 638–644.
- [52] M. Elangovan, R. Day, A. Periasamy, Nanosecond fluorescence resonance energy transfer-fluorescence lifetime imaging microscopy to localize the protein interactions in a single living cell, *J. Microsc.* 205 (2002) 3–14.
- [53] C. Tshangana, T. Nyokong, Photophysical properties gallium octacarboxy phthalocyanines conjugated to CdSe@ ZnS quantum dots, *Spectrochim. Acta A Mol. Biomol. Spectrosc.* 151 (2015) 397–404.

4.1.1 Paper 3 - Supplementary information

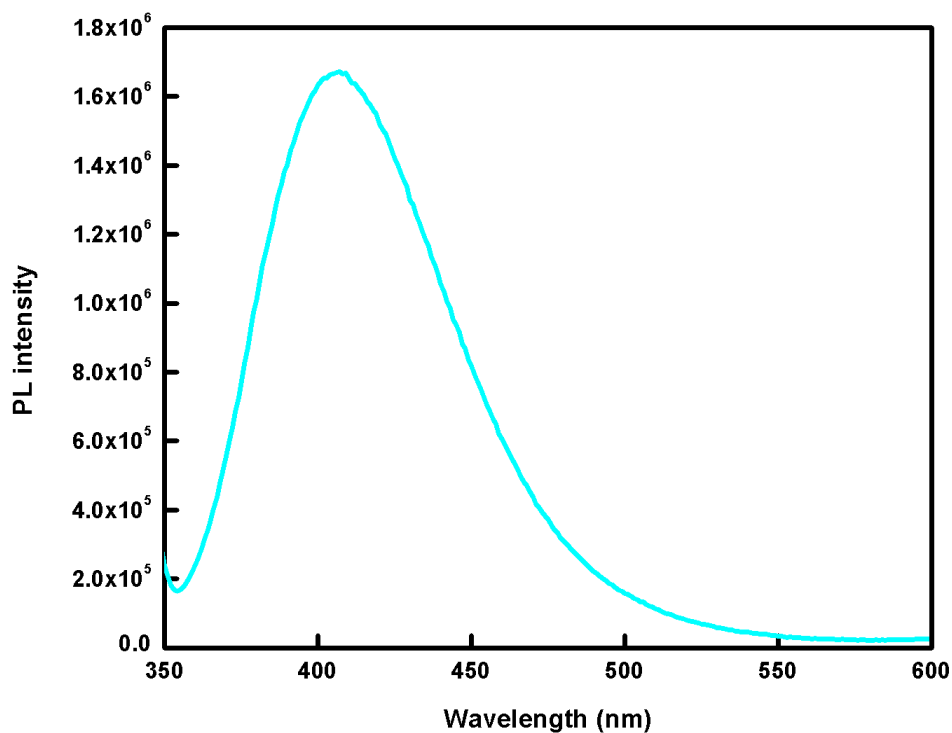


Fig. S1. Fluorescence spectrum of TCS ($1.4 \times 10^{-5} \text{ mol L}^{-1}$) at excitation wavelength 310 nm.

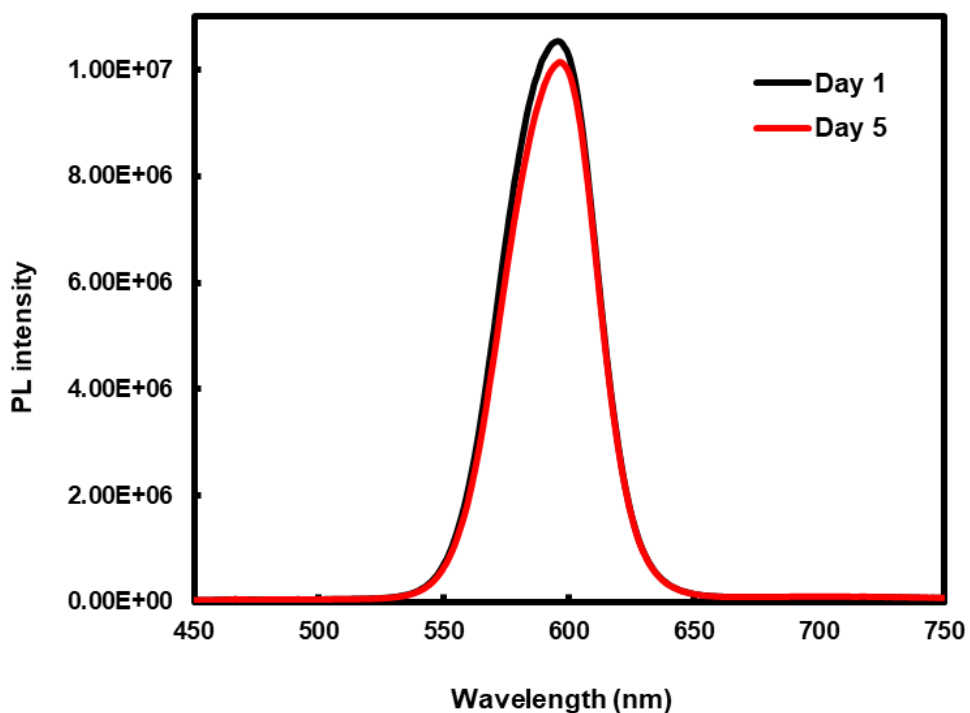
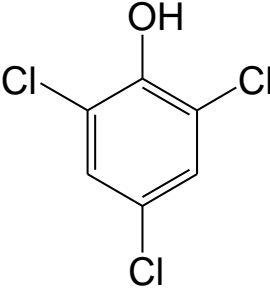
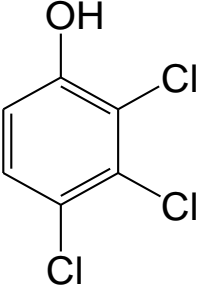
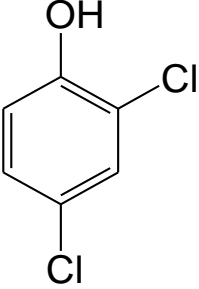
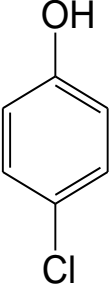


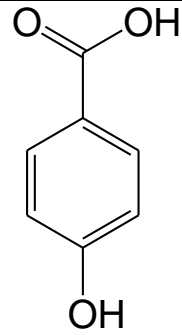
Fig.S2. PL stability of the hydrophilic CdSe/ZnS QDs measured before and after 5 days of exposure to ambient light. The experimental conditions were GSH-CdSe/ZnS QDs 1.5 mg in 3.0 mL Millipore water; excitation wavelength, 300 nm; slit widths of excitation and emission, 5 nm.

Table S1

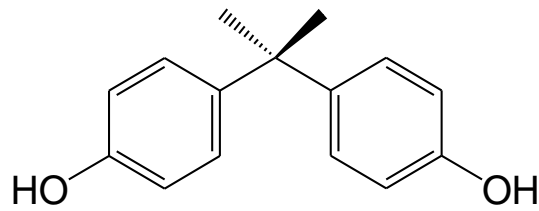
Chemical structures of potentially interfering analytes.

Name	Structure
2,4,6-trichlorophenol (2,4,6-TCP)	
2,3,4-trichlorophenol (2,3,4-TCP)	
2,4-dichlorophenol (2,4-DCP)	
4-chlorophenol (4-CP)	

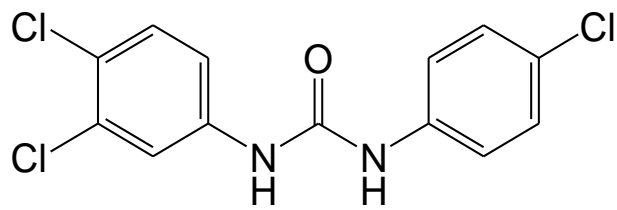
4-hydroxybenzoic acid
(Paraben)



Bisphenol A
(BPA)



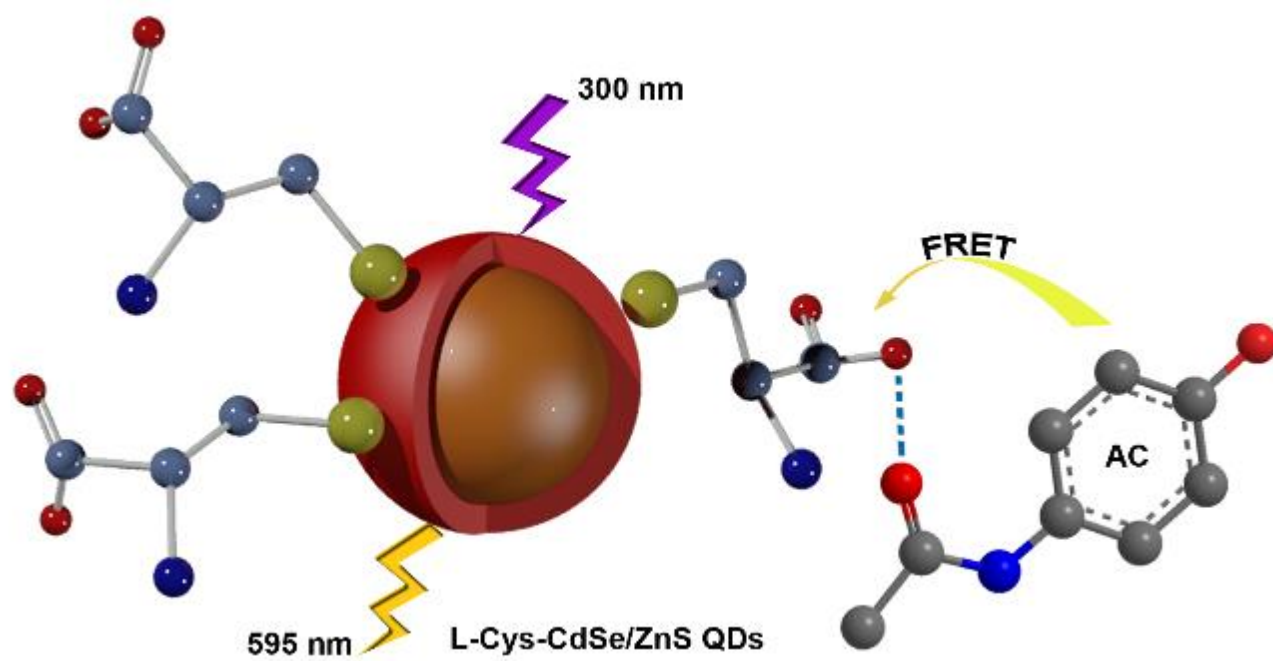
Triclocarban
(TCC)



4.2 Paper 4

This paper was formatted in accordance with the journal *South African Journal of Chemistry* where it has been submitted for review.

Graphical abstract



Development of a thiol-capped core/shell quantum dot sensor for acetaminophen

Hanieh Montaseri, Oluwasesan Adegoke, Patricia B.C. Forbes*

Department of Chemistry, Faculty of Natural and Agricultural Sciences, University of Pretoria, Lynnwood Road, Pretoria 0002, South Africa

ABSTRACT

Acetaminophen (AC) is a frequently used pharmaceutical which has been detected in water systems and is of concern due to its potential environmental impacts. In this study, three quantum dot (QD)-ligand systems, namely L-cysteine (L-cys)-, N-acetyl-L-cysteine (NAC)- and glutathione (GSH)-capped CdSe/ZnS quantum dots, were synthesized and tested for the fluorescence detection of acetaminophen. Among the synthesized aqueous core/shell quantum dots, L-cys-CdSe/ZnS QDs were found to be optimal with high sensitivity for the fluorescence detection of acetaminophen. The L-cys-CdSe/ZnS QDs were of a zinc blende crystal structure and displayed excellent fluorescence intensity and photostability and provided a photoluminescence quantum yield of 77%. The fluorescence of L-cys-CdSe/ZnS QDs was enhanced by the introduction of AC enabling the development of a fast and simple method for the detection of AC. Under optimal conditions, $F-F_0$ was linearly proportional to the concentration of AC from 3.0-100 nmol L⁻¹ with limits of detection and quantification of 1.6 and 5.3 nmol L⁻¹ respectively. Some related pharmaceutical compounds including epinephrine hydrochloride (EP), L-ascorbic acid (AA), uric acid (UA), dopamine hydrochloride (DA) and 4-aminophenol (4-AP) did not interfere with the sensing of AC. The probe was also successfully applied in the determination of AC in tap and river water matrices.

KEYWORDS

Acetaminophen; FRET; Pharmaceuticals; Quantum dots; Fluorescence spectroscopy.

* Corresponding author. Tel.: +27 12 420 5426.
E-mail address: patricia.forbes@up.ac.za (P.B.C. Forbes).

1. Introduction

Acetaminophen or paracetamol (N-acetyl-p-aminophenol, Figure 1) is an acylated aromatic amide with $\log K_{ow}$ 0.46 ¹, which was introduced in 1893 by Von Mering as antipyretic/analgesic medicine. It has a pK_a of 9.46 ² with a solubility of 1.4×10^4 mg L⁻¹ in water at 25 °C ³.

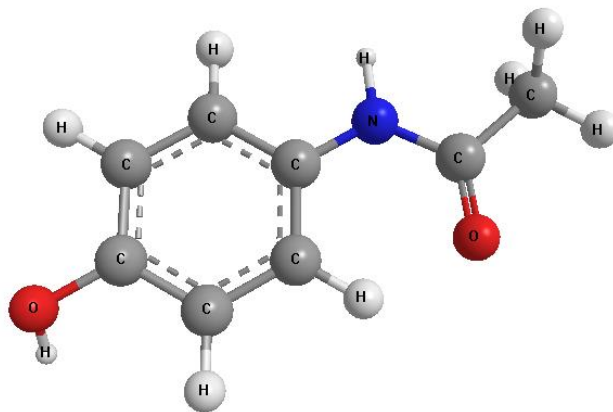


Figure 1 Structure of acetaminophen.

Acetaminophen (AC) is frequently prescribed or purchased over the counter, and falls within the pharmaceuticals and personal care products (PPCPs) a subclass of organic contaminants. Studies have shown that a large volume of pharmaceutical compounds is constantly entering the aquatic environment as well as sewers and drains from hospital waste, improper disposal of pharmaceutical waste, and from healthcare and veterinary facilities ⁴. In spite of the fact that the detected concentrations thereof are low, a wide variety of potential deleterious effects, including acute and chronic toxicity on the aquatic environment ⁵ and accumulation in tissues ⁶ have been reported even at these low levels.

In order to avoid adverse effects of PPCPs to humans, fast and sensitive analytical methods are needed for detecting low concentrations of PPCPs in water systems.

At present, detection of PPCPs is carried out under laboratory conditions utilizing highly expensive instruments, trained personnel, environmentally unfriendly solvent use and long analysis times. Techniques include high performance liquid chromatography ⁷, electrochemical analysis ⁸, spectrophotometry ⁹ and chemiluminescence ¹⁰. To circumvent these issues, simple analytical methods are being developed to detect low concentrations of AC. Among them, optical measurement methods have gained attention due to advantages including high sensitivity, ease of implementation, and generally fast response times ¹¹. Fluorescence techniques are a popular subset of optical methods, which use a fluorophore material as a sensing receptor to detect the analyte(s). Examples of fluorophore nanomaterials are carbon nanoparticles (CNPs), graphene quantum dots (QDs) and semiconductor QDs of the class of group II-VI and III-V ¹².

QDs are comprised of a semiconductor core and a shell which protects them against oxidation and photodegradation. In addition, QDs are photo electrochemically active which make them reliable optical labels in environmental analysis ¹³.

QD-based sensing applications are due to Förster resonance energy transfer (FRET) where QDs serve as donor, and reports of their application as acceptor are less common. The photoluminescence (PL) “turn-on” mode is more desirable compared to the “turn-off” mode, as many other factors can also induce the PL “off” state resulting in false positives ¹⁴.

It has been previously shown that high lattice mismatch (~16%) between ZnS and CdTe may cause incomplete coating of the core QDs with ZnS which makes the QDs susceptible to degradation ¹⁵. Lower lattice mismatch (~12%) for CdSe and ZnS however, results in less degradation ¹⁶. Therefore CdSe/ZnS QDs are more stable and less toxic than CdTe/ZnS QDs. Moreover, CdSe/ZnS QDs have exhibited the least cytotoxicity and the most biocompatibility with high sensing ability among CdSe, CdSe/ZnS and CdSe/CdS QDs ¹⁷.

Core/shell QDs have a number of advantageous properties regarding their use as analytical sensors and they have found many applications across disciplines ^{18, 19}.

Acetaminophen is being continuously introduced into the environment which can cause detrimental impacts on human, animals and aquatic environment. Moreover, the acute and chronic toxicity of AC to the aquatic environment may lead to unpredicted long-term toxic effects even at low concentrations. Even though AC has been detected by several analytical techniques, there is still a lack of a reliable, fast and cost effective screening method for this analyte. Herein, three QD-thiol ligand combinations were synthesized and their sensitivity towards AC detection was examined in order to find the optimum QD-ligand system. We then describe a simple turn-on fluorescence detection approach for AC sensing based on L-cys-CdSe/ZnS QDs as these provided the highest sensitivity. Although many studies have been published regarding the application of CdSe/ZnS QDs, there is no study to date regarding their use in the determination of AC in environmental water samples.

2. Experimental procedures

2.1. Materials

Cadmium oxide (99.5%), octadec-1-ene (ODE, 90%), L-cysteine (L-cys, 96%), sulfur powder ($\geq 99.5\%$), trioctylphosphine oxide (TOPO, 90%), zinc oxide (99%), oleic acid (OA, 90%), N-acetyl-L-cysteine (NAC, $\geq 99\%$) and acetaminophen (AC, analytical standard) were purchased from Sigma Aldrich (St. Louis, MO, USA). Epinephrine hydrochloride (EP, 95%), L-ascorbic acid (AA, reagent grade), dopamine hydrochloride (DA, $\geq 98\%$), and uric acid (UA, $\geq 99\%$) and 4-aminophenol (4-AP, 99.9%) as potential interfering analytes were also purchased from Sigma Aldrich. Methanol (99.5%), acetone (99.5%), sulfuric acid (98%),

potassium hydroxide (85%), chloroform (99%), glutathione (GSH, $\geq 98\%$) and selenium powder (99%) were purchased from Merck (Darmstadt, Germany). Water was provided by an ultrapure Milli-Q Water System (18.0 M Ω .cm at 25 °C).

2.2. Instrumentation

A Horiba Jobin Yvon Fluoromax-4 spectrofluorometer was employed to record fluorescence emission spectra and UV–vis absorption spectra were taken using a Cary Eclipse (Varian) spectrophotometer.

The PL quantum yields of the QDs in Millipore water were determined as previously reported ²⁰. A PANalytical X'Pert Pro powder diffractometer in θ - θ configuration with a X'Celerator detector, variable divergence and receiving slits with Fe filtered Co-K α radiation ($\lambda=1.789\text{\AA}$) was used to analyze powder X-ray diffraction (XRD) patterns. IR measurements were obtained from a Spectrum RXI FT-IR System from Perkin Elmer. Transmission electron microscopy (TEM) images were recorded using a JEOL JEM 2100F operated at 200 kV. The particle size distributions of QDs were estimated using ImageJ software (<http://imagej.nih.gov/ij/>, U.S. National Institutes of Health [NIH], Bethesda, Maryland, USA). Raman spectra were recorded using a WITec Alpha 300 micro-Raman imaging system with 488 nm excitation laser and CCD detector at room temperature with laser power below 2 mW in order to minimize heating effects. All pH measurements were made with a Metrohm 780 pH-meter that was calibrated with Accsen standards of pH 4.0 and 7.0. Energy dispersive X ray spectroscopy (EDS) analysis was carried out using a HRSEM integrated EDS Zeiss Crossbeam 540 with software AZtech version 3 by Oxford Instruments. PhotochemCAD was used to compute the Förster distance ²¹.

2.3. Fabrication of water-soluble CdSe/ZnS core/shell QDs

A one pot organometallic approach was utilized for the preparation of the CdSe/ZnS core/shell QDs which has previously been reported by our group ²⁰. Conversion of hydrophobic QDs to water-soluble QDs was then carried out by a ligand exchange reaction. A stock solution of thiol ligand–KOH in 40 mL methanol was prepared using 2 g of thiol ligand (L-cys, GSH or NAC) and 3.0 g of KOH with ultrasonication. After purification, the hydrophobic capped CdSe and CdSe/ZnS QDs were re-dispersed separately in chloroform and the ligand exchange solution was added followed by Millipore water. In order to separate the organic phase from the aqueous phase, the solutions were stirred for 1 h. The water-soluble CdSe and CdSe/ZnS QDs were then purified using ethanol and acetone to efficiently remove all hydrophobic capping substituents. The purified water soluble QDs were finally dried in a fume hood.

2.4. Fluorescence experiments

1.0 mg of water-soluble CdSe/ZnS QDs was dissolved in 3 mL Millipore water and a standard solution containing a specific amount of AC was added and after 5 min the resulting PL spectrum was determined. The same conditions were applied for all PL measurements: 5 nm slit width was chosen for the excitation and emission of the spectrofluorometer with a 300 nm excitation wavelength. An AC stock solution ($1.4 \times 10^{-3} \text{ mol L}^{-1}$) was prepared by dissolution of the solid in Millipore water and was diluted to prepare standard solutions. Sensing was carried out as follows: 2 mL of QDs solution was placed in a quartz cuvette followed by addition of 500 μL of AC standard solution. The PL intensity was taken after 5 min as F and F_0 was PL intensity of QDs in 500 μL of water. A series of $F-F_0$ values were obtained by varying the AC concentration.

Real water samples for fluorescence measurements were collected in pre-cleaned glass bottles from a river and municipal tap in Pretoria, South Africa and were transported to the laboratory in a cooler box filled with icepacks. The water samples were centrifuged at 4500 rpm for 5 min and filtered using 110 mm pore size filter paper prior to analysis.

3. Result and discussion

3.1. Comparison of PL intensity of L-cys-CdSe/ZnS, NAC-CdSe/ZnS and GSH-CdSe/ZnS QDs

The synthesized CdSe/ZnS QDs capped with three different capping agents, L-cys, NAC and GSH respectively, were utilized to investigate the optimum QD-ligand system for the determination of AC. The relative fluorescence intensity of the QD-ligand combinations was measured by the amount of enhancement observed for 5.0 nmol L^{-1} of AC relative to the fluorescence signal of the QDs in the presence of Millipore water. It was observed that the NAC-capped CdSe/ZnS QDs provided the lowest sensitivity while the fluorescence intensities of the L-cys and GSH-CdSe/ZnS QDs were easily influenced by the addition of AC and showed greater sensitivity (Figure 2). There was a 23% increase in the relative PL intensity of the L-cys-capped core/shell QDs while only an increase of 2% was found for the NAC-capped QDs and 21% for the GSH-capped QDs. In contrast, GSH-CdSe/ZnS QDs were previously found to provide sensitive detection of triclosan by our group²⁰. In this case, L-cys-CdSe/ZnS QDs provided the most sensitivity and were thus chosen as a fluorescent sensor for the determination of AC and all subsequent characterizations and experiments were performed on L-cys-CdSe/ZnS core/shell QDs.

In a previous study²⁰, the Förster distance was found to be 4.0 nm for the system of GSH-CdSe/ZnS QDs-TCS while this distance in the case of L-Cys- and NAC-CdSe/ZnS QDs for TCS was 7.9 nm and 7.8 nm, respectively. Therefore, GSH-CdSe/ZnS QDs provided higher

sensitivity with better energy transfer. In this study, the calculated Förster distance for both L-cys- and NAC-CdSe/ZnS QDs for AC target molecules were 6.1 nm (the Förster distance of L-cys-CdSe/ZnS QDs-AC system is discussed in Section 3.11). It was therefore concluded that the lower sensitivity of NAC-CdSe/ZnS QDs arose most likely from the structure of NAC which could not efficiently H-bond to AC molecules relative to L-cys for which three H-bonds are possible.

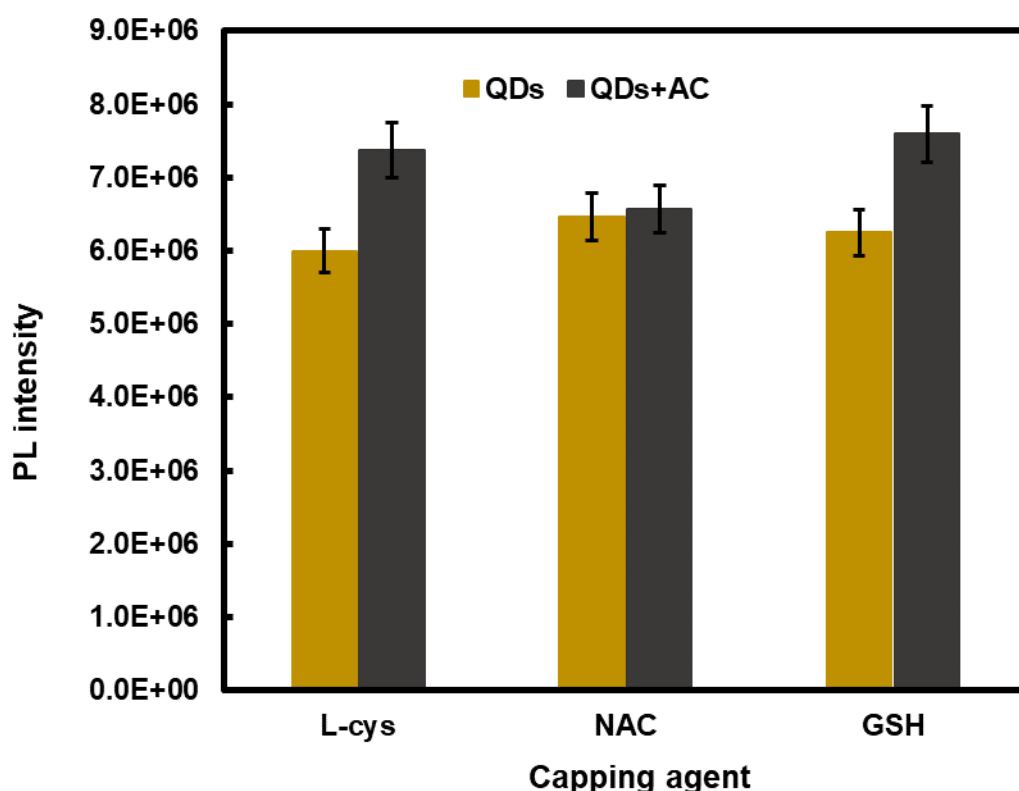


Figure 2 Comparison of the sensitivity of three QD-ligand systems (L-cys-CdSe/ZnS, NAC-CdSe/ZnS and GSH-CdSe/ZnS QDs) towards 5.0 nmol L⁻¹ of AC.

3.2. Optical characterization of aqueous L-cys-CdSe and L-cys-CdSe/ZnS QDs

An overlay of the emission and absorption spectra of core and core/shell QDs is shown in Fig. S1, where a characteristic broad absorption and narrow emission peak are evident. Table 1 compares the optical parameters of the water-soluble core and core-shell QDs.

Surface passivation with the ZnS shell increased the size of the core-shell QDs, as evident from the red shift. Stokes shift is one of the most important parameters of semiconductor QDs for the elucidation of their optical properties which is known as the red shift of the emission spectra in respect of the absorption spectra²². Accordingly, the Stokes shift of L-cys-CdSe and L-cys-CdSe/ZnS QDs were determined to be 30 nm and 15 nm, respectively. The significant fluorescence enhancement of CdSe/ZnS QDs is a result of the influence of the larger band gap induced by the ZnS shell which efficiently traps the electrons in the core, and

also due to the removal of dangling surface bonds in the QD core upon addition of the shell²³.

The extinction coefficient of L-cys-CdSe and L-cys-CdSe/ZnS QDs were calculated according to a published method²⁴. The concentrations of L-cys-CdSe and L-cys-CdSe/ZnS QDs in Millipore water can be therefore calculated from the Beer-Lambert law.

The calculated emission band gap values for the synthesized QDs were calculated to be 2.18 and 2.09 nm for L-cys-CdSe and L-cys-CdSe/ZnS QDs, respectively. The PLQY of core/shell QDs increased dramatically due to the passivation of surface vacancies and non-radiative recombination sites after coating with the ZnS shell²⁵. A red shift of 26 nm was observed in the PL emission of L-cys-CdSe/ZnS QDs in comparison to the L-cys-CdSe core at the optimum excitation wavelengths, which is due to the formation of the shell layer. The strong PL band with narrow FWHM of L-cys-CdSe/ZnS QDs provides evidence for the formation of a uniform particle distribution¹⁷.

Table 1 Optical characterization values of the water-soluble L-cys-CdSe and L-cys-CdSe/ZnS QDs.

QDs	Excitonic peak (nm)	PL peak (nm)	Extinction coefficient (L mol ⁻¹ cm ⁻¹)	PLQY (%)	Stokes shift (nm)	FWHM (nm)	Calculated band gap energy value (eV)
L-cys-CdSe QDs	460 (shoulder) 539	569	9.3×10 ⁴	5.4	30	40.0	2.18
L-cys-CdSe/ZnS QDs	580	595	2.04×10 ⁵	77	15	38.5	2.09

3.3. Structural and composition characterization of L-cys-capped core/shell QDs

EDS analysis was performed to prove the presence of the metal components in the structure of the L-cys-CdSe and L-cys-CdSe/ZnS QDs (Fig. S2). The signals of Cd and Se were found in the core while the presence of Zn and S in the core/shell QDs confirmed the addition of the ZnS shell on the core. The elemental composition for L-cys-CdSe and L-cys-CdSe/ZnS QDs are compared in Table S1. In the EDS spectra additional C, N and O signals arose from the capping ligand L-cys. For these core QDs, the capping agent also resulted in a S signal.

The X-ray diffraction patterns of L-cys-CdSe and L-cys-CdSe/ZnS QDs were compared. Fig. S3 indicates a typical zinc blende crystal structure with planes at {111}; 2θ=31.56, {220}; 2θ=52.71 and {311}; 2θ= 62.74 for CdSe/ZnS QDs. The peaks for CdSe QDs were at 29.57°, 49.18° and 58.44° corresponding to {111}, {220} and {311} according to the standard JCPDS (Card No.19-0191) of bulk cubic CdSe. The diffraction peaks for the CdSe/ZnS QDs were

shifted slightly to higher Bragg angles compared to the CdSe core. The broadening of the diffraction peak can also be attributed to the nano-sized dimensions of the nanocrystals²⁶. The zinc blende crystal structure was still predominant for CdSe QDs but with weaker diffraction peaks compared to CdSe/ZnS QDs.

FT-IR analysis allowed for the characterization of the functional groups on the surface of the QDs (Figure 3). Functional groups and IR absorption bands of L-cys-CdSe and L-cys-CdSe/ZnS QDs are summarized in Table S2. Carboxylic acid and amino groups were found on the surface of the L-cys capped CdSe/ZnS and CdSe QDs while the S-H group vibration was absent on the surface of the QDs, which is attributed to the formation of ZnS onto the surface of the core, and core/shell QDs.

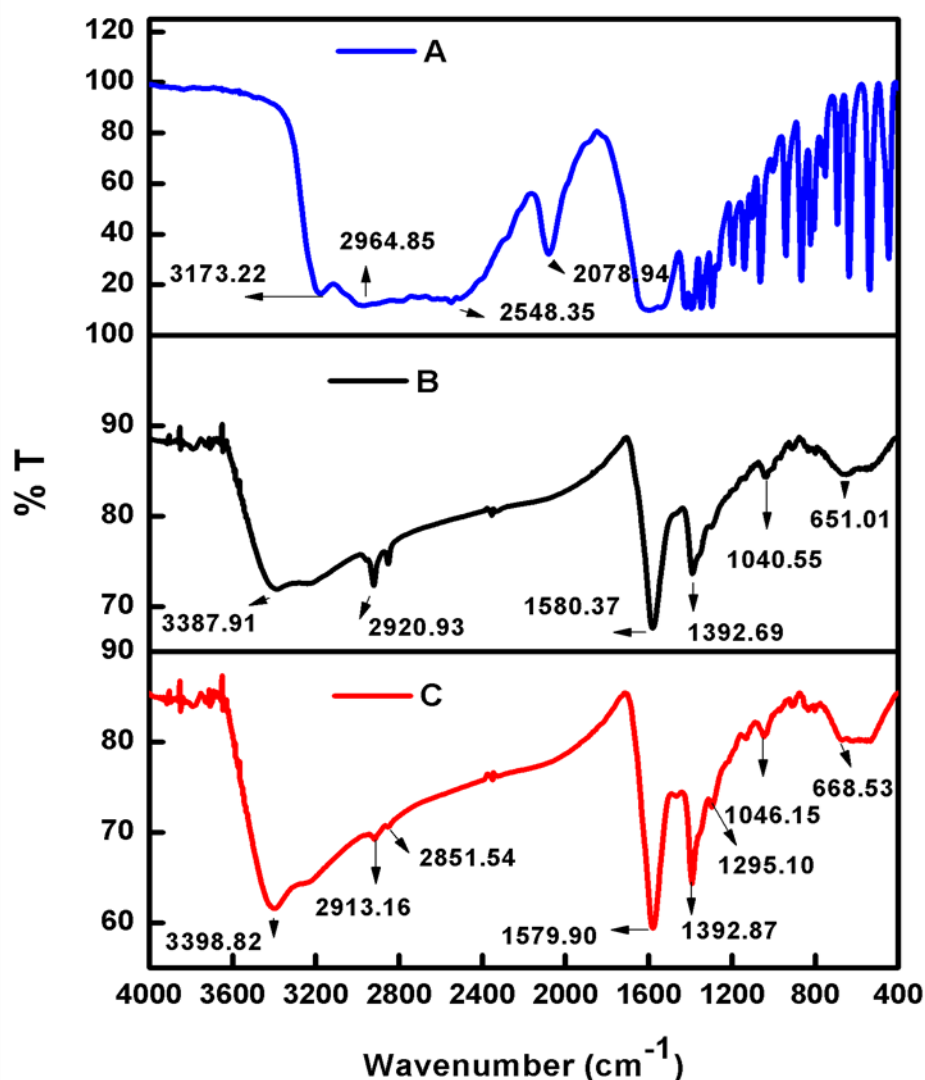


Figure 3 The FT-IR spectra of (A) L-cys, (B) L-cys-CdSe QDs and (C) L-cys-CdSe/ZnS QDs.

3.4. Raman analysis

The Raman spectra of L-cys CdSe and L-cys-CdSe/ZnS QDs are shown in Fig. S4. Generally, nanomaterials with small dimensions from group II-VI show broad spectra. The Raman lines of the CdSe core illustrate longitudinal optical LO and 2LO phonons in the region of 200 cm^{-1} and 400 cm^{-1} respectively while a weaker mode of the second order transverse acoustic (TA) appeared at around 103 cm^{-1} ²⁷. This multi phonon scattering in semiconductor QDs is characteristic of the resonantly excited Raman processes ²⁸. The Raman lines of LO and 2LO phonons in CdSe/ZnS QDs are located at around 190.5 cm^{-1} and 577 cm^{-1} respectively. Moreover, the LO line of the ZnS shell was observed at about 300 cm^{-1} . The D-band at 1350 cm^{-1} confirms the presence of disorder in sp^2 -hybridized carbon systems and the G-band (1580 cm^{-1}) arises from the stretching of the C-C bond of all pairs of sp^2 -hybridized carbon atoms in both the rings and chains ²⁹ which are evidence of the presence of L-cys.

3.5. Comparison of particle size of the water-soluble L-cys-CdSe/ZnS QDs

The particle size of L-cys-capped core and core/shell QDs were estimated by using three approaches including first excitonic absorption peak, XRD and HRTEM (Table 2).

The particle size of the L-cys-CdSe and L-cys-CdSe/ZnS QDs determined from the first excitonic absorption peak using a published method ²⁴ and the average crystallite size of the L-cys-CdSe and L-cys-CdSe/ZnS QDs were estimated from the Debye Scherrer's equation ³⁰. The average particle size of the core/shell QDs shows that each particle of the synthesized L-cys-CdSe/ZnS QDs consists of 2 or more individual crystallites.

In addition, the average particle size distributions \pm standard deviation of the QDs were estimated to be 2.1 ± 0.5 and 5.1 ± 0.8 nm for L-cys-CdSe and L-cys-CdSe/ZnS QDs, respectively from the TEM micrographs, which were in agreement with the sizes estimated from the first excitonic absorption peak. As an indirect approach ³¹ the shell thickness of ZnS was calculated to be 1.5 nm. The morphological display of the QDs showed that they were nearly homogenous in nature, monodispersed and also spherical in shape (Figure 4 A and B). HRTEM also showed narrow particle size distributions for L-cys-CdSe and L-cys-CdSe/ZnS QDs with a standard deviations below 1% (Figure 4 A1-B1).

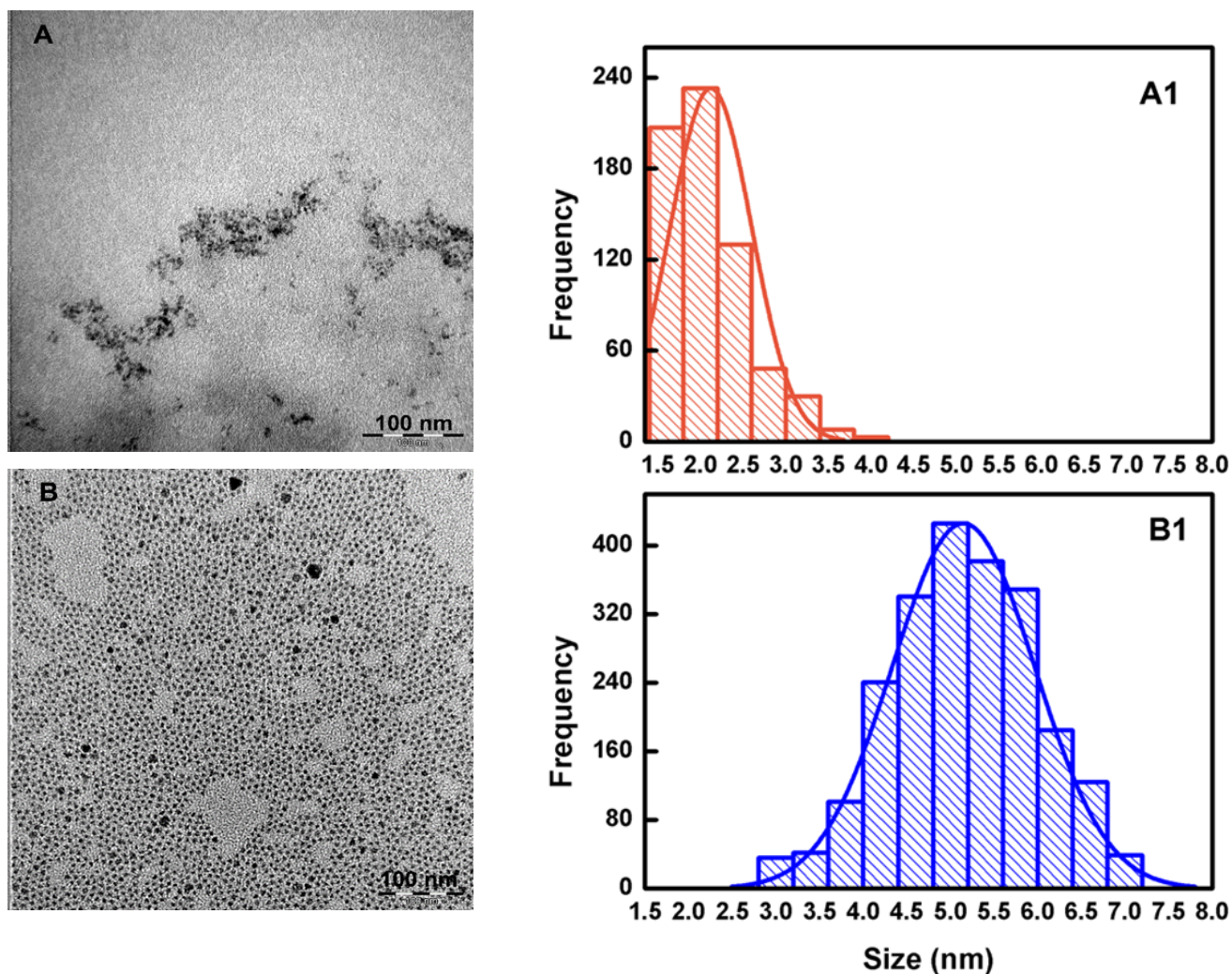


Figure 4 TEM images of (A) L-cys-CdSe QDs and (B) L-cys-CdSe/ZnS QDs, scale bar 100 nm; and (A1) particle size distribution of L-cys-CdSe QDs and (B1) L-cys-CdSe/ZnS QDs.

Table 2 Comparison of the particle size of L-cys-CdSe and L-cys-CdSe/ZnS QDs.

Method	L-cys-CdSe QDs (nm)	L-cys-CdSe/ZnS QDs (nm)
First excitonic peak	2.8	4.0
XRD	3.00	3.03
HRTEM	2.1±0.5	5.1±0.8

3.6. Fluorescence properties of AC

The possible influence of AC on the PL spectrum of L-cys-CdSe/ZnS QDs was evaluated by recording its PL using different excitation wavelengths as AC itself fluoresces. The highest emission intensity was around 400 nm at the excitation wavelength of 300 nm (Fig. S5). FRET is therefore a possible mechanism for the fluorescence enhancement noted upon interaction

of AC with the QDs, because there are overlapping bands between the absorption spectrum of the QDs and the emission spectrum of AC in the range 350-650 nm.

3.7. Investigation of photostability

The fluorescence intensity of L-cys-CdSe/ZnS QDs in Millipore water increased over time and became stable after 24 hrs. No major changes in the fluorescence intensity of 1.0 mg/3.0 mL QD solutions were noted even after storage for 5 days in solution under ambient light conditions (Fig. S6) although the band gap of the L-cys-CdSe/ZnS QDs decreased which can be seen from the red shift in the PL emission of the QDs. Aggregation can induce such a red shift in the QD fluorescence which would also be accompanied by PL quenching although quenching in fluorescence intensity may also be attributed to the inability of the thiol ligand to suppress the electron much deeper into the interior of the QDs. The slight decrease in fluorescence intensity between day 1 to day 5 may also be due to desorption of L-cys from the surface of CdSe/ZnS QDs, as L-cys acts as a surface passivating agent, which eliminates surface defects ³². Subsequent analytical measurements were thus performed after the fluorescence intensity of QDs had become stable after one day.

3.8. Optimization of aqueous L-cys-CdSe/ZnS QD concentration and incubation time

Taking into consideration that the concentration of QDs can influence the fluorescence intensity, different concentrations of L-cys-CdSe/ZnS QDs (1.0, 1.5, 2.0, 2.5, and 3.0 mg in 3.0 mL water) were prepared and 5.0 nmol L⁻¹ of AC was added to each. Briefly, 500 µL of a fixed concentration of AC was added to 2 mL of each concentration of QDs and the fluorescence intensity was recorded after 5 min. It was observed that the sensitivity reduced at high concentrations of water-soluble L-cys-CdSe/ZnS QDs likely due to self-quenching or agglomeration effects, whereas very low concentrations of QDs led to a narrowing of the linear range. The optimum concentration of 1.0 mg of L-cys-CdSe/ZnS QDs in 3.0 mL water was found, indicating an increase in the interaction of AC with QDs in solution (Figure 5).

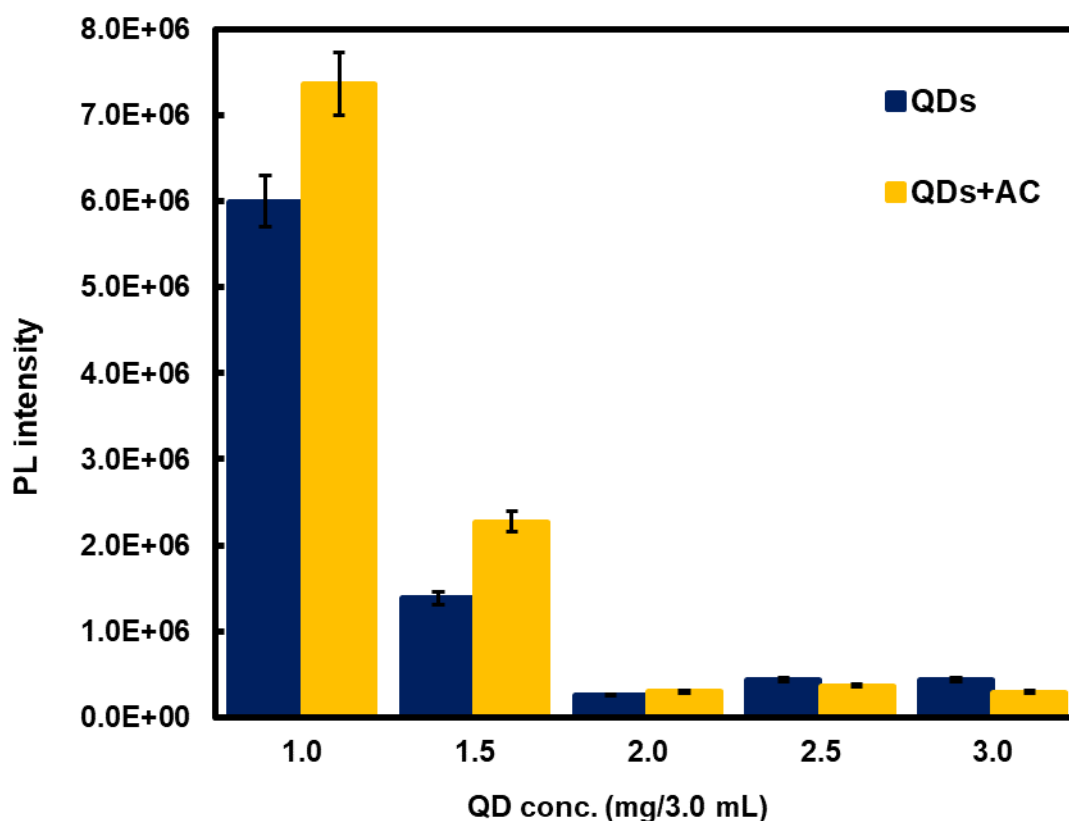


Figure 5 Effect of the concentration of aqueous L-cys-CdSe/ZnS QDs on fluorescence in the absence and presence of 5.0 nmol L⁻¹ AC at excitation wavelength 300 nm (values are the average of three measurements).

In order to determine the optimum interaction time of L-cys-CdSe/ZnS QDs with AC, the fluorescence intensity of the system was examined at different time intervals in the presence of 5.0 nmol L⁻¹ AC (Fig. S7). The data obtained showed the highest fluorescence enhancement after 5 min incubation time and thereafter a quenching effect of the PL intensity of the QDs was observed after 10 min, indicating a potential reversible interaction. The results show that although AC can be detected within 5 to 35 min of incubation time, a shorter incubation time is more effective.

3.9. Influence of AC on the fluorescence behavior of L-cys-CdSe/ZnS QDs

Under optimal conditions (i.e. 1.0 mg/3.0 mL of L-cys-CdSe/ZnS QDs and 5 min as incubation time), the introduction of acetaminophen to the L-cys-CdSe/ZnS QDs solution led to luminescence enhancement (Figure 6A). This signal enhancement could be due to FRET from analyte which served as donor to QDs. The emission of the acceptor enhances and simultaneously the luminescence of the donor quenches. In this case, due to the weak fluorescence intensity of the AC, the quenching of AC fluorescence could not be seen in Figure 6A.

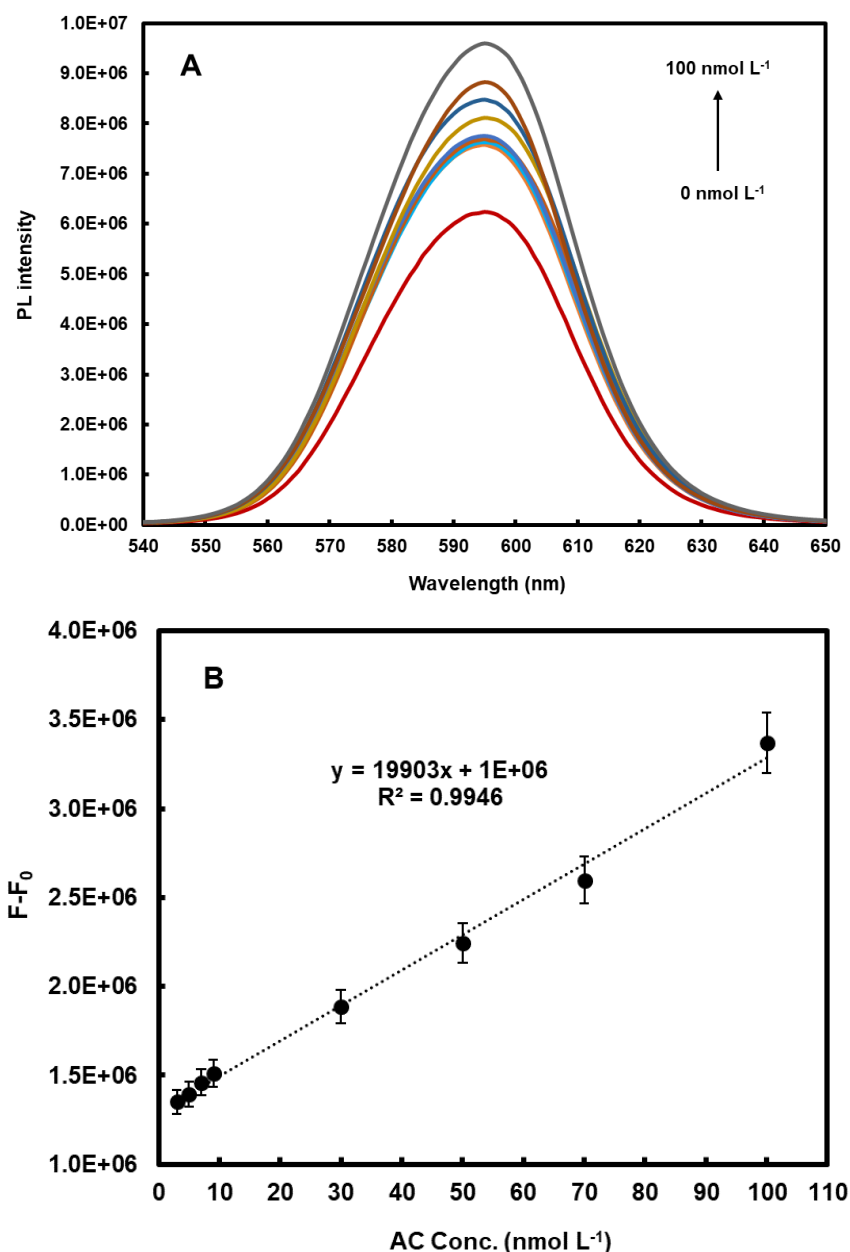


Figure 6 (A) PL “turn-on” emission spectra for the determination of AC using L-cys-CdSe/ZnS QDs for different concentrations of AC at an excitation wavelength of 300 nm and (B) linear graph of $F-F_0$, versus AC concentration (values are the average of three measurements).

3.10. Analytical figures of merit

The fluorescence calibration curve of $F-F_0$ versus AC concentration is illustrated in Figure 6B, where F_0 and F are the fluorescence intensities of the QDs in the presence and absence of different concentrations of acetaminophen, respectively. A good linear relationship between $F-F_0$ and $[AC]$ was found from 3.0-100 nmol L⁻¹ at an emission wavelength of 595 nm ($r^2 = 0.99$). Thus, AC can be sensed fluorescently using this method.

The limit of detection (LOD) and quantification (LOQ) are defined as $3\delta/m$ and $10\delta/m$, respectively where δ is the standard deviation of blank measurement (with $n=10$) and m is the slope of the calibration curve. LOD and LOQ were found to be 1.6 nmol L⁻¹ and 5.3 nmol L⁻¹,

respectively. The data thus revealed that the proposed method is suitable for the determination of AC at environmentally relevant levels. The LOD value is lower than the guidance value of 1.3×10^3 nmol L⁻¹ (or 200 ppb) for acetaminophen in drinking water given by the Department of Health in Minnesota ³³.

The linear range and detection limit of some other methods for the detection of AC in water samples are summarized in Table 3 for comparison purposes. The results indicate the potential of our sensor for detecting the low concentrations of AC typically present in water samples.

Table 3 Comparison of some published analytical methods for the determination of AC in water.

Detection method	Linear range (nmol L ⁻¹)	Detection limit (nmol L ⁻¹)	Quantification limit (nmol L ⁻¹)	Recovery (%)	Sample matrix	Reference
Biocatalytic spectrophotometry	2,000-1,4000	550	8,300	88-112	Commercial potable bottled water, tap water and treated wastewater effluent	9
CNTPE/surfactant system	1,5000-180,000 (DPV)	290 (DPV)	960 (DPV)	98-103	Tap and domestic wastewater	34
	1,5000-120,000 (SWV)	4,400 (SWV)	14,800 (SWV)			
LC-MS/MS	<LOQ-0.23	0.01	0.06	NR	Surface water	35
SPE/CZE-DAD	6.6-97.0	3.04	NR	51-64	Influent wastewater	36
	3.4-11.0				Effluent wastewater	
Fluorescence using L-cys-CdSe/ZnS QDs	3.0-100	1.6	5.3	90-108	Tap and river water	This work

CNTPE, Carbon nanotubes paste electrode; DPV, Differential pulse voltammetry; LC-MS/MS, Liquid chromatography/tandem mass spectrometry; NR, Not reported; SPE/CZE-DAD, Solid phase extraction/capillary zone electrophoresis diode array detector; SWV, Square wave voltammetry.

3.11. Proposed mechanism

In theory, Förster resonance energy transfer (FRET) is a non-radiative process and if the emission spectra of target compounds overlap with the absorption spectra of the QDs, energy transfer from the analyte to the QDs could occur upon excitation ³⁷. In this study, the absorption spectrum of L-cys-CdSe/ZnS QDs at 430-650 nm (the highest absorbance is at 580 nm) (Figure 7A) overlaps with the emission spectrum of acetaminophen at 350-650 nm (Figure

7B). Hence the QDs can absorb the emission energy from acetaminophen resulting in the enhancement of the PL emission of QDs, which was also found experimentally.

Scheme 1 shows the enhancement mechanism of the QDs in the presence of the AC via FRET. The electrons of AC can absorb energy resulting in an excited state. When the excited electron of AC returns to the ground state, the electrons of the QDs can transit to the excited states due to the polar-polar resonance of the donor acceptor. The coupled transitions result in quenching of the fluorescence of donor (AC molecules) and enhancement in fluorescence intensity of the acceptor (L-cys-CdSe/ZnS QDs) ³⁸.

The distance between donor and acceptor is also a critical parameter of FRET processes since FRET depends on the donor quantum yield and will occur over a limited distance (Förster distance (Å)) when the overlap between the emission spectrum of the donor and the absorption spectrum of the acceptor is greater than 30% and the distance is less than 10 nm ³⁹. The Förster distance in the L-cys-CdSe/ZnS QDs-AC system was found to be 6.1 nm which meets this distance requirement for FRET to occur.

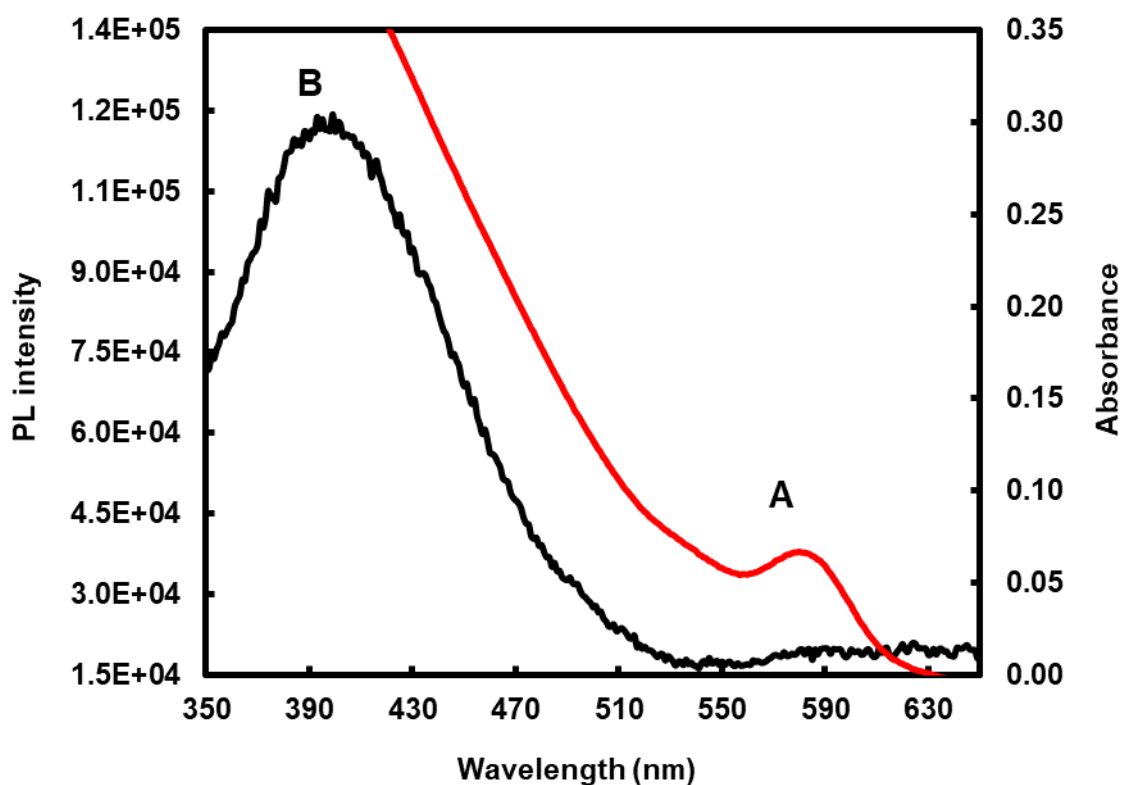
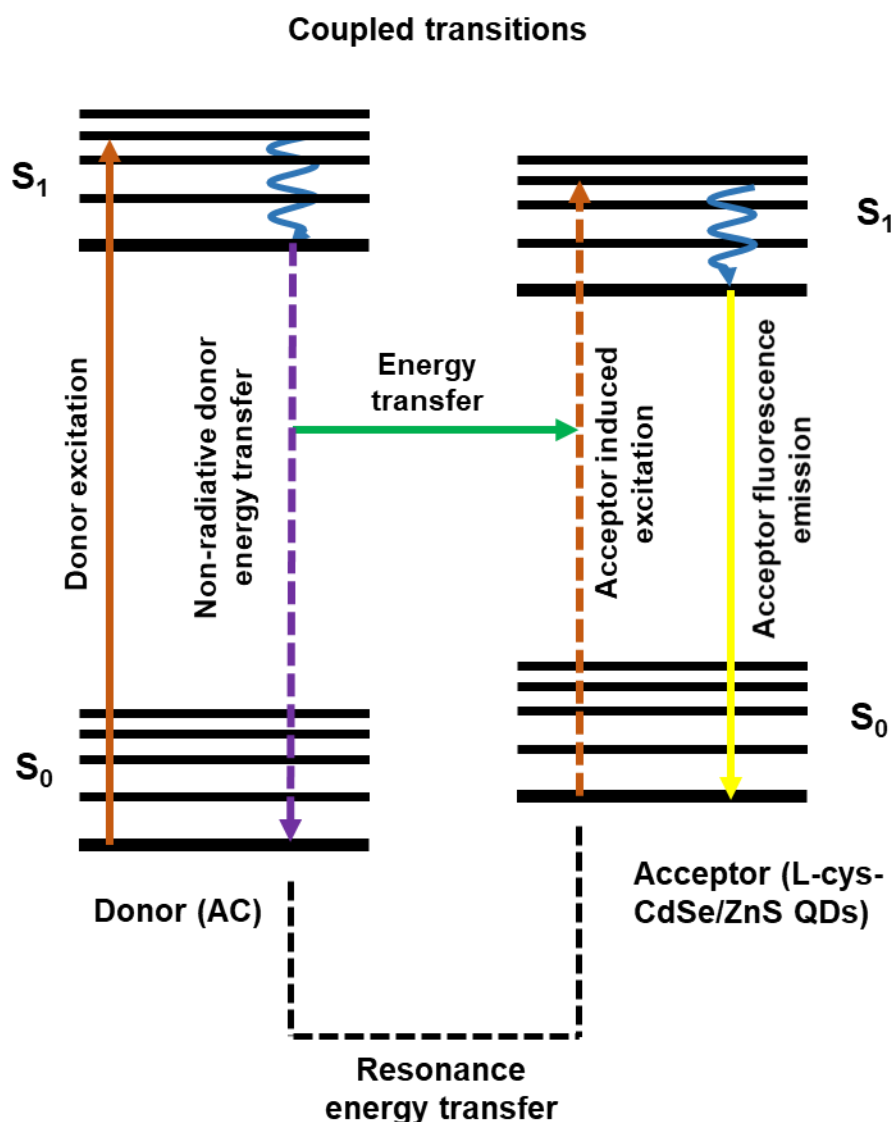


Figure 7 UV-Vis absorption spectrum of (A) L-cys-CdSe/ZnS QDs and (B) fluorescence spectrum of acetaminophen (1.0×10^{-5} mol L⁻¹) at excitation wavelength 300 nm.



Scheme 1. Fluorescence resonance energy transfer from AC to the L-cys-CdSe/ZnS QDs.

3.12. Effect of potential interfering analytes on the fluorescence of L-cys-CdSe/ZnS QDs

The possible influence of other related pharmaceutical analytes was assessed under optimum conditions of 2 mL of 1.0 mg/3.0 mL L-cys-CdSe/ZnS QDs and 5 min equilibrium time. Although the photoluminescence intensity of the L-cys-CdSe/ZnS QDs was slightly enhanced in the presence of these pharmaceutical analytes (Figure 8), it is clear that the prototype QD probe is the most sensitive to AC which provided the highest relative fluorescence intensity whereas the other analytes investigated did not produce as significant a fluorescence enhancement with the QDs (Table S3). These compounds therefore do not interfere significantly with the detection of AC. The selectivity of the QDs sensor could be enhanced by the application of a surface molecularly imprinted polymer, for example, should other structurally related compounds be found to interfere with the detection of AC.

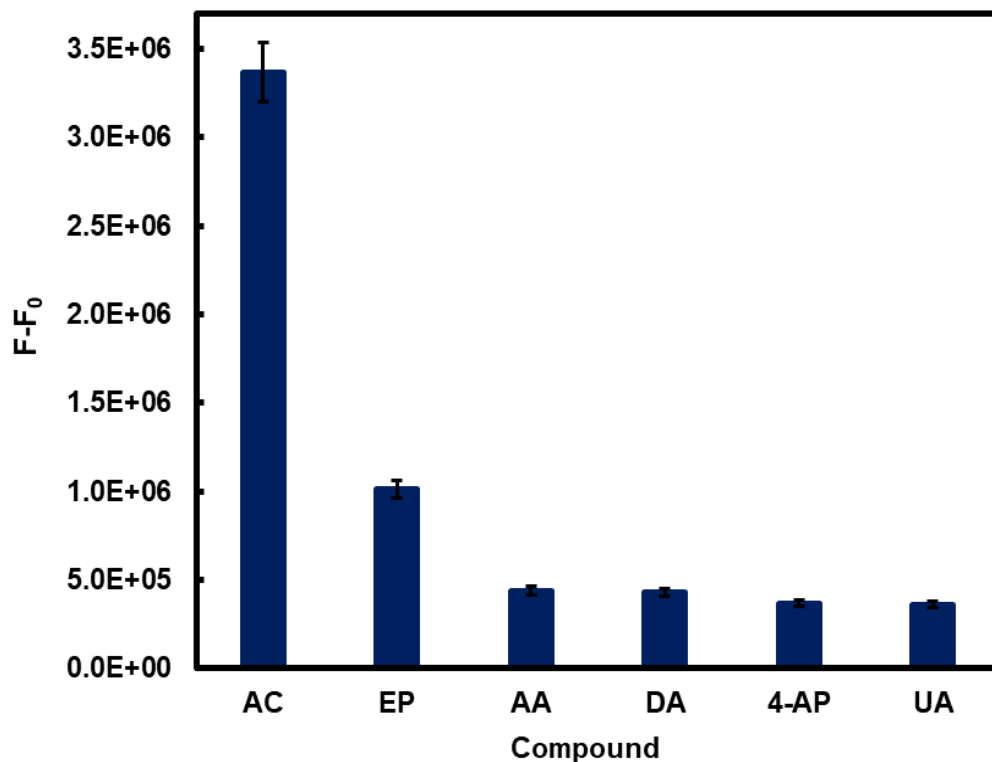


Figure 8 Fluorescence intensity change of 1.0 mg/3.0 mL of L-cys-CdSe/ZnS QDs in the presence of AC and various analytes (100 nmol L⁻¹) at an excitation and emission wavelengths of 300 nm and 595 nm respectively. Epinephrine hydrochloride (EP), L-ascorbic acid (AA), uric acid (UA), dopamine hydrochloride (DA), 4-aminophenol (4-AP), (values are the average of three measurements).

3.13. Sensing application

The method was applied to AC in water from a river and tap to investigate the effectiveness of the fluorescence sensor for AC determinations in real samples. As can be seen from Table 4, the recoveries of different known amounts of AC spiked in both types of water ranged from 95 to 108 % and 90 to 108 % respectively. The fluorescence sensing method developed in this study was thus found to be practical and reliable for the determination of AC in the aqueous environment.

Regarding the effect of pH, the average three replicate pH value of L-cys-CdSe/ZnS QDs in Millipore water was 7.6 while after addition of 500 μ L of tap or river water into 2 mL of L-cys-CdSe/ZnS QDs solution (containing 0.67 mg of L-cys-CdSe/ZnS QDs), the pH values changed to 7.1 and 7.5 respectively. Therefore, no significant pH changes took place upon addition of real water samples to the L-cys-CdSe/ZnS QDs solution and the effect of sample pH can consequently be considered negligible. HPLC-MS/MS analysis confirmed that AC was not present in both the tap and river water samples.

Table 4 Analytical results for the determination of recoveries of AC spiked in tap and river water samples using L-cys-CdSe/ZnS QDs.

	AC Spiked (nmol L ⁻¹)	Determined AC (mean ± RSD; n=3, nmol L ⁻¹)	Recovery (%)
Tap water	10	10.1±0.1	101
	50	54.0±0.1	108
	100	95.0±0.2	95
River water	10	10.8±0.7	108
	50	53.0±0.1	106
	100	90.0±0.2	90

4. Conclusion

A comparison study was performed by applying three water soluble L-cys, NAC and GSH functionalized CdSe/ZnS QDs to optimize a QD-ligand system for acetaminophen fluorescence sensing. L-cys-CdSe/ZnS QDs were selected due to their enhanced sensitivity for use as a fluorescence sensor for the determination of acetaminophen in water for the first time. The operating mechanism of the designed probe was based on the fluorescence “turn-on” mode. Advantages of this method include its simplicity, as well as stability and resistivity of QDs against photobleaching under ambient light conditions. Under optimum conditions, with the addition of acetaminophen to QDs in aqueous solution, the original PL intensity of the QDs was enhanced most likely due to fluorescence resonance energy transfer from analytes to QDs which was found to be linear within the concentration range of 3.0-100 nmol L⁻¹ AC with detection and quantification limits of 1.6 and 5.3 nmol L⁻¹ respectively. The method could therefore be applied to detect AC at environmentally relevant nanomolar concentrations.

Acknowledgment

Research funding from the University of Pretoria, the Water Research Commission (Grant K5/2438/1 and K5/2752) as well as the Photonics Initiative of South Africa (Grant PISA-15-DIR-06) is gratefully acknowledged. We also thank the Microscopy and Microanalysis Laboratory of the University of Pretoria, for assistance with microscopy measurements and Wiebke Grote of UP for the XRD measurements.

References

- 1 P. Westerhoff, Y. Yoon, S. Snyder and E. C. Wert, Fate of endocrine-disruptor, pharmaceutical, and personal care product chemicals during simulated drinking water treatment processes, *Environ. Sci. Technol.*, 2005, 39, 6649-6663.
- 2 Y. Ishihama, M. Nakamura, T. Miwa, T. Kajima and N. Asakawa, A rapid method for pKa determination of drugs using pressure-assisted capillary electrophoresis with photodiode array detection in drug discovery, *J. Pharm. Sci.*, 2002, 91, 933-942.
- 3 A. Achilleos, M. Ines Vasquez Hadjilyra, E. Hapeshi, C. Michael, S. M. Monou, M. and D. Fatta Kassinos, presented in part at the International Conference on the Protection and Restoration of the Environment IX, Kefalonia, Greece, 29 June - 03 July 2008.
- 4 K. H. Langford and K. V. Thomas, Determination of pharmaceutical compounds in hospital effluents and their contribution to wastewater treatment works, *Environ. Int.*, 2009, 35, 766-770.
- 5 M. Crane, C. Watts and T. Boucard, Chronic aquatic environmental risks from exposure to human pharmaceuticals, *Sci. Total Environ.*, 2006, 367, 23-41.
- 6 M. M. Schultz, E. T. Furlong, D. W. Kolpin, S. L. Werner, H. L. Schoenfuss, L. B. Barber, V. S. Blazer, D. O. Norris and A. M. Vajda, Antidepressant pharmaceuticals in two US effluent-impacted streams: occurrence and fate in water and sediment, and selective uptake in fish neural tissue, *Environ. Sci. Technol.*, 2010, 44, 1918-1925.
- 7 Ş. Dinç, Ö. A. Dönmez, B. Aşçı and A. E. Bozdoğan, Chromatographic and chemometrics-assisted spectrophotometric methods for the simultaneous determination of allobarbitol, adiphenine hydrochloride, and paracetamol in suppository, *J. Liq. Chromatogr. Relat. Technol.*, 2014, 37, 560-571.
- 8 B. Zheng, C. Li, Y. Li, Y. Gu, X. Yan, L. Tang, R. Chen and Z. Zhang, One-step electrochemical preparation of a reduced graphene oxide/poly (sulfosalicylic acid) nanocomposite film for detection of acetaminophen and its application in human urine and serum studies, *Anal. Methods*, 2015, 7, 8248-8254.
- 9 A. Méndez-Albores, C. Tarín, G. Rebollar-Pérez, L. Dominguez-Ramirez and E. Torres, Biocatalytic spectrophotometric method to detect paracetamol in water samples, *J. Environ. Sci. Health A.*, 2015, 50, 1046-1056.
- 10 D. Easwaramoorthy, Y.-C. Yu and H.-J. Huang, Chemiluminescence detection of paracetamol by a luminol-permanganate based reaction, *Anal. Chim. Acta.*, 2001, 439, 95-100.
- 11 L. Yuan, W. Lin, K. Zheng, L. He and W. Huang, Far-red to near infrared analyte-responsive fluorescent probes based on organic fluorophore platforms for fluorescence imaging, *Chem. Soc. Rev.*, 2013, 42, 622-661.

- 12 Q. Liu, Q. Zhou and G. Jiang, Nanomaterials for analysis and monitoring of emerging chemical pollutants, *Trends Anal. Chem.*, 2014, 58, 10-22.
- 13 R. Gill, M. Zayats and I. Willner, Semiconductor quantum dots for bioanalysis, *Angew.Chem.Int. Ed.* 2008, 47, 7602-7625.
- 14 H. Xu, R. Miao, Z. Fang and X. Zhong, Quantum dot-based “turn-on” fluorescent probe for detection of zinc and cadmium ions in aqueous media, *Anal. Chim. Acta.*, 2011, 687, 82-88.
- 15 S. Ithurria, P. Guyot-Sionnest, B. Mahler and B. Dubertret, Mn^{2+} as a radial pressure gauge in colloidal core/shell nanocrystals, *Phys. Rev. Lett.* 2007, 99, 265501.
- 16 K. T. Yong, W. C. Law, I. Roy, Z. Jing, H. Huang, M. T. Swihart and P. N. Prasad, Aqueous phase synthesis of CdTe quantum dots for biophotonics, *J. Biophotonics.*, 2011, 4, 9-20.
- 17 R. K. Ratnesh and M. S. Mehata, Investigation of biocompatible and protein sensitive highly luminescent quantum dots/nanocrystals of CdSe, CdSe/ZnS and CdSe/CdS, *Spectrochim. Acta A. Mol. Biomol. Spectrosc.*, 2017, 179, 201-210.
- 18 A. J. Nozik, M. C. Beard, J. M. Luther, M. Law, R. J. Ellingson and J. C. Johnson, Semiconductor quantum dots and quantum dot arrays and applications of multiple exciton generation to third-generation photovoltaic solar cells, *Chem. Rev.*, 2010, 110, 6873-6890.
- 19 H. Huang and J.-J. Zhu, The electrochemical applications of quantum dots, *Analyst*, 2013, 138, 5855-5865.
- 20 H. Montaseri and P. B. Forbes, A triclosan turn-ON fluorescence sensor based on thiol-capped core/shell quantum dots, *Spectrochim. Acta A. Mol. Biomol. Spectrosc.*, 2018, 204, 370-379.
- 21 H. Du, R. C. A. Fuh, J. Li, L. A. Corkan and J. S. Lindsey, PhotochemCAD: A computer-aided design and research tool in photochemistry, *Photochem. Photobiol.*, 1998, 68, 141-142.
- 22 A. Bagga, P. K. Chattopadhyay and S. Ghosh, Stokes shift in quantum dots: Origin of dark exciton, *Physics of Semiconductor Devices, 2007. IWPSD 2007. International Workshop on, IEEE, 2007*, pp. 876-879.
- 23 O. Adegoke, T. Nyokong and P. B. C. Forbes, Structural and optical properties of alloyed quaternary CdSeTeS core and CdSeTeS/ZnS core-shell quantum dots, *J. Alloys Compd.*, 2015, 645, 443-449.
- 24 W. W. Yu, L. Qu, W. Guo and X. Peng, Experimental determination of the extinction coefficient of CdTe, CdSe, and CdS nanocrystals, *Chem. Mater.*, 2003, 15, 2854-2860.
- 25 B. O. Dabbousi, J. Rodriguez-Viejo, F. V. Mikulec, J. R. Heine, H. Mattoussi, R. Ober, K. F. Jensen and M. G. Bawendi, (CdSe) ZnS core-shell quantum dots: synthesis and

- characterization of a size series of highly luminescent nanocrystallites, *J. Phys. Chem. B.*, 1997, 101, 9463-9475.
- 26 O. Adegoke, M.-W. Seo, T. Kato, S. Kawahito and E. Y. Park, Gradient band gap engineered alloyed quaternary/ternary CdZnSeS/ZnSeS quantum dots: An ultrasensitive fluorescence reporter in a conjugated molecular beacon system for the biosensing of influenza virus RNA, *J. Mater. Chem. B.*, 2016, 4, 1489-1498.
- 27 A. V. Baranov, Y. P. Rakovich, J. F. Donegan, T. S. Perova, R. A. Moore, D. V. Talapin, A. L. Rogach, Y. Masumoto and I. Nabiev, Effect of ZnS shell thickness on the phonon spectra in CdSe quantum dots, *Phys. Rev. B.*, 2003, 68, 165306.
- 28 M. Klein, F. Hache, D. Ricard and C. Flytzanis, Size dependence of electron-phonon coupling in semiconductor nanospheres: The case of CdSe, *Phys. Rev. B.*, 1990, 42, 11123-11132.
- 29 S. N. Alam, N. Sharma and L. Kumar, Synthesis of graphene oxide (GO) by modified hummers method and its thermal reduction to obtain reduced graphene oxide (rGO), *Graphene*, 2017, 6, 1-18.
- 30 D. K. Gupta, M. Verma, K. Sharma and N. S. Saxena, Synthesis, characterization and optical properties of CdSe/CdS and CdSe/ZnS core-shell nanoparticles, *Indian J. Pure Appl. Phys.*, 2017, 55, 113-121.
- 31 C.-T. Cheng, C.-Y. Chen, C.-W. Lai, W.-H. Liu, S.-C. Pu, P.-T. Chou, Y.-H. Chou and H.-T. Chiu, Syntheses and photophysical properties of type-II CdSe/ZnTe/ZnS (core/shell/shell) quantum dots, *J. Mater. Chem.*, 2005, 15, 3409-3414.
- 32 M. Koneswaran and R. Narayanaswamy, L-Cysteine-capped ZnS quantum dots based fluorescence sensor for Cu²⁺ ion, *Sens. Actuators B. Chem.*, 2009, 139, 104-109.
- 33 Toxicological Summary for: Acetaminophen. (2010). Retrieved from www.health.state.mn.us/divs/eh/risk/guidance/dwec/sumacetamin.pdf. Date of access: February 2018.
- 34 F. A. Gorla, E. H. Duarte, E. R. Sartori and C. R. T. Tarley, Electrochemical study for the simultaneous determination of phenolic compounds and emerging pollutant using an electroanalytical sensing system based on carbon nanotubes/surfactant and multivariate approach in the optimization, *Microchem. J.*, 2016, 124, 65-75.
- 35 C. D. S. Pereira, L. A. Maranhão, F. S. Cortez, F. H. Pusceddu, A. R. Santos, D. A. Ribeiro, A. Cesar and L. L. Guimarães, Occurrence of pharmaceuticals and cocaine in a Brazilian coastal zone, *Sci. Total Environ.*, 2016, 548, 148-154.
- 36 L. Capka, P. Lacina and M. Vavrova, Development and application of SPE/CZE method for detection and determination of selected non-steroidal anti-inflammatory drugs in wastewater, *Fresen. Environ. Bull.*, 2012, 21, 3312-3317.

- 37 K. E. Sapsford, L. Berti and I. L. Medintz, Materials for fluorescence resonance energy transfer analysis: beyond traditional donor–acceptor combinations, *Angew. Chem. Int. Ed.*, 2006, 45, 4562-4589.
- 38 X. Wang, J. Yu, Q. Kang, D. Shen, J. Li and L. Chen, Molecular imprinting ratiometric fluorescence sensor for highly selective and sensitive detection of phycocyanin, *Biosens. Bioelectron.*, 2016, 77, 624-630.
- 39 M. Elangovan, R. Day and A. Periasamy, Nanosecond fluorescence resonance energy transfer-fluorescence lifetime imaging microscopy to localize the protein interactions in a single living cell, *J. Microsc.*, 2002, 205, 3-14.

4.2.1 Paper 4 - Supplementary information

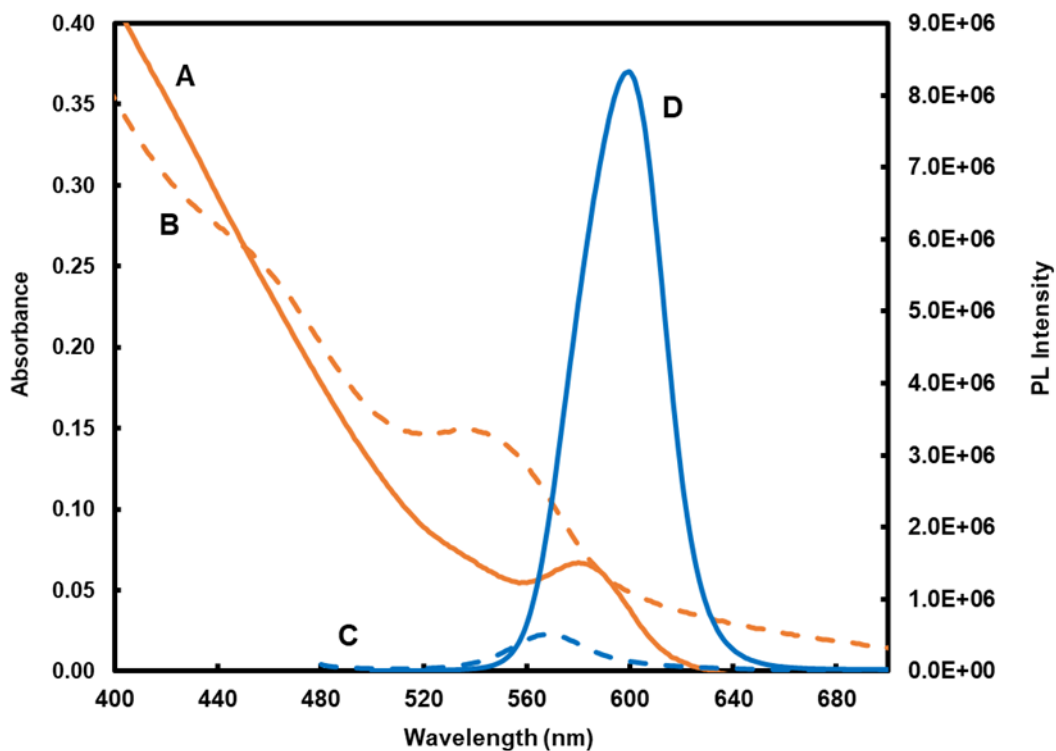


Fig. S1. Absorption spectra of the water-soluble (A) L-cys-capped CdSe/ZnS QDs; (B) L-cys-CdSe QDs in Millipore water; (C) PL emission spectra of the water-soluble L-cys-capped CdSe QDs at excitation wavelength 470 nm; (D) L-cys-capped CdSe/ZnS QDs at excitation wavelength 410 nm measured in Millipore water.

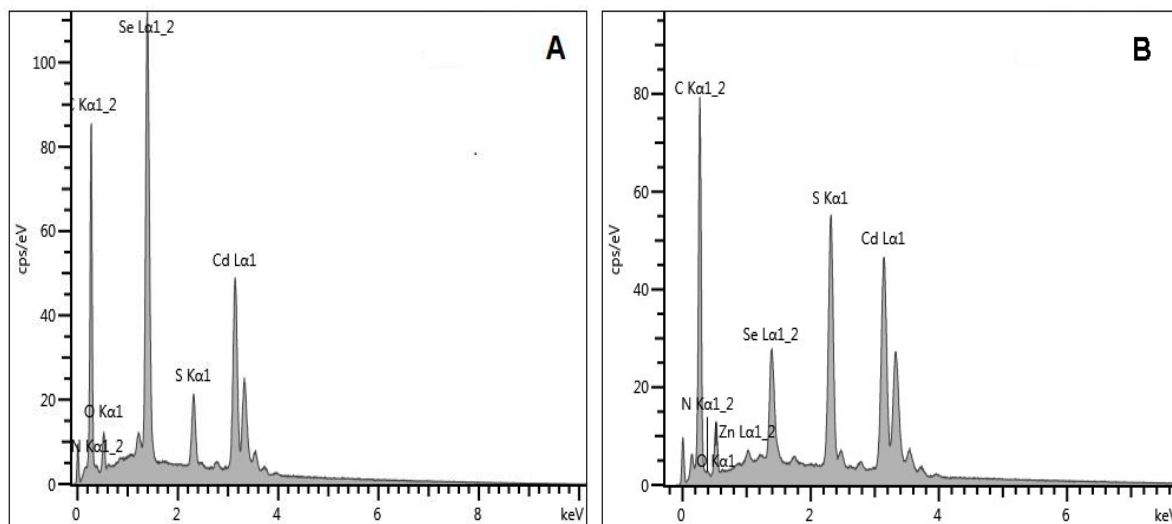


Fig. S2. EDS spectra of (A) L-cys-CdSe QDs and (B) L-cys-CdSe/ZnS QDs.

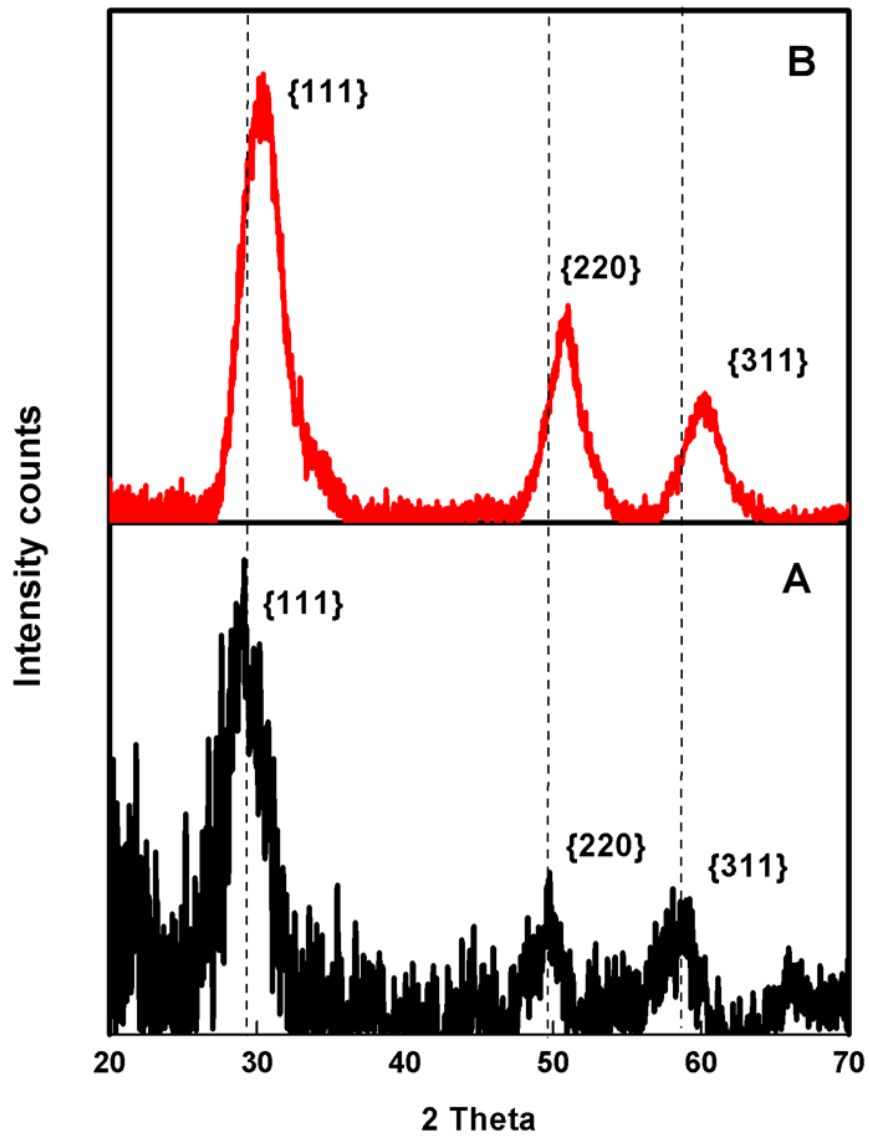


Fig. S3. Powder XRD pattern of the (A) L-cys-CdSe and (B) L-cys-CdSe/ZnS QDs.

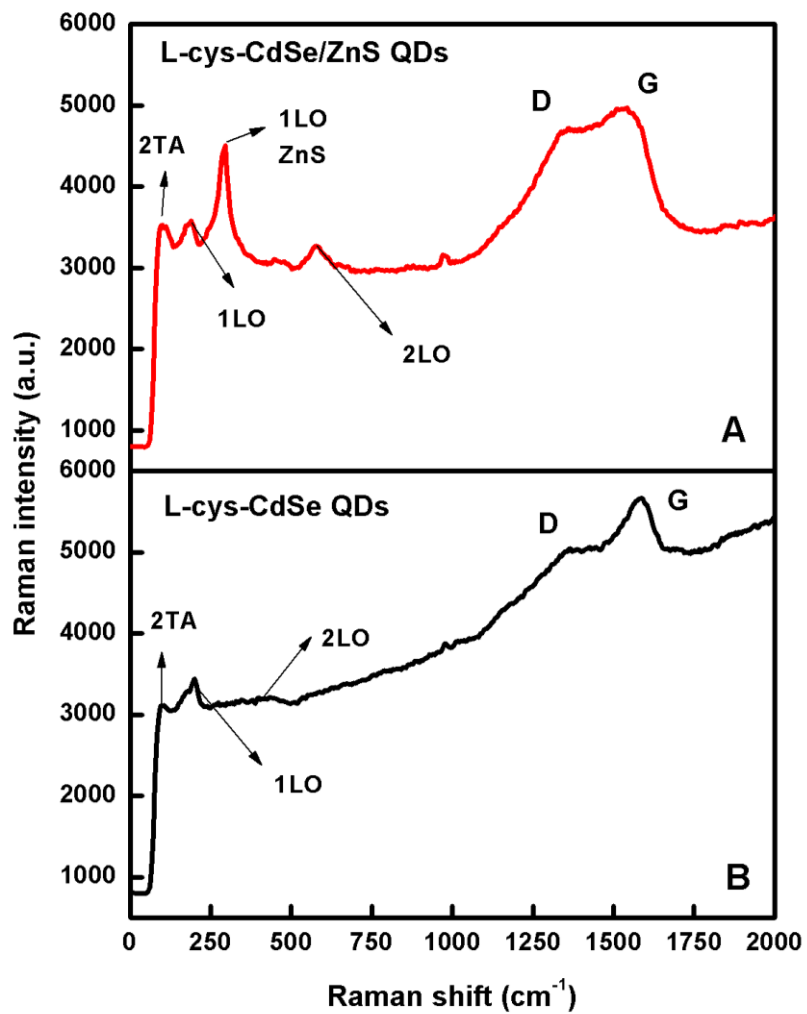


Fig. S4. Raman spectra of (A) L-cys-CdSe and (B) L-cys-CdSe/ZnS QDs.

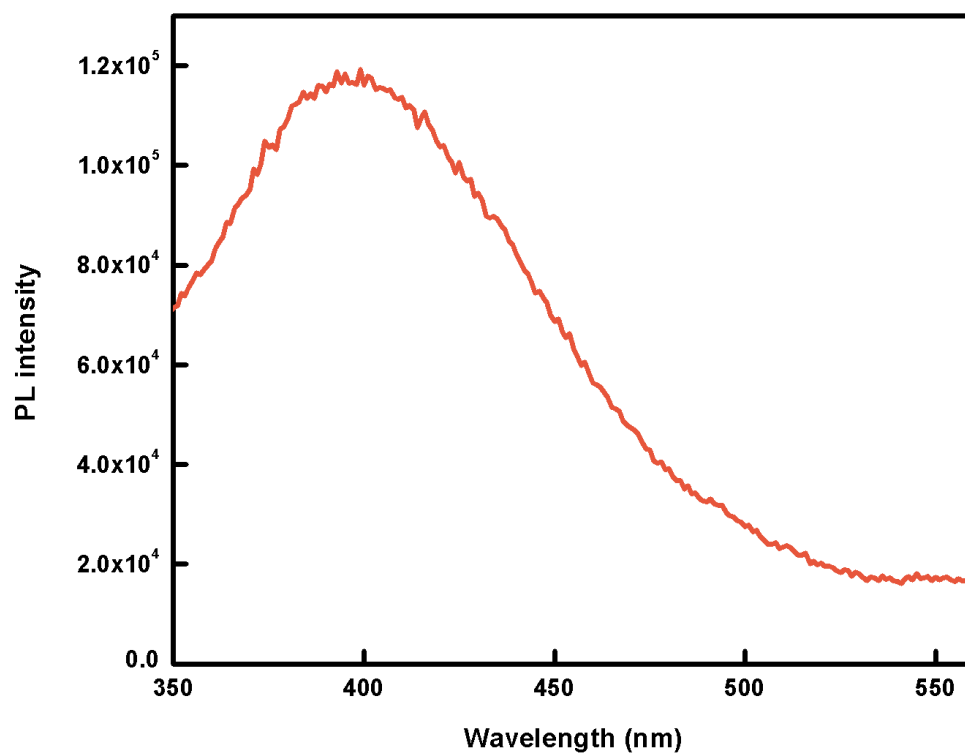


Fig. S5. Fluorescence spectrum of acetaminophen in water (1.0×10^{-5} mol L⁻¹) at an excitation wavelength of 300 nm.

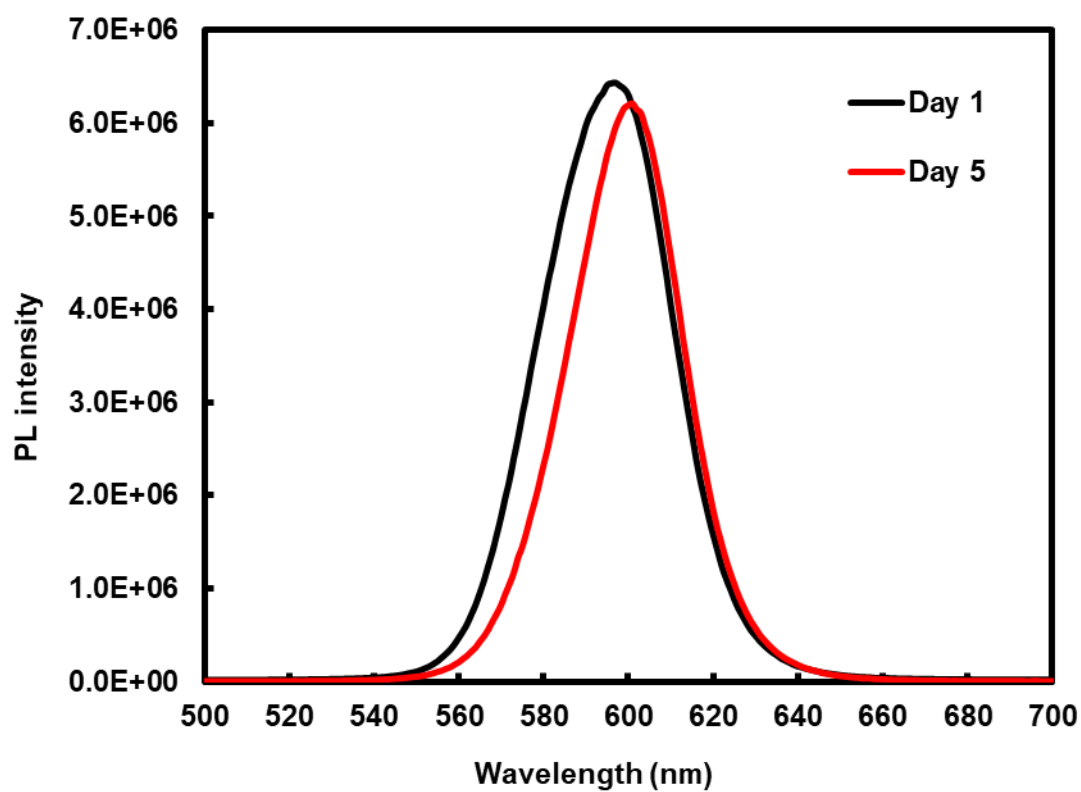


Fig. S6. PL stability of the hydrophilic QDs measured before and after 5 days of exposure to ambient light (300 nm excitation).

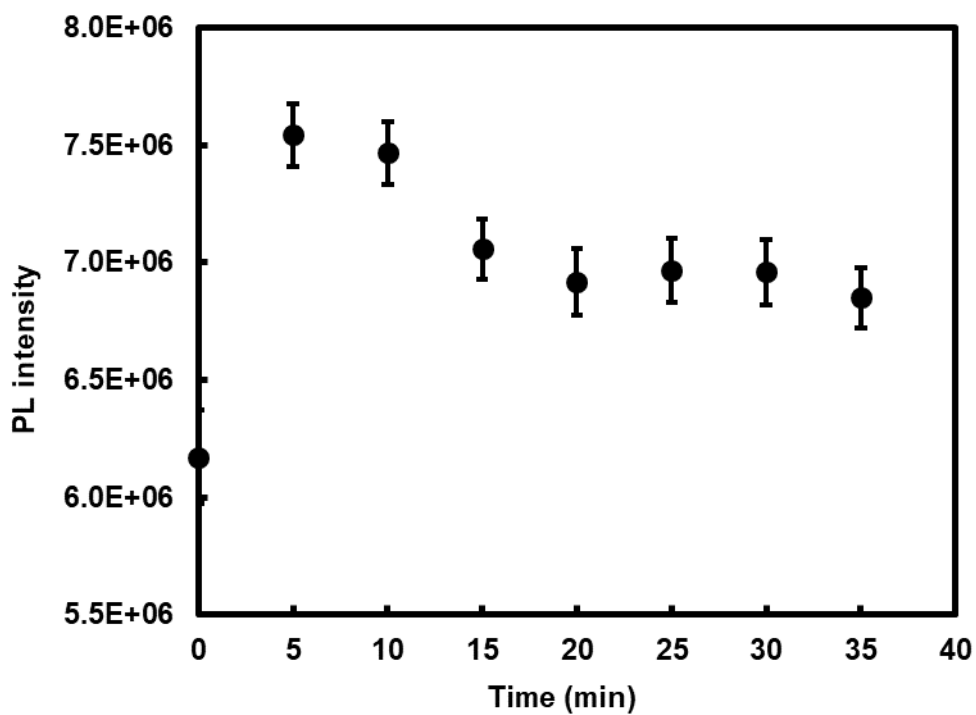


Fig. S7. Effect of interaction time on the fluorescence intensity of the L-cys capped CdSe/ZnS QD-AC system at an excitation wavelength of 300 nm (values are the average of three measurements).

Table S1

Elemental compositions of L-cys-CdSe and L-cys-CdSe/ZnS QDs by using EDS.

Element (Wt %)	C	N	O	S (ligand and shell)	Cd	Se	Zn
L-cys-CdSe QDs	22.5	0.4	2.7	3.60	45.3	25.6	-
L-cys-CdSe/ZnS QDs	23.7	0.01	4.0	12.3	52.7	6.50	0.8

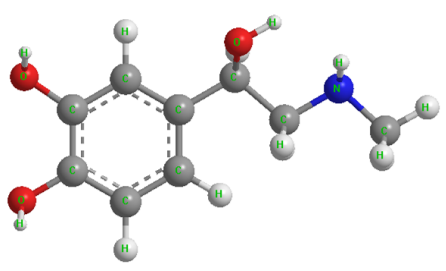
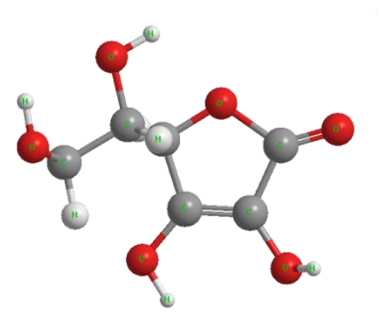
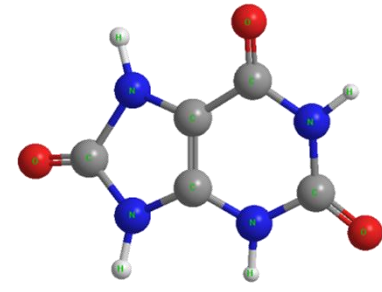
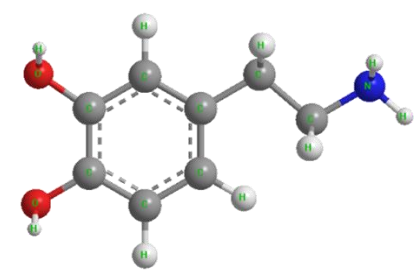
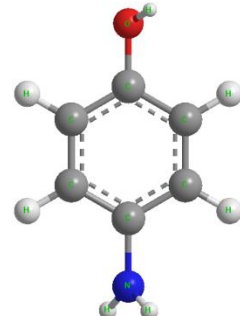
Table S2

IR absorption bands of the L-cys-CdSe and L-cys-CdSe/ZnS QDs.

Functional group	IR band (cm ⁻¹)
-COO-	1550-1600 (strong) 1400 (medium)
-OH	3000-3500
-NH ₂	2900-3420
C-S	600-800
S-H	2550-2750

Table S3

Chemical structures of potentially interfering analytes.

Name	Structure
Epinephrine hydrochloride (EP)	
L-ascorbic acid (AA)	
Uric acid (UA)	
Dopamine hydrochloride (DA)	
4-aminophenol (4-AP)	

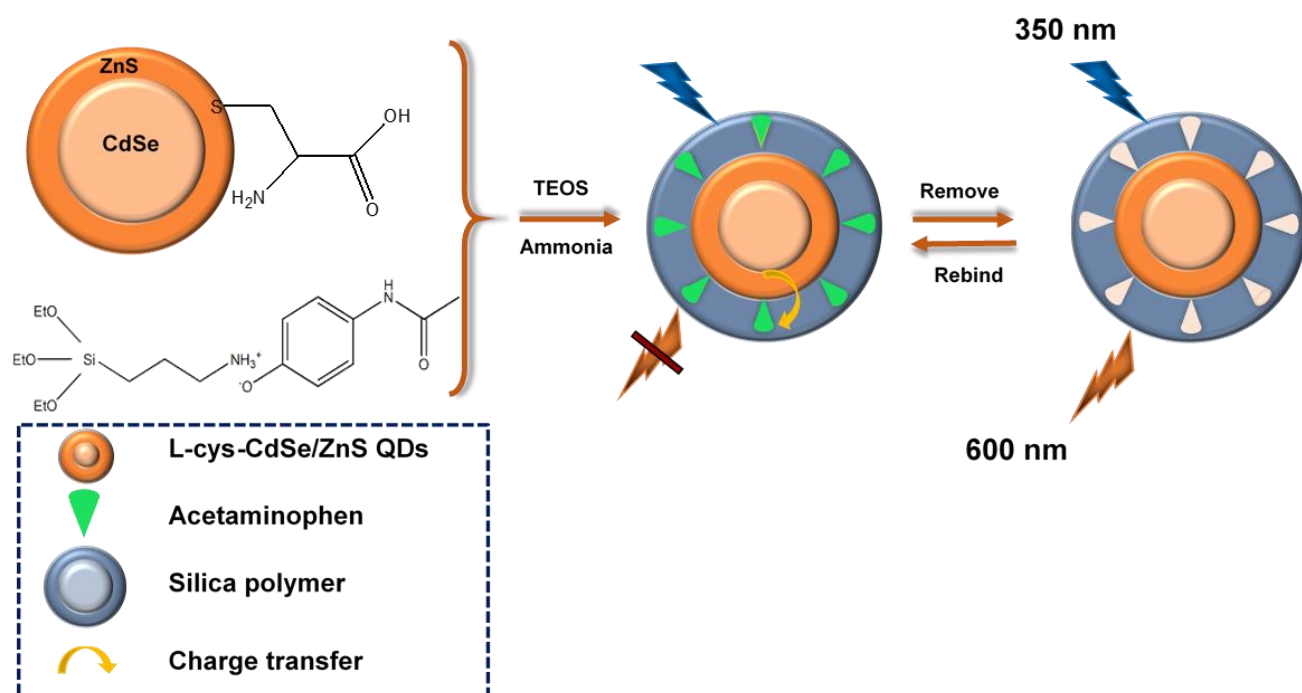
4.3 Paper 5

This paper was formatted in accordance with the journal *Materials Today Communications*, an Elsevier journal in which it has been published:

Montaseri, H., & Forbes, P.B.C. (2018). Molecularly imprinted polymer coated quantum dots for fluorescence sensing of acetaminophen, *Materials Today Communications*, 17, 480-492.

<https://doi.org/10.1016/j.mtcomm.2018.10.007>

Graphical abstract





Molecularly imprinted polymer coated quantum dots for fluorescence sensing of acetaminophen

Hanieh Montaseri, Patricia B.C. Forbes

Department of Chemistry, Faculty of Natural and Agricultural Sciences, University of Pretoria, Lynnwood Road, Pretoria 0002, South Africa

ARTICLE INFO

Keywords:

Molecularly imprinted polymer
Quantum dots
Fluorescence spectroscopy
Pharmaceuticals
Acetaminophen

ABSTRACT

A molecularly imprinted coating with acetaminophen (AC) as template molecule was grafted onto L-cys-CdSe/ ZnS quantum dots (QDs) using 3-aminopropyltriethoxysilane as the functional monomer and tetraethyl orthosilicate as the cross-linker via an adapted Stöber method, in order to develop a selective and sensitive fluorescence sensor for the determination of AC in water samples. The resulting MIP@QDs were characterized by Fourier-transform infrared spectroscopy, high resolution transmission electron microscopy, energy dispersive X-ray spectroscopy, thermogravimetric analysis and fluorescence spectrophotometry which confirmed the polymer coating. The fluorescence quenching of the sensor provided good linearity over the AC concentration range of 1.0–300 nmol L⁻¹ with a detection limit of 0.34 nmol L⁻¹ and the sensor showed good photostability over 5 days. The recoveries of AC in water samples at various spiking levels varied from 95% to 114%.

1. Introduction

Acetaminophen (AC) is a common analgesic and antipyretic drug which is prescribed and purchased over the counter for the relief of minor pain such as fever and headaches. AC has no toxic effect in normal therapeutic doses while large doses particularly with simultaneous consumption of alcohol or other drugs can cause nephrotoxicity, skin rashes, inflammation of the pancreas and liver disorders [1]. A few reports have been published regarding the presence of acetaminophen in potable water, such as Frick et al. [2], and on the potential chronic health effects related to long term ingestion of AC in water [3].

Conventional methods for the detection of AC in real water samples are based on electrochemistry [4], chromatography [5] and spectrophotometry [6]. A fluorescence probe approach offers an alternative with significant advantages including easy operation, low cost, a fast and simple experimental process, and high sensitivity towards different molecular structures with different emission wavelengths [7]. Semiconductor quantum dots (QDs) have a number of attractive properties that render them suitable as fluorescence probes for in vivo or in vitro imaging, as well as in fluorescence immunoassays and toxin detection [8]. This is due to their unique chemical and physical properties including high fluorescence quantum yields, narrow spectral line widths, size-dependent fluorescence, independence of emission on the excitation wavelength and stability against photobleaching [9]. Furthermore, because of their large surface to volume ratios, their surface activity,

and their strong adsorption affinity to other nanoparticles, their utilization can be advantageous over that of larger particles. QDs have size-dependent optical properties, which means that their absorption and emission properties can be tuned by changing the surface structure and particle shape and size [10]. Through surface modification strategies, they have found various applications across disciplines. Reviews have been published on their application in solar cells [11], as biological labels [12], in microelectronics [13] and in electrochemistry [14].

Core/shell nanoparticles have gained considerable research interest due to their distinct advantages over core QDs, including higher quantum yields, higher photoluminescence efficiencies, improved optical properties, increased half-life times and easy detection of emission spectra, because they are shifted towards longer wavelengths in the visible range. In addition, due to their improved electronic properties (band gap and band alignment), they possess better structural (lattice mismatch) properties than core QDs. Stabilization of the core QDs with an inorganic shell such as ZnS and also surface coating with a capping agent (e.g. L-cysteine or glutathione) can reduce ion leakage thereby reducing toxicity in use. The shell layer also protects the core from air oxidation [15] and more importantly it reduces surface defects which arise from coordinative unsaturation [16].

The use of QDs is limited when coexisting interfering compounds produce a similar photoluminescence response to the target analyte. Molecularly imprinted polymers (MIPs) are a promising way to enhance the selectivity of QDs. They are synthetic polymeric materials

Corresponding author.

E-mail address: patricia.forbes@up.ac.za (P.B.C. Forbes).

<https://doi.org/10.1016/j.mtcomm.2018.10.007>

Received 17 August 2018; Received in revised form 8 October 2018; Accepted 8 October 2018

Available online 09 October 2018

2352-4928/ © 2018 Elsevier Ltd. All rights reserved.

possessing specific recognition sites complementary to the template molecule in terms of functional groups, size and shape. In molecular imprinting, functional monomers are located around the template molecules by reversible covalent or non-covalent interaction, followed by polymerization and template removal. In so doing, a molecular 'memory' is fabricated within the imprinted polymer allowing for the target molecule to be selectively distinguished from other molecules [17]. MIPs have been considered as alternatives for natural receptors [18,19] in chemical assays or sensors due to their low cost, long lifetime, intrinsic robustness and their tailor-made recognition sites for target analytes [20].

In 2012, a simple and sensitive assay of acetaminophen was proposed based on the quenching of the fluorescence intensity of L-cysteine capped CdTe nanoparticles (NPs) in aqueous solution. Under optimal experimental conditions, the relative fluorescence intensity ($\Delta I = I_0/I$) of L-cysteine capped CdTe NPs versus the concentration of acetaminophen was linear over the range of 10–160 nmol L⁻¹ with a detection limit of 4.2 nmol L⁻¹. The applicability of the method was tested for the analysis of AC in pharmaceutical tablets [21].

A bio-mimetic bulk acoustic wave (BAW) sensor was fabricated using a molecularly imprinted polymer with two functional monomers of 4-vinylpyridine (4-VP) and methacrylic acid (MAA) for the determination of acetaminophen over the linear range of 5.0–100 nmol L⁻¹ with a detection limit of 5.0 nmol L⁻¹. The biosensor was then applied for the determination of acetaminophen in human serum and urine samples [22].

Recently, amphiphilic pillar[5]arene (amPA5) functionalized reduced graphene oxide (amPA5-RGO) as a receptor has been applied as a 'turn on' fluorescence sensing platform for the determination of AC in serum samples. The mechanism was based on competitive host–guest interaction between two analytes of acridine orange (AO)/acetaminophen which led to a change in fluorescence signal of the dye molecule. The prototype sensor gave a linear concentration range over 1.0×10^2 – 4.0×10^3 and 4.0×10^3 – 3.2×10^4 nmol L⁻¹ with a detection limit of 50 nmol L⁻¹ [23].

In another study for the simultaneous spectrophotometric determination of acetaminophen and gentamicin in tablets, ampoules and blood serum samples, silver nanoparticles were synthesized and applied over the concentration range of 5.0×10^3 – 1.0×10^5 nmol L⁻¹ with a detection limit of 1.2×10^2 nmol L⁻¹ [24].

In this study, the high sensitivity of QDs was integrated with the selectivity of MIPs via the preparation of a QD-based MIP composite. L-cys-CdSe/ZnS QDs were synthesized and entrapped in the layers of 3-aminopropyltriethoxysilane (APTES) and tetraethyl orthosilicate (TEOS) through a sol-gel polymerization approach. The sol-gel technique has many advantages over other polymerization techniques, including simple preparation at room temperature, preventing problems associated with thermal and chemical decomposition. Furthermore, environmentally friendly solvents such as Millipore water or ethanol can be used in radical polymerisation instead of toluene, acetonitrile or chloroform [17,20].

A surface molecular imprinting process using AC as a template was applied to synthesize the fluorescent sensor which places the binding sites in the vicinity of the MIP surface and enhances selectivity and mass transfer. In comparison with bulk polymerisation which generates MIPs with poor binding capacity and low binding kinetics, the surface imprinting technique facilitates complete removal of the template due to the thin imprinting layers and also provides accessible sites for rebinding of the target analyte leading to high binding capacities, in addition to good synthesis reproducibility [17,25].

This is the first time that the detection of AC based on the application of surface molecular imprinting of core/shell quantum dots has been reported. AC could be detected at low levels based on the fluorescence quenching of MIP@QDs likely through charge transfer induced fluorescence quenching from the MIP@QDs to AC, allowing for the

application of the fluorescence sensor to AC monitoring in real water samples. A simple sensor for AC molecules is thus reported which detects this analyte selectively and can be applied to improve water quality, as AC can accumulate in water systems and cause long term health effects, even at low concentrations.

2. Experimental section

2.1. Reagents and materials

Octadec-1-ene (ODE), trioctylphosphine oxide (TOPO), zinc oxide, cadmium oxide, oleic acid (OA), sulfur powder, L-cysteine (L-cys), hydrochloric acid, potassium hydroxide, acetaminophen (AC), 3-aminopropyltriethoxysilane (APTES) and tetraethyl orthosilicate (TEOS) were purchased from Sigma Aldrich. Anhydrous ethanol and ammonia solution were purchased from Merck. Potential interfering analytes, namely L-ascorbic acid (AA), dopamine hydrochloride (DA), epinephrine hydrochloride (EP), uric acid (UA), 4-aminophenol (4-AP), L-tryptophan (TRY), ketoprofen (KTP), sulfamethoxazole (SM), estradiol (ES), L-Dopa and diclofenac sodium salt (Dic) were purchased from Sigma Aldrich. An ultrapure Milli-Q Water System (18.0 MΩ cm at 25 °C) was used for sample preparation.

2.2. Characterization

A Horiba Jobin Yvon Fluoromax-4 spectrofluorometer was employed to record fluorescence emission spectra. High resolution transmission electron microscopy (HRTEM) images were taken using a JEOL JEM 2100 F operated at 200 kV. The estimated particle size distribution of QDs was determined using ImageJ software (<http://imagej.nih.gov/ij/>, U.S. National Institutes of Health [NIH], Bethesda, Maryland, USA). High resolution scanning electron microscopy (HRSEM) measurements were carried out using an FE-SEM Zeiss Ultra Plus. IR measurements (4000–400 cm⁻¹) in KBr were taken using a Spectrum RXI FT-IR System from Perkin Elmer and UV–vis absorption spectra were recorded using a Cary Eclipse (Varian) spectrophotometer. Energy dispersive X-ray spectroscopy (EDS) analysis was carried out using HRTEM integrated EDS (Oxford INCAx-sight, 20 keV range and 150 s acquisition) with Oxford INCA Suite 4.11 software. Thermal analysis was performed using a TA Instruments SDT Q600 thermogravimetric analyzer (TGA) using a heating rate of 10 °C min⁻¹ from 25 to 1200 °C, under nitrogen atmosphere at a rate of 100 mL min⁻¹.

2.3. Synthesis of water-soluble CdSe/ZnS QDs

CdSe/ZnS core/shell QDs were synthesized according to previous reports [26]. Conversion of hydrophobic QDs to water soluble QDs was performed as follows: methanolic stock solution of L-cys–KOH was prepared separately by adding 2 g of L-cys to 3.0 g of KOH in 40 mL methanol followed by ultrasonication. The purified hydrophobic capped CdSe and CdSe/ZnS QDs were redispersed in chloroform and the ligand exchange solution was subsequently added. Millipore water was then separately added to each QD solution. In order to separate the organic phase from the aqueous phase, the solutions were stirred for 1 h. The water-soluble QDs were then purified with ethanol followed by acetone via centrifugation to efficiently remove all unreacted organic substituents. The purified water soluble QDs were dried in a fume hood.

2.4. Synthesis of MIP-capped L-cys-CdSe/ZnS QDs

20 mg of AC (template) in 20 mL anhydrous ethanol and 100 μL of APTES (functional monomer) were added to a flask followed by stirring for 1 h. 5 mL of L-cys-CdSe/ZnS QDs, 100 μL of TEOS (cross linker) and 100 μL of ammonia were then injected into the mixture solution and stirred for 24 h. Anhydrous ethanol was utilized to purify and wash the

resultant MIP-capped CdSe/ZnS QDs at 5000 rpm for 10 min until the fluorescence intensity of MIP-capped CdSe/ZnS QDs remained constant. Lastly, the MIP-capped CdSe/ZnS QDs (MIP@QDs) were dried under vacuum at room temperature and stored in a desiccator for further use. The non-imprinted polymers (NIP@QDs) were also prepared in the same manner but without the addition of AC to compare with MIP@QDs [27].

2.5. Optimization experiments

Regarding the optimization of the MIP@QDs concentration, the experimental procedure is described as follows: different concentrations of MIP@QDs (0.2, 0.4, 0.6, 0.8, 1.0 and 1.2 mg) were prepared in 3.0 mL of Millipore water and 200 μL of a standard solution of AC (300 nmol L^{-1}) was then injected to 2 mL of each solution separately. The PL of the resulting solution was then determined.

In order to optimize the incubation time, 0.8 mg of MIP@QDs was dissolved in 3 mL Millipore water and 200 μL a standard solution containing 300 nmol L^{-1} of AC was injected and the corresponding PL spectra were then recorded after different time intervals. The values of F_0 and F were recorded for each optimization which were the PL intensity of MIP@QDs in the absence and presence of AC respectively.

Inter-day and intra-day photostability of MIP@QDs and NIP@QDs were also performed by preparing 0.8 mg in 3 mL Millipore water of each polymer. 2 mL of this solution was placed in a quartz cuvette and PL spectra were recorded after 10 min intervals for 40 min. In order to examine inter-day photostability, the solution of each polymer was kept in the fridge for 5 days and the PL corresponding spectra were recorded.

The following conditions were applied for all optimization measurements: the excitation and emission slit width of the spectrofluorometer was 5 nm and the fluorescence intensity was measured at an excitation wavelength of 350 nm.

2.6. Sample analysis

Tap water samples for fluorescence measurements were collected from a municipal tap in Pretoria, South Africa using cleaned glass bottles. River water samples were also collected from the LC de Villiers sports grounds of the University of Pretoria. The sample bottles were filled and immediately placed in cooler boxes containing icepacks and

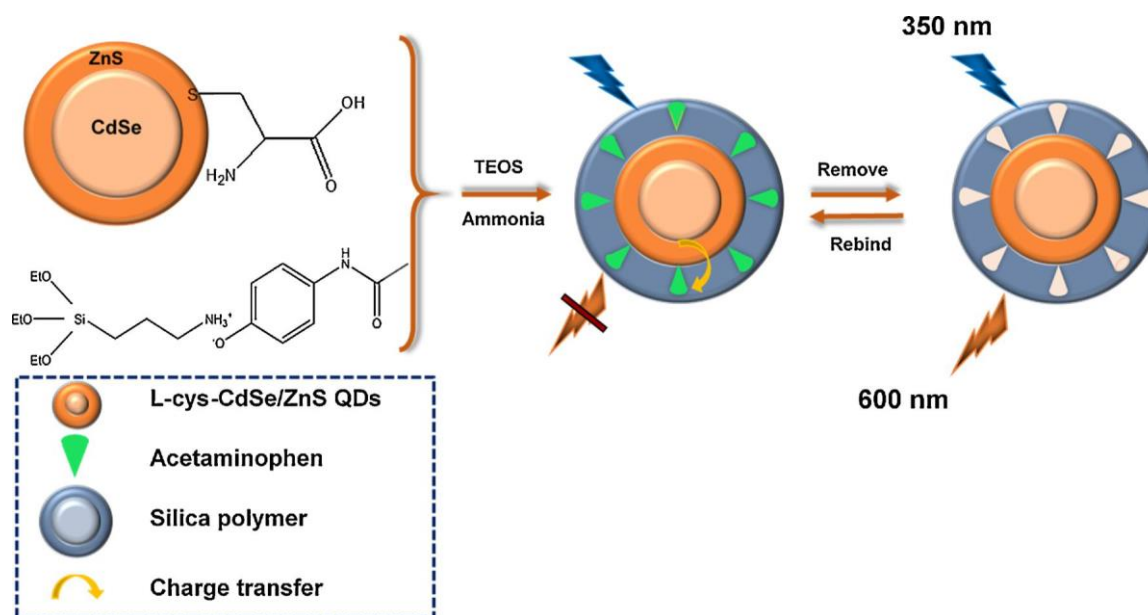
transferred to the laboratory for storage at 4 °C prior to analysis. The collected tap and river water samples were centrifuged at 4500 rpm for 5 min and filtered through 110 mm pore size filter paper before analysis to eliminate particulate matter before storage in pre-cleaned glass bottles. As no AC was detected in collected water samples by HPLC-MS/MS, a spiking method (over the concentration range of 1.0–300 nmol L^{-1}) was adopted with different known amounts of AC dissolved in Millipore water and the AC concentration was determined based on the fluorescence quenching of the MIP@QDs. Sensing was carried out by placing 2 mL of 0.8 mg of MIP@QDs in 3 mL of Millipore water in a quartz cuvette followed by addition of 200 μL of a standard solution containing different amounts of AC. The PL intensity after 14 min stabilization time was set as F_0 and the PL intensity of MIP@QDs in the absence of AC was set as F . Through the variation of AC concentration, a series of F_0/F values were obtained.

3. Results and discussion

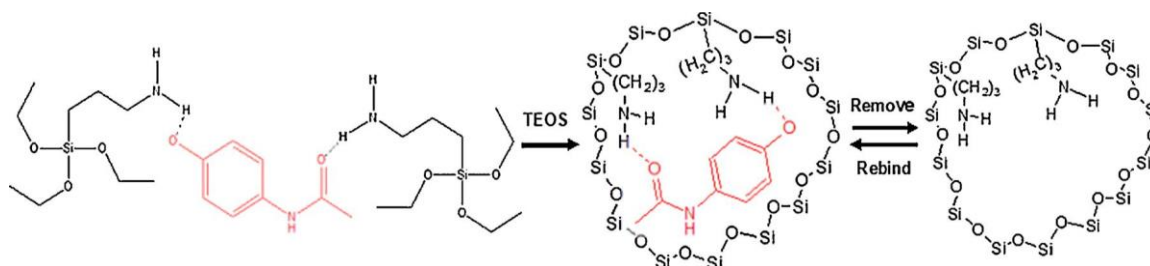
3.1. Preparation and characterization of MIP- and NIP-capped CdSe/ZnS QDs

A MIP layer was anchored on the surface of the L-cys-CdSe/ZnS QDs using 3-aminopropyltriethoxysilane (APTES) as the functional monomer, tetraethyl orthosilicate (TEOS) as the cross-linker, aqueous ammonia solution as the catalyst and AC as a template via an adapted Stöber method to produce MIP capped L-cys-CdSe/ZnS QDs (Scheme 1) [27]. The L-cys-CdSe/ZnS QDs were used as scaffolds and fluorescence detection sources while the silica shell provided highly selective recognition sites. The silica shell also provides a rigid matrix and a hydrophilic surface [28, 29], making it a good choice for the imprinting process.

Carboxylic groups of L-cys-CdSe/ZnS QDs can interact with APTES and TEOS to enable the formation of sol-gel MIP@QDs. In addition, the amino groups of APTES can render strong non-covalent interactions with the hydroxyl group, carboxylic or amino group of AC through hydrogen bonding [30] which drives template molecules into the silica matrix as illustrated in Scheme 2. The silanization reaction of APTES and TEOS was adopted in order to immobilize AC templates into the matrix of silica to form L-cys-CdSe/ZnS QDs@MIP-AC. After extracting AC templates from the silica matrix using absolute ethanol to disrupt



Scheme 1. Schematic illustration of the preparation of MIP@QDs and the sensing mechanism for AC.



Scheme 2. Schematic illustration of the molecular imprinting mechanism of AC in a silica matrix through hydrogen bond interactions (the third H-bond is between the amine group of AC and a hydroxyl group of L-cys associated with the QDs – not shown).

the hydrogen bond interactions, the AC-imprinted sites with anchored amino groups surrounding the cavity were created in the silica matrix forming MIP@QDs [31].

As can be seen from Fig. S1, the fluorescence intensity of MIP@QDs partly decreased compared to the core/shell QDs. Fluorescence quenching may be attributed to an electric field caused by a single charge which is in the proximity of the surface of QDs arising from Si₂O groups, hydroxyl ions or ammonium ions which may also cause a red shift [32,33]. This phenomenon was also noted by Yu et al. and Xu et al. [25,34] where QD@MIPs and dummy molecularly imprinted

polymer capped QDs (DMIP@QDs) were applied for the detection of 4-nitrophenol and 2,4,6-trinitrotoluene respectively. It has also been suggested that the attachment of fully hydrolyzed and condensed silica to the surface of the QDs can cause a red shift [31,33]. Furthermore, the slight red shift from 595 nm to 600 nm can be ascribed to the size effect of MIP@QDs relative to the core/shell QDs.

Although the PL of MIP@QDs decreased, they still showed bright PL (Fig. S1, inset c) and the sharp PL intensity provided evidence for the homogenous size of the MIP@QDs [30] (Fig. S1). The lower intensity observed for NIP@QDs was possibly due to the denser silica layers on

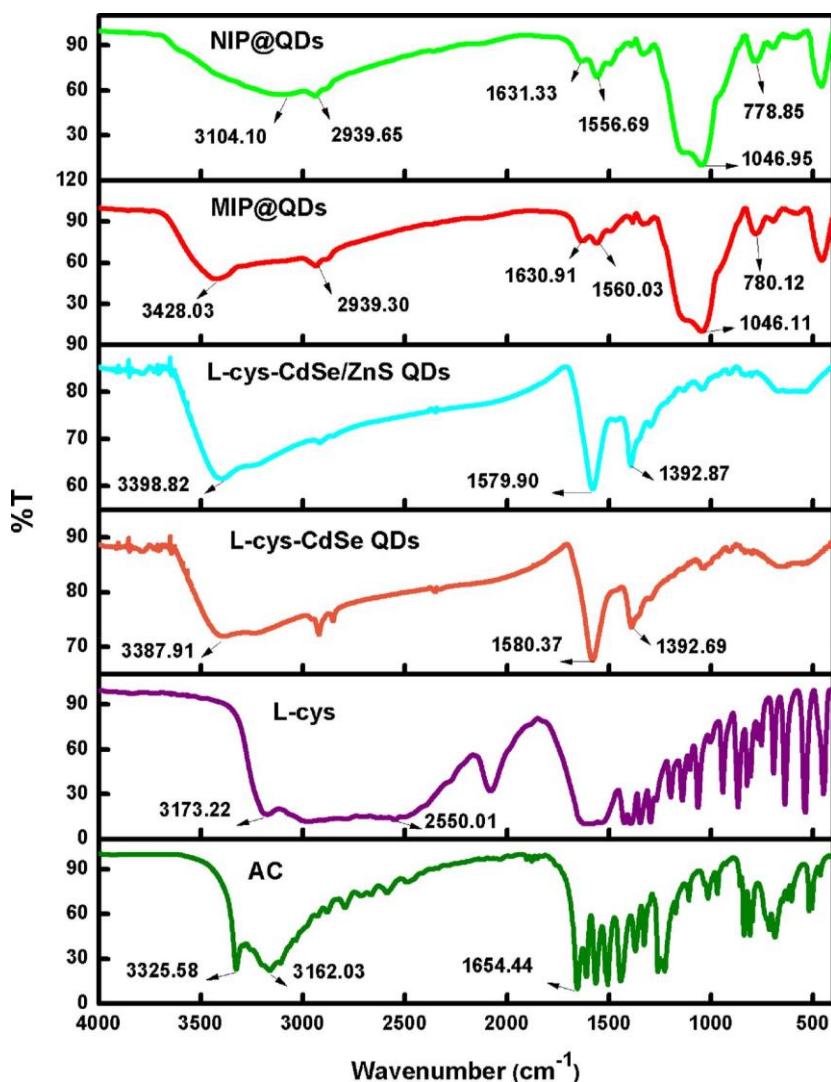


Fig. 1. FT-IR spectra of AC, L-cys, L-cys-CdSe QDs, L-cys-CdSe/ZnS QDs, MIP@QDs (with template removed) and NIP@QDs.

the NIP@QDs particles compared with MIP@QDs (Fig. S2) [35].

Band gap energy values of L-cys-CdSe QDs, L-cys-CdSe/ZnS QDs, MIP@QDs and NIP@QDs were estimated to be 2.18, 2.09, 2.07 and 2.07 eV respectively.

3.2. FT-IR analysis

In order to confirm that the MIP was well coated onto the QDs, FTIR of MIP@QDs, NIP@QDs, original L-cys-CdSe core QDs, L-cys-CdSe/ZnS core/shell QDs, L-cys and AC were compared (Fig. 1).

Carboxylic acid and amino groups of L-cys around $1550\text{--}1600\text{ cm}^{-1}$ and $2900\text{--}3420\text{ cm}^{-1}$ were evident for the L-cys capped CdSe/ZnS and CdSe QDs, while the SeH group vibration ($2550\text{--}2750\text{ cm}^{-1}$) was absent in the spectra of the L-cys-CdSe/ZnS QDs which is due to the formation of covalent bonds between thiols and the surface of ZnS in the L-cys capped CdSe/ZnS QDs and the formation of Cd-S bonds in the L-cys-CdSe QDs. After the coating of MIP onto the surface of the QDs, a strong band at 1046 cm^{-1} corresponded to the asymmetric stretching vibration of Si-O-Si groups. The bands at $3100\text{--}3500\text{ cm}^{-1}$ and 1630 cm^{-1} in the spectra of MIP@QDs and NIP@QDs can be due to the stretching

and bending vibrations of N-H groups from the APTES which suggested the presence of aminopropyl groups on the surface of the materials. The band at 2940 cm^{-1} could be ascribed to the $\text{-CH}_2\text{-}$ bond while the band at around 780 cm^{-1} is due to the vibration of Si-O groups. All of these bands revealed that APTES and TEOS were successfully grafted onto the surface of the L-cys-capped CdSe/ZnS QDs.

3.3. HRTEM analysis

Modification of the surface of QDs with MIP was further confirmed by HRTEM analysis. The HRTEM images of original L-cys-CdSe QDs, L-cys-CdSe/ZnS QDs, MIP@QDs and NIP@QDs are shown in Fig. 2A–D. They all had a nearly spherical morphology and were well dispersed in the aqueous solution. The estimated average particle size distributions of the QDs were 2.1 ± 0.5 and 5.1 ± 0.8 nm (average particle size \pm standard deviation) for L-cys-CdSe QDs and L-cys-CdSe/ZnS QDs respectively. The diameters of MIP@QDs increased after coating with APTES to 6.2 ± 0.9 nm in comparison with core/shell QDs. NIP@QDs particles were also spherical and monodispersed in the solution with the size of 5.6 ± 0.4 nm. It is thus expected that any difference in AC

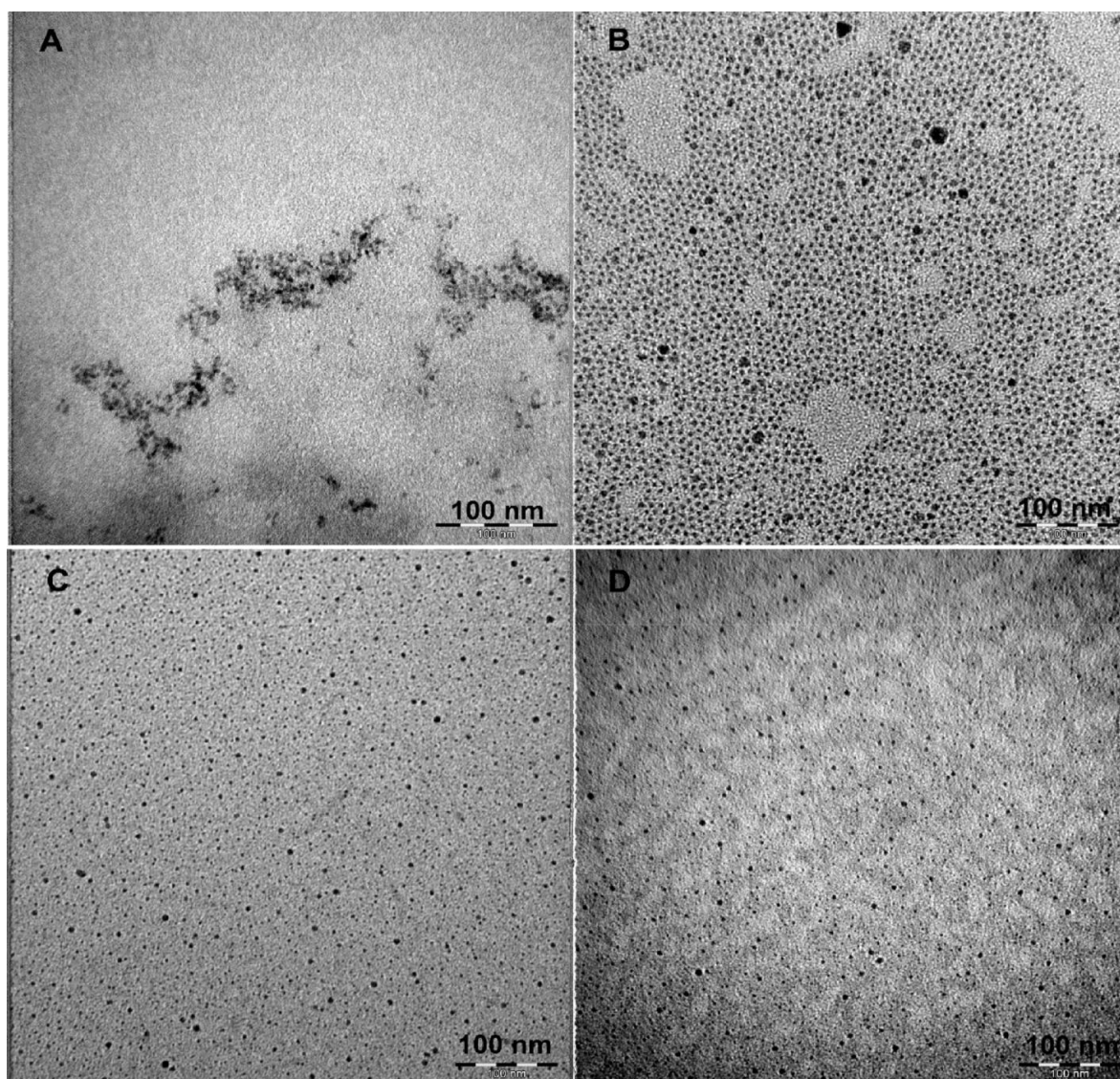


Fig. 2. HRTEM images of (A) L-cys-CdSe QDs (B) L-cys-CdSe/ZnS QDs (C) MIP@QDs and (D) NIP@QDs.

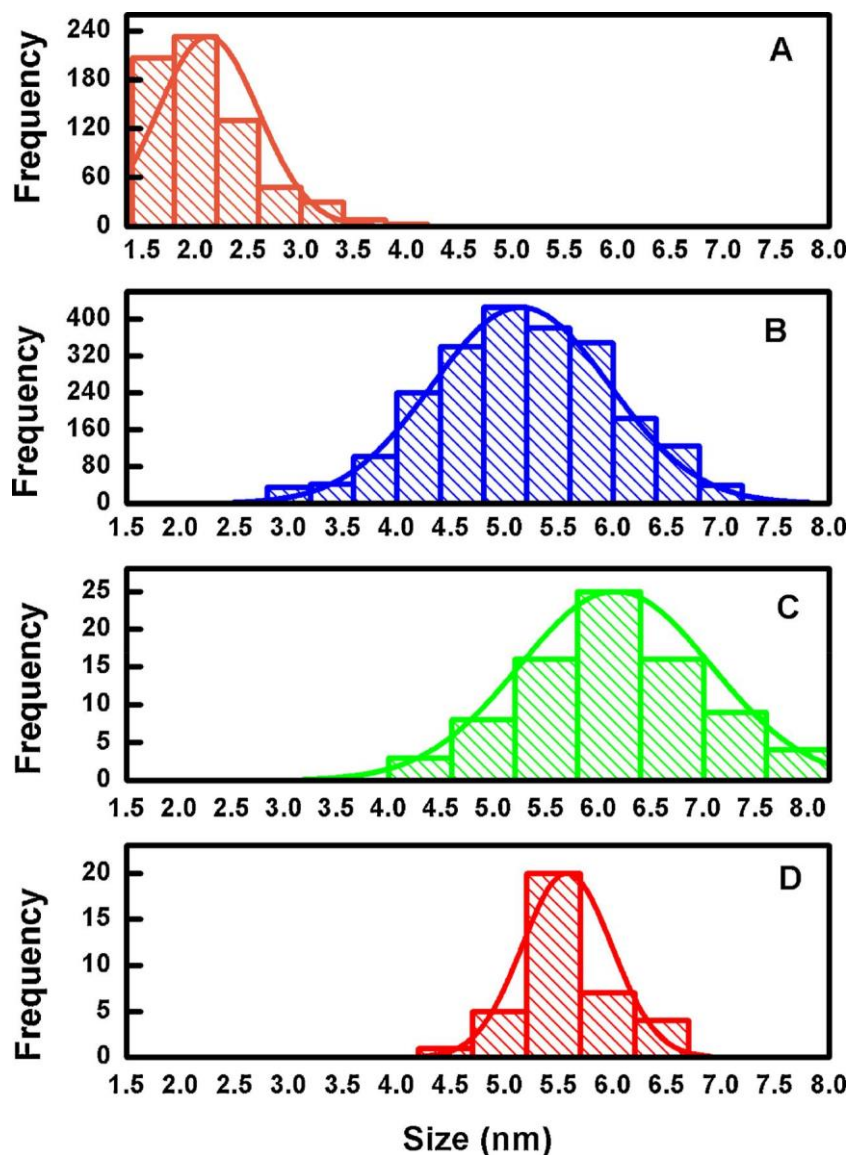


Fig. 3. Size distribution histogram of (A) L-cys-CdSe QDs (B) L-cys-CdSe/ZnS QDs, (C) MIP@QDs and (D) NIP@QDs.

recognition behavior between MIP@QDs and NIP@QDs is due to the imprinting factor rather than a morphological difference. As an indirect approach [36], the shell thickness of silica was calculated by subtracting the average particle size of MIP@L-cys-CdSe/ZnS QDs from L-cys-CdSe/ZnS QDs which was estimated to be 0.55 nm. The size distribution of L-cys-CdSe QDs, L-cys-CdSe/ZnS QDs, MIP@QDs and NIP@ QDs are shown in Fig. 3A–D.

3.4. EDS analysis

EDS analysis was carried out to confirm the presence of the metal components within the MIP@QDs and NIP@QDs structures (Fig. S3 A and B). Similar spectra were obtained, where the presence of Cd, Se, Zn and S showed the presence of core/shell QDs in both cases, while the additional Si and O signals provided evidence for the presence of the polymer. The approximate elemental composition for MIP@QDs was Si (14%), O (43%) and NIP@QDs was Si (14%) and O (46%) which provided evidence for successful polymerisation.

3.5. TGA analysis

Thermogravimetric (TG) and derivative thermogravimetric (DTG) analysis were conducted on the washed MIP@QDs and NIP@QDs (Fig. 4). A mass loss of approximately 6% and 9% occurred for the washed MIP@QDs and NIP@QDs polymers at 68 °C and 65 °C respectively, which was probably due to the remaining adsorbed absolute ethanol from the template removal step [37]. At 111 °C, the loss of residual water occurred which produced a 20% mass loss of the washed polymers. The mass of the polymers decreased sharply from ~450 °C to ~550 °C due to the degradation of the carbon skeleton of the polymers. The washed NIP@QDs showed a slightly higher overall mass loss compared to the washed MIP@QDs which were 39% and 37% respectively. The difference might have been caused by structural variations arising from the template removal process and the difference in the coating thicknesses of the washed MIP@QDs and NIP@QDs [38,39]. Further increase in temperature from 700 °C to 1200 °C showed no mass loss for both the washed MIP@QDs and NIP@QDs.

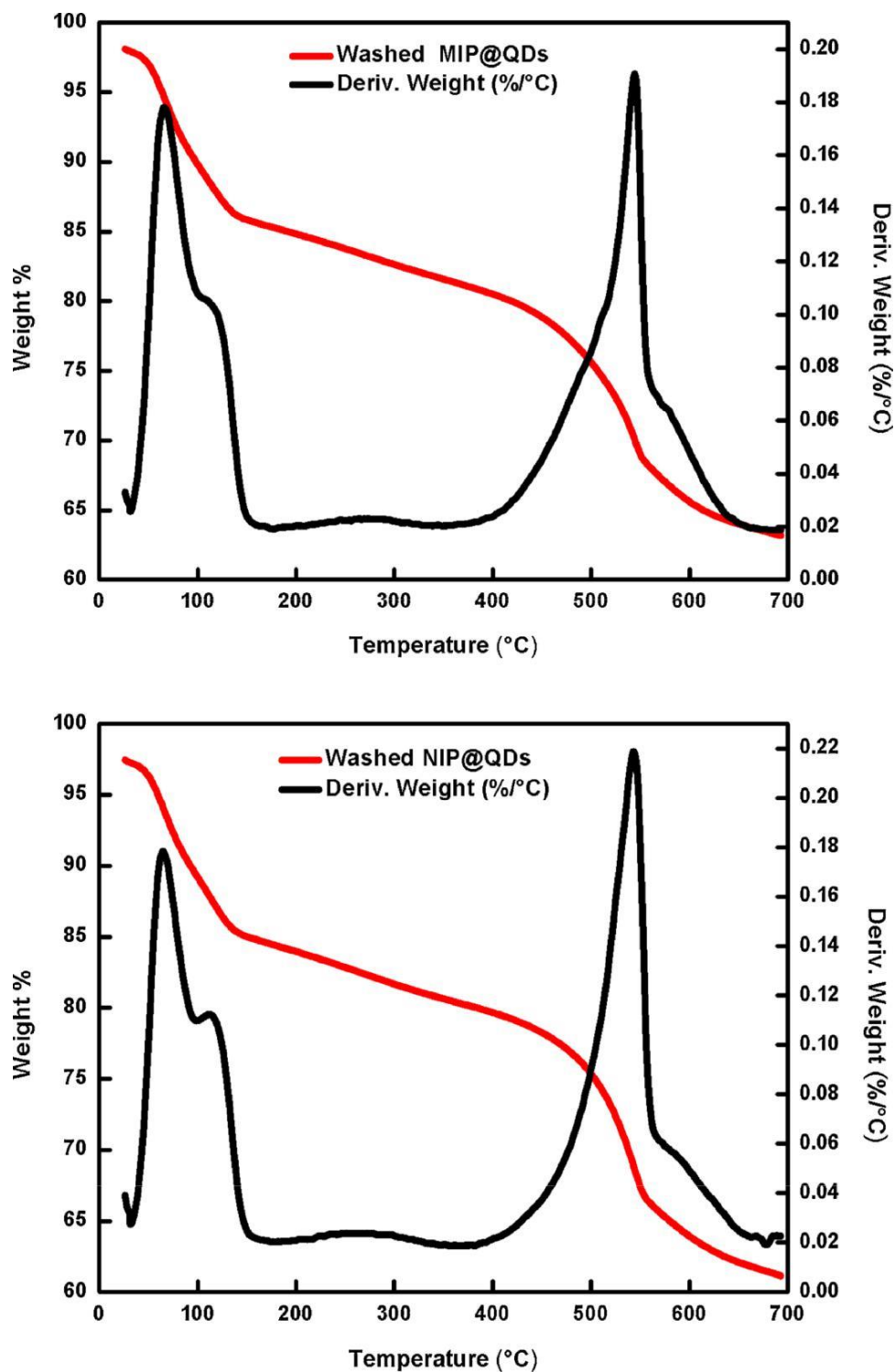


Fig. 4. Thermogravimetric analysis of the synthesized MIP@QDs and NIP@QDs.

3.6. Optimization of sensing variables

The aim of this work was to develop a sensor material which is selective and sensitive towards AC molecules. The effects of MIP@QDs concentration and incubation time on the fluorescence quenching of MIP@QDs were thus studied in order to optimize these experimental variables and allow for control thereof in subsequent application experiments.

3.6.1. Concentration of MIP@QDs

The amount of MIP@QDs was varied from 0.2 to 1.2 mg in 3.0 mL of Millipore water and a fixed concentration of AC was used ($300.0 \text{ nmol L}^{-1}$). The highest degree of quenching was achieved at the concentration of 0.8 mg in 3.0 mL (Fig. 5) which was therefore used for subsequent experiments. At higher concentrations (over 1.0 mg in 3.0 mL) possible self-quenching occurs thus only concentrations of MIP@QDs below 1.0 mg in 3.0 mL were investigated.

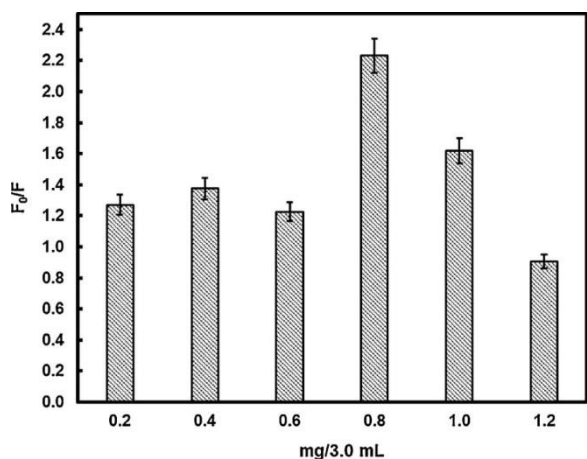


Fig. 5. Effect of the MIP@QD concentration on PL quenching efficiency ($n = 3$). The concentration of AC was fixed at $300.0 \text{ nmol L}^{-1}$. The experimental conditions were excitation wavelength 350 nm ; slit widths of excitation and emission, 5.0 nm .

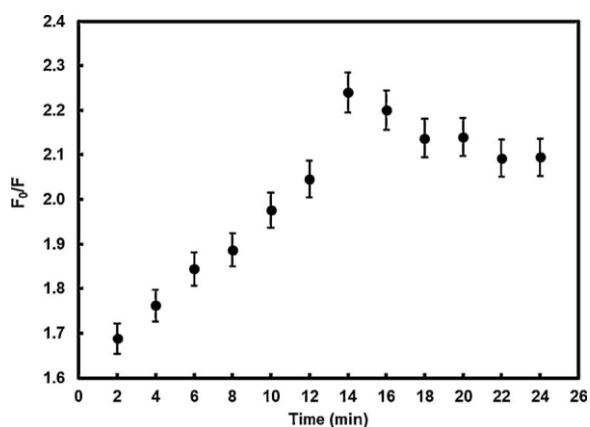


Fig. 6. Effect of incubation time on relative fluorescence of MIP@QDs with AC ($n = 3$). The experimental conditions were MIP@QDs: 0.8 mg in 3.0 mL^{-1} ; AC: $300.0 \text{ nmol L}^{-1}$; excitation wavelength, 350 nm ; slit widths of excitation and emission, 5 nm .

3.6.2. Effect of incubation time

The experimental results for the incubation time of MIP@QDs at a fixed concentration of AC showed a notable increase up to 14 min and thereafter decreased slightly (Fig. 6). Not only did the recognition cavities in the structure of MIP@QDs provide high accessibility for AC, but it can also be seen from the HRTEM images that the imprinting silica layer was ultrathin ($\sim 0.55 \text{ nm}$) which facilitated fast response of the MIP@QDs to AC [40]. Therefore 0.8 mg of MIP@QDs in 3.0 mL and an incubation time of 14 min were chosen for subsequent experiments.

3.7. Photostability study

The photostability of MIP@QDs was investigated over 40 min which showed no significant change in PL intensity (Fig. 7). It is known that when QDs are entrapped in silica layers, they may be protected from the environment and the fluorescence lifetime will be longer than without a silica shield [41]. In addition, carboxyl groups around L-cys-QDs can interact with the amino groups of APTES resulting in tight binding of the QDs in the polymer layer. As a result, the fluorescence emission of MIP@QDs did not decrease significantly over time [41]. Fluorescence stability was investigated up to 40 min as the highest relative fluorescence intensity of MIP@QDs towards AC was achieved after only 14 min.

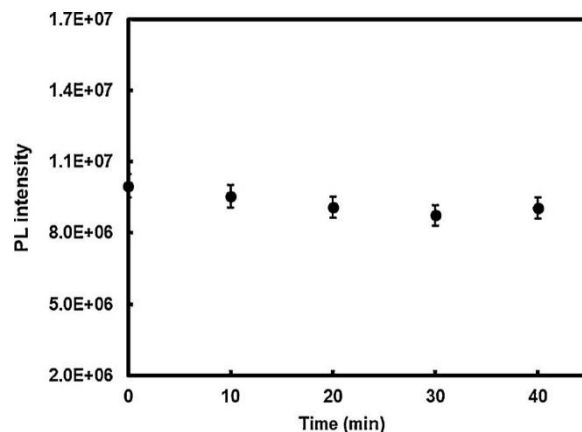


Fig. 7. Photostability of MIP@QDs over 40 min (values are the average of three measurements). The experimental conditions were MIP@QDs, 0.8 mg in 3.0 mL ; excitation wavelength, 350 nm ; slit widths of excitation and emission, 5.0 nm .

The stabilities of MIP@QDs and NIP@QDs were then evaluated over 5 days. The FL intensity of MIP@QDs was stable for 2 days, and then declined slightly over the next 3 days, while the change in fluorescence intensity of NIP@QDs over 5 days was not significant (Fig. S4). Therefore the prototype polymer displayed acceptable storage stability over time which indicated effective protection of L-cys-CdSe/ZnS QDs by the silica layers of the polymer.

3.8. Fluorescence sensing of acetaminophen using AC-templated molecularly imprinted polymer-quantum dots

AC-templated MIP@QDs were prepared and used as a homogenous fluorescence sensing platform for the determination of AC in aqueous media under optimized conditions of 0.8 mg MIP@QDs in 3.0 mL^{-1} with an incubation time of 14 min. The functional groups ($-\text{NH}_2$) of the silica shell interact with the AC molecules via hydrogen bonding during the synthesis process. After removing AC molecules via solvent extraction, imprinted binding cavities remained in the nanoparticle material that enabled rebinding of the AC molecules selectively.

The binding affinity of MIP@QDs and NIP@QDs towards different concentrations of AC were investigated by fluorescence analysis (Fig. 8A and B). The quenching mechanism can be described according to the Stern-Volmer equation [31]:

$$\frac{F_0}{F} = 1 + K_{SV} [Q]$$

Here F_0 and F are the fluorescence intensities in the absence and presence of the quencher, respectively, K_{SV} is the quenching constant of the quencher, and $[Q]$ is the concentration of the quencher.

With the introduction of AC, the fluorescence intensity of the MIP@QDs was quenched linearly in the concentration range of $1.0\text{--}300 \text{ nmol L}^{-1}$ (Fig. 8A) with detection and quantification limits of 0.34 and 1.1 nmol L^{-1} respectively. The limit of detection (LOD) and quantification (LOQ) are defined by $3\delta/m$ and $10\delta/m$, where δ is the standard deviation of the blank measurement ($n = 10$) and m is the slope of the calibration curve. The LOD value is lower than the guidance value of $1.3 \times 10^3 \text{ nmol L}^{-1}$ (200 ppb) for acetaminophen in drinking water given by the Minnesota Department of Health (MDH) [42].

As a comparison, the binding affinity of NIP@QDs was also examined with different concentrations of AC (Fig. 8B). It was observed that the NIP@QDs could not bind AC as effectively, resulting in lower sensitivity with detection and quantification limits of 10.0 and 33.0 nmol L^{-1} respectively. The decrease of fluorescence intensity of the MIP@QDs was considerably more than for NIP@QDs at the same concentration of AC indicating better quenching efficiency of MIP@QDs

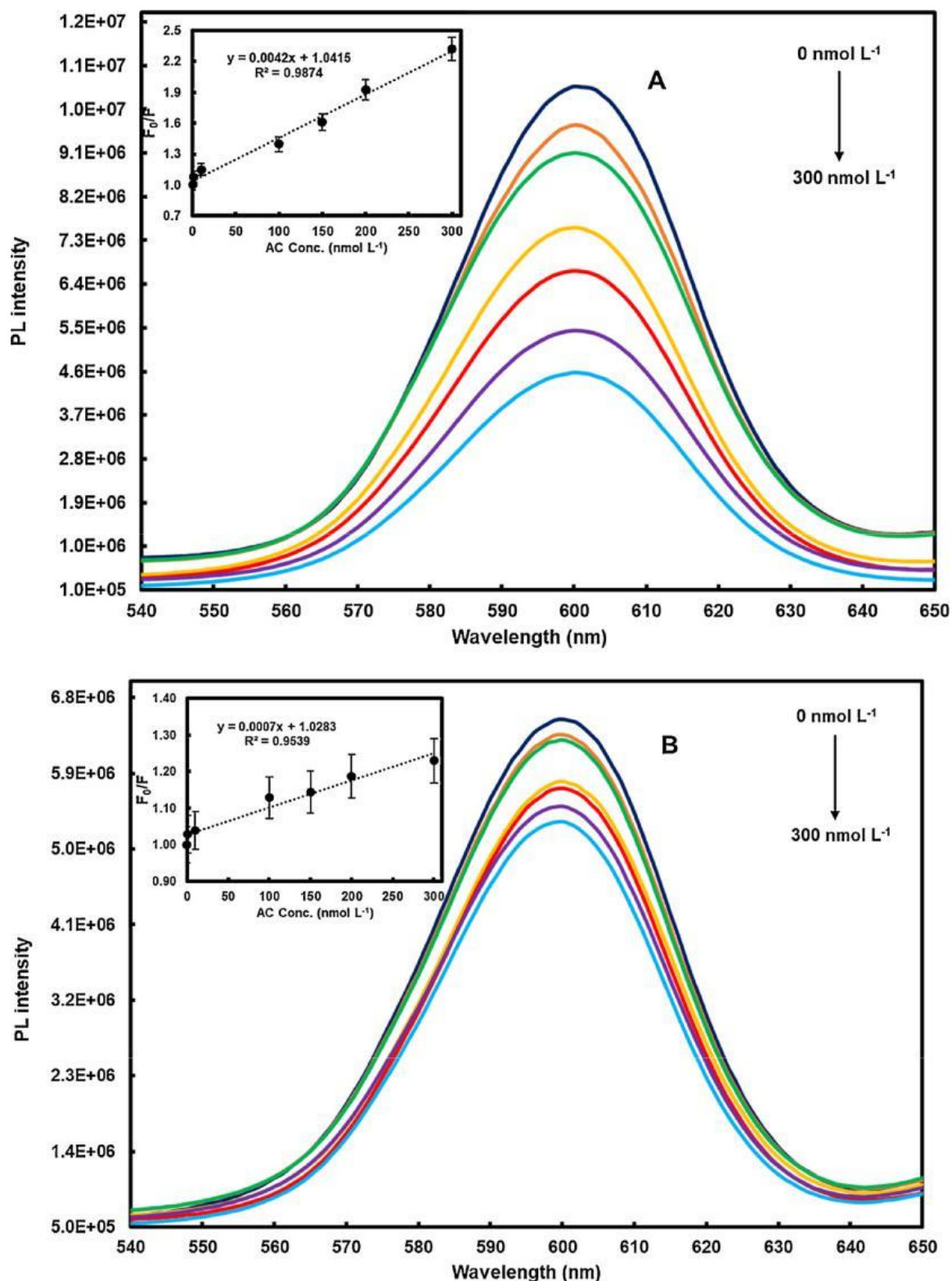


Fig. 8. Fluorescence emission spectra of MIP@QDs (A) and NIP@QDs (B) in the presence of varying concentrations of AC. The experimental conditions were MIP@ QDs or NIP@QDs at 0.8 mg in 3.0 mL; excitation wavelength, 350 nm; slit widths of excitation and emission, 5 nm. The inset graphs display the corresponding Stern–Volmer plots of MIP@QDs and NIP@QDs with the addition of AC (all results are the average of three replicates).

and thus an increasing in spectral sensitivity of MIP@QDs to AC. Furthermore, due to the absence of specific recognition cavities in the structure of NIP@QDs, AC could not entrap properly into the polymer and only the QDs located on the proximity of the surface of the NIP@ QDs could be quenched. Consequently, the fluorescence intensity of

many of the QDs is expected to have remained unchanged [28,43].

The imprinting factor is of great importance in estimating the selectivity of imprinted materials which is defined as the ratio of $K_{SV,MIP}$ to $K_{SV,NIP}$. Under optimum conditions, a high imprinting factor of 6.0 was found in this study, indicating that the MIP@QDs possessed higher

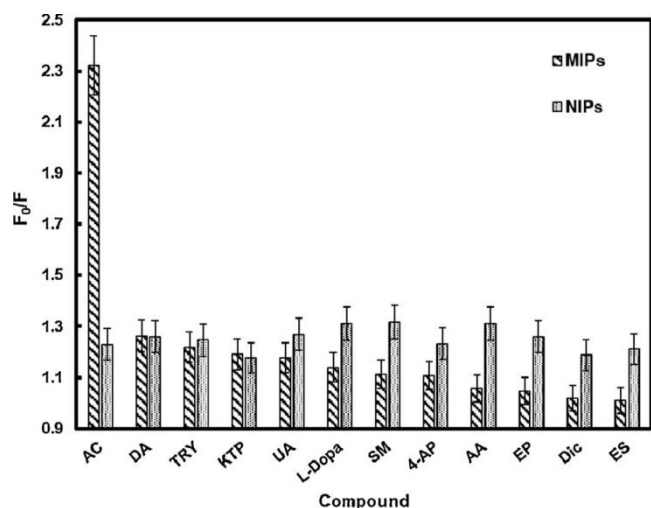


Fig. 9. Fluorescence quenching of MIP@QDs and NIP@QDs by different ana-lytes at $300.0 \text{ nmol L}^{-1}$. The experimental conditions were MIP@QDs, or NIP@ QDs 0.8 mg in 3.0 mL ; excitation wavelength 350 nm ; 5 nm excitation and emission slit widths. L-tryptophan (TRY), ascorbic acid (AA), epinephrine hy-drochloride (EP), uric acid (UA), dopamine hydrochloride (DA), ketoprofen (KTP), sulfamethoxazole (SM), diclofenac sodium salt (Dic), estradiol (ES), L-3,4-dihydroxyphenylalanine (L-Dopa) and 4-aminophenol (4-AP) (results are the average of three replicates).

molecular selectivity and sensing specificity than NIP@QDs. Generally, AC can bind to the $-\text{NH}_2$ groups at the surface of MIP@QDs and NIP@ QDs through hydrogen bonds. Although both MIP@QDs and NIP@QDs showed fluorescence quenching in the presence of AC, for the MIP@ QDs, the specific binding affinity of the imprinted cavities played an important role in the fluorescence quenching while non-specific adsorption was the likely cause of fluorescence quenching in NIP@QDs [27], which is supported by the poorer reproducibility (larger standard deviation) of the NIP@QDs measurements (refer to Fig. 8B).

Reproducibility is an important factor for the application of MIP@ QDs. For three replicate detections of AC with three AC-imprinted sensing materials under optimum conditions, the precision was 3.7% (relative standard deviation).

3.9. Selectivity of the sensor to AC

The selectivity of MIP@QDs was examined towards different analytes with similar structures to AC, including vitamins (AA), catecholamines (EP, DA, L-Dopa), aminophenols (4-AP), analgesics and antipyretics (KTP, Dic), antiseptics (SM), essential amino acids (TRY), hormones (ES) and UA (Table S1). Significant fluorescence quenching was observed for the MIP@QDs in the presence of AC (Fig. 9), while this response was not as significant for the other analytes. During the synthesis of MIP@QDs, well-defined imprinted cavities with the shape and size of AC were produced on the surface of the MIP@QDs, allowing for interaction of AC with the rebinding sites of the prototype MIP@ QDs through hydrogen bonds causing a noticeable fluorescence change. In other words, the imprinted cavities left by the removal of the template provided easier access to the recognition sites for AC molecules [31].

In spite of the fact that other analytes could produce hydrogen bond interactions with APTES on the surface of MIP@QDs resulting in the fluorescence quenching, they were not complementary to the recognition sites of the MIP in terms of functionality, size and shape of the template. Therefore, the imprinted cavities of MIP@QDs were not ap-propriate to accommodate other analytes thus significantly less fluor-escence quenching was observed.

Moreover, the difference in spatial structure, molecular weight and interaction with APTES between AC and its analogues can cause this difference [28]. The hydroxyl group of AC in the para position acted as electron donor through π bonds, i.e., through resonance structures with a double bond to oxygen (positive mesomeric effect), while DA had another hydroxyl group in the meta position which had electron-withdrawing properties through sigma bonds (negative inductive effect). Therefore DA could bind to the imprinting sites and cause fluorescence quenching to some extent but not as much as that of AC. As for L-Dopa and EP, electron withdrawing effects of the hydroxyl group in the meta position could weaken hydrogen bonding with APTES. In addition, the size and spatial structure of L-Dopa and EP were different to those of the recognition cavities. Regarding TRY, KTP, ES and AA, molecular weight, size and spatial structure resulted in much less fluorescence quenching compared to AC. Low fluorescence quenching of UA, Dic and SM might be due to the absence of hydroxyl functional groups in their structures as well as the difference in the size and shape

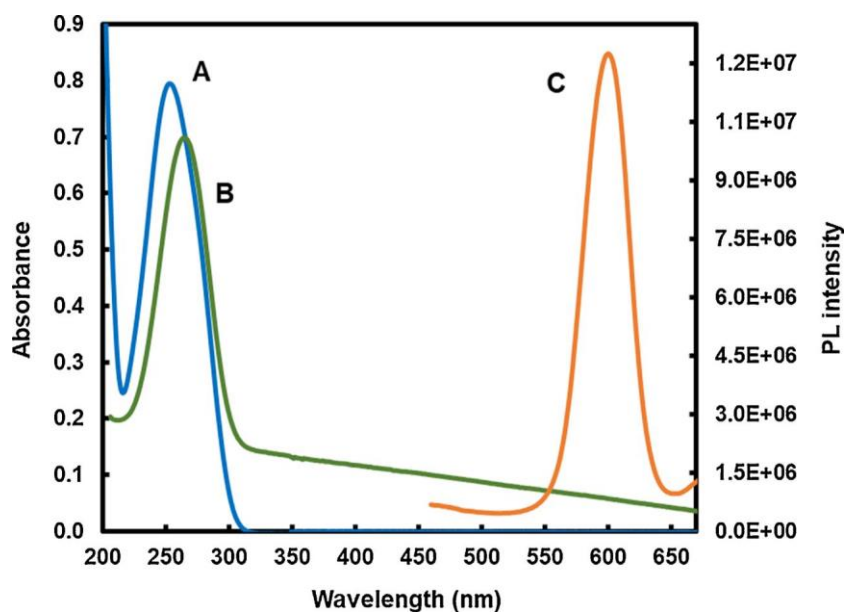
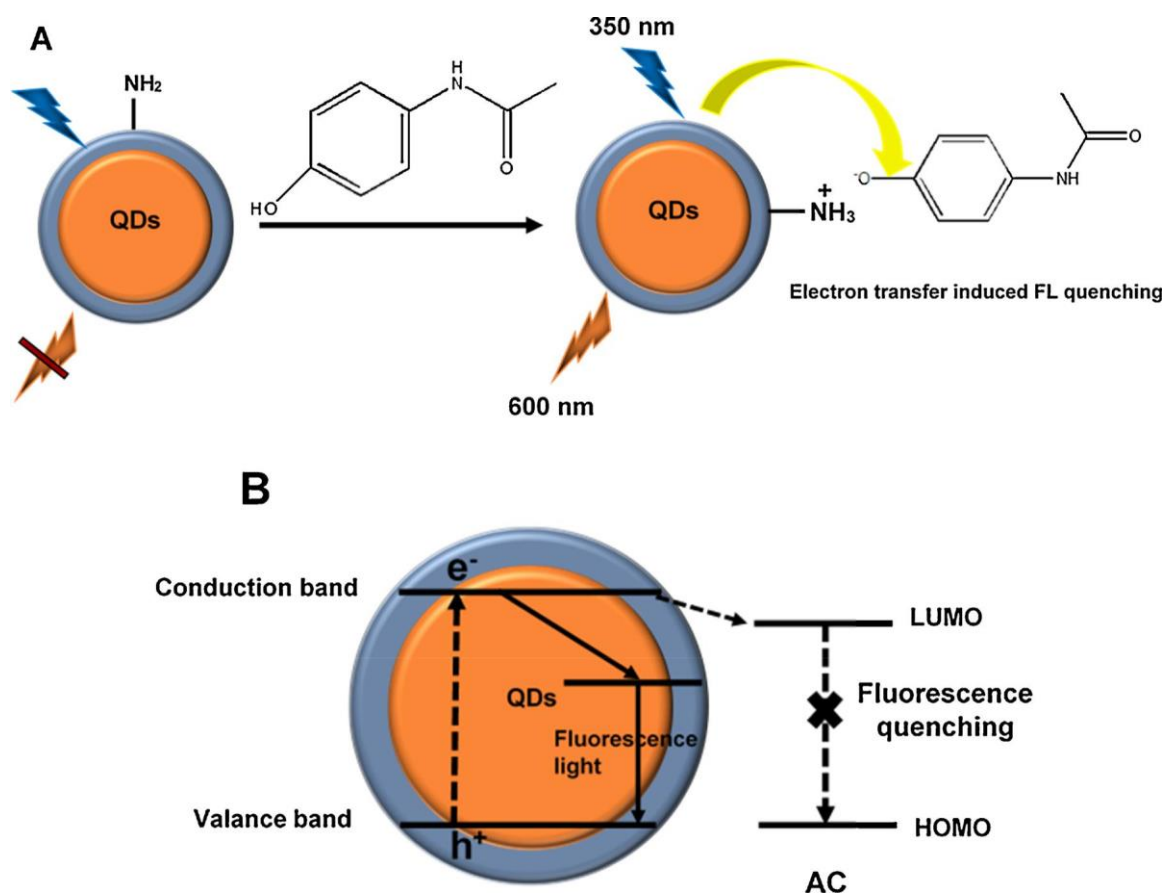


Fig. 10. UV/Vis absorption spectrum of AC (A) and MIP@QDs (B) and fluorescence emission spectrum of MIP coated QDs (C).



Scheme 3. (A) Schematic representation of the MIP@QDs fluorescence quenching mechanism based on electron transfer-induced energy transfer and (B) schematic of the fluorescence quenching of MIP@QDs according to molecular orbital theory (B).

of these compounds compared to AC, which caused very weak binding with imprinting cavities. Furthermore, the presence of a chloride group in the structure of Dic can reduce the strength of hydrogen bonding. With respect to 4-AP, it could only form two hydrogen bond interactions while AC possessed three positions for hydrogen bonding and the size of 4-AP is smaller than AC to fit in the recognition sites. Consequently, the following order of fluorescence quenching was found: AC > DA > TRY > KTP > UA > L-Dopa > SM > 4-AP > AA > EP > Dic > ES.

Fig. 9 also shows the quenching of NIP@QDs with AC and the other analytes. In this case there was much less of a difference between the sensor response to AC and other competitive compounds, i.e. significantly less selectivity. These results revealed the higher selectivity of MIP@QDs to AC molecules which thus provided a selective fluorescence response.

3.10. Proposed sensing mechanism of the MIP-capped CdSe/ZnS QDs

Fluorescence resonance energy transfer (FRET) from MIP@QDs to AC can be excluded as there is no spectral overlap between the absorption spectra of AC and the fluorescence emission of the MIP@QDs (Fig. 10 A and C). A Meisenheimer complex could form between AC and the amino group of APTES, as shown in Scheme 3A [28,34], which could consequently lead to energy transfer from the MIP@QDs to this complex and fluorescence quenching of the MIP@QDs as a result.

In addition, the UV–vis absorption of AC was located at 253 nm (Fig. 10A) which is near the band gap of MIP@QDs at 264 nm (Fig. 10B). Therefore, in the presence of AC, an excited electron may directly transfer from the conduction band of MIP@QDs to the lowest unoccupied molecular orbital (LUMO) of AC (Scheme S1 in the

Supplementary Information) followed by non-radiative relaxation (Scheme 3B).

Such a charge transfer mechanism has been also reported by Jia et al. in the case of SiO₂@QDs@mesoporous-MIPs for the fluorescence determination of 2,4-dichlorophenoxyacetic acid [28] and Yu et al. for the determination of 4-nitrophenol via molecularly imprinted polymer coated thioglycolic acid capped CdTe QDs [25].

3.11. Practical application and performance comparison

The synthesized MIP@QDs were applied to determine AC in real water samples. HPLC-MS/MS analysis was also performed as a comparative method which confirmed that the background concentration of AC in the tap and river water samples was below the detection limit of 150.0 ng L⁻¹. As AC was not present in these samples, they were spiked

Table 1

Spiked recovery results for the determination of AC in water samples using 2 mL of 0.8 mg of MIP@QDs in 3 mL of Millipore water and 200 μL of AC standard solution (n = 3).

Sample	Spiked AC (nmol L ⁻¹)	Determined AC (mean ± RSD; n = 3, nmol L ⁻¹)	Recovery (%)
Tap water	50	52.0 ± 0.1	104
	150	146.0 ± 0.4	97
	300	320.0 ± 0.1	107
River water	50	57.0 ± 0.3	114
	150	142.0 ± 0.01	95
	300	301.0 ± 0.1	100

Table 2

Comparison of the proposed fluorescence method with other recently reported methods for AC determination in water samples.

Sensor system	Linear range (nmol L ⁻¹)	LOD (nmol L ⁻¹)	Sample matrix	Reference
CS/CPE	8.0 × 10 ² –2.0 × 10 ⁵	7.1 × 10 ²	River water	[4]
(SWV)	4.0 × 10 ⁵ –1.0 × 10 ⁶	6.8 × 10 ²	Seawater	[44]
HPLC-DAD	3.8 × 10 ¹ –3.9 × 10 ²	< 66.2	Surface water	
Biocatalytic spectrophotometry	2.0 × 10 ³ –1.4 × 10 ⁴	390.3	Wastewater influent	[6]
MWCNT/PE/surfactant (DPV)	1.5 × 10 ⁴ –1.8 × 10 ⁵	5.5 × 10 ²	Potable, tap water and treated wastewater effluent	
MWCNT/PE/surfactant (SWV)	1.5 × 10 ⁴ –1.2 × 10 ⁵	3.0 × 10 ²	Tap and domestic wastewater	[45]
MIP-capped L-cys CdSe/ZnS QDs	1.0–300	4.4 × 10 ³	Tap and river water	This work

CS/CPE, Chitosan modified carbon paste electrode; DPV, Differential pulse voltammetry; HPLC-DAD, High-performance liquid chromatography-diode array detector; LOD, Limit of detection; MWCNT/PE/surfactant, Multi-walled carbon nanotubes/paste electrode in the presence of a surfactant; SWV, Square wave voltammetry.

with three different concentrations of AC. The fluorescence of the MIP@QDs was notably quenched upon addition of the samples, suggesting the existence of imprinted cavities with the size and shape of AC molecules. The average triplicate value of the pH of MIP@QDs in Millipore water was 6.935 while after injecting 200 µL of river or tap water into 2 mL of MIP@QDs (containing 0.53 mg of MIP@QDs), the pH changed to 7.062 and 6.952 respectively. Therefore, no significant changes occurred in the pH of the MIP@QDs upon the addition of real water samples and the effect of sample pH can be considered negligible.

For each sample, the experiments were conducted three times at three spiking levels and the recoveries varied from 95% to 114% (Table 1), indicating the potential application of the prototype sensor for the determination of AC in real water samples.

Although numerous studies have been reported regarding the detection of AC in different matrices, there are limited reports for water samples. However, the performance of the synthesized MIP@QDs AC sensor with that of other reported methods for real water samples are compared in Table 2.

Although the linear range is smaller compared to square wave voltammetry, for example, both the selectivity and sensitivity of the developed MIP@QDs sensor have been markedly enhanced (LOD = 0.34 nmol L⁻¹) compared to other reported methods. As a new material, our developed MIP@QDs fluorescence sensor is thus a promising candidate for the selective and sensitive detection of AC in water.

4. Conclusion

The nano-molar level fluorescence detection of AC was achieved with the utilization of L-cys-CdSe/ZnS QDs embedded in a MIP, likely via a charge transfer induced fluorescence quenching process from MIP@QDs to AC. The structures of QDs, MIP@QDs and NIP@QDs were characterized by fluorescence spectroscopy, FTIR, HRTEM and TGA. EDS analysis also confirmed the presence of silica in the structure of the sensor material. Quenching of the photoluminescence of the synthesized MIP@QDs enabled the determination of AC at concentrations as low as 0.34 nmol L⁻¹ and over the linear concentration range of 1.0–300 nmol L⁻¹. The prepared MIP@QDs were highly selective to AC with outstanding reproducibility (3.7%). The simple and economical preparation of the MIP@QDs, good photostability as well as selectivity towards AC, allowed for this novel sensor material to be successfully applied in the analysis of nanomolar concentrations of AC in water samples with recoveries of 95% to 114%.

Data availability statement

Additional raw/processed data required to reproduce these findings is available on request.

Acknowledgments

Funding from the University of Pretoria, the Water Research Commission (Grant K5/2438/1 and K5/2752) and the Photonics Initiative of South Africa (Grant PISA-15-DIR-06) is gratefully acknowledged. We thank the Microscopy and Microanalysis Laboratory of the University of Pretoria, for their assistance with microscopy measurements and Wiebke Grote, Lielzel van der Merwe and Marilé Landman of UP for assistance with XRD and TGA measurements and molecular modeling, respectively.

Appendix A. Supplementary data

Supplementary material related to this article can be found, in the online version, at doi:<https://doi.org/10.1016/j.mtcomm.2018.10.007>.

References

- [1] B.C. Lourencao, R.A. Medeiros, R.C. Rocha-Filho, L.H. Mazo, O. Fatibello-Filho, *Talanta* 78 (2009) 748–752.
- [2] E.A. Frick, A.K. Henderson, D.M. Moll, E.T. Furlong, M.T. Meyer. In: K.J. Hatcher, editor. *Proceedings of the 2001 Georgia Water Resources Conference*, March 26–27, at the University of Georgia, Athens, Georgia: Institute of Ecology, The University of Georgia, 2001.
- [3] K. Kümmerer, *Introduction: pharmaceuticals in the environment*, *Pharmaceuticals in the Environment*, Springer, 2001, pp. 1–8.
- [4] Y.E.L. Bouabi, A. Farahi, N. Labjar, S. El Hajjaji, M. Bakasse, M.A. El Mhammedi, *Mater. Sci. Eng. C* 58 (2016) 70–77.
- [5] E. Gracia-Lor, J.V. Sancho, F. Hernández, *J. Chromatogr. A* 1217 (2010) 622–632.
- [6] A. Méndez-Albores, C. Tarin, G. Rebollar-Pérez, L. Dominguez-Ramirez, E. Torres, *J. Environ. Sci. Health A* 50 (2015) 1046–1056.
- [7] L. Li, R. Bian, Y. Ding, M. Yu, D. Yu, *Mater. Chem. Phys.* 113 (2009) 905–908.
- [8] M.N. Rhyner, A.M. Smith, X. Gao, H. Mao, L. Yang, S. Nie, *Nanomedicine* 1 (2006) 209–217.
- [9] W.Y. William, E. Chang, R. Drezek, V.L. Colvin, *Biochem. Biophys. Res. Commun.* 348 (2006) 781–786.
- [10] M.F. Frasco, N. Chaniotakis, *Sensors* 9 (2009) 7266–7286.
- [11] A.J. Nozik, M.C. Beard, J.M. Luther, M. Law, R.J. Ellingson, J.C. Johnson, *Chem. Rev.* 110 (2010) 6873–6890.
- [12] S. Jin, Y. Hu, Z. Gu, L. Liu, H.-C. Wu, *J. Nanomater.* 2011 (2011) 1–13.
- [13] F.D. De Menezes, A.G. Brasil, W.L. Moreira, L.C. Barbosa, C.L. Cesar, R.C. Ferreira, P.M.A. De Farias, B.S. Santos, *Microelectron. J.* 36 (2005) 989–991.
- [14] H. Huang, J.-J. Zhu, *Analyst* 138 (2013) 5855–5865.
- [15] Y. Su, Y. He, H. Lu, L. Sai, Q. Li, W. Li, L. Wang, P. Shen, Q. Huang, C. Fan, *Biomaterials* 30 (2009) 19–25.
- [16] R.E. Galian, M. de la Guardia, *Trends Anal. Chem.* 28 (2009) 279–291.
- [17] L. Chen, X. Wang, W. Lu, X. Wu, J. Li, *Chem. Soc. Rev.* 45 (2016) 2137–2211.
- [18] X. Wang, J. Yu, J. Li, Q. Kang, D. Shen, L. Chen, *Sens. Actuators B Chem.* 255 (2018) 268–274.
- [19] X. Wang, S. Yu, W. Liu, L. Fu, Y. Wang, J. Li, L. Chen, *ACS Sens* 3 (2018) 378–385.
- [20] L. Chen, S. Xu, J. Li, *Chem. Soc. Rev.* 40 (2011) 2922–2942.
- [21] L. Li, Y. Lu, Y. Ding, Y. Cheng, W. Xu, F. Zhang, *J. Fluoresc.* 22 (2012) 591–596.
- [22] Y. Tan, Z. Zhou, P. Wang, L. Nie, S. Yao, *Talanta* 55 (2001) 337–347.
- [23] G. Zhao, L. Yang, S. Wu, H. Zhao, E. Tang, C.P. Li, *Biosens. Bioelectron.* 91 (2017) 863–869.
- [24] M. Bahram, S. Alizadeh, T. Madrakian, *Sens. Lett.* 14 (2016) 127–133.
- [25] J. Yu, X. Wang, Q. Kang, J. Li, D. Shen, L. Chen, *Environ. Sci. Nano.* 4 (2017) 493–502.

- [26] H. Montaseri, P.B. Forbes, *Spectrochim. Acta A Mol. Biomol. Spectrosc.* 204 (2018) 370–379.
- [27] L. Jiang, H. Liu, M. Li, Y. Xing, X. Ren, *Anal. Methods* 8 (2016) 2226–2232.
- [28] M. Jia, Z. Zhang, J. Li, H. Shao, L. Chen, X. Yang, *Sens. Actuators B. Chem.* 252 (2017) 934–943.
- [29] L. Madikizela, N. Tavengwa, V. Pakade, *Molecularly imprinted polymers for pharmaceutical compounds: synthetic procedures and analytical applications*, *Recent Research in Polymerization, InTech*, 2018.
- [30] K. Chullasat, P. Nurerk, P. Kanatharana, F. Davis, O. Bunkoed, *Sens. Actuators B.* 254 (2018) 255–263.
- [31] H. Li, Y. Li, J. Cheng, *Chem. Mater.* 22 (2010) 2451–2457.
- [32] L.-W. Wang, *J. Phys. Chem. B* 105 (2001) 2360–2364.
- [33] S.A. Empedocles, M.G. Bawendi, *Science* 278 (1997) 2114–2117.
- [34] S. Xu, H. Lu, J. Li, X. Song, A. Wang, L. Chen, S. Han, *ACS Appl. Mater. Interfaces* 5 (2013) 8146–8154.
- [35] M.-R. Chao, C.-W. Hu, J.-L. Chen, *Microchim. Acta.* 181 (2014) 1085–1091.
- [36] C.-T. Cheng, C.-Y. Chen, C.-W. Lai, W.-H. Liu, S.-C. Pu, P.-T. Chou, Y.-H. Chou, H.-T. Chiu, *J. Mater. Chem.* 15 (2005) 3409–3414.
- [37] G. Székely, J. Bandarra, W. Heggie, F.C. Ferreira, B. Sellergren, *Sep. Purif. Technol.* 86 (2012) 190–198.
- [38] S.S. Zunngu, L.M. Madikizela, L. Chimuka, P.S. Mdluli, *Comp. Rendus Chim.* 20 (2017) 585–591.
- [39] Z. Xia, Z. Lin, Y. Xiao, L. Wang, J. Zheng, H. Yang, G. Chen, *Biosens. Bioelectron.* 47 (2013) 120–126.
- [40] X. Wang, J. Yu, Q. Kang, D. Shen, J. Li, L. Chen, *Biosens. Bioelectron.* 77 (2016) 624–630.
- [41] H.D. Duong, C.V.G. Reddy, J.I. Rhee, T. Vo-Dinh, *Sens. Actuators B Chem.* 157 (2011) 139–145.
- [42] **Toxicological Summary for: Acetaminophen, (2010)** Retrieved from www.health.state.mn.us/divs/eh/risk/guidance/dwec/sumacetamin.pdf.
- [43] X. Wang, J. Yu, X. Wu, J. Fu, Q. Kang, D. Shen, J. Li, L. Chen, *Biosens. Bioelectron.* 81 (2016) 438–444.
- [44] F.O. Agunbiade, B. Moodley, *Environ. Monit. Assess.* 186 (2014) 7273–7291.
- [45] F.A. Gorla, E.H. Duarte, E.R. Sartori, C.R.T. Tarley, *Microchem. J.* 124 (2016) 65–75.

4.3.1 Paper 5 - Supplementary information

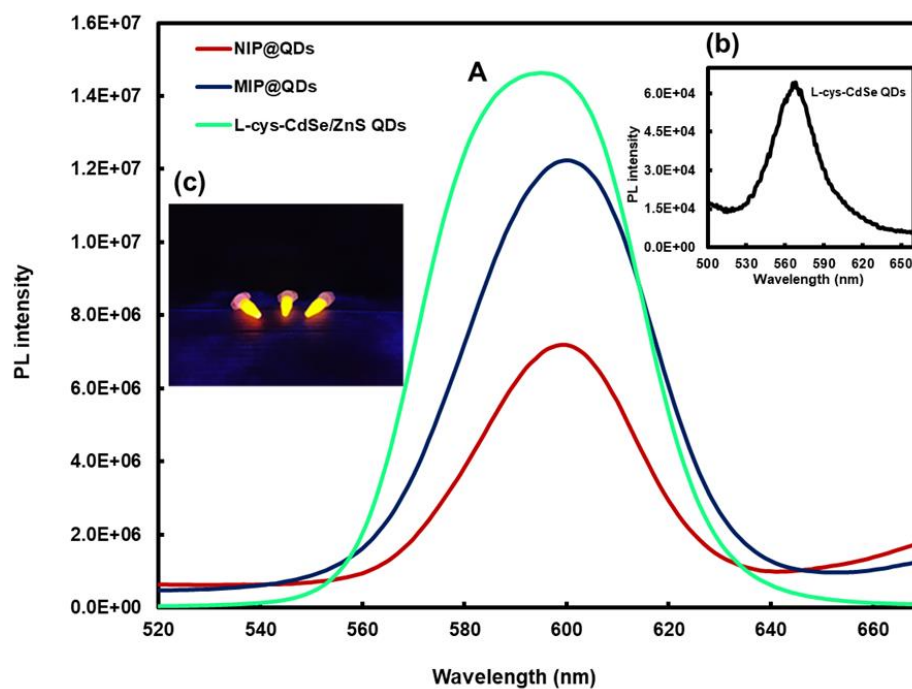


Fig. S1. (A) Photoluminescence spectra of the L-cys-CdSe/ZnS QDs, MIP@QDs and NIP@QDs in Millipore water, excitation wavelength 350 nm; slit widths of excitation and emission, 5 nm. (Inset: (b) photoluminescence spectra of the L-cys-CdSe QDs with an intensity of 6.4×10^4 at an emission wavelength of 568 nm which could not be included in graph (A) due to the low intensity, (c) L-cys-CdSe/ZnS QDs (left) MIP@QDs (middle) and NIP@QDs (right) under UV irradiation with an excitation wavelength of 365 nm).

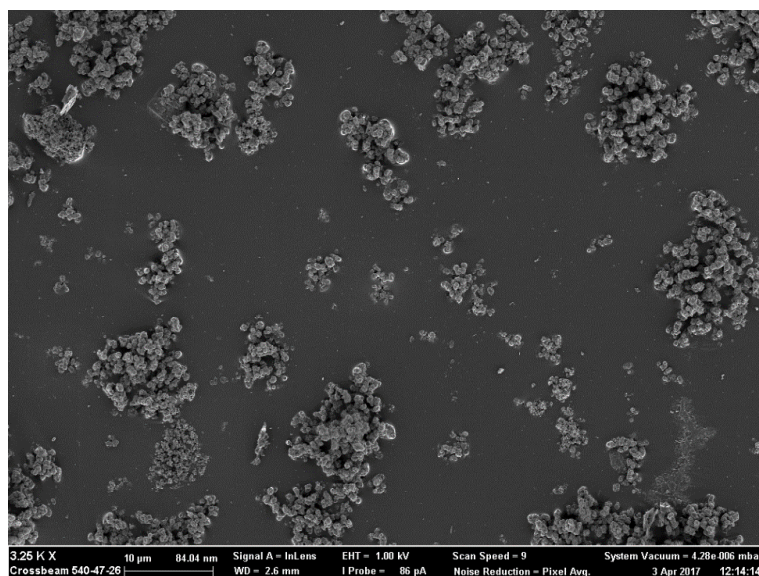


Fig. S2. HRSEM image of NIP@QDs.

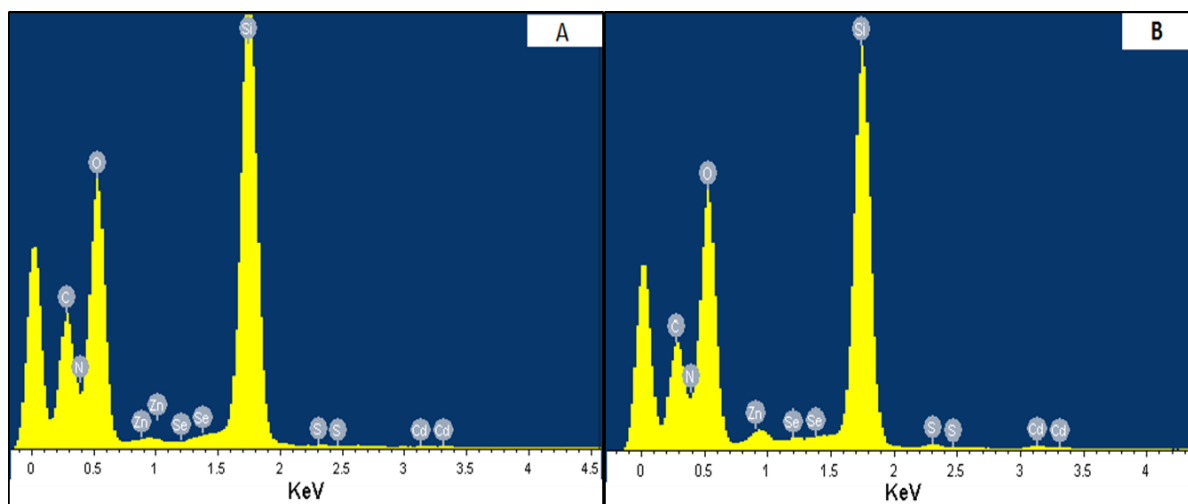


Fig. S3. EDS spectra of MIP@QDs (A) and NIP@QDs (B).

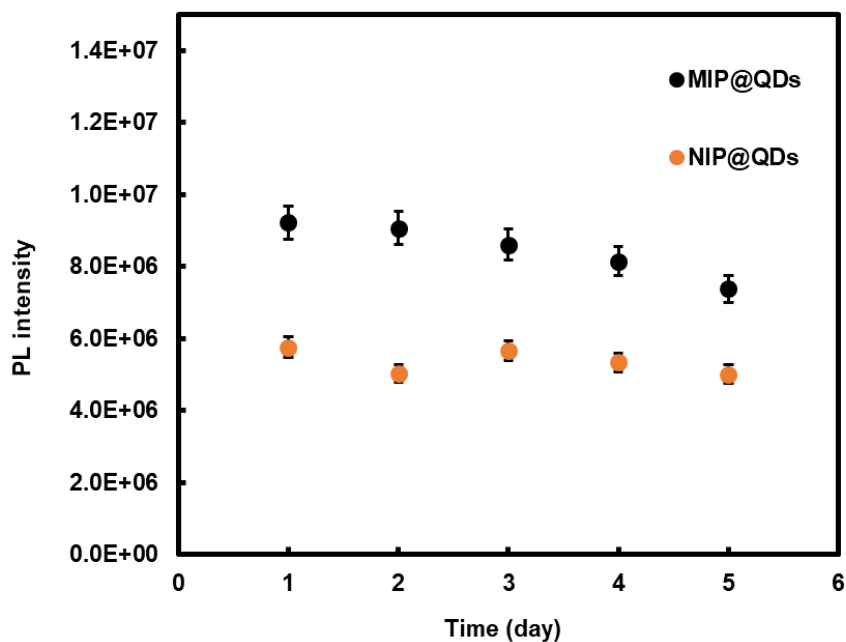
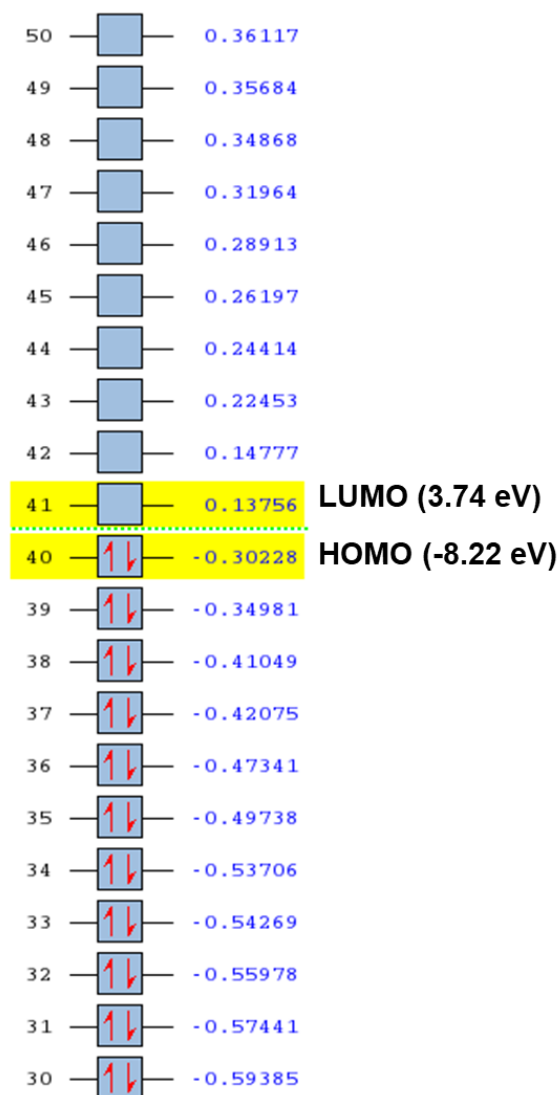


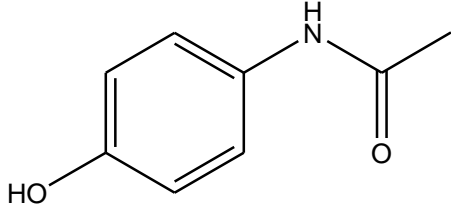
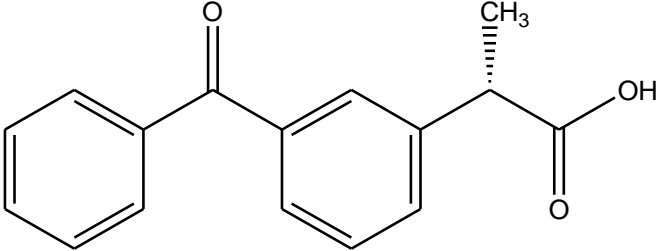
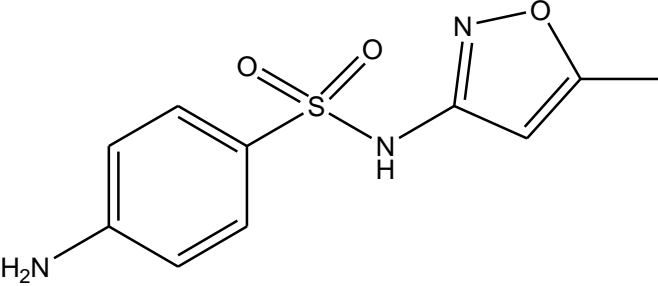
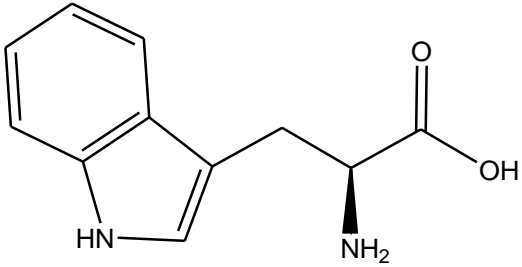
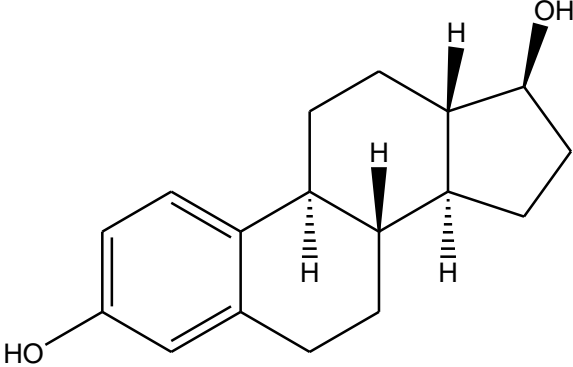
Fig. S4. Average photostability of MIP@QDs and NIP@QDs over 5 days (n=3). The experimental conditions were MIP@QDs or NIP@QDs, 0.8 mg in 3.0 mL⁻¹; excitation wavelength, 350 nm; slit widths of excitation and emission, 5.0 nm.

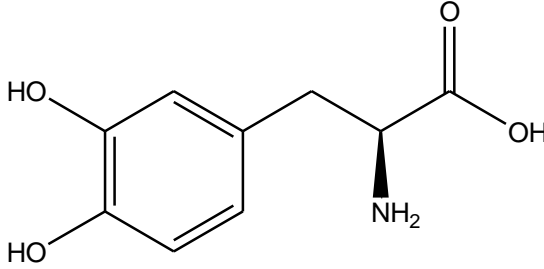
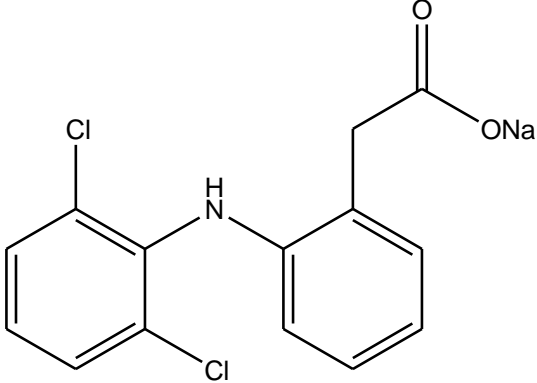
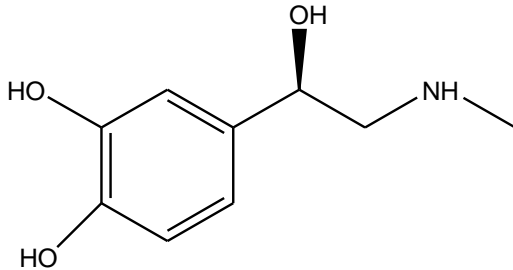
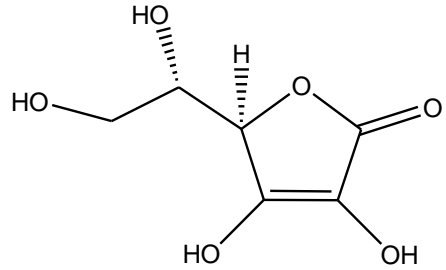
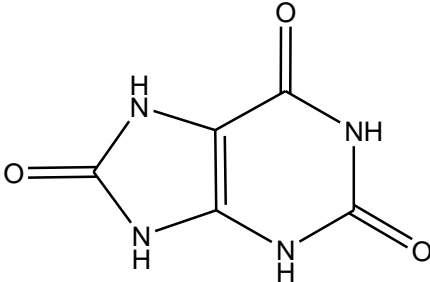
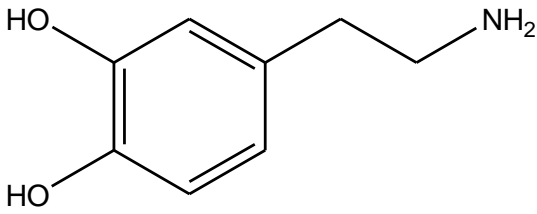


Scheme S1 Molecular orbital diagram of AC. The molecular orbital diagram of acetaminophen was generated with a gas phase single point calculation in the Gaussian 09 program package [1] from the crystal structure (COTZAN02) in the CCDC database. Hartree-Fock level of theory was used with a 3-21g basis set.

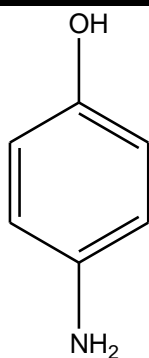
Table S1

Chemical structures of potential interfering analytes.

Name	Structure	pK _a	Reference
AC		9.46	[2]
KTP		4.14	[2]
SM		5.60	[3]
TRY		2.46 9.41	[4]
ES		10.71	[5]

L-Dopa		2.32 8.72	[4]
Dic		3.99	[2]
EP		8.66 9.95	[4]
AA		4.04 11.7	[4]
UA		5.4 11.3	[4]
DA		8.9 10.6	[4]

4-AP



5.48
10.30

[4]

References

- [1] M. Frisch, G. Trucks, H. Schlegel, G. Scuseria, M. Robb, J. Cheeseman, et al., Gaussian 09, Revision D.01, Gaussian Inc., Wallingford, CT, 2010.
- [2] Y. Ishihama, M. Nakamura, T. Miwa, T. Kajima, N. Asakawa, J. Pharm. Sci. 91 (2002) 933-942.
- [3] B.C. Rudy, B.Z. Senkowski, Sulfamethoxazole, Analytical profiles of drug substances, Elsevier, 1973, pp. 467-486.
- [4] D.R. Lide, Physical Constants of Organic Compounds", in CRC Handbook of Chemistry and Physics, Internet Version 2005, <<http://www.hbcnetbase.com>>, CRC Press, Boca Raton, FL, 2005.
- [5] K. Lewis, R. Archer, Steroids, 34 (1979) 485-499.

Chapter 5 Overall Conclusions and Future Work

5.1 Overall conclusions

Nanomaterial science has opened up new opportunities for the design of useful materials in technological, industrial and medical applications. Semiconductor quantum dots (QDs) are emerging as excellent nanomaterials for various applications with high stability, fluorescence intensity and quantum efficiency. Among Cd-based QDs, CdSe/ZnS core/shell QDs have gained considerable research interest due to their superior optical properties and low toxicity after over-coating with the non-toxic ZnS shell layer.

In this work, CdSe/ZnS QDs were fabricated and modified for application as sensitive fluorescence sensors for detection of two emerging chemical pollutants in water, specifically triclosan (TCS) and acetaminophen (AC). In South African surface waters, TCS has been reported to occur in the range of 3.04 – 30.1 nmol L⁻¹ (Lehutso *et al.*, 2017; Madikizela *et al.*, 2014) and AC was reported to occur within the 6.55 – 11.8 nmol L⁻¹ range (Matongo *et al.*, 2015a, 2015b). The CdSe/ZnS QDs that were fabricated were shown to be sensitive and selective in detecting these compounds at low concentrations, thus demonstrating the growing importance of nanomaterials in the development of fluorescence sensing systems for environmental monitoring of contaminants at low concentrations.

Firstly, glutathione (GSH)-capped CdSe/ZnS QDs as thiol-capped core/shell QDs were fabricated and characterized for the detection of a personal care product, namely triclosan. The synthesized QDs displayed excellent stability and a high photoluminescence quantum yield of 89%. Interaction of the QDs with triclosan resulted in fluorescence enhancement and allowed for the utilization of these QDs as a fluorescence probe for the detection of triclosan over the concentration range of 10-300 nmol L⁻¹. Förster resonance energy transfer (FRET) from triclosan to the QDs was responsible for a “turn-on” effect of the probe because of the overlap between the emission spectrum of analyte and the absorption spectrum of the QDs. An in-depth evaluation of the fluorescence enhancement mechanism showed that the Förster distance was about 4.0 nm, suggesting that the fluorescence enhancement was due to direct interaction of the analyte with the QDs.

The applicability of the fluorescence probe towards the detection of triclosan was examined by using standard solutions and real water samples in the presence of different structural analogues. GSH-CdSe/ZnS QDs showed higher sensitivity and selectivity towards triclosan among similar structure compounds. Investigation of a comparative method demonstrated that triclosan can be detected in river and tap water samples at nanomolar levels of 3.7 nmol L⁻¹ which were environmentally relevant, with good recoveries of 94-117.5%. The LOD value was lower than the guidance value for triclosan in drinking water which is 173 nmol L⁻¹ (50 ppb) as recommended by the US Minnesota Department of Health.

Following this, a CdSe/ZnS QDs fluorescence sensor was synthesized by a one-pot organometallic approach. The QDs were then functionalized with different thiol capping agents, namely L-cysteine (L-cys), N-acetyl-L-cysteine (NAC) and glutathione (GSH), for the quantification of acetaminophen. The performance of these three QD-ligand systems with respect to sensitivity for acetaminophen sensing was investigated to determine the best performing QD-ligand system. L-cys-CdSe/ZnS QDs were found to provide greater sensitivity for the fluorescence determination of acetaminophen. The procedure for the synthesis of L-cys-CdSe/ZnS QDs was simple and reproducible which also provided QDs with high fluorescence quantum yield (77%). The fabrication of the hydrophilic QDs was confirmed by various means including Fourier-transform infrared spectroscopy, powder X-ray diffraction, high resolution transmission electron microscopy, energy dispersive X-ray spectroscopy and Raman analysis. Under optimum conditions, the calibration plot of $F-F_0$ versus acetaminophen concentration showed a linear PL “turn-on” response over the range of 3.0-100 nmol L⁻¹. Investigation of the mechanism showed that Förster resonance energy transfer (FRET) from acetaminophen to the QDs led to the enhancement in the fluorescence intensity of the QDs. Moreover, L-cys-CdSe/ZnS QDs provided high selectivity towards acetaminophen as compared to its biologically important analogues. Finally, the potential application of the proposed methodology was evaluated for the determination of acetaminophen in spiked real water samples in which standard addition was utilized to correct for any matrix effects. The method allowed for the nanomolar detection (1.6 nmol L⁻¹) of acetaminophen in river and tap water samples.

Furthermore, anchoring of molecularly imprinted polymer (MIP) onto the surface of the L-cys-CdSe/ZnS QDs (MIP@QDs) as a receptor for acetaminophen sensing was also successfully attempted in this work, where the selectivity of the MIP and sensitivity of the QDs were integrated to fabricate a fluorescence probe. Characterization analysis of MIP@QDs confirmed the fabrication of the polymer coating. The response mechanism of MIP@QDs was also investigated and showed that charge transfer from MIP@QDs to acetaminophen produced fluorescence quenching according to the Stern–Volmer model. The sensor allowed for the quantitative determination of acetaminophen over the concentration range of 1.0-300 nmol L⁻¹ and provided a lower detection limit of 0.34 nmol L⁻¹ for acetaminophen in comparison with L-cys-QDs in this work and other analytical techniques from other studies. The sensor was successfully applied for the detection of acetaminophen in tap and river water samples in the presence of structural analogues and good recoveries from 95% to 114% were obtained at three spiking levels of acetaminophen. Amino groups of the monomer (APTES) formed hydrogen bonds with acetaminophen during the synthesis process. After removal of the acetaminophen template, imprinted cavities left in the polymer provided selectively upon

acetaminophen rebinding. Therefore, this method brought significant advantages of selectivity and sensitivity for practical applications with good reproducibility of 3.7%.

The results presented in this thesis demonstrate novel applications of the synthesized QDs and MIP@QDs provide a valuable contribution to the design of nanosensors for the target analytes, both in terms of sensitivity and efficacy of the resulting sensor probes.

In conclusion, the combination of molecular imprinting technology and fluorescence detection using core/shell QDs opens a new window of interest in the exploration of functionalized polymers and provides new opportunities for real applications involving the highly selective recognition of target species at low concentrations.

5.2 Future work

Although there has been great progress in the fabrication and synthesis of nanomaterials in the last few years, there is still need for sustainable and more environmentally friendly approaches.

The application of water soluble quantum dots as fluorescence probes is of particular value when the systems can be transferred to larger scales for real applications in which the size and biocompatibility of the sensor are critical. It is envisaged that other novel quantum dots with unique properties will be developed by using economical approaches to fabricate photostable and high-performance quantum dots to make the processes safer, faster and cleaner.

There are vast possibilities to utilize the quantum dots for *in-situ* analysis by encapsulation of the quantum dots into polymers like polydimethylsiloxane (PDMS) to minimize leaching of the toxic metals and to facilitate their utilization in optical devices. Further improvement could include quantum dots in lab-on-a-chip and in miniaturized devices for continuous monitoring of the contaminants. In addition, highly sensitive QD-based sensors with reduced toxicity can be applied in a great number of *in vivo* and *in vitro* systems for therapeutic and diagnostic purposes.

Regarding the application of molecularly imprinted polymers, computational chemistry could assist in the selection of the functional monomers, cross linker and templates in order to optimize the binding affinity of the synthesized polymers with target analytes. This system could also be applied to the removal of multiple analytes (contaminants) from contaminated waters by fabrication of multiple recognition cavities during polymerisation.

It is fortunate that the arrival of nanotechnology and nanosensors can usher in a new direction in producing devices for routine and extensive monitoring of PPCPs in water systems all

around the globe. The application of quantum dots can be considered as a breakthrough in the nano-revolution which will shape future developments. New aspects of quantum dot applications will certainly be revealed as thorough scientific research continues.

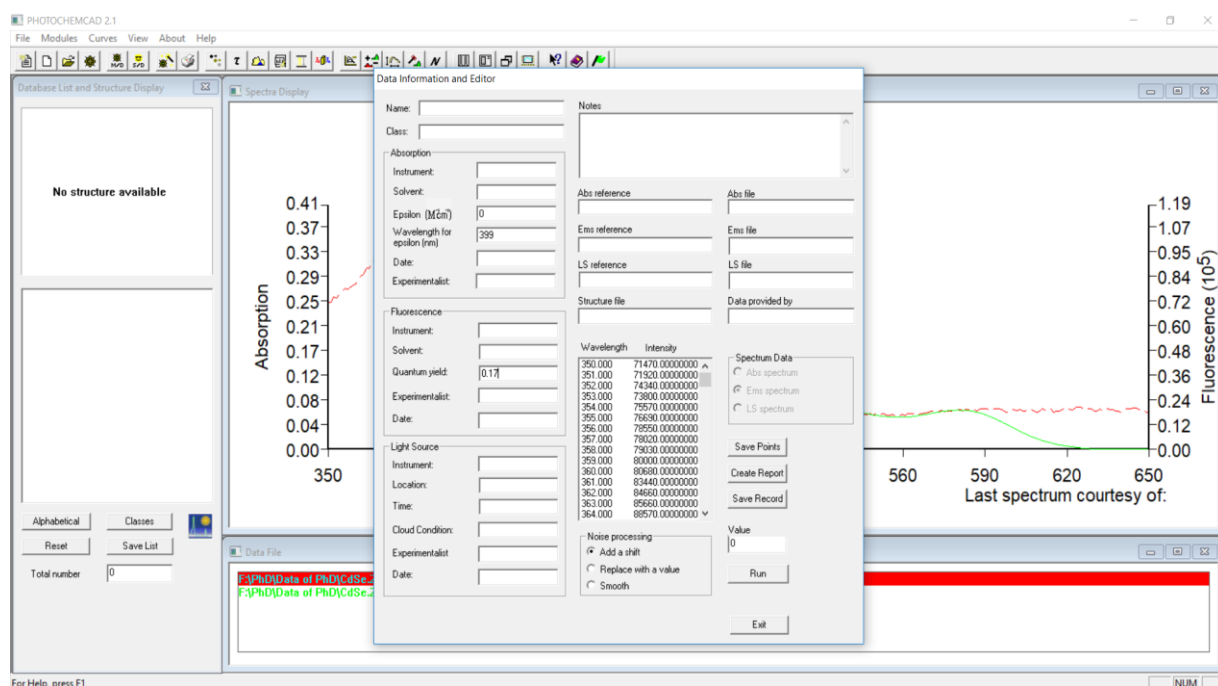
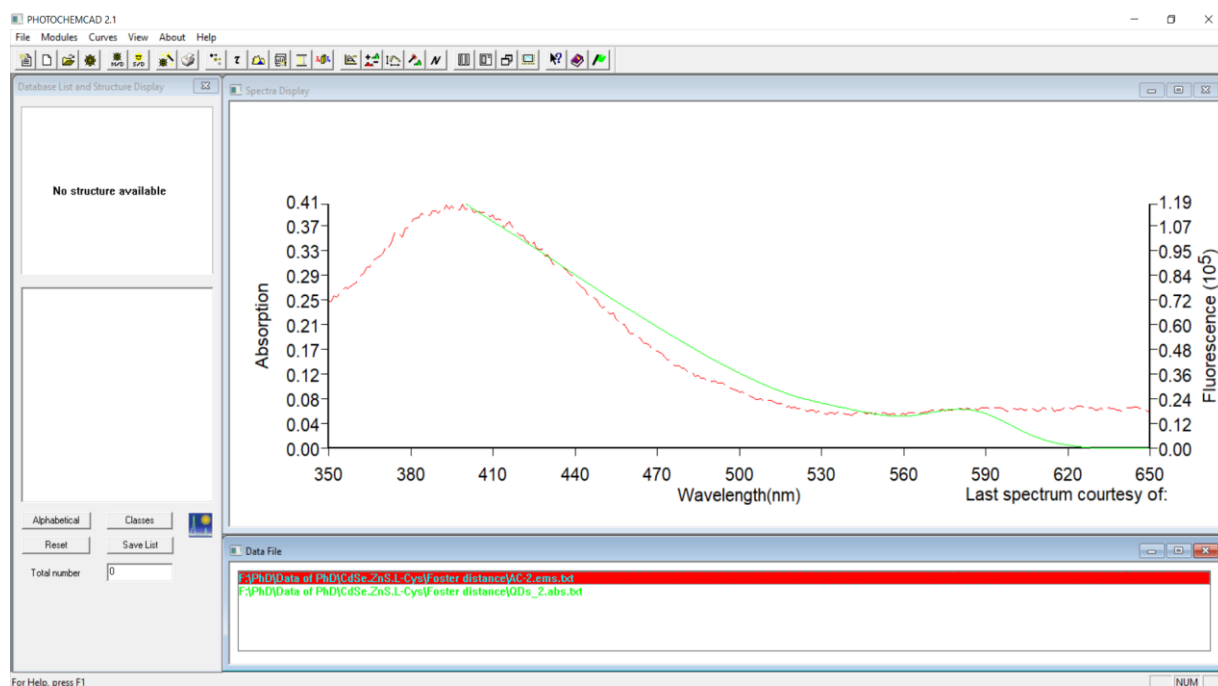
5.3 References

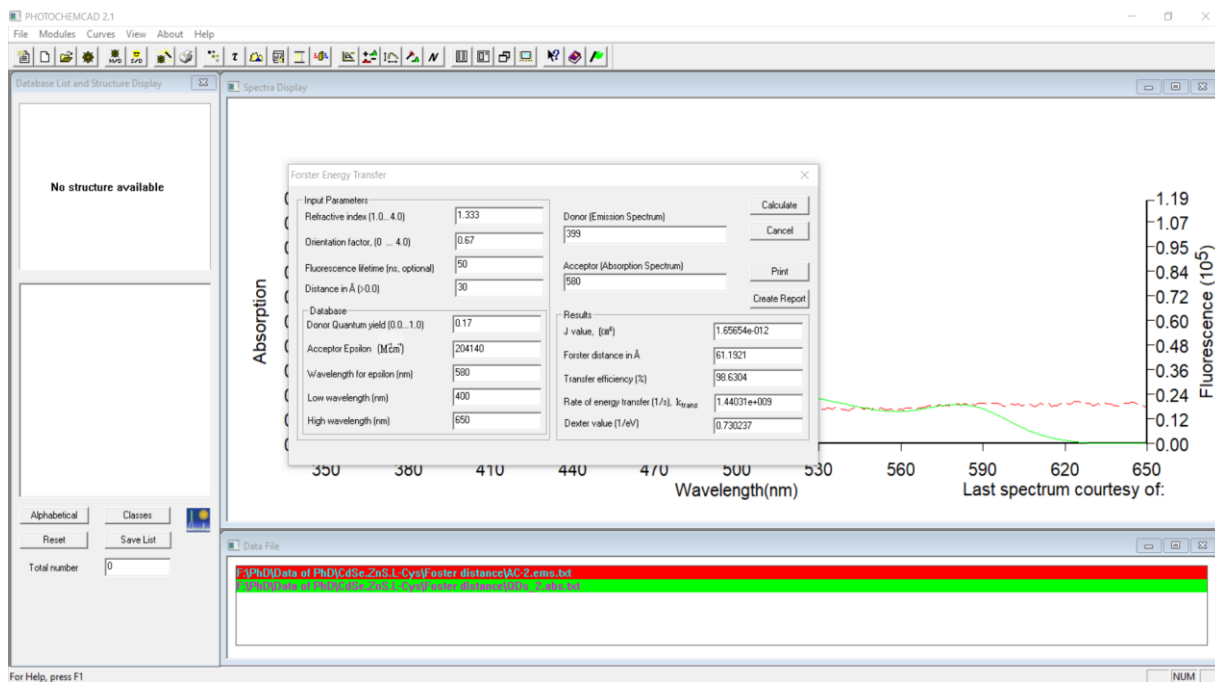
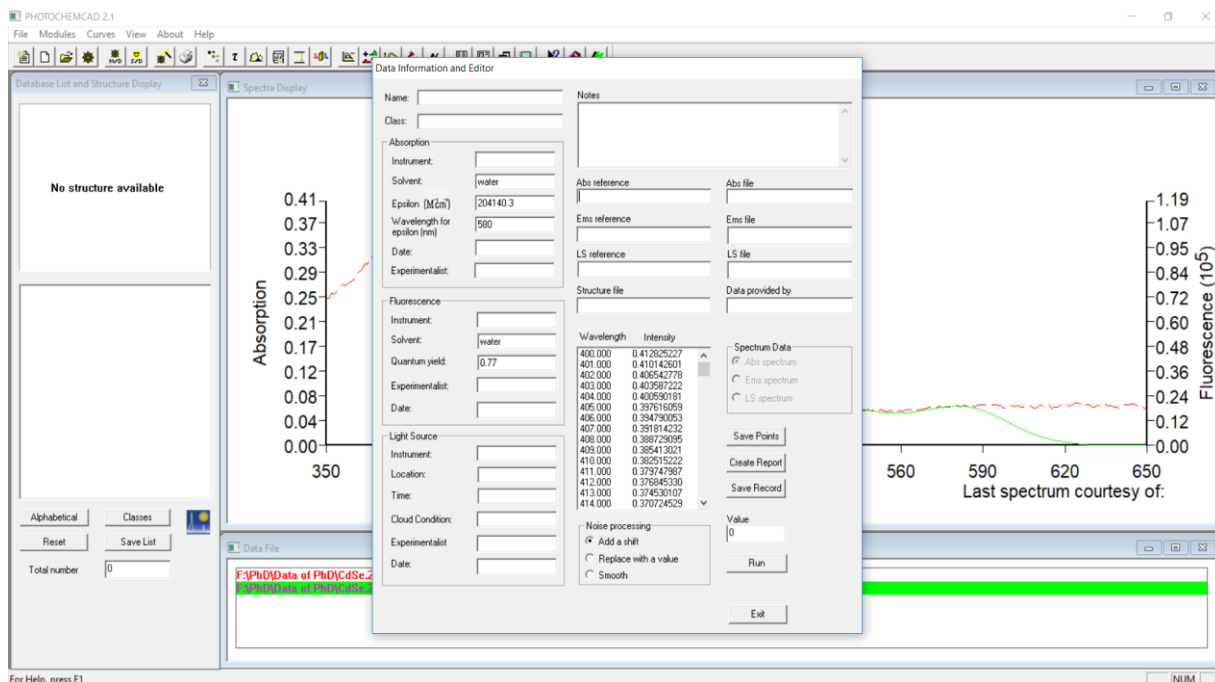
- Lehutso, R.F., Daso, A.P., & Okonkwo, J.O. (2017). Occurrence and environmental levels of triclosan and triclocarban in selected wastewater treatment plants in Gauteng Province, South Africa. *Emerging Contaminants*, 3(3), 107-114.
- Madikizela, L.M., Muthwa, S.F., & Chimuka, L. (2014). Determination of triclosan and ketoprofen in river water and wastewater by solid phase extraction and high performance liquid chromatography. *South African Journal of Chemistry*, 67, 143-150.
- Matongo, S., Birungi, G., Moodley, B., & Ndungu, P. (2015a). Occurrence of selected pharmaceuticals in water and sediment of Umgeni River, KwaZulu-Natal, South Africa. *Environmental Science and Pollution Research*, 22(13), 10298-10308.
- Matongo, S., Birungi, G., Moodley, B., & Ndungu, P. (2015b). Pharmaceutical residues in water and sediment of Msunduzi River, Kwazulu-Natal, South Africa. *Chemosphere*, 134, 133-140.

Appendices

Appendix A

The screenshots below show the PhotochemCAD program which was used to compute the Förster distance for L-cys-CdSe/ZnS QDs-AC system.





Appendix B

In this work solid phase extraction (SPE) followed by ultra-high performance liquid chromatography-high definition mass spectrometry (UHPLC-HDMS) was used for the confirmation of AC and TCS in tap and river water samples. The experimental procedure is described as follows:

The collected tap and river water samples were centrifuged at 4500 rpm for 5 min and filtered through 110 mm pore size filter paper before analysis to eliminate particulate matter before storage in pre-cleaned glass bottles.

Oasis HLB (60 mg) cartridges were conditioned with 3 mL of methanol and 3 mL of HPLC-grade water. 100 mL of the samples were then passed through the cartridge by gravity (flow rate $\sim 3 \text{ mL min}^{-1}$). After drying under vacuum, analytes were eluted by 5 mL of methanol. The extract was evaporated to dryness under a fume hood and finally reconstituted with 1 mL methanol-water (10:90 v/v) (Gracia-Lor *et al.*, 2010). Analysis was conducted by injecting 5 μL of the final extract into the UHPLC-HDMS system.

Analysis was performed using using a Waters® Synapt G2 high definition mass spectrometry system (Waters Inc., Milford, Massachusetts, USA). The system comprises of a Waters Acquity ultra-high performance liquid chromatography (UHPLC®) system hyphenated to a quadrupole-time-of-flight (QTOF) instrument which was operated with MassLynx™ (version 4.1) software (Waters Inc., Milford, Massachusetts, USA) for data acquisition and processing.

The source conditions were as follows: the capillary voltage for electrospray ionisation (ESI) was 2.8 kV for positive mode ionisation. The source temperature was set at 120 °C, the sampling cone voltage at 30 V, extraction cone voltage at 4.0 V and cone gas (nitrogen) flow at 10.0 L hr⁻¹. The desolvation temperature was set at 300 °C with a gas (nitrogen) flow of 600.0 L hr⁻¹.

Quantitative data-independent acquisition (DIA) was performed using two simultaneous acquisition functions with low and high collision energy (MS^E approach) with a QTOF instrument. The high energy MS scan can be time aligned with the low energy scan in order to predict which fragment ions belong to which precursor ions, consequently the full mass spectrum is acquired. Fragmentation patterns can thus be used for qualitative confirmation. Fragmentation was done using high energy collision induced dissociation (CID). The fragmentation energy was set at 2 eV and 3 eV for the trap and collision energy, respectively.

Mass spectral scans were collected every 0.3 seconds. The raw data was collected in the form of a continuous profile. Mass to charge ratios (m/z) between 50 and 1200 Da were recorded.

Separation was completed using a reverse phase step gradient elution scheme with water: methanol both containing 0.1% formic acid (Table B.1). Formic acid was added to the solution as buffer (pH correction), preservative and proton source for ionisation. A Kinetex® 1.7 µm EVO C18 100 Å (2.1 mm ID x 100 mm length) column was used. The column temperature was kept constant at 40 °C and the flow rate was set at 0.3 mL min⁻¹ for the entire run giving a total run time of 9 min.

Table 1. Water: methanol percentage gradient elution.

Time (min)	% water	% methanol
initial	95	5
1.5	95	5
2.0	70	30
3.0	50	50
5.0	30	70
6.0	10	90
7.0	10	90
7.1	95	5
9.0	95	5

Reference

Gracia-Lor, E., Sancho, J.V., & Hernández, F. (2010). Simultaneous determination of acidic, neutral and basic pharmaceuticals in urban wastewater by ultra-high-pressure liquid chromatography-tandem mass spectrometry. *Journal of Chromatography A*, 1217(5), 622-632.

Appendix C

Two additional journal papers were produced as a co-author responsible for the characterisation of the synthesised quantum dots.

C.1 Paper 1

Adegoke, O., Montaseri, H., Nsibande, S.A., & Forbes, P.B.C. (2017). Alloyed quaternary/binary core/shell quantum dot-graphene oxide nanocomposite: Preparation, characterization and application as a fluorescence “switch ON” probe for environmental pollutants. *Journal of Alloys and Compounds*, 720, 70-78. Impact Factor 3.779. <https://doi.org/10.1016/j.jallcom.2017.05.242>



Alloyed quaternary/binary core/shell quantum dot-graphene oxide nanocomposite: Preparation, characterization and application as a fluorescence “switch ON” probe for environmental pollutants



Oluwasesan Adegoke^{*}, Hanieh Montaseri, Sifiso A. Nsiband, Patricia B.C. Forbes^{**}

Department of Chemistry, Faculty of Natural and Agricultural Sciences, University of Pretoria, Lynnwood Road, Pretoria, 0002, South Africa

ARTICLE INFO

Article history:

Received 2 March 2017

Received in revised form

15 May 2017

Accepted 23 May 2017

Available online 24 May 2017

Keywords:

Graphene oxide

Quantum dots

Polycyclic aromatic hydrocarbon

Photoluminescence

Fluorescence probe

ABSTRACT

Alloyed L-cysteine-capped CdSeTeS/ZnS quantum dots (QDs) have been covalently linked to graphene oxide (GO) to form a new QD-GO nanocomposite material. Transmission electron microscopy, scanning electron microscopy, Raman, energy dispersive X-ray spectroscopy, X-ray diffraction, FT-IR, UV/vis and fluorescence spectrophotometry were used to characterize the nanocomposite material. Covalent binding of GO to the QDs quenched the fluorescence (“switch OFF”) of the QDs. The planar structure of GO and its π electron rich surface enables the adsorption of π rich aromatic analytes. Environmental pollutants, belonging to the class of polycyclic aromatic hydrocarbons (PAHs) were used as model analytes to test their affinity to adsorb onto GO via π - π interaction and trigger fluorescence transduction changes (“switch ON”) in the conjugated QDs. Our investigation showed that the affinity of the four PAH analytes tested to switch on the fluorescence of the nanocomposite probe followed the order phenanthrene > anthracene > naphthalene > pyrene.

© 2017 Elsevier B.V. All rights reserved.

1. Introduction

Nanocomposites, composed of hierarchically-structured composite materials with one or more components of a nanostructured domain, have the potential to pave the way for the next-generation of device materials for sensor nanotechnologies. Selection of the appropriate nanostructured materials as building blocks, and the development of methods to assemble these materials to meet targeted applications, is a requisite to produce nanocomposite materials with unique optical, electronic and mechanical properties [1].

Graphene is a nanomaterial which is characterized by sp^2 hybridized carbon atoms which are covalently bonded to three other atoms and has a monolayer thickness of ~ 0.34 nm [2–5]. The carbon atoms are assembled in a honeycomb-like crystal lattice and exhibit a unique array of unparalleled electrical, mechanical and structural properties [6–10]. Other carbon-based materials such as graphite, fullerene and carbon nanotubes are known to derive their basic structure from graphene [11–13]. With respect to nanodevice

applications, many technological and scientific breakthroughs have been reported using graphene, the most common being in the development of chemical sensors and biosensors [14–16]. A limitation of graphene is its tendency to aggregate when used in bulk quantities during adsorption reactions as well as its susceptibility to restack to graphite. To improve chemisorption, graphene needs to be functionalized or bonded with other materials of interest [17,18]. The presence of oxygen functional groups in the basal edges and planes renders graphene oxide (GO) highly soluble in water when compared to reduced graphene. It is known that the degree of oxidation of GO influences the assembly of oxide functional groups as well as their identity while the structural atomic nature should mostly resemble that of a 2D amorphous sheet of carbon atoms with partially bonded oxygen atoms, rather than an exact graphene sheet with oxidized surface [19]. For direct conjugation to other materials and for biocompatibility, single layer GO nano-sheets are highly desirable.

Fluorescent semiconductor quantum dot (QDs) nanocrystals have in the last two decades generated enormous interest due to their unique optical properties which are far superior to fluorescent organic dyes. Their broad absorption and narrow fluorescence emission, large extinction coefficient, brightness, high resistance to photodegradation, excellent photostability and multiplex detection

^{*} Corresponding author.

^{**} Corresponding author.

E-mail addresses: adegoke.sesan@mailbox.co.za (O. Adegoke), patricia.forbes@up.ac.za (P.B.C. Forbes).

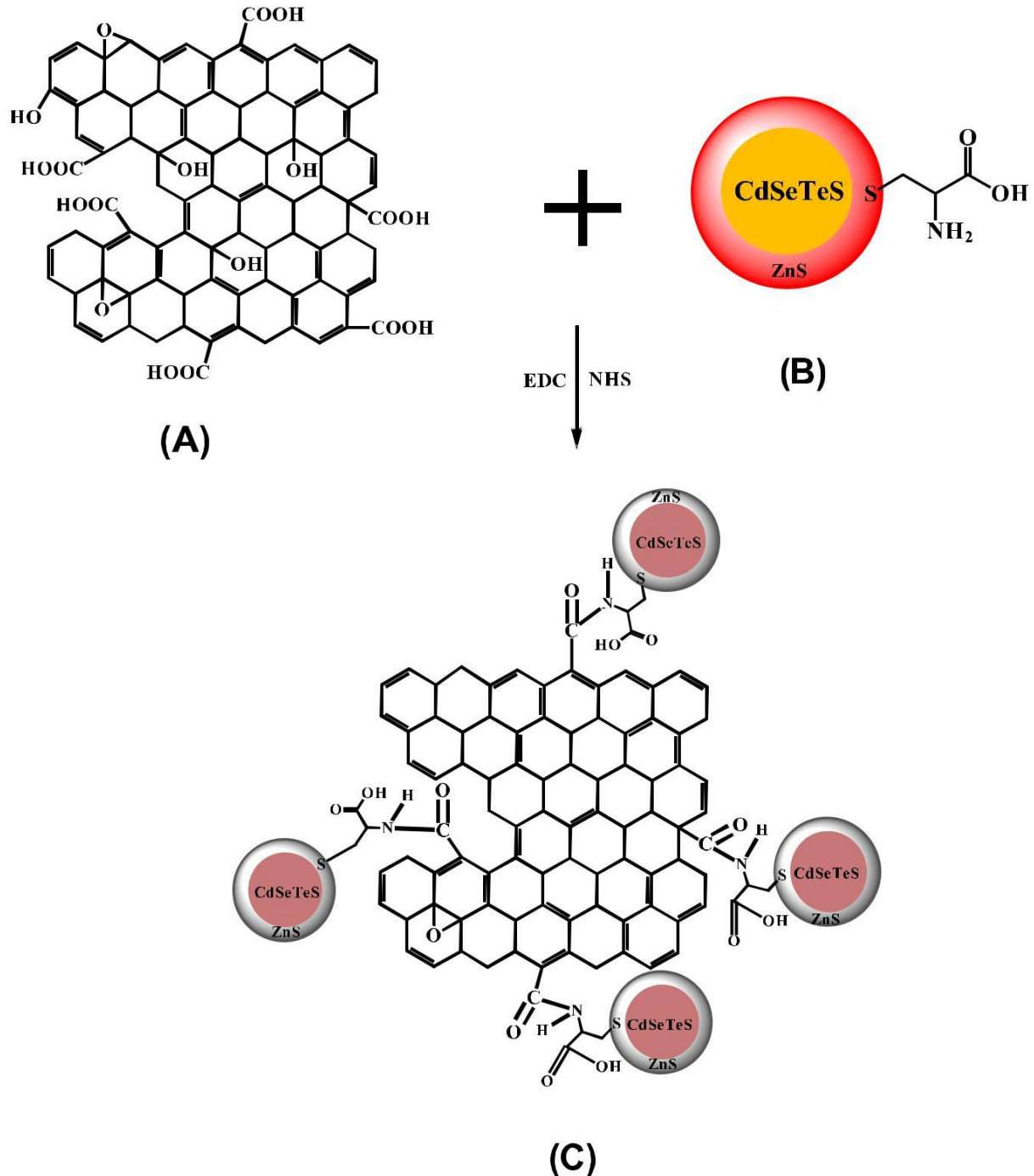
<http://dx.doi.org/10.1016/j.jallcom.2017.05.242>

0925-8388/© 2017 Elsevier B.V. All rights reserved.

capabilities have made them a powerful tool as nanodevices in biology, chemistry and physics applications [20-22]. QDs represent an excellent choice of nanocrystalline material for bonding to GO due to their surface biocompatibility, stability and unique optical properties. To meet the demand for highly sensitive detection in sensor design, the choice of QDs is crucial. Following recent developments in bandgap engineering of QDs, alloyed QDs composed of two or more semiconductor metals have been reported to generate improved sensitivity for analyte sensing than conventional QDs systems [23,24]. This makes their use as fluorescence reporters interesting.

In this work, we report on the preparation, characterization and

chemical sensing application of a L-cysteine-capped alloyed CdSeTeS/ZnS quaternary/binary core/shell QD-GO nanocomposite. A non-toxic ZnS shell was passivated onto the cadmium-based alloyed QD core to reduce leaching of Cd from the core and thereby render the nanocrystals environmentally safe. Alloyed L-cysteine-capped CdSeTeS/ZnS QDs and GO were synthesized, characterized and chemically bonded via covalent coupling chemistry. The structural and optical properties of the new QD-GO nanocomposite were studied and thereafter applied as a fluorescent probe for environmental water pollutants belonging to the class of polycyclic aromatic hydrocarbons (PAHs). PAHs are ubiquitous environmental pollutants, known to be persistent in the



Scheme 1. Conjugation of GO (A) to alloyed L-cysteine-capped CdSeTeS/ZnS QDs (B) to form the QD-GO nanocomposite (C).

environment and are released into the environment during the incomplete combustion of organic substances [25]. Many of the PAH molecules are known to be mutagenic and carcinogenic [26], hence there is a need to develop efficient probes to detect them.

Our approach exploits the unique adsorption properties of GO. The π electron rich surface of GO allows π - π interactions with organic compounds containing benzene rings or C=C bonds such as PAHs. Our detection principle is based on the quenching of the fluorescence of the QDs by GO (“switch OFF”) due to their strong binding effect whilst the subsequent adsorption of PAH on the GO surface, triggers the fluorescence recovery (“switch ON”) process of the QDs in a concentration-dependent manner. Our work is the first to exploit a QD-GO as an OFF/ON sensor for PAHs.

2. Experimental

2.1. Materials

Cadmium oxide, trioctylphosphine oxide, N-Hydroxysuccinimide, N-(3-dimethylaminopropyl)-N-ethylcarbodiimide hydrochloride, sulphur, octadecene, tellurium powder, oleic acid, L-cysteine and PAH standards consisting of anthracene (Ant), naphthalene (Naph), phenanthrene (Phe) and pyrene (Py) were purchased from Sigma Aldrich. Sulphuric acid, hydrogen peroxide, methanol, zinc powder, absolute ethanol, sodium nitrate, acetone, chloroform, selenium powder, hydrochloric acid, potassium hydroxide, potassium permanganate and graphite powder were purchased from Merck. Water dispensed from an ultrapure Milli-Q Water System was used as the measurement medium.

2.2. Apparatus

Fluorescence emission measurements were performed using a Horiba Jobin Yvon Fluoromax-4 spectrofluorometer. UV-vis absorption spectra were performed using a Cary Eclipse (Varian) spectrophotometer. Powder X-ray diffraction (PXRD) analyses were performed using a PANalytical X'Pert Pro powder diffractometer in θ - θ configuration with an X'Celerator detector, variable divergence and receiving slits with Fe filtered Co-K α radiation ($\lambda = 1.789 \text{ \AA}$). Transmission electron microscopy (TEM) images were taken using a JEOL JEM 2100F operated at 200 kV. Raman analyses were performed using a T64000 micro-Raman spectrometer (HORIBA Scientific Jobin Yvon Technology) equipped with a triple monochromator system to eliminate contributions from the Rayleigh line. Scanning electron microscopy (SEM) measurements were performed using a JEOL JSM-5800LV operated at 20 kV, whilst high resolution scanning electron microscopy (HRSEM) measurements were obtained using an FE-SEM Zeiss Ultra Plus. A RX system from Perkin Elmer was used for FT-IR analyses. Energy dispersive X-ray spectroscopy (EDS) analysis was carried out using a SEM integrated EDS Zeiss Crossbeam 540 with software AZtech version 3 by Oxford Instruments.

2.3. Synthesis of L-cysteine-capped CdSeTeS/ZnS alloyed QDs

The synthesis of L-cysteine-capped CdSeTeS/ZnS alloyed QDs has previously been reported by our group [27] and here we provide a brief description. Firstly, hydrophobic alloyed CdSeTeS/ZnS QDs were synthesized via the hot organometallic route. To a solution of cadmium oxide (1.3 g) in 30 mL oleic acid and 50 mL octadecene at $\sim 280 \text{ C}$, precursor solutions of selenium (0.3 g selenium + 1.93 g trioctylphosphine oxide + 25 mL octadecene), tellurium (0.48 g tellurium + 1.93 g trioctylphosphine oxide + 25 mL octadecene) and sulphur (0.16 g sulphur + 20 mL oleic acid + 30 mL octadecene) were added to grow the quaternary alloyed CdSeTeS QDs. After

satisfactory growth of the core QDs, ZnS shell precursor solution consisting of zinc ($\sim 0.4 \text{ g}$ zinc + 20 mL oleic acid + 30 mL octadecene) and sulphur (as used in the growth of the core QDs) were added. The hydrophobic CdSeTeS/ZnS QDs were allowed to grow with time and harvested thereafter. Purification was performed using methanol and acetone.

Conversion of the hydrophobic CdSeTeS/ZnS QDs to water-soluble QDs was performed by a ligand exchange reaction utilising a potassium hydroxide-methanolic-L-cysteine-water solution. This separated the organic-phase soluble QDs from the water-soluble QDs. The latter were purified by acetone and chloroform.

2.4. Synthesis of GO nanosheets

The synthesis of GO nanosheets has previously been reported by our group [28] and here we provide a brief description. GO was synthesized via a modified Hummer's method [29]. Briefly, 7.5 g of potassium permanganate was used to oxidize an acidic solution of 2.5 g graphite and 1.25 g sodium nitrate in 60 mL of sulphuric acid. The solution was kept under ice for few hours and stirred until the following day. A pasty light brown solution was formed to which 75 mL of ultrapure deionized water was added and the solution was stirred at 60 C overnight. A solution of 30% hydrogen peroxide (25 mL) was added into the reaction mixture which was then centrifuged using 5% hydrogen chloride and ultrapure deionized water. This produced graphene oxide with a yield of 4.0 g after drying at 65 C. Graphite oxide (0.8 g), dissolved in ultrapure deionized water was exfoliated to GO nanosheets by ultrasonication for 3 h followed by purification using 5% hydrogen chloride. After drying at 65 C, the yield of GO was 0.4 g.

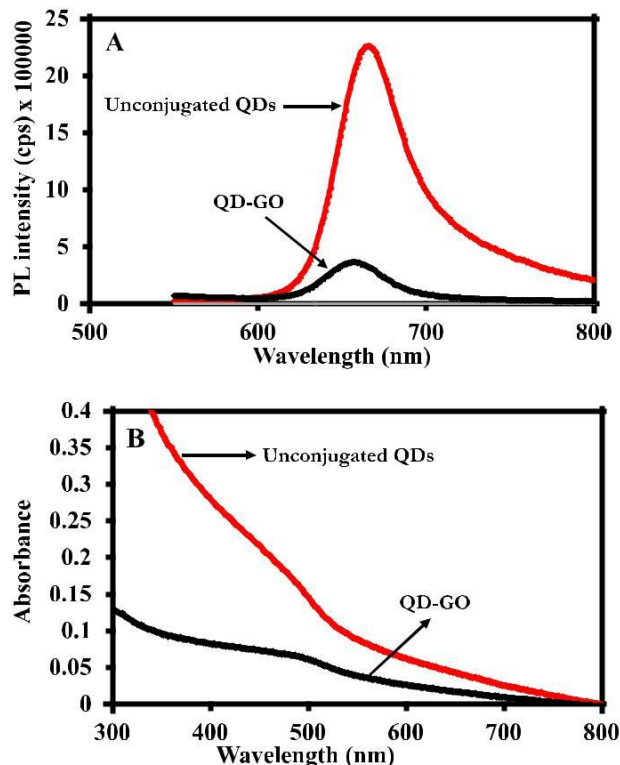


Fig. 1. PL emission (A) and UV-vis absorption spectra (B) of unconjugated L-cysteine-capped CdSeTeS/ZnS QDs and the QD-GO nanocomposite.

2.5. Preparation of CdSeTeS/ZnS QD-GO nanocomposite

The descriptive preparation of the QD-GO nanocomposite is shown in Scheme 1. A 5 mL solution of 0.1 M EDC was used to activate the carboxylic groups of GO (Scheme 1A) (20 mg in 5 mL of ultrapure deionized water) for ~30 min. A 5 mL solution of the QDs (Scheme 1B) (20 mg) was then added followed by 5 mL of 0.1 M NHS to stabilize the amide bond. The reaction was stirred at ambient temperature for ~24 h. The QD-GO (Scheme 1C) nanocomposite was purified by centrifugation with acetone.

2.6. Procedure for the fluorescence “switch ON” detection of PAHs

Four PAHs (Py, Naph, Ant and Phe) which are in the list of the

sixteen priority PAHs documented by the US Environmental Protection Agency [30] were tested in this work. The four selected PAHs are commonly detected in water systems [31,32]. PAH standards (1×10^{-7} - 5×10^{-7} M) were prepared in an ethanol: water (1:2) mixture and were added into the QD-GO nanocomposite solution (~0.7 mg/mL) and allowed to equilibrate for ~5 min. The probe solution was excited at 470 nm and the fluorescence emission measuring range was 480–800 nm.

3. Results and discussion

3.1. Fluorescence quenching effect of GO on the QDs

Structurally, GO has several oxygen containing functional

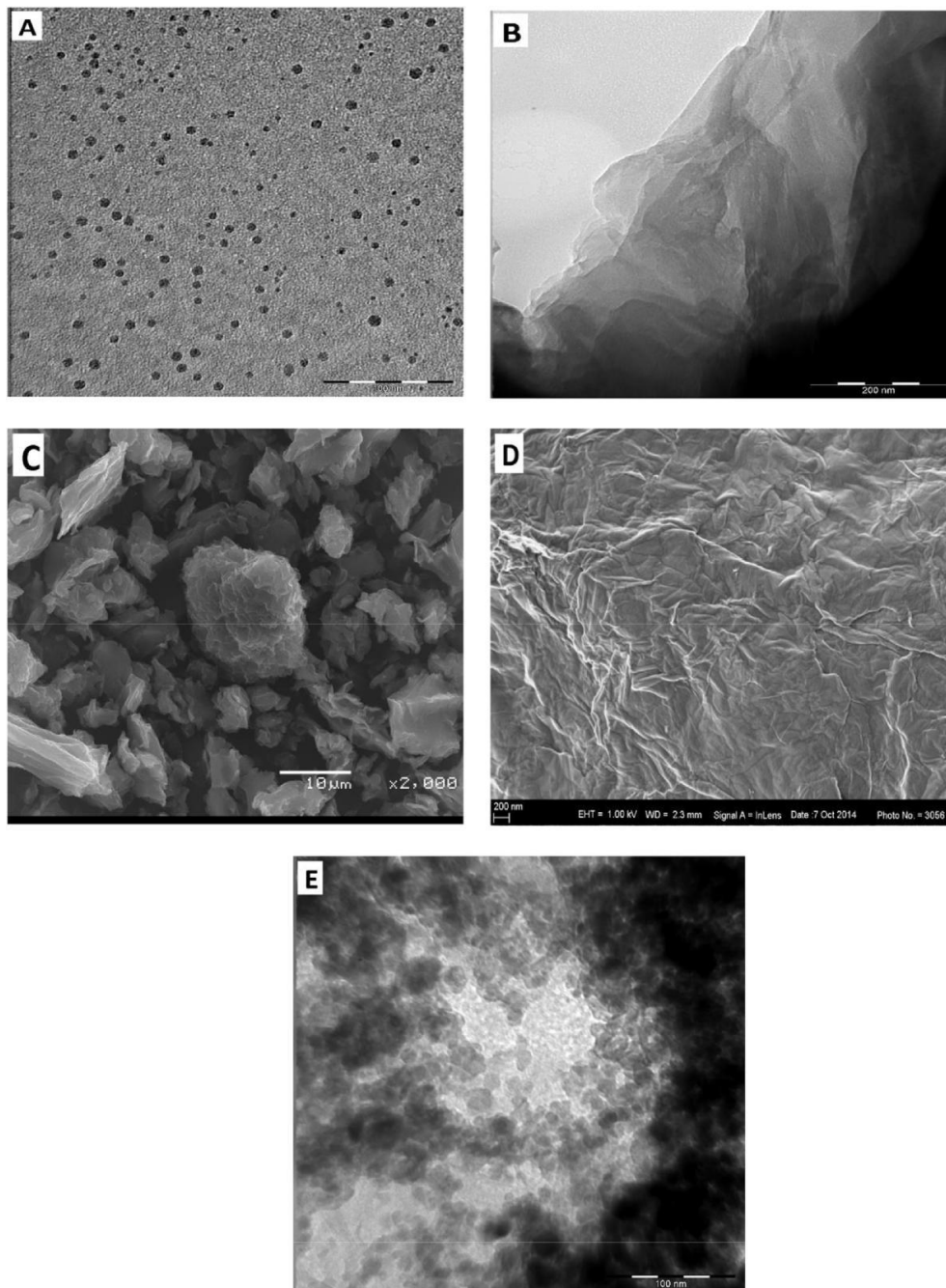


Fig. 2. TEM images of (A) L-cysteine CdSeTeS/ZnS QDs and (B) GO. (C) SEM image of GO and (D) HRSEM image of GO. (E) TEM image of the QD-GO nanocomposite.

groups on its carbon surface such as hydroxyl, epoxy and carboxylic groups. It is believed that the exact structure and composition of GO is difficult to ascertain as this depends on the synthetic method used [33]. In our work, we employed the modified Hummer's method, hence GO should exhibit hydroxyl/epoxy functional groups on the basal plane and carboxylic functional groups at the edges of its planar structure (Scheme 1A). The Hummer's method is applicable for producing high yield water-soluble GO nanosheets.

The fluorescence quenching effect of the QDs after covalent binding to GO is shown in Fig. 1A whilst the corresponding UV/vis absorption spectra are shown in Fig. 1B. The fluorescence emission maximum of the QDs before conjugation was 666 nm and upon binding to GO a slight blue shift to 658 nm was observed. The blue shift reflects a possible increase in the QDs band gap and the lack of agglomerated nanocrystals upon binding to GO. Changes in the absorption spectrum of the nanocomposite also reflects the binding effect of the QDs to GO. There are three possible mechanisms associated with the quenching effect as proposed in the literature [34]; (i) nano-metal surface energy transfer (NSET), (ii) Forster resonance energy transfer (FRET) and (iii) a charge transfer or electron-donor-acceptor mechanism. With respect to the three possible mechanisms, the QDs act as the donor and GO acts as the acceptor. For the charge transfer mechanism, the distance between the QD fluorophore and the GO quencher induces electronic charge transfer from the donor to the acceptor whilst in the case of FRET, energy transfer from the QDs to GO induces the quenching effect which is also made possible by the distance (d) that separates the QDs donor from the GO acceptor. This energy transfer efficiency is inversely proportional to the separation distance ($1/d^6$) for FRET and $1/d^4$ for NSET [35,36]. It has been reported that the higher the separation distance of the donor from the acceptor, the lower the energy transfer efficiency, with the degree of energy transfer efficiency being greater for NSET-based processes than FRET-based processes when a nanoparticle is the acceptor [35].

GO exhibits a weak absorption in the UV region [33], hence making the possibility of charge or energy transfer mechanisms difficult. Li and co-workers [34] proposed that the NSET mechanism dominates the quenching of CdSe/ZnS QDs by GO and this theory has also been supported by another group [37]. However, based on the poor absorption of GO as evidenced from the UV/vis spectrum measured in this work (data not shown), we believe that bonding of GO to CdSeTeS/ZnS QDs may have introduced surface defect states to the QDs fluorescence, hence resulting in the observed quenching.

3.2. Morphology of the QDs, GO and QD-GO nanocomposite

A TEM image of L-cysteine CdSeTeS/ZnS QDs shown in Fig. 2A reveal a mono-dispersed particle size distribution averaging 5.5 nm. The morphology of GO as characterized by TEM (Fig. 2B), shows layers of GO nanosheets interlocking with each other, and rolled into connected networks of sheets. The SEM image in Fig. 2C, showed that the surfaces of GO were wrinkled into curling edges, with connected networks of interlocking flakes, which will enable strong interaction with other conjugated entities. The corresponding HRSEM image (Fig. 2D) also showed the rolling up of GO into interconnected sheets. The TEM image of the QD-GO displays the binding effect of the QDs onto the GO. It is difficult to see individual QDs anchored onto the GO due to the strong inter-connecting layers of GO. The coarse nature of the image showed its difference from the TEM images of GO and the QDs and thus indicate the bonding of QDs to GO via covalent interaction.

3.3. Crystal structure of the QDs, GO and QD-GO nanocomposite

Fig. 3 shows the XRD patterns for GO, the QDs and QD-GO

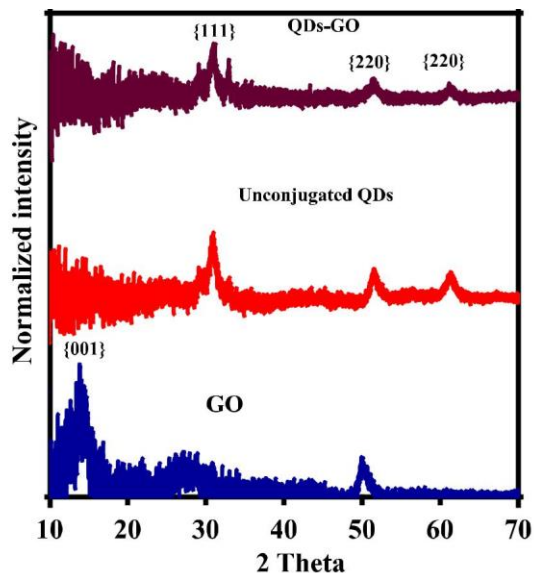


Fig. 3. PXRD spectra of GO, unconjugated QDs and the QD-GO nanocomposite.

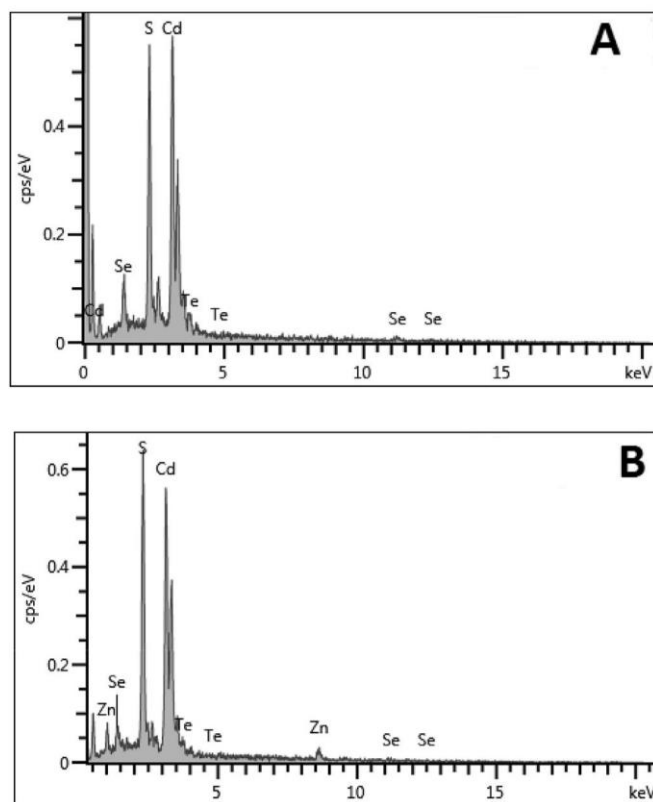


Fig. 4. EDS spectra of (A) CdSeTeS core and (B) CdSeTeS/ZnS QDs.

nanocomposite. GO displayed a typical peak at $2\theta = 13.83^\circ$ [28]. For the QDs, the diffraction pattern fits to a typical zinc-blende crystal structure with the three notable peaks at planes {111}, {220} and {311}, thus corresponding to the JCPDS Card No. 19-0191 for CdSe QDs. The three peaks were displayed at $2\theta = 30.97^\circ$, $2\theta = 51.53^\circ$ and $2\theta = 61.39^\circ$. For the XRD pattern of the QD-GO nanocomposite, we could observe that the zinc-blende crystal structure of the QDs prevailed but with weaker diffraction peaks in

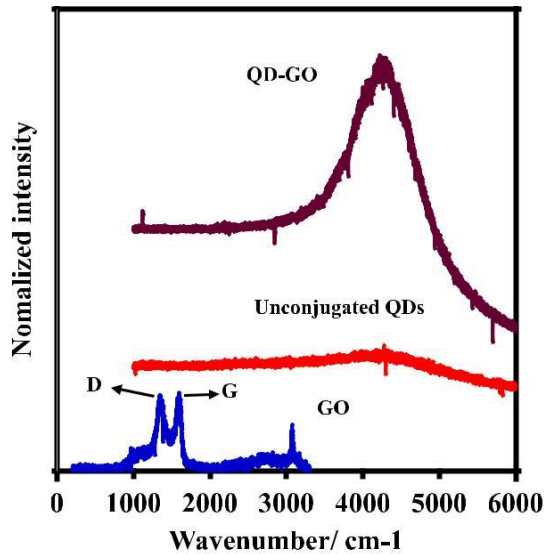


Fig. 5. Raman spectra of GO, unconjugated QDs and the QD-GO nanocomposite.

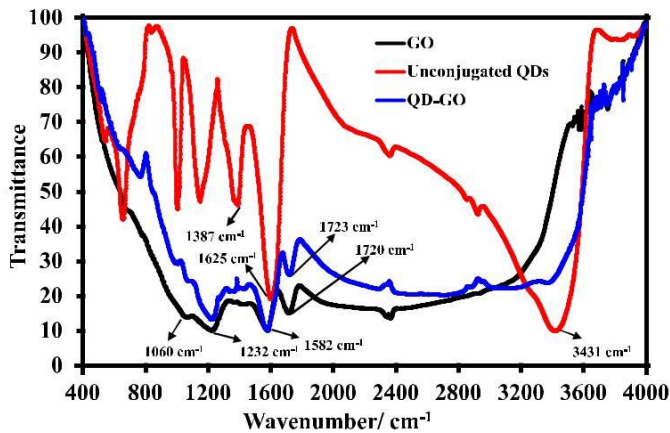


Fig. 6. FT-IR spectra of GO, unconjugated QDs and the QD-GO nanocomposite.

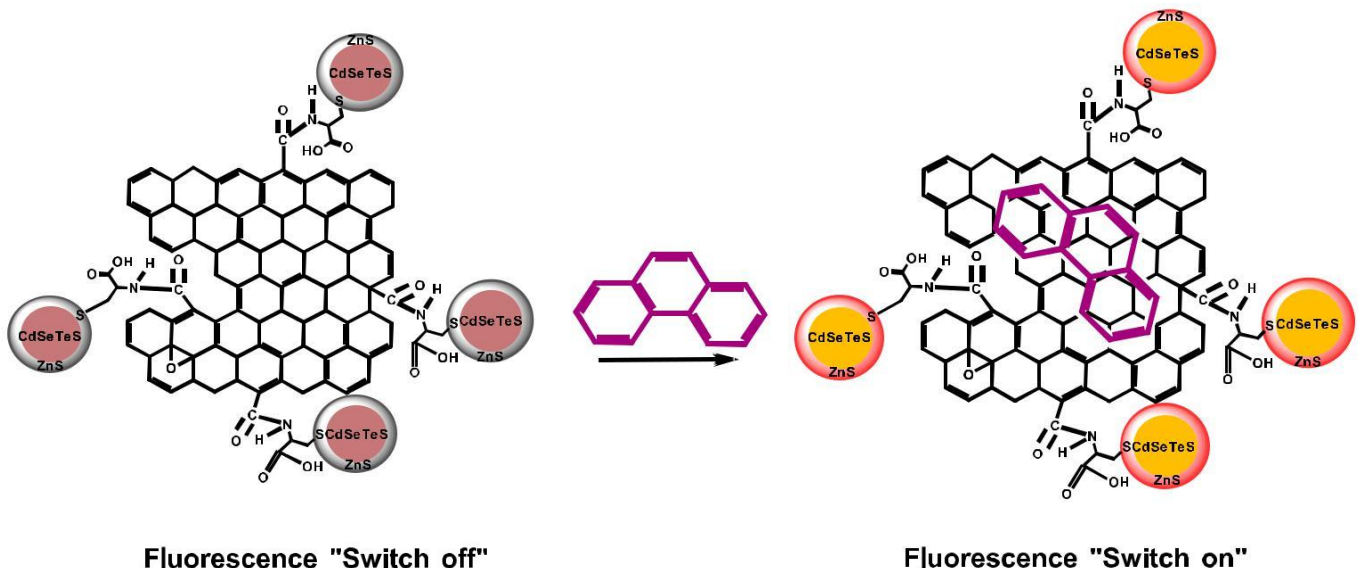
comparison to those of the unconjugated QDs. It is difficult to see the peak of GO in the diffraction pattern of the nanocomposite probably due to the weak intensity thereof. The diffraction peaks of the nanocomposite were displayed at $2\theta = 31.17^\circ$, $2\theta = 51.43^\circ$ and $2\theta = 61.16^\circ$. Comparing the diffraction peak position of the unconjugated QDs with the QD-GO nanocomposite, we observed no significant peak shift. This suggests that the binding of GO to the QDs did not alter the structural nature of the QDs.

3.4. EDS analysis of the QDs

EDS analysis was carried out to semi-quantitatively determine the semiconductor metal components present in the CdSeTeS core and CdSeTeS/ZnS core/shell structures (Fig. 4A and B). The presence of Cd, Se, Te and S were effectively identified in both the core and core/shell spectra while the additional Zn metal component in the core/shell structure was evident. The approximate elemental composition for the CdSeTeS core was Cd (69%), Se (7%), Te (5%) and S (19%) and that for the CdSeTeS/ZnS core/shell was Cd (66.43%), Se (3.37%), Te (3.05), Zn (5.67%) and S (21.48%). An increase in the Zn and S content and decrease in the Cd content of the core/shell QDs relative to the core QDs was a direct evidence of the effects of shell layering.

3.5. Raman analysis of the QDs, GO and QD-GO nanocomposite

The Raman spectrum of GO [28] shown in Fig. 5 displayed the characteristic D and G band at 1350 cm^{-1} and 1596 cm^{-1} respectively. The D band is generally assigned to vibration of sp^3 hybridized carbon atoms of defects which can break the selection rule and symmetry, while the G band is ascribed to the sp^2 hybridized carbon domain entailed with E_{2g} mode [38]. For the Raman spectrum of the QDs, a broad and weak peak around the region of $4000\text{--}4600\text{ cm}^{-1}$ was observed. The Raman spectrum of the QDs is typical for fluorescent-emitting nanocrystals [28]. For the QD-GO nanocomposite, we observed that the QDs dominated the Raman spectrum. The interesting feature is that the Raman spectrum of the nanocomposite was stronger and more refined than the unconjugated QDs. This is strongly induced by the binding effect of GO.



Scheme 2. Schematic representation of the π - π induced PAH adsorption on GO which triggers the fluorescence enhancement of the conjugated QDs.

3.6. FT-IR spectra of the QDs, GO and QD-GO nanocomposite

The FT-IR spectrum of GO (Fig. 6) exhibited characteristic bands at ν_{C-O} = 1060 cm^{-1} (alkoxy), ν_{C-O} = 1232 cm^{-1} (epoxy), ν_{C-O} = 1582 cm^{-1} (aromatic), $\nu_{C=O}$ = 1720 cm^{-1} (carbonyl and carboxylic) and ν_{O-H} = 3000 - 3050 cm^{-1} (hydroxyl) [28]. For the unconjugated QDs, the symmetric and asymmetric carboxylic bands appeared at ν_{C-O} = 1387 and 1625 cm^{-1} while the hydroxyl functional group appeared at ν_{O-H} = 3431 cm^{-1} . A careful assessment of the FT-IR spectrum of the QD-GO nanocomposite indicated a slight resemblance to GO. This is due to the strong binding effect of GO to the QDs. The formation of the amide linkage between GO and the QDs is difficult to ascertain from the FT-IR spectrum due to remaining unconjugated moieties on the GO, however the band at 1723 cm^{-1} is in the region for CO-NH formation.

3.7. Fluorescence detection principle

Studies have shown that drugs, pesticides, phenolic compounds, humic acids and PAHs [12,28,33] can adsorb onto graphene-related materials. There are five possible mechanistic pathways by which aromatic-based analytes can interact with the surface of carbon-based materials, namely (i) π - π interactions, (ii) hydrophobic effects, (iii) electrostatic interactions, (iv) covalent interactions and hydrogen bonds [33]. For graphene-based materials, most studies have found π - π interaction to play the dominant role for adsorption [12,33], although hydrophobic effects may also play a role when considering interactions with non-polar organic species in water. Scheme 2 shows the proposed mechanism for the detection of the targeted PAHs by the QD-GO nanocomposite (Scheme 2A), using Phe as an example. Upon binding of GO to the QDs, the fluorescence of the QDs is quenched ("switched OFF"), whilst interaction of the targeted PAH analytes with the QD-GO probe switched on the fluorescence of the conjugated QDs. The PAH analytes were able to adsorb onto graphene via π - π in-teractions of their aromatic ring system with the π electron rich carbon system of GO (Scheme 2B). The adsorption process then remediates the surface defect states on the QD-GO surface leading to fluorescence enhancement.

3.8. Relative fluorescence enhancement effects of different PAHs on the QD-GO nanocomposite

The affinity of Py, Naph, Ant and Phe to switch on the fluorescence of the QD-GO nanocomposite probe was investigated. It is expected that each of the PAH compounds can adsorb onto GO and trigger fluorescence transduction changes in the conjugated QDs. However, the degree of fluorescence enhancement may vary amongst the PAH analytes due to structural differences. Fig. 7A shows the enhancement effects of the PAH analytes (at a fixed concentration) on the fluorescence of the nanocomposite probe. Each of the tested PAH analytes showed affinity for the nano-composite probe. The variation in affinity based on the relative % fluorescence enhancement followed the order Py < Naph < Ant < Phe.

3.9. Effect of incubation time and nanocomposite concentration

The effect of incubation time on the PL intensity of the QD-GO nanocomposite probe was studied. Fig. 7B shows the time-dependent (5-40 min) fluorescence intensity change for the detection of a fixed concentration of Phe (5×10^{-7} M). The data obtained shows that the fluorescence enhancement, and thereby nanocomposite/analyte interactions, were greatest after 5 min incubation and thereafter a steady decrease in the fluorescence

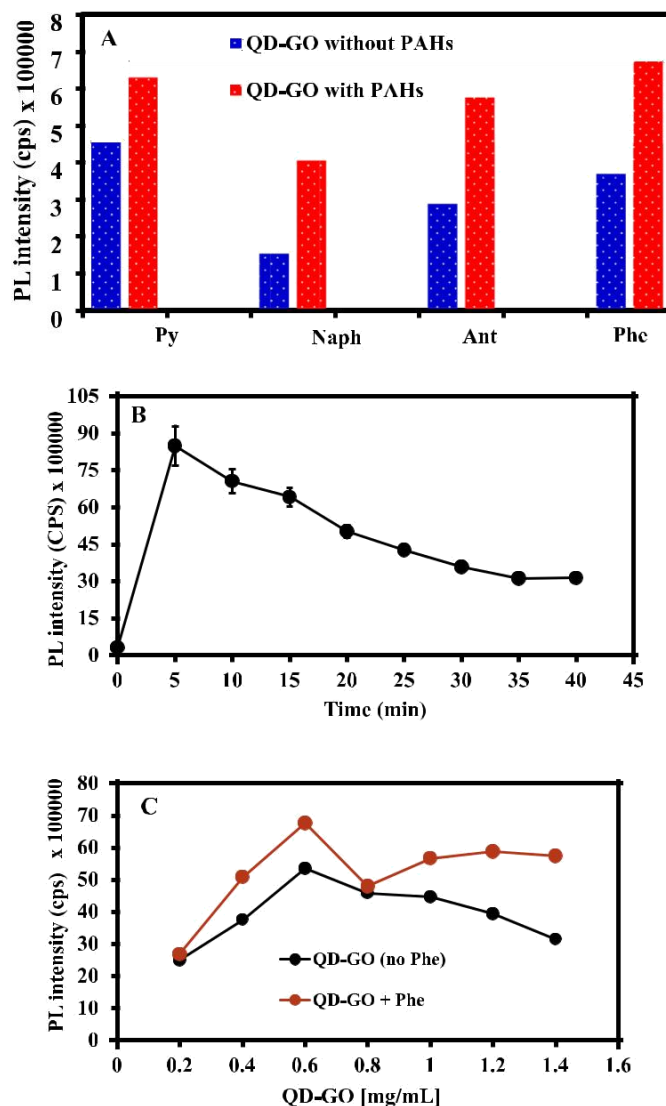


Fig. 7. Effects of PAHs on the PL emission of QD-GO nanocomposite. [PAH] = 5×10^{-7} M. Effect of incubation time (0-40 min) (B) and concentration (C) on the PL emission of the QD-GO nanocomposite in the presence of 5×10^{-7} M Phe target. Error bars represent standard deviation of 3 successive measurements.

intensity occurred from 10 min to 40 min. The results indicate that Phe can be detected between 5 and 40 min of incubation time but shorter incubation time is more favourable due to the greater enhancement in fluorescence signal. The effect of the QD-GO concentration on the detection of a fixed concentration of Phe is shown in Fig. 7C. With the exception of 0.2 mg/mL and 0.8 mg/mL (which may be considered an outlier) concentration of the QD-GO which exhibited low fluorescence signal enhancement, the rest of the concentrations showed appreciable fluorescence signal enhancement. It appears that there is an increase in PL intensity up to a concentration of 0.6 mg/mL of nanocomposite, indicating an increased interaction of the analyte with the nanocomposite as more of the latter is available in solution. Thereafter, it appears that the nanocomposite is in excess, as there was no further increase in PL intensity with additional increase in concentration of the nanocomposite. In fact, it appears that some degree of self-quenching or agglomeration may have occurred at the higher nanocomposite concentrations due to the slight decrease in PL intensity.

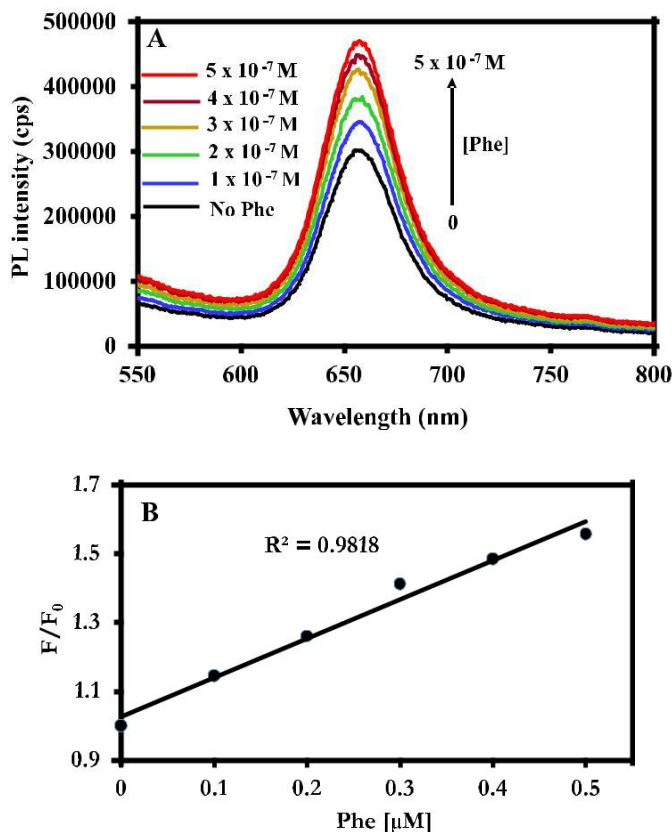


Fig. 8. (A) PL “switch ON” emission spectra for the detection of Phe using the QD-GO nanocomposite for a range of phenanthrene concentrations and (B) corresponding fluorescence signal calibration curve.

3.10. Fluorescence “switch ON” detection of phenanthrene

Phe, used as a typical test PAH analyte, was detected by the nanocomposite probe at different concentrations. Fig. 8A shows the fluorescence detection of Phe by the nanocomposite probe. At increasing concentration of Phe, the fluorescence of the conjugated QDs was switched on. No noticeable peak shift was observed as the target Phe was detected. This implies that the fluorescence of the QD-GO nanocomposite remained stable during the detection process. The corresponding fluorescence calibration curve is shown in Fig. 8B and the limit of detection (LOD) was estimated as three times the standard deviation of blank measurements ($n = 9$) divided by the slope of the linear calibration curve. The LOD of Phe was 2.26×10^{-9} M or 0.4 $\mu\text{g/L}$. The nanocomposite developed in this work is not only suitable for the detection of PAHs but will be sensitive to analytes having fused benzene rings in which their electron rich system can result in adsorption onto the surface of graphene and trigger fluorescence changes in the bonded fluorophore. We believe our detection system is simple, cheap and sensitive.

4. Conclusions

A new nanocomposite material involving the conjugation of L-cysteine-capped CdSeTeS/ZnS QDs to GO has been developed. Characterization of the nanocomposite has been performed using transmission electron microscopy, scanning electron microscopy, Raman, X-ray diffraction, FT-IR, UV/vis and fluorescence spectrophotometry. We have taken advantage of the π electron rich system of GO and its planar structure as a mechanism for the adsorption

of the π electron rich aromatic system of PAHs. The affinity of four different PAH analytes to switch on the fluorescence of the conjugated QDs based on π - π interaction with the surface of GO followed the order Phe > Ant > Naph > Py and the LOD for Phe was 2.26×10^{-9} M.

Acknowledgements

A postdoctoral fellowship offered by the University of Pretoria is gratefully appreciated by O. Adegoke. This work is based on research supported in part by the National Research Foundation of South Africa, Grant Numbers: 90720 and 93394 (P. Forbes), as well as the Department of Science and Technology (DST) through the Photonics Initiative of South Africa (PISA Grant PISA-15-DIR-06), and the Water Research Commission (WRC Grant K5/2438/1). Wirsam Scientific, South Africa is thanked for their support of this research. We thank the Laboratory for Microscopy and Microanalysis of the University of Pretoria (UP), for assistance with the microscopy measurements and Wiebke Grote of UP for the XRD analyses.

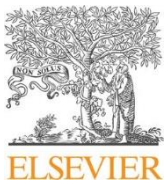
References

- [1] J. Kao, K. Thorkelsson, P. Bai, B.J. Rancatore, T. Xu, Toward functional nano-composites: taking the best of nanoparticles, polymers, and small molecules, *Chem. Soc. Rev.* 42 (2013) 2654–2678.
- [2] K.S. Novoselov, A.K. Geim, S.V. Morozov, D. Jiang, Y. Zhang, S.V. Dubonos, I.V. Grigorieva, A.A. Firsov, Electric field effect in atomically thin carbon films, *Science* 306 (2004) 666–669.
- [3] T.P. Kaloni, Y.C. Cheng, R. Faccio, U. Schwingenschlög, Oxidation of mono-vacancies in graphene by oxygen molecules, *J. Mater. Chem.* 21 (2011) 18284–18288.
- [4] Y.C. Cheng, T.P. Kaloni, Z.Y. Zhu, U. Schwingenschlög, Oxidation of graphene in ozone under ultraviolet light, *Appl. Phys. Lett.* 101 (2012) 073110.
- [5] T.P. Kaloni, M. Upadhyay Kahaly, R. Faccio, U. Schwingenschlög, Modelling magnetism of C at O and B monovacancies in graphene, *Carbon* 64 (2013) 281–287.
- [6] W. Choi, I. Lahiri, R. Seelaboyina, Y.S. Kang, Synthesis of graphene and its applications: a review, *Crit. Rev. Solid State* 35 (2010) 52–71.
- [7] Y. Si, E.T. Samulski, Synthesis of water soluble graphene, *Nano Lett.* 8 (2008) 1679–1682.
- [8] E.W. Hill, A. Vijayaraghavan, K. Novoselov, Graphene sensors, *IEEE Sens. J.* 11 (2011) 3161e3170.
- [9] V. Singh, D. Joung, L. Zhai, S. Das, S.I. Khondaker, S. Seal, Graphene based materials: past, present and future, *Prog. Mater. Sci.* 56 (2011) 1178–1271.
- [10] L. Gomez De Arco, Y. Zhang, C.W. Schlenker, K. Ryu, M.E. Thompson, C. Zhou, Continuous, highly flexible, and transparent graphene films by chemical vapor deposition for organic photovoltaics, *ACS Nano* 4 (2010) 2865–2873.
- [11] M.J. Allen, V.C. Tung, L. Gomez De Arco, Z. Xu, L.M. Chen, K.S. Nelson, C. Zhou, R.B. Kaner, Y. Yang, Soft transfer printing of chemically converted graphene, *Adv. Mater.* 21 (2009) 2098–2102.
- [12] S. Basua, P. Bhattacharyya, Recent developments on graphene and graphene oxide based solid state gas sensors, *Sens. Actuat. B-Chem.* 173 (2012) 1–21.
- [13] Y. Zhang, Y.W. Tan, H.L. Stormer, P. Kim, Experimental observation of the quantum Hall effect and Berry's phase in graphene, *Nature* 438 (2005) 201–204.
- [14] T. Kuila, S. Bose, P. Khanra, A.K. Mishra, N.H. Kim, J.H. Lee, Recent advances in graphene-based biosensors, *Biosens. Bioelectron.* 26 (2011) 4637–4648.
- [15] N. Tombros, C. Jozsa, M. Popinciuc, H. Jonkman, B. van Wees, Electronic spin transport and spin precession in single graphene layers at room temperature, *Nature* 448 (2007) 571–574.
- [16] T.J. Booth, P. Blake, R.R. Nair, D. Jiang, E.W. Hill, U. Bangert, A. Bleloch, M. Gass, K.S. Novoselov, M.I. Katsnelson, A.K. Geim, Macroscopic graphene membranes and their extraordinary stiffness, *Nano Lett.* 8 (2008) 2442–2446.
- [17] B. Lang, A LEED study of the deposition of carbon on platinum crystal surfaces, *Surf. Sci.* 53 (1975) 317–329.
- [18] M. Pumera, A. Ambrosi, A. Bonanni, E.L.K. Chng, H.L. Poh, Graphene for electrochemical sensing and biosensing, *Trac-Trend Anal. Chem.* 29 (2010) 954–965.
- [19] R.M. Singh, R. Kumar, D.P. Singh, Graphene oxide: strategies for synthesis, reduction and frontier applications, *RSC Adv.* 6 (2016) 64993–65011.
- [20] M. Han, X. Gao, J.Z. Su, S. Nie, Quantum-dot-tagged microbeads for multiplexed optical coding of biomolecules, *Nat. Biotechnol.* 19 (2001) 631–635.
- [21] A.P. Alivisatos, The use of nanocrystals in biological detection, *Nat. Biotechnol.* 22 (2004) 47–52.
- [22] N.L. Rosi, C.A. Mirkin, Nanostructures in biodiagnostics, *Chem. Rev.* 105 (2005) 1547–1562.
- [23] O. Adegoke, T. Kato, E.Y. Park, An ultrasensitive alloyed near-infrared

- quinternary quantum dot-molecular beacon nanodiagnostic bioprobe for influenza virus RNA, *Biosens. Bioelectron.* 80 (2016) 483-490.
- [24] O. Adegoke, M.-W. Seo, T. Kato, S. Kawahito, E.Y. Park, Gradient band gap engineered alloyed quaternary/ternary CdZnSeS/ZnSeS quantum dots: an ultrasensitive fluorescence reporter in a conjugated molecular beacon system for the biosensing of influenza virus RNA, *J. Mater. Chem. B* 4 (2016) 1489-1498.
- [25] H. Richter, J.B. Howard, Formation of polycyclic aromatic hydrocarbons and their growth to soot: a review of chemical reaction pathways, *Prog. Energ. Combust.* 26 (2000) 565-608.
- [26] G. Falco, J.L. Domingo, J.M. Llobet, A. Teixido, C. Casas, L. Muller, Polycyclic aromatic hydrocarbons in foods: human exposure through the diet in Catalonia, Spain, *J. Food. Prot.* 66 (2003) 2325-2331.
- [27] O. Adegoke, T. Nyokong, P.B.C. Forbes, Structural and optical properties of alloyed quaternary CdSeTeS core and CdSeTeS/ZnS core-shell quantum dots, *J. Alloy Compd.* 645 (2015) 443-449.
- [28] O. Adegoke, P.B.C. Forbes, L-cysteine-capped core/shell/shell quantum dot-graphene oxide nanocomposite fluorescence probe for polycyclic aromatic hydrocarbon detection, *Talanta* 146 (2016) 780-788.
- [29] W.S. Hummers Jr., R.E. Offeman, Preparation of graphitic oxide, *J. Am. Chem. Soc.* 80 (1958) 1339.
- [30] US Environmental Protection Agency, Guidelines Establishing Test Procedures for the Analysis of Pollutants, Proposed Regulations, Federal Register, vol. 49, no. 209, USEPA, Washington, DC.
- [31] L. Chimuka, P. Sibiya, R. Amdany, E. Cukrowska, P.B.C. Forbes, Status of PAHs in environmental compartments of South Africa: a country report, *Polycycl. Aromat. Comp.* 36 (2015) 376-394.
- [32] E. Martinez, M. Gros, S. Lacorte, D. Barcelo, Simplified procedures for the analysis of polycyclic aromatic hydrocarbons in water, sediments and mussels, *J. Chrom. A* 1047 (2004) 181-188.
- [33] S. Wang, H. Sun, H.M. Ang, M.O. Tade, Adsorptive remediation of environmental pollutants using novel graphene-based nanomaterials, *Chem. Eng. J.* 226 (2013) 336-347.
- [34] M. Li, X. Zhou, S. Guo, N. Wu, Detection of lead (II) with a "turn-on" fluorescent biosensor based on energy transfer from CdSe/ZnS quantum dots to graphene oxide, *Biosens. Bioelectron.* 43 (2013) 69-74.
- [35] H. Tao, X. Liao, M. Xu, X. Xie, F. Zhong, Z. Yi, Detection of immunoglobulin G based on nanoparticle surface energy transfers from fluorescein isothiocyanate to gold nanoparticles, *Anal. Methods* 6 (2014) 2560-2565.
- [36] X. Huang, I.H. El-Sayed, W. Qian, M.A. El-Sayed, Cancer cells assemble and align gold nanorods conjugated to antibodies to produce highly enhanced, sharp, and polarized surface Raman spectra: a potential cancer diagnostic marker, *Nano Lett.* 7 (2007) 1591-1597.
- [37] S. Jander, A. Kornowski, H. Weller, Energy transfer from CdSe/CdS nanorods to amorphous carbon, *Nano Lett.* 11 (2011) 5179-5183.
- [38] X.-j. Hu, Y.-g. Liu, H. Wang, A.-w. Chen, G.-m. Zeng, S.-m. Liu, Y.-m. Guo, X. Hu, T.-t. Li, Y.-q. Wang, L. Zhou, S.-h. Liu, Removal of Cu(II) ions from aqueous solution using sulfonated magnetic graphene oxide composite, *Sep. Purif. Technol.* 108 (2013) 189-195.

C. 2 Paper 2

Adegoke, O., Montaseri, H., Nsibande, S.A., & Forbes, P.B.C. (2019). Passivating effect of ternary alloyed AgZnSe shell layer on the structural and luminescent properties of CdS quantum dots. *Materials Science in Semiconductor Processing*. 90, 162-170. Impact Factor 2.593. <https://doi.org/10.1016/j.mssp.2018.10.025>



Contents lists available at ScienceDirect

Materials Science in Semiconductor Processing

journal homepage: www.elsevier.com/locate/mssp

Passivating effect of ternary alloyed AgZnSe shell layer on the structural and luminescent properties of CdS quantum dots



Oluwasesan Adegoke*, Hanieh Montaseri, Sifiso A. Nsibandé, Patricia B.C. Forbes*

Department of Chemistry, Faculty of Natural and Agricultural Sciences, University of Pretoria, Lynnwood Road, Pretoria 0002, South Africa

ARTICLE INFO

Keywords:

Quantum dots
Surface defects
Photoluminescence
Quantum yield
Alloyed

ABSTRACT

The surface passivation of luminescent CdS quantum dots (QDs) via epitaxial overgrowth of new alloyed ternary AgZnSe shell layer is reported here. Two synthetic fabrication strategies were used to tune the optical properties of CdS/AgZnSe core/alloyed shell QDs across the visible region. Transmission electron microscopy, powder X-ray diffraction, Raman, UV/vis and fluorescence spectrophotometric techniques were used to characterize the nanocrystals. Analysis of the internal structure of the QDs revealed that homogeneity of the particle reduced as the size increased, thus indicating that the QDs growth transitioned from an interfacial epitaxial homogenous state to a heterogeneous state. The crystal structure of the QDs revealed a distinct zinc-blende diffraction pattern for CdS while CdS/AgZnSe core/alloyed shell QDs kinetically favoured a phase change process from the zinc-blende phase to a wurtzite phase. Analysis of the photophysical properties revealed varying degrees of interfacial defect state suppression in CdS/AgZnSe QDs which was dependent on the QDs size. Specifically, the fluorescence quantum yield (QY) of CdS/AgZnSe QDs was at most ~5-fold higher than the CdS core and varied from 35% to 73%. We found that band gap modulation via the synthetic fabrication strategy employed, influenced the optical properties of the core/alloyed shell QDs. The CdS/AgZnSe QDs produced in this work hold great promise in light-emitting optoelectronic applications.

1. Introduction

The wide electro-luminescent applications of colloidal semiconductor quantum dot (QD) nanocrystals in various fields of chemistry, biology and physics, stem from their unique optoelectronic properties [1,2]. Particularly, the size-dependent optical and electronic properties of QDs which are governed by the associated quantum confinement feature, allows tuning of the photoluminescence (PL) emission from the ultraviolet/visible (UV/vis) region to the far infrared region [3–6]. In contrast to bulk semiconductors in which the surface represents a tiny fraction of the bulk material, colloidal QDs have their size typically in the range of 2–10 nm. This unique characteristic enables a large number of atoms to be embedded on the QD surface [7].

The QD surface represents a highly sensitive region that is exposed to its surrounding environment (matrices, solvents and various other species in solution) and it is typically coordinated by chemical ligands, surfactants or stabilizers that influence the QD optoelectronic properties [7]. The synergistic effects of precursor material which create low numbers of coordinated surface atoms may lead to highly reactive or localized electronic sites that are susceptible to redox and chemical processes. Thus, it is very likely for midgap, shallow or deep surface

defect states to be formed and induce the pathway for poor PL properties. The characteristic phenomenon is nonradiative recombination exciton (electron and hole) states associated with low PL quantum yield (QY) [8,9]. One of the widely used strategies to eliminate surface traps is to passivate the QD core surface with a wider band gap shell material [10–13]. This strategy shifts the surface defects to the outer domain of the shell layer, thus improving the PL QY [4]. The electron and hole being localized in the core, represents a signature process associated with the low probability of the outer surface state being subjected to trapped photogenerated charge carriers [14,15].

Over the past two decades, the most studied class of semiconductor QDs are the group II-VI metal chalcogenides with CdSe-based QDs being the most popular for fabricating new synthetic routes [16], shell passivation [17], ligand dynamics [18] and alloying [19]. On the other hand, CdS nanocrystals are probably the second most studied QD system [20–23], exhibiting an exciton Bohr radius of 3.0 nm [24] and a bulk band gap of 2.48 eV [25]. Its characteristic PL emission is known to be highly prone to surface defects which results in low PL QY [26]. Nonetheless, it is widely used as a shell layer to overcoat the surface of CdSe-based QDs. The well-known strategy to isolate the exciton wave function from the surface of the core QDs with embedded surface

* Corresponding authors.

E-mail addresses: adegoke.sesan@mailbox.co.za (O. Adegoke), patricia.forbes@up.ac.za (P.B.C. Forbes).

<https://doi.org/10.1016/j.mssp.2018.10.025>

Received 6 October 2018; Received in revised form 21 October 2018; Accepted 24 October 2018
1369-8001/ © 2018 Elsevier Ltd. All rights reserved.

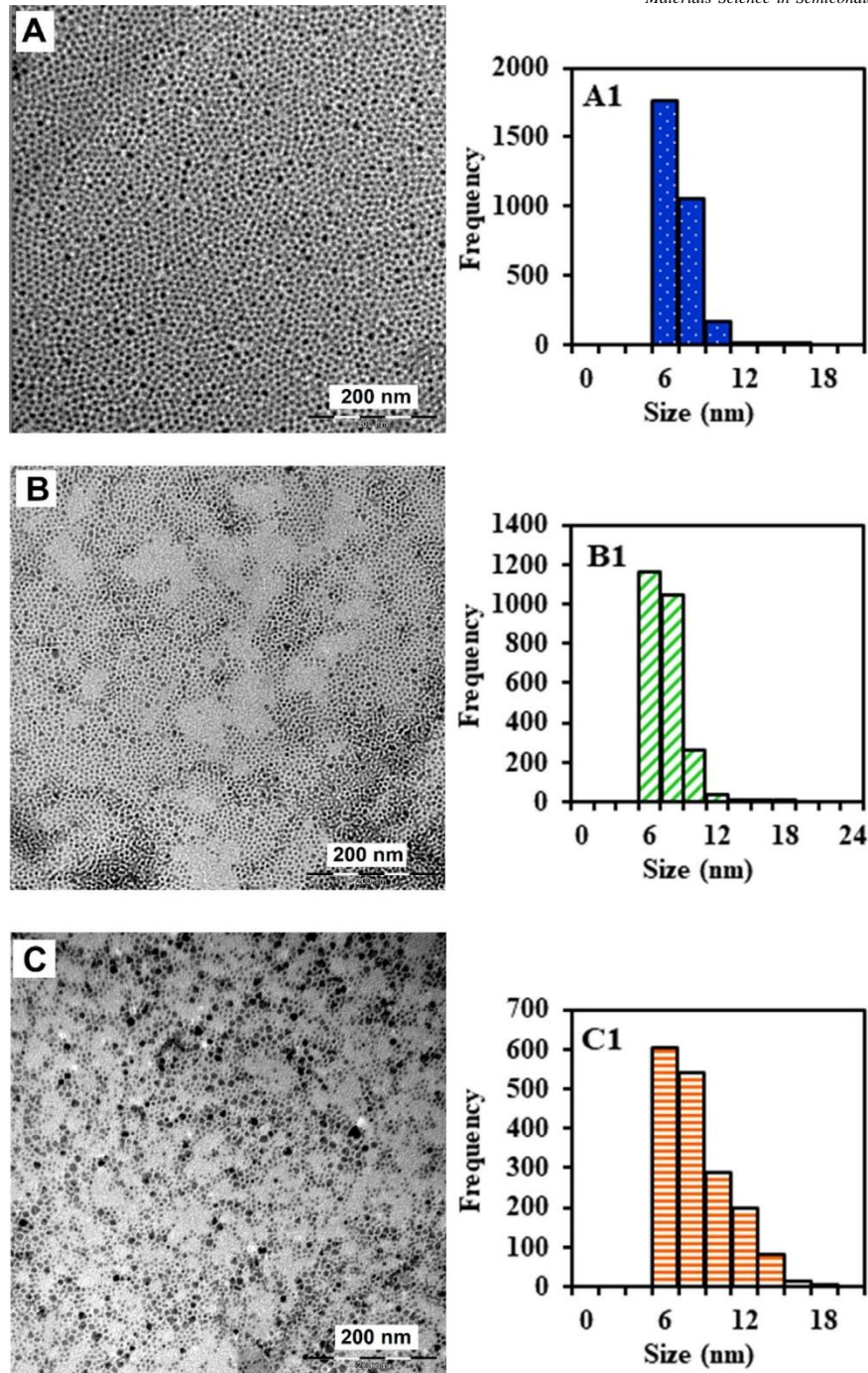


Fig. 1. TEM images (A, B and C) and average particle size distribution (A1, B1 and C1) of CdS core QDs.

defects and dangling bonds is to coat with a shell layer of a wide band gap [27]. However, it is important to note that lattice mismatch between the core and binary shell material at the interface can also induce surface defects that degrade the luminescence of the core/shell QDs, thus lowering the PL QY [28].

Another strategy which has drawn significant interest in improving the PL QY of binary core QDs is to coat the surface with an alloyed ternary shell layer. Alloyed QDs (AB_xC_{1-x}) have become important in mainstream nanoscale optical engineering due to the added degree of freedom in tuning the exciton energy for either extended PL emission range or improved optical properties [29–32]. The coating of an alloyed ternary shell around binary core QDs to improve the PL efficiency has mostly been reported for CdSe-based QDs [33,34] with rare reports for

CdS-based QDs [13]. It is noteworthy that apart from the formation of a smooth gradient band gap, the lattice strain of the core/shell QDs can be relaxed due to alloying [35]. Furthermore, it has been demonstrated that shell alloying suppressed Auger exciton recombination in core/alloyed shell/shell QDs, thus increasing the PL QY [36].

Overcoating a shell layer around the CdS core to improve the PL QY of QDs has rarely been studied. Thus, in this paper, we report on a new strategy to suppress the surface defect states of CdS QDs by coating with a new ternary alloyed shell layer. CdS QDs, characterized by low PL QY due to embedded surface defects were synthesized in this work via the organometallic synthetic route. We have demonstrated for the first time that improved PL QY in CdS QDs can be achieved via passivation with a ternary alloyed AgZnSe shell layer. To the best of our knowledge, our

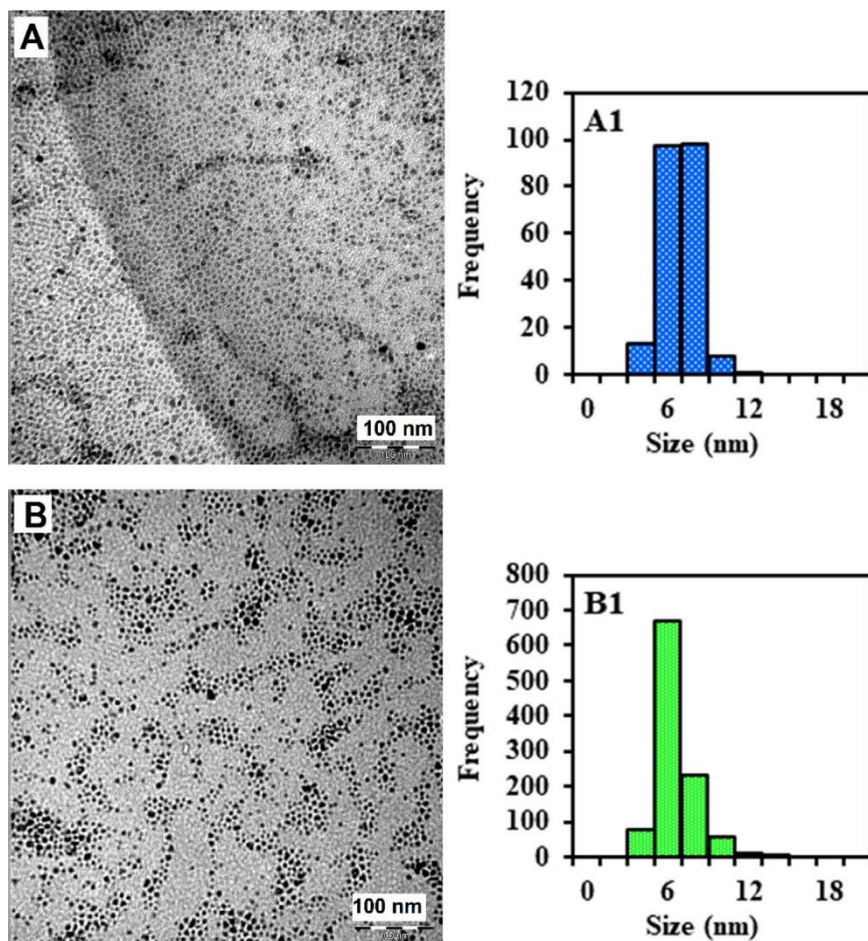


Fig. 2. TEM images (A, B, C and D) and average particle size distribution (A1, B1, C1 and D1) of CdS/AgZnSe core/alloys shell QDs synthesized via method 1.

work is the first to overcoat a AgZnSe shell around CdS core QDs with the sole aim of suppressing interfacial defect states in the core QDs. The organic-phase CdS/AgZnSe core/alloys shell QDs produced in this work hold great promise in light-emitting optoelectronic applications.

2. Experimental section

2.1. Materials

Cadmium oxide (CdO), myristic acid, trioctylphosphine oxide (TOPO), hexadecylamine (HDA), trioctylphosphine (TOP), octadecene (ODE), oleic acid, sulphur (S), L-cysteine, diethylzinc (Et_2Zn) and zinc oxide (ZnO) were purchased from Sigma Aldrich. Silver nitrate (AgNO_3) was purchased from Saarchem. Selenium (Se) was purchased from Merck. Methanol, acetone, hexane and chloroform were purchased from ACE Chemicals.

2.2. Characterization

UV/vis absorption spectra were obtained using a Cary Eclipse (Varian) spectrophotometer. PL emission measurements were carried out using a Horiba Jobin Yvon Fluoromax-4 spectrofluorometer. Powder X-ray diffraction (PXRD) measurements were determined using a $\text{Cu}(K_\alpha)$ radiation ($\lambda = 1.54184 \text{ \AA}$) on a Bruker D2 Phaser. Transmission electron microscopy (TEM) images were produced using a JEOL JEM 2100 F operated at 200 kV. Raman spectra were recorded using a WITec Alpha 300 micro-Raman imaging system with a 488 nm excitation laser and CCD detector at ambient temperature with the laser power below 2 mW in order to reduce heating effects.

2.3. Preparation of the precursors

2.3.1. TOPSe

To prepare the Se precursor, 0.12 g Se was dissolved in 5 mL TOP and sonicated until complete dissolution of Se, thus resulting in a clear solution. The solution was then stirred at room temperature prior to use and was stable for 3 days.

2.3.2. TOPZn

To prepare the Zn precursor from Et_2Zn , 1.93 g TOPO was firstly dissolved in 10 mL ODE and 5 mL of oleic acid. The solution was then heated up until the complete dissolution of TOPO surfactant, thus resulting in a clear solution. Thereafter, 2 mL Et_2Zn and 1 mL TOP were added and the solution was stirred at room temperature before use.

To prepare the Zn precursor from ZnO, 0.4 g ZnO was added to a mixture of 15 mL ODE and 10 mL oleic acid and sonicated for a few minutes. Thereafter, the precursor solution was stirred at room temperature prior to use.

2.3.3. TOPAg

Ag precursor was prepared by mixing 0.5 g AgNO_3 with 5 mL TOP. The solution was then heated up until complete dissolution of the AgNO_3 which was evident by the change in colour from colourless to brownish black.

2.3.4. TOPS

To prepare the TOPS precursor used in method 1 synthesis of CdS/AgZnSe QDs (refer to Section 2.4), 1.93 g TOPO was first dissolved in 15 mL ODE and 10 mL oleic acid followed by the addition of 0.16 g S

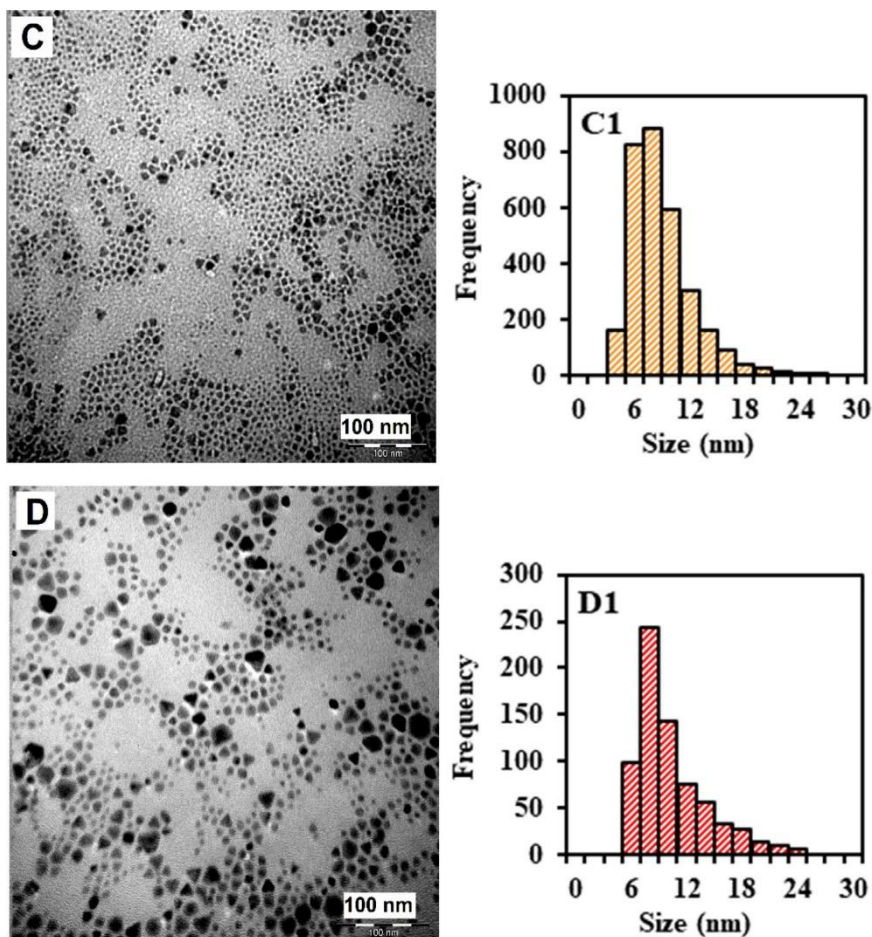


Fig. 2. (continued)

and 1 mL TOP. For method 2 synthesis of CdS/AgZnSe QDs (Section 2.5), 1.93 g TOPO was dissolved in 10 mL ODE and 5 mL oleic acid, then 0.08 g S and 1 mL TOP was added thereafter. The solutions were sonicated and heated up to aid complete dissolution of the S and thereafter stirred at room temperature prior to use.

2.4. Synthesis of CdS/AgZnSe core/alloyed shell QDs (method 1)

The synthesis of CdS/AgZnSe core/alloyed shell QDs was carried out via the organometallic one-pot synthetic route but with modifications [37]. Complexation between the Cd ion, surfactants and capping ligands was formed by mixing 1.3 g CdO, 1.2 g myristic acid, 1.93 g TOPO and 1.2 g HDA with 50 mL ODE and 30 mL of oleic acid. The solution was bubbled with Ar gas and heated up until complete dissolution of the Cd ion which was evident by a change in colour of the solution from pale brown to colourless. At ~ 220 °C, TOPS solution was added into the Cd precursor solution to form the CdS core QDs. Once satisfactory growth of the QD core was achieved, a fraction of the growth solution was injected into a beaker. To form the core/alloyed shell QDs, 1 mL of TOPSe solution was added into the CdS growth solution followed swiftly by the addition of 1 mL TOPAg and TOPZn (using ZnO). Portions of the core/shell QDs were taken out at different time intervals.

2.5. Synthesis of CdS/AgZnSe QDs (method 2)

Method 2 synthesis was carried out according to the fabrication steps detailed in method 1 but with slight modifications of the precursor concentrations. For the complexation of Cd ion with the precursor materials, 2 mL TOP, 0.4 g CdO, 0.6 g HDA and 0.6 g myristic acid were

mixed with 20 mL ODE and 15 mL oleic acid. The synthetic process of method 1 was thereafter followed by adding TOPS (prepared specifically for method 2) to form the CdS QDs. Formation of the core/alloyed shell QDs was followed according to method 1 except that TOPZn prepared from ET_2Zn was used.

3. Results and discussion

3.1. Fabrication of the QDs

One-pot organometallic synthesis of metal precursors in the presence of surfactants, organic-capping ligands and a non-coordinating solvent (ODE) was used to engineer the structure of the QDs. It is well known that the growth kinetics influences the PL emission and absorption evolution of the QDs [38]. The nature of the precursor material with respect to the concentration, quantity, time of injection, temperature and the interplay between them are reaction conditions that influence the growth of the QDs. We have therefore exploited these reaction conditions to engineer the optical properties of CdS/AgZnSe core/alloyed shell QDs.

In method 1 synthesis, higher quantities of the Cd metal precursor, surfactants, organic ligands and the non-coordinating solvent were used to aid the Cd-precursor complexation for the subsequent nucleation and growth of CdS QDs. Conversely, lower concentrations of the Cd precursor, surfactants and ligands were employed in method 2 synthesis of the QDs. Before adding the TOPS precursor, the Cd precursor solution was heated up to > 200 °C to aid complete dissolution and complexation of the Cd precursor. The change in colour of the solution from brown to colourless confirmed the complexation process which was accompanied by injection of the TOPS precursor. As the CdS core QDs

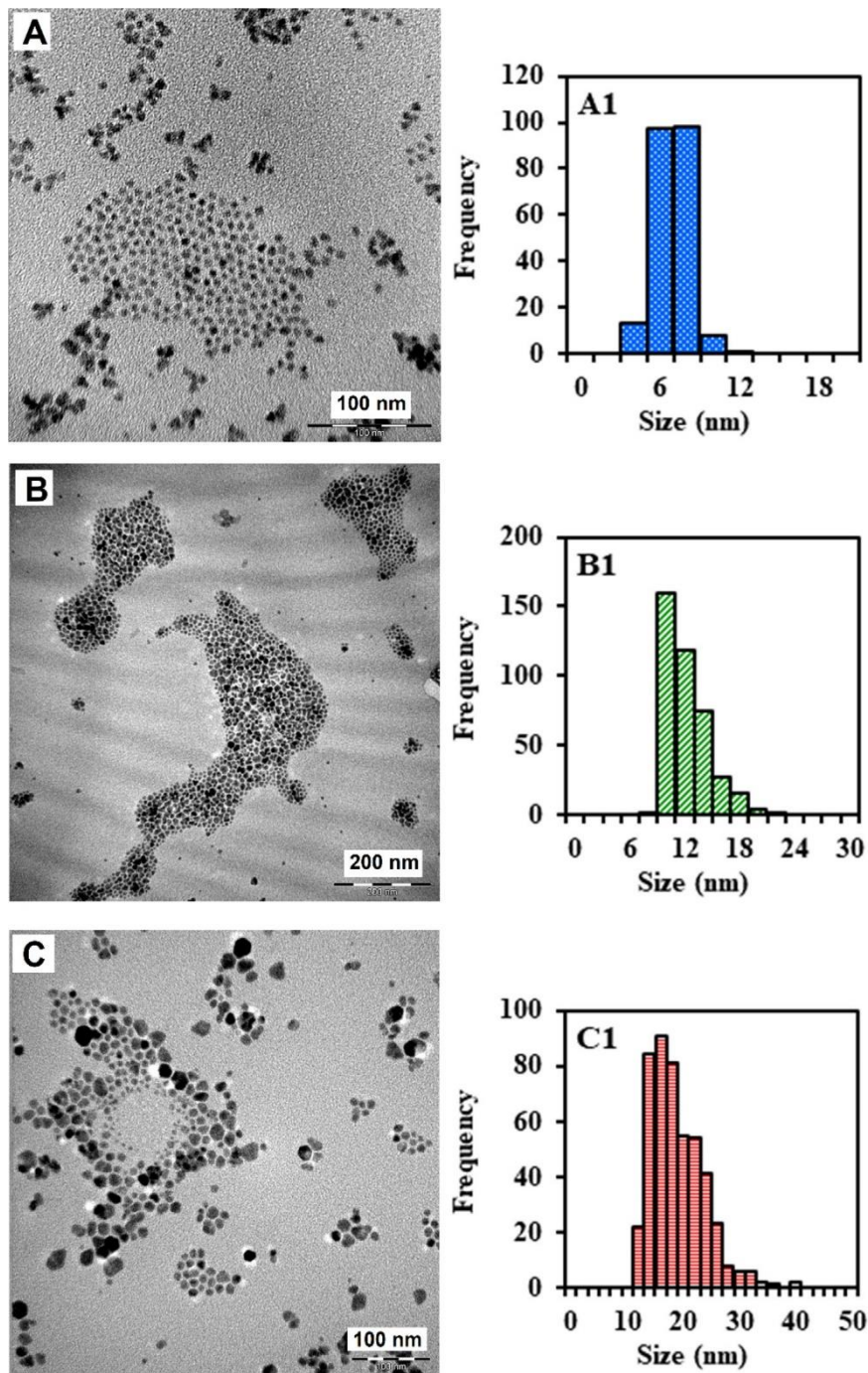


Fig. 3. TEM images (A, B and C) and average particle size distribution (A1, B1 and C1) of CdS/AgZnSe core/alloyed shell QDs synthesized via method 2.

nucleated, the temperature of the growth solution increased steadily and was accompanied by a concomitant change in the colour. During this period, a fraction of the CdS core QDs was removed in order to probe the structural and optical properties thereof in comparison to the core/alloyed shell QDs.

The temperature at which the AgZnSe alloyed shell was overcoated on the CdS core surface is very crucial to the overall optical properties of the CdS/AgZnSe core/alloyed shell QDs. At higher temperature and longer reaction time, CdS QDs size distribution is expected to deteriorate and lead to broadening of the spectral line widths. On the other hand, overcoating the shell layer at relatively low temperature could either reduce the crystallinity of CdS/AgZnSe core/alloyed shell QDs or lead to incomplete decomposition of the precursor materials [39].

Therefore, an appropriate temperature was determined independently for each method used to fabricate the core/alloyed shell QDs. The concentration and rate at which the AgZnSe shell precursor is added is also crucial in influencing the optical properties of the QDs. Slow addition of the precursor shell materials prevents homogenous nucleation and induces most of the AgZnSe shell to grow heterogeneously on the CdS nuclei. Hence, the precursor solutions for the shell layering were injected into the CdS growth solution in swift succession. Addition of TOPSe, TOPZn and TOPAg precursors to the CdS growth solution triggered a progressive change in the colour of the solution from orange to red and to dark brown. Different sizes of the CdS/AgZnSe QDs were thereafter harvested at different time intervals whilst the QDs were purified with acetone, chloroform/acetone and chloroform/acetone/

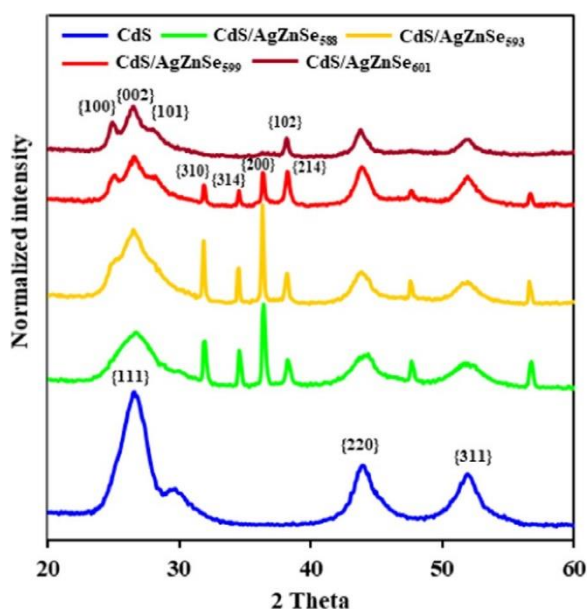


Fig. 4. PXRD plots of CdS, CdS/AgZnSe₅₈₈, CdS/AgZnSe₅₉₃, CdS/AgZnSe₅₉₉ and CdS/AgZnSe₆₀₁ QDs.

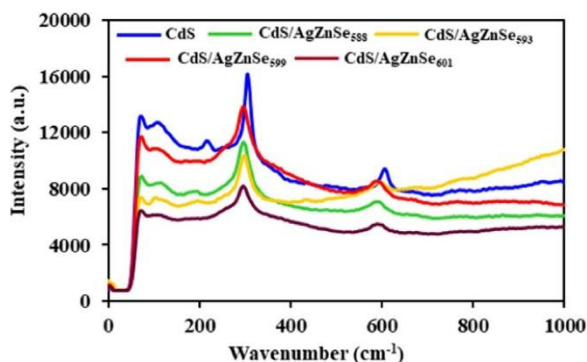


Fig. 5. Raman spectra of CdS, CdS/AgZnSe₅₈₈, CdS/AgZnSe₅₉₃, CdS/AgZnSe₅₉₉ and CdS/AgZnSe₆₀₁ QDs.

ethanol mixture.

3.2. Structural properties

3.2.1. Surface morphology

TEM analysis was used to qualitatively probe the internal structure of the QDs with respect to the shape, size distribution, and shell coverage. Fig. 1A–C shows the TEM images of three different-sized CdS QDs with average sizes of 6.0 ± 0.5 , 6.5 ± 0.5 and 7.5 ± 1.2 nm respectively. Our aim was to synthesize uniform-sized CdS QDs in order to effectively understand the structural effects of shell layering. Looking closely at each TEM micrograph, a uniform size distribution, embedded with a mixture of spherical and quasi-spherical shapes was observed. Thus, the monodispersed particle size distribution provides direct indication of homogenous nucleation and growth of the core QDs.

Alloyed semiconductor QD nanocrystals can be grouped as having either a gradient internal structure derived from varying the alloy composition or a uniform internal structure ascribed to homogenous alloying. In our work, a fixed composition of the shell precursor was used to engineer the structure of the core/alloyed shell QDs. Fig. 2A–D shows the representative TEM images of CdS/AgZnSe core/alloyed shell QDs synthesized via method 1 with average particle sizes of 5.1 ± 0.6 , 5.5 ± 0.7 , 7.9 ± 1.6 and 9.1 ± 1.9 nm respectively. The striking feature was the decrease in the core/alloyed shell QDs particle size

relative to the core which is an unusual phenomenon as the size of the core/shell QDs is expected to increase after shell passivation. Since shell passivation of the 7.5 nm CdS QDs led to rapid nucleation and growth of the different sized CdS/AgZnSe QDs, it is imperative to suggest that either CdS was buried within the shell domain or an intermediate formation of CdS/CdSe occurred before the growth of CdS/AgZnSe QDs.

As the CdS/AgZnSe QDs grew, a steady transformation in the particle morphology with respect to the size distribution was observed. The homogeneity of the particle reduced as the size increased, thus indicating that the QDs growth transitioned from an interfacial epitaxial homogenous state to a heterogeneous state. During the period of harvesting each of the different-sized QDs, the temperature of the solution increased from ~ 240 – 310 °C and this should tentatively influence the nucleation and growth of the QDs. It is also noteworthy to emphasize that the transition in homogeneity of the QDs correlated significantly to the shape engineering of the particle. Looking closely at the TEM monograph of 7.9 nm and 9.1 nm-sized CdS/AgZnSe QDs (Figs. 2C and 2D), the emergence of trigonal-shaped particles was observed. Tentatively, we could attribute the shape engineering of the QDs to the passivating effect of AgZnSe shell, thus implying that the electronic structure of CdS/AgZnSe QDs led to different confinement levels for electron and hole. The hole may be strongly confined to the CdS core while the electron may be delocalised into the shell layer [40].

Three different sizes of CdS/AgZnSe QDs were harvested using method 2 synthetic route. The corresponding TEM images and particle size histograms are shown in Fig. 3. The particle size distribution revealed a prolate heterogeneous particle morphology, resembling an anisotropic-like growth pattern. The anisotropic growth pattern can be understood in terms of the reaction conditions used in the synthesis as it applies to low reactivity precursors and low volume of coordinating solvent. Under these reaction conditions, CdS/AgZnSe heteroepitaxial growth is kinetically controlled (i.e., AgZnSe formation at the surface is the rate-limiting step, rather than the precursor diffusion) and slow. Thus, the high reactivity of the Ag, Zn and Se of the AgZnSe shell layer will favour anisotropic-type growth [41].

Generally, the mechanism of nucleation and growth of CdS/AgZnSe QDs can be understood in terms of Ostwald ripening. At relatively low temperature (220 – 240 °C), Ostwald ripening dominated as a result of dissolution and surface energy of small particles which redissolve to allow subsequent growth of larger particles. At higher temperature (> 260 °C), Brownian motion will increase in the synthetic system due to higher thermal energy. Hence it is more likely that the increase in motion will allow the particles to interact at the exact crystallographic orientation, leading to orientated attachment [42].

3.2.2. Crystal phase analysis

The crystal structure of CdS core and CdS/AgZnSe QDs was studied using PXRD. From the diffraction pattern of the CdS core (Fig. 4), a pure zinc-blende crystal structure with three prominent peaks at planes {111}, {220} and {311} was observed. The three planes exhibited Bragg angles at 26.5° , 43.9° and 51.9° respectively. Comparison of the diffraction pattern of CdS/AgZnSe core/alloyed shell QDs with CdS QDs reveal notable differences. Firstly, the three-notable peaks (associated with zinc-blende crystal structure) present in CdS were observed in CdS/AgZnSe₅₈₈. However, the appearance of four additional peaks between 30° and 40° and two additional peaks at higher Bragg angle (47.6° and 56.8°) provides direct evidence that the shell alloying process induced crystal phase changes in the QDs. Since the CdS/AgZnSe QDs size was tuned by fixed shell alloying, it is interesting to note the phase transition changes in the core/alloyed shell QDs. As the size of CdS/AgZnSe QDs increased, a steady transformation in the diffraction pattern as it relates to changes in the diffraction peaks was observed. A close assessment of the diffraction pattern of CdS/AgZnSe₅₉₃, revealed detailed formation of a duplet peak at low Bragg angle which can be attributed to the steady phase transition from a zinc-blende diffraction pattern to a wurtzite diffraction pattern. Further growth of the core/

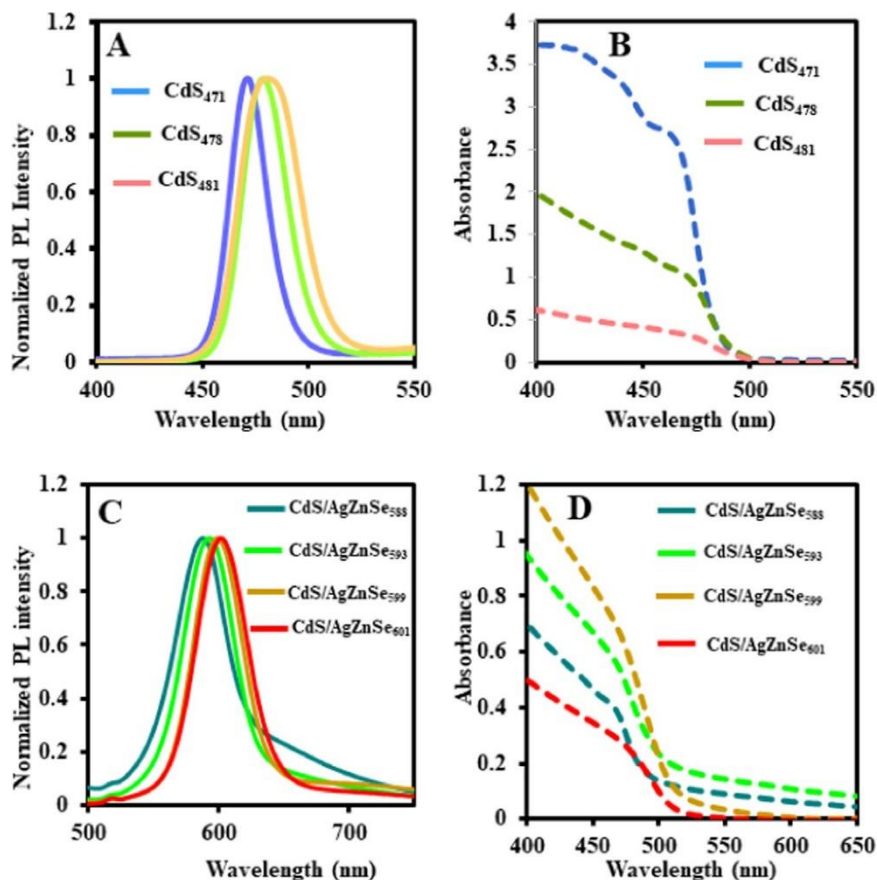


Fig. 6. PL and UV/vis absorption spectra of the different sized CdS (A and B) and CdS/AgZnSe core/alloyed shell QDs (C and D) synthesized via method 1.

Table 1

Summary of the photophysical properties of the different-sized CdS core and CdS/AgZnSe QDs.

QDs- λ_{Emi} (nm)	λ_{Abs} (nm)	FWHM (nm)	Band gap (eV)	PL QY (%)
CdS ₄₇₁	458	20	2.64	16
CdS ₄₇₈	471	26	2.60	4
CdS ₄₈₁	476	33	2.58	8
^a CdS/AgZnSe ₅₈₈	464	41	2.11	48
^b CdS/AgZnSe ₅₉₁	449	34	2.10	73
^a CdS/AgZnSe ₅₉₃	468	42	~2.10	50
^a CdS/AgZnSe ₅₉₉	473	40	2.07	49
^a CdS/AgZnSe ₆₀₁	477	45	~2.07	51
^b CdS/AgZnSe ₆₀₂	473	39	2.06	35
^b CdS/AgZnSe ₆₁₂	481	40	2.03	42

^a Method 1 synthesis.

^b Method 2 synthesis.

alloyed shell QDs led to the formation of a triplet peak at low angle as observed from the diffraction pattern of CdS/AgZnSe₅₉₉. Further assessment of the diffraction pattern of CdS/AgZnSe₆₀₁ revealed the formation of a pure wurtzite diffraction pattern. Thus it can be concluded that CdS core QDs favoured a zinc-blende crystal structure while the CdS/AgZnSe core-alloyed QDs kinetically favoured a phase change from a zinc-blende diffraction pattern to a wurtzite diffraction pattern.

3.2.3. Raman analysis

Core/shell QDs have been proven to reduce Auger recombination rates, which is important in multiexciton recombination and OFF/ON blinking process [43]. It is also believed that the core/shell interfacial alloying region is associated with a graded interface [44]. Hence, the potential of Raman to probe the internal structure of the core/alloyed shell QDs interface was investigated. Fig. 5 shows the Raman spectra for

CdS core and the different-sized CdS/AgZnSe QDs. The similarities with reference to the peak position of CdS longitudinal optical phonon (LO) bulk frequency at $\sim 300\text{ cm}^{-1}$ and CdS overtone at $\sim 600\text{ cm}^{-1}$ with those of CdS/AgZnSe₅₈₈ and CdS/AgZnSe₅₉₃, provides strong indication of the homogenous growth of the core/alloyed shell QDs. For CdS/AgZnSe₅₉₉ and CdS/AgZnSe₆₀₁, we observed significant changes in the peak position when compared to the CdS core. Specifically, the peak position of CdS/AgZnSe₅₉₉ exhibited similar frequency to CdS LO frequency but the peak at the CdS overtone region was more blue-shifted in frequency. Conversely, the peak frequencies of CdS/AgZnSe₅₉₉ relative to CdS LO and the overtone region were more red-shifted in comparison to the CdS core. The degree of frequency shift in CdS/AgZnSe₅₉₉ and CdS/AgZnSe₆₀₁ peak position relative to CdS can be understood in terms of the growth morphology and the degree of interfacial defect states in the QDs. Thus, the frequency shift and strain relaxation in the core/alloyed shell interface will differ due to the QDs size and shell thickness. The relatively less-pronounced peaks below 220 cm^{-1} for the core/alloyed shell QDs can be ascribed to a surface optical phonon feature which is inherent in finite sized crystals and also from the varying degree of alloying at the interface between CdS core and AgZnSe shell [45,46]. The variation in the intensity of the modes below 220 cm^{-1} could probably also account for the differences in alloying efficiency of the AgZnSe shell relative to the CdS core.

3.3. Optical properties

The QDs surface is influenced by the nature and chemical reaction of the synthetic constituents (surfactants, capping ligands and solvents) used in fabricating its structure. The atomistic effects of these constituents form the basis for assessing the quality of the QDs surface as it relates to the optical properties, such as the PL stability, spectral

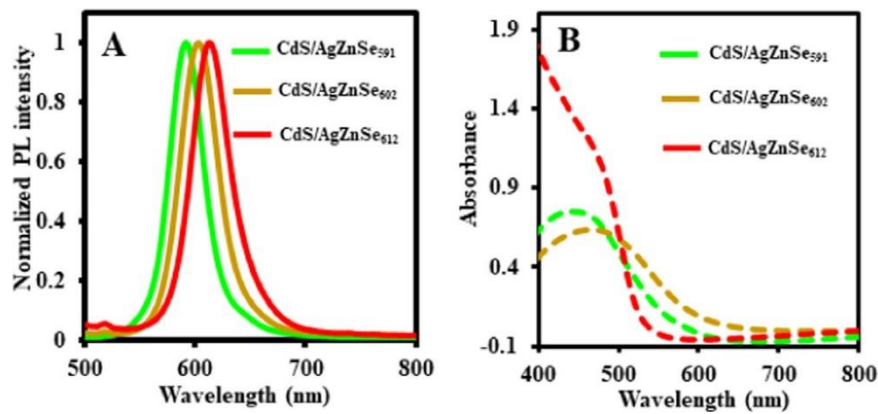


Fig. 7. PL (A) and UV/vis absorption (B) spectra of the different sized and CdS/AgZnSe core/alloyed shell QDs synthesized via method 2.

features and PL QY. The formation of midgap, deep and shallow states as surface traps provides the basis to which nonradiative electron-hole recombination degrades the QDs fluorescence. The suppression or total elimination of surface trap states in core QDs via coating of a shell layer is useful for light-associated applications and it provides a platform for better understanding of synthetic fabrication strategies required to construct high-quality QD nanocrystals. Our objective is to investigate the influence of a new shell layer (AgZnSe) on the luminescent properties of colloidal CdS QDs. We have utilized the shell alloying process to unravel how the QDs band gap and synthetic fabrication strategy influences the PL properties of CdS/AgZnSe core/alloyed shell QDs. The PL QY was determined according to the equation:

$$\Phi_F^{QD} = \Phi_F^{Std} \frac{F_{QDs} \cdot OD_{Std}(\lambda_{exc}) \cdot n_{water}^2}{F_{Std} \cdot OD_{QDs}(\lambda_{exc}) \cdot n_{ethanol}^2} \quad (1)$$

where Φ_F^{Std} is the PL quantum yield of rhodamine 6G standard in ethanol ($\Phi = 0.95$); F_{Std} and F_{QDs} are the integrated sum of the fluorescence intensity of the standard and QDs; $OD_{QD}(\lambda_{exc})$ and $OD_{Std}(\lambda_{exc})$ are the optical densities of the QDs and standard while $n_{ethanol}$ and n_{water} are the refractive indices of ethanol and water used to prepare the standard and QDs respectively.

Fig. 6A and B shows the evolution of the PL emission and absorption spectra of three different-sized CdS core QDs and Table 1 summarizes the corresponding photophysical properties as they relate to the absorption wavelength maximum, full width at half maximum (FWHM), band gap and PL QY. We harvested three-sized CdS core QDs with the sole aim of assessing their optical properties in comparison to the different-sized CdS/AgZnSe core/alloyed shell QDs. A small red shift in PL emission was observed for the harvested different-sized CdS core QDs with the absorption wavelength maximum and FWHM increasing in relation to the core size. The striking feature is the low PL QY which was increasingly tuned from 4% to 16% and also dependent on each core size. We observed that CdS₄₇₁ produced the highest PL QY of 16% while the lowest PL QY value of 4% was exhibited by CdS₄₇₈. Based on the relatively low PL QY, CdS core QDs suffers significantly from interfacial surface defects and residual strain in which the degree of defect states depends on the core size.

To effectively understand the effect of ternary AgZnSe shell alloying on the PL properties of CdS QDs, we employed two synthetic fabrication strategies. The most obvious and direct evidence of shell alloying comes from the PL emission and absorption spectra shown in Fig. 6C. The evolution of the PL emission of CdS/AgZnSe QDs synthesized via method 1 was tuned from 588 to 601 nm while the absorption spectra (Fig. 6D) was tuned from 464 nm to 477 nm. AgZnSe shell precursors used in method 1 synthesis of CdS/AgZnSe QDs was added into the growth solution after harvesting fraction of CdS₄₈₁ core QDs. The striking feature is the blue-shifted absorption wavelength and corresponding red shift in PL emission of CdS/AgZnSe₅₈₈ relative to CdS₄₈₁

QDs. The shift reveals that the shell alloying strategy, induced band gap modulation of the QDs in the visible region of the electromagnetic spectrum. For CdS/AgZnSe QDs synthesized via method 2, the PL emission spectra was tuned from 591 to 612 nm (Fig. 7A) while the absorption spectra were tuned from 449 to 481 nm (Fig. 7B). Despite the PL emission being more red-shifted relative to the CdS core, the absorption spectrum of CdS/AgZnSe₅₉₁ was significantly blue-shifted. From Table 1, the efficiency of band gap modulation of CdS/AgZnSe QDs was observed to vary narrowly from 2.07 to 2.11 eV for method 1 synthesis and from 2.03 to 2.10 eV for method 2 synthesis of the QDs.

To determine if the band gap modulation of CdS/AgZnSe QDs originated from the intrinsic optical properties of the core/alloyed nanostructures, a deeper assessment of the PL QY values (Table 1) was performed. The most striking observation is the variation in the PL QY of CdS/AgZnSe QDs synthesized via method 1 and 2 and the remarkable increase in comparison to the values obtained for CdS core. Via method 1 synthesis, the PL QY of CdS/AgZnSe QDs was tuned from 48% to 51% but via method 2 synthesis the PL QY was tuned from 35% to 73%. It is noteworthy that shell alloying of CdS QDs suppressed interfacial defect states in the core/alloyed shell nanocrystals due to the remarkable increase in the PL QY. However, it is important to emphasize that the defect state suppression efficiency varied amongst the QDs size and was dependent on the quality of the fabrication method.

Examining closely how the shell alloying process influenced the optical properties of the QDs, we have probed the correlation between the band gap modulation and the PL QY. It is a well-established phenomenon that a semiconductor band gap can be reduced by residual strain, thus leading to deformed potential [47,48]. Therefore, the low PL QY reveals that CdS core QDs suffer from residual strain due to surface traps embedded within the nanocrystals. The narrow band gap (2.07–2.11 eV) exhibited by the different-sized CdS/AgZnSe QDs (synthesized via method 1), correlated precisely to the small difference in PL QY (48–51%). This suggests that suppression of surface defect states in CdS QDs was with a very small margin across the core/alloyed shell QDs size. However, a wider margin in defect state suppression was observed for CdS/AgZnSe QDs synthesized via method 2, due to the wider difference in PL QY from 35% to 73%. Two important features are the maximum PL QY of 73% and the precise correlation in the margin of difference between the band gap and the PL QY. It is also noteworthy that the high PL QY implies much of the surface defects were suppressed by the shell alloying process while the variation in PL QY correlated precisely to the efficiency of surface defect suppression.

4. Conclusions

The passivation of CdS QDs with a new ternary alloyed AgZnSe shell layer was obtained via the organometallic synthetic route. The band gap of CdS/AgZnSe core/alloyed shell QDs was tuned across the visible

region with the nanocrystals exhibiting varying PL QYs. We observed a precise correlation in the margin of difference between the band gap of the QDs and the PL QY. The effect of shell alloying was observed in the QDs growth morphology in which the QDs growth transitioned from a homogeneous state to a heterogeneous state. Transition in the phase structure of the QDs from a zinc blende diffraction pattern to a wurtzite diffraction pattern was also observed. Generally, we have established that AgZnSe shell passivation on luminescent CdS QDs suppressed interfacial defect states in the CdS core QDs with the degree of suppression dependent on the size of the QDs derived from the finely-tuned synthetic fabrication strategy.

Acknowledgement

Financial support from the Water Research Council (WRC) project K5/2752, South Africa and the University of Pretoria is gratefully acknowledged.

References

- [1] T.V. Duncan, M.A. Mendez Polanco, Y. Kim, S.-J. Park, Improving the quantum yields of semiconductor quantum dots through photoenhancement assisted by reducing agents, *J. Phys. Chem. C* 11 (2009) 7561–7566.
- [2] A. Hassinen, I. Moreels, K. De Nolf, P.F. Smet, J.C. Martins, Z. Hens, Short-chain alcohols strip X-type ligands and quench the luminescence of PbSe and CdSe Quantum dots, acetonitrile does not, *J. Am. Chem. Soc.* 134 (2012) 20705–20712.
- [3] M. Nasilowski, P. Spinicelli, G. Patriarche, B. Dubertret, Gradient CdSe/CdS quantum dots with room temperature biexciton unity quantum yield, *Nano Lett.* 15 (2015) 3953–3958.
- [4] P. Reiss, M. Potié, L. Li, Core/shell semiconductor nanocrystals, *Small* 5 (2009) 154–168.
- [5] D.V. Talapin, J.-S. Lee, M.V. Kovalenko, E.V. Shevchenko, Prospects of colloidal nanocrystals for electronic and optoelectronic applications, *Chem. Rev.* 110 (2010) 389–458.
- [6] O. Chen, J. Zhao, V.P. Chauhan, J. Cui, C. Wong, D.K. Harris, H. Wei, H.-S. Han, D. Fukumura, R.K. Jain, M.G. Bawendi, Compact high-quality CdSe–CdS core–shell nanocrystals with narrow emission linewidths and suppressed blinking, *Nat. Mater.* 12 (2013) 445–451.
- [7] C. Giansante, I. Infante, Surface traps in colloidal quantum dots: a combined experimental and theoretical perspective, *J. Phys. Chem. Lett.* 8 (2017) 5209–5215.
- [8] M. Nirmal, B.O. Dabbousi, M.G. Bawendi, J.J. Macklin, J.K. Trautman, T.D. Harris, L.E. Brus, Fluorescence intermittency in single cadmium selenide nanocrystals, *Nature* 383 (1996) 802–804.
- [9] A. Efros, M. Rosen, Random telegraph signal in the photoluminescence intensity of a single quantum dot, *Phys. Rev. Lett.* 78 (1997) 1110–1113.
- [10] Y. Altintas, M.Y. Talpur, M. Ünlü, E. Mutlugün, Highly efficient cd-free alloyed core/shell quantum dots with optimized precursor concentrations, *J. Phys. Chem. C* 120 (2016) 7885–7892.
- [11] J. Bang, J. Park, J.H. Lee, N. Won, J. Nam, J. Lim, B.Y. Chang, H.J. Lee, B. Vhon, J. Shin, J.B. Park, H. Choi, K. Cho, S.M. Park, T. Joo, S. Kim, ZnTe/ZnSe (core/shell) type-II quantum dots: their optical and photovoltaic properties, *Chem. Mater.* 22 (2010) 233–240.
- [12] M.D. Tessier, D. Dupont, K. De Nolf, J. De Roo, Z. Hens, Economic and Size-tunable synthesis of InP/ZnE (E = S, Se) colloidal quantum dots, *Chem. Mater.* 27 (2015) 4893–4898.
- [13] W. Jiang, A. Singhal, J. Zheng, C. Wang, W.C.W. Chan, Optimizing the synthesis of red- to near-ir-emitting CdS-capped CdTe_xSe_{1-x} alloyed quantum dots for biomedical imaging, *Chem. Mater.* 18 (2006) 4845–4854.
- [14] P. Tyagi, P. Kambhampati, Independent control of electron and hole localization in core/barrier/shell nanostructures, *J. Phys. Chem. C* 116 (2012) 8154–8160.
- [15] M. Nasilowski, P. Spinicelli, G. Patriarche, B. Dubertret, Gradient CdSe/CdS quantum dots with room temperature biexciton unity quantum yield, *Nano Lett.* 15 (2015) 3953–3958.
- [16] M. Wang, M. Zhang, J. Qian, F. Zhao, L. Shen, G.D. Scholes, M.A. Winnik, Enhancing the photoluminescence of polymer-stabilized CdSe/CdS/ZnS core/shell/shell and CdSe/ZnS core/shell quantum dots in water through a chemical-activation approach, *Langmuir* 25 (2009) 11732–11740.
- [17] W. Liu, H. Soo Choi, J.P. Zimmer, E. Tanaka, J.V. Frangioni, M. Bawendi, Compact cysteine-coated CdSe(ZnCdS) quantum dots for in vivo applications, *J. Am. Chem. Soc.* 129 (2007) 14530–14531.
- [18] K. Yu, S. Singh, N. Patrio, V. Chu, Effect of reaction media on the growth and photoluminescence of colloidal CdSe nanocrystals, *Langmuir* 20 (2004) 11161–11168.
- [19] R.E. Bailey, S. Nie, Alloyed semiconductor quantum dots: tuning the optical properties without changing the particle size, *J. Am. Chem. Soc.* 125 (2003) 7100–7106.
- [20] J. Quyang, C.I. Ratcliffe, D. Kingston, B. Wilkinson, J. Kuijper, X. Wu, J.A. Ripmeester, K. Yu, Gradiently alloyed Zn_xCd_{1-x}S colloidal photoluminescent quantum dots synthesized via a noninjection one-pot approach, *J. Phys. Chem. C* 112 (2008) 4908–4919.
- [21] R. Gui, A. Wan, H. Jin, H. Li, C. Zhou, Acetyl acetonate-stabilized Mn²⁺:cds quantum dots: aqueous synthesis and reversible fluorescence tuned by redox re- action, *Mater. Lett.* 98 (2013) 190–193.
- [22] R. Gui, X. An, H. Su, W. Shen, Z. Chen, X. Wang, A near-infrared-emitting CdTe/CdS core/shell quantum dots-based OFF–ON fluorescence sensor for highly selective and sensitive detection of Cd²⁺, *Talanta* 94 (2012) 257–262.
- [23] R. Gui, X. An, Layer-by-layer aqueous synthesis, characterization and fluorescence properties of type-II CdTe/CdS core/shell quantum dots with near-infrared emission, *RSC Adv.* 3 (2013) 20959–20969.
- [24] M.V. Rama Krishna, R.A. Friesner, Quantum confinement effects in semiconductor clusters, *J. Chem. Phys.* 95 (1991) 8309–8322.
- [25] I. Hernandez-Calderon, II-VI semiconductor materials and their applications, in: M.C. Tamargo, M.O. Manasreh (Eds.), *Optoelectronic Properties of Semiconductors and Superlattices*, 12 Taylor & Francis Inc, New York, 2002, pp. 136–138.
- [26] A.I. Ekimov, I.A. Kudryavtsev, M.G. Ivanov, A.L. Efros, Spectra and decay kinetics of radiative recombination in CdS microcrystals, *J. Lumin.* 46 (1990) 83–95.
- [27] K. Gong, D.F. Kelley, Lattice strain limit for uniform shell deposition in zincblende CdSe/CdS quantum dots, *J. Phys. Chem. Lett.* 6 (2015) 1559–1562.
- [28] C.-C. Hung, S.-J. Ho, C.-W. Yeh, G.-H. Chen, J.-H. Huang, H.-S. Chen, Highly luminescent dual-color-emitting alloyed [Zn_xCd_{1-x}Se_yS_{1-y}] quantum dots: investigation of bimodal growth and application to lighting, *J. Phys. Chem. C* 121 (2017) 28373–28384.
- [29] L.A. Swafford, L.A. Weigand, M.J. Bowers, J.R. McBride, J.L. Rapaport, T.L. Watt, S.K. Dixit, L.C. Feldman, S.J. Rosenthal, Homogeneously alloyed Cd_xSe_{1-x} nanocrystals: synthesis, characterization, and composition/size-dependent band gap, *J. Am. Chem. Soc.* 128 (2006) 12299.
- [30] Z. Pan, K. Zhao, J. Wang, H. Zhang, Y.Y. Feng, X. Zhong, Near infrared absorption of Cd₆Te_{1-x} alloyed quantum dot sensitized solar cells with more than 6% efficiency and high stability, *ACS Nano* 7 (2013) 5215–5222.
- [31] A. Kigel, M. Brumer, A. Sashchiuk, L. Amirav, E. Lifshitz, PbSe/PbSe_xS_{1-x} core-alloyed shell nanocrystals, *Mater. Sci. Eng., C* 25 (2005) 604–608.
- [32] H. Jin, R. Gui, Z. Wang, J. Xia, M. Yang, F. Zhang, S. Bi, Facile fabrication of water-dispersible AgInS₂ quantum dots and mesoporous AgInS₂ nanospheres with visible photoluminescence, *RSC Adv.* 5 (2015) 68287–68292.
- [33] P. Yang, M. Ando, N. Murase, Highly luminescent CdSe/Cd_xZn_{1-x}S quantum dots coated with thickness-controlled SiO₂ shell through silanization, *Langmuir* 27 (2011) 9535–9540.
- [34] K. Boldt, N. Kirkwood, G.A. Beane, P. Mulvaney, Synthesis of highly luminescent and photo-stable, graded shell CdSe/Cd_xZn_{1-x}S nanoparticles by in situ alloying, *Chem. Mater.* 25 (2013) 4731–4738.
- [35] S.M. Fairclough, E.J. Tyrrell, D.M. Graham, P.J.B. Lunt, S.J.O. Hardman, A. Pietzsch, F. Hennies, J. Moghal, W.R. Flavell, A.A.R. Watt, J.M.J. Smith, Growth and characterization of strained and alloyed Type-II ZnTe/ZnSe core–shell nanocrystals, *Phys. Chem. C* 16 (2012) 26898–26907.
- [36] W.K. Bae, L.A. Padilha, Y.-S. Park, H. McDaniel, I. Robel, J.M. Pietryga, V.I. Klimov, Controlled alloying of the core-shell interface in CdSe/CdS quantum dots for suppression of Auger recombination, *ACS Nano* 7 (2013) 3411–3419.
- [37] O. Adegoke, K. Takemura, E.Y. Park, Plasmonic oleylamine-capped gold and silver nanoparticle-assisted synthesis of luminescent CdZnSeS quantum dots, *ACS Omega* 3 (2018) 135–1366.
- [38] J. Quyang, C.I. Ratcliffe, D. Kingston, B. Wilkinson, J. Kuijper, X. Wu, J.A. Ripmeester, K. Yu, Gradiently alloyed Zn_xCd_{1-x}S colloidal photoluminescent quantum dots synthesized via a noninjection one-pot approach, *J. Phys. Chem. C* 112 (2008) 4908–4919.
- [39] B.O. Dabbousi, Rodríguez-Viejo, F.V. Mikulec, J.R. Heine, H. Mattoussi, R. Ober, K.F. Jensen, M.G. Bawendi, (CdSe)ZnS core-shell quantum dots: synthesis and characterization of a size series of highly luminescent nanocrystallites, *J. Phys. Chem. B* 101 (1997) 9463–9475.
- [40] D.V. Talapin, I. Mekis, S. Götzinger, A. Kornowski, O. Benson, H. Weller, CdSe/CdS/ZnS and CdSe/ZnSe/ZnS core-shell-shell nanocrystals, *J. Phys. Chem. B* 108 (2004) 18826–18831.
- [41] P.T.K. Chin, C. de Mello Donega, S.S. van Bavel, S.C.J. Meskers, N.A.J.M. Sommerdijk, R.A.J. Janssen, Highly luminescent CdTe/CdSe colloidal heteronanocrystals with temperature-dependent emission color, *J. Am. Chem. Soc.* 129 (2007) 14880–14886.
- [42] N.T.K. Thanh, N. Maclean, S. Mahiddine, Mechanisms of nucleation and growth of nanoparticles in solution, *Chem. Rev.* 114 (2014) 7610–7630.
- [43] F. Garcia-Santamaría, S. Brovelli, R. Viswanatha, J.A. Hollingsworth, H. Htoon, S.A. Crooker, V.I. Klimov, Breakdown of volume scaling in Auger recombination in CdSe/CdS heteronanocrystals: the role of the core-shell interface, *Nano Lett.* 11 (2011) 687–693.
- [44] G.E. Cragg, A.L. Efros, Suppression of auger processes in confined structures, *Nano Lett.* 10 (2009) 313–317.
- [45] F. Comas, N. Studart, G.E. Marques, Optical phonons in semiconductor quantum rods, *Solid State Commun.* 130 (2004) 477–480.
- [46] H. Lange, M. Artemyev, U. Woggon, C. Thomsen, Geometry dependence of the phonon modes in CdSe nanorods, *Nanotechnology* 20 (2009) 045705.
- [47] J. Kim, M.V. Fischetti, Electronic band structure calculations for biaxially strained Si, Ge, and III-V Semiconductors, *J. Appl. Phys.* 108 (2010) 013710.
- [48] J. Kim, M.V. Fischetti, S. Aboud, Structural, electronic, and transport properties of silicene nanoribbons, *Phys. Rev. B* 86 (2012) 205323.